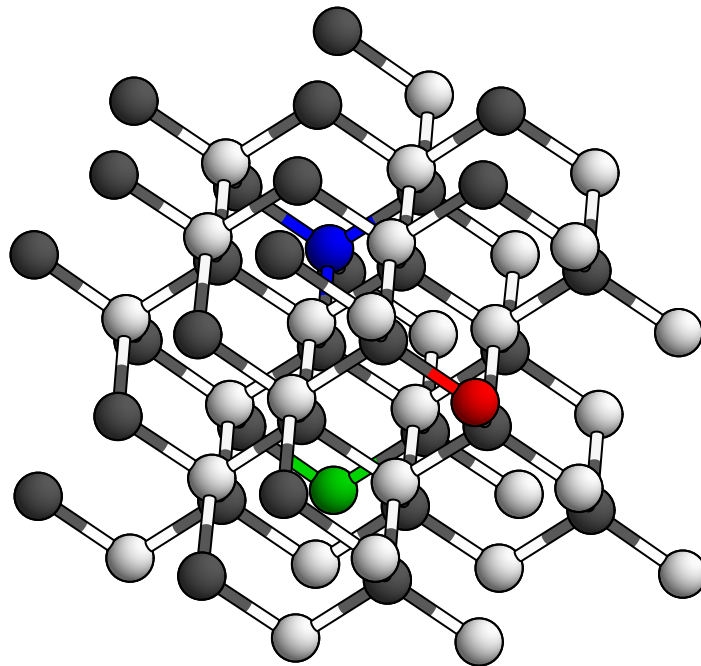


Rare Earth point defects in GaN

Simone Sanna



The Rare Earths perplex us in our researches, baffle us in our speculations, and haunt us in our very dreams. They stretch like an unknown before us, mocking, mystifyng, and murmuring strange revelations and possibilities.

Sir William Crooke, 1832-1919

Rare Earth point defects in GaN

Dissertation zur Erlangung des akademischen Grades

Doktor der Naturwissenschaften (Dr. rer. nat.)

vorgelegt dem

Fachbereich Physik der Fakultät für Naturwissenschaften

Universität Paderborn

Dipl. Phys. Simone Sanna

Paderborn, 2007

Dem Department Physik der Fakultät für Naturwissenschaften als Dissertation vorgelegt.

Eingereicht am: 29.10.2007
Tag der mündlichen Prüfung: 14.12.2007

Promotionskommission

Vorsitzender	Prof. Dr. Siegmund Greulich-Weber
Erstgutachter	Prof. Dr. Thomas Frauenheim
Zweitgutachter	Prof. Dr. Wolf Gero Schmidt
Beisitzer	Prof. Dr. Donat Josef As

Archiv

Elektronische Dissertationen und Habilitationen der Universität Paderborn
<http://www.ub.upb.de/ebibliothek/hochschulschriften/ediss>

Simone Sanna, *Rare Earth point defects in GaN*.

PhD Thesis (in English), Department of Physics, Faculty of Science, University of Paderborn, Germany (2007). 157 Pages, 64 Figures, 30 Tables.

Abstract

In this work we investigate rare earth doped GaN, by means of theoretical simulations. The optical emission from rare earth ions (RE) consists of very sharp lines (ranging from the UV to IR), whose wave length is determined by the energy of the corresponding transition within the $4f$ -shell. Rare earth doped GaN has been used as phosphors in the realisation of GaN-based flat panel displays, even if the RE luminescence could not be related up to date to a singular or to a group of lanthanide defects and few is known about the mechanisms leading to the emission.

The huge unit cells necessary to model the experimental system, where dilute amount of rare earth ions are used, are handled with the charge self consistent density-functional based-tight binding (SCC-DFTB) calculational scheme. The method has been extended to include LDA+ U and simplified self interaction corrected (SIC)-like potentials for the simulation of systems with localised and strongly correlated electrons. This approach attempts to combine the efficiency of the tight-binding with the accuracy of more sophisticated *ab initio* methods allowing the treatment of highly correlated electrons also for very large systems.

A set of tight-binding parameters has been created to model the interaction of GaN with some dopants, including a selection of lanthanide ions interesting due to their optical or magnetic properties (Pr, Eu, Gd, Er and Tm). The f -electrons were treated as valence electrons. The validity of the parameters was thoroughly tested against experimental data, in particular bulk ErN in the rock-salt phase is investigated in detail and found to be a half-metal in the ferromagnetic phase.

In addition, the TB approach opens the possibility to overcome one of the most relevant problems of the density-functional theory (DFT) calculations in the local density approximation (LDA), the considerable underestimation of the band gap. A qualitatively correct description of the band gap is crucial for the simulation of rare earth doped GaN, because the luminescence intensity of the implanted samples depends on the size of the host band gap and because the rare earths could introduce charge transition levels near the conduction band. In this work these levels are calculated with the Slater-Janak (SJ) transition state model, which allows an approximate calculation of the charge transition levels by analysing the Kohn-Sham eigenvalues of the DFT. Unfortunately, the usual LDA and its gradient extensions fail in describing the Kohn-Sham eigenvalues of the lanthanides sufficiently well. We show (analytically and by means of representative examples) that the SJ-transition state becomes a powerful tool if applied self-consistently within a LDA+ U extension of DFT. The simulations confirmed that the lanthanide ions prefer the Ga lattice site. Isolated substitutionals RE_{Ga} are very stable defects, present in the C_{3v} symmetry. RE_{Ga} are found to introduce only a small distortion in the host lattice and in the charge distribution of the ligands and are therefore easily incorporated in the GaN host. Rare earth interstitials are found not to be stable against the kick-out of a neighbouring Ga which is replaced by the rare earth. Complexes formed by lanthanide substitutionals and N-interstitials or anti-sites (I_{N} and Ga_{N} or N_{Ga}) are characterised by high formation and low binding energies and are unlikely to be formed under equilibrium conditions. Among the defects which can be related with the luminescence we have found the close pairs formed by RE_{Ga} substitutionals and vacancies or O_{N} substitutionals. These complexes are stable (bound) at typical annealing temperatures and introduce localised levels in the GaN band gap. On the basis of these results we conclude our work with a possible model for the mechanisms leading to the luminescence, where the nitrogen vacancies in RE_{Ga} V_{N} pairs act as assistant for the energy transfer to the f -shell of the lanthanides.

Keywords

density functional theory, DFT, tight-binding, LDA+ U , strongly correlated electrons, point defects, rare earth, lanthanides, GaN, gallium nitride

Simone Sanna, *Seltene Erde Punktdefekte in GaN*.

Dissertation (in englischer Sprache), Department Physik, Fakultät für Naturwissenschaften, Universität Paderborn (2007). 157 Seiten, 64 Abbildungen, 30 Tabellen.

Kurzfassung

In dieser Arbeit wird seltene Erde dotiertes GaN mit Hilfe von Computersimulationen untersucht. Die Emissionsspektren der seltenen Erde Ionen (SE) sind von scharfen Linien gekennzeichnet, die dem zugehörigen Übergang in der f -Schale entsprechen. SE-dotiertes GaN wurde erfolgreich für die Herstellung von flachen Displays benutzt, auch wenn die SE-Lumineszenz bis zum heutigen Tag keinem bestimmten Defektzustand zugeordnet werden konnte.

Die sehr großen Einheitszellen, die erforderlich sind, um die experimentellen Konzentrationen zu reproduzieren, werden mit dem Ladung-selbstkonsistenten dichtefunktionalbasierten Tight-Binding Verfahren (SCC-DFTB) untersucht. Die Methode wurde auf orbitalabhängigen Potentiale erweitert, die für die Simulation von Systemen mit stark korrelierten Elektronen notwendig sind, nämlich LDA+ U und Self-Interaction Correction (pSIC) Methode. Das Verfahren kombiniert die Effizienz der Tight-Binding Methode mit der Genauigkeit von anspruchsvolleren *ab initio* Verfahren und ermöglicht so die Untersuchung von stark lokalisierten Elektronen auch in größeren Systemen.

Ein Satz von Tight-Binding Parameter wurde erzeugt, um die Wechselwirkung von GaN mit einer Auswahl von SE-Dotiersubstanzen zu modellieren, welche wegen ihrer optischen oder magnetischen Eigenschaften von Interesse sind (Pr, Eu, Gd, Er, Tm). Dabei wurden die f -Elektronen als Valenzelektronen behandelt. Die Tauglichkeit der Parameter wurde anhand von experimentell bekannten Testsystemen überprüft. Insbesondere, ErN in der Kochsalz Struktur ist ausführlich untersucht worden und ist in der DFTB-Darstellung ein Halbmetall in der ferromagnetischen Phase.

DFTB bietet die Möglichkeit eines der größten Probleme der dichtefunktionaltheoretischen Rechnungen (DFT) in der Lokaldichte-Näherung (LDA) zu umgehen, nämlich die Unterschätzung der elektronischen Bandlücke. Eine qualitativ korrekte Beschreibung der Bandlücke ist dabei eine Grundvoraussetzung für die Simulation von SE-dotierten Halbleitern, weil die Lumineszenzintensität der dotierten Probe von der Größe der Bandlücke abhängt und weil die Störatome Umladungsniveaus in der Nähe der Leitungsbandkante einfügen. Diese Umladungen wurden in dieser Arbeit mit dem Slater-Janak (SJ) Modell berechnet, das eine annähernde Berechnung von elektronischen Umladungen durch die Analyse der Kohn-Sham DFT Eigenwerte ermöglicht.

Die Simulationen haben bestätigt, dass SE den Ga-Platz bevorzugen. Isolierte SE_{Ga} sind sehr stabile Defekte mit C_{3v} Symmetrie. SE_{Ga} verursachen eine relativ kleine Gitterverzerrung in GaN, ändern nur geringfügig die Ladungsverteilung der N-Liganden und werden daher leicht in dem GaN-Host aufgenommen. Seltene Erde in Zwischengitterstellen (I_{SE}) sind nicht stabil und gehen in die energetisch günstigere $SE_{Ga} I_{Ga}$ Konfiguration über.

Die von einem SE_{Ga} und einem N-Zwischengitteratom oder Antisite gebildeten Defektkomplexe (I_N und GaN oder N_{Ga}) sind von großer Formationsenergie und niedriger Bindungsenergie gekennzeichnet, so dass sie mit großer Wahrscheinlichkeit bei Gleichgewichtsbedingungen nicht vorkommen und, falls nach Implantation vorhanden, die Probenausheilung nicht überstehen würden. Unter den Defekten, die mit der Lumineszenz in Verbindung gebracht werden können, sind die von SE_{Ga} und benachbarten Leerstellen oder O_N Substitutionellen gebildeten Paare besonders wichtig. Diese Konfigurationen sind auch bei typischen Ausheilungstemperaturen stabil und induzieren zusätzliche lokalisierte Zustände in die Bandlücke. Anhand dieser Ergebnisse wird ein Modell für die Emissionsmechanismen vorgeschlagen, in dem die Energie der Ladungsträger über diese zusätzlich eingefügten Assistenz-Niveaus übermittelt wird.

Schlagwörter

DFT, Dichtefunktionaltheorie, Tight-Binding, LDA+ U , Punktdefekte, seltene Erde, Lanthanide, GaN, Galliumnitrid

Introduction

Starting from the work of Ennen *et al.* in 1983 [1] the study of the optical properties of rare earth (RE) doped III-V semiconductors has attracted more and more the attention of the scientific community. The emission spectrum of the RE ions is characterised by very sharp optical emissions ranging from the ultraviolet (UV) to the infrared (IR), which are related to intra- f electronic transitions. The RE ions have a strongly localised and partially filled $4f$ -shell which is screened by the outer $5s$ and $5p$ orbitals. Due to the screening effects the wavelengths of these emissions are only determined by the energy of the transition between the $4f$ -states and are quite independent from the host material. The latter only influences the radiative transition probability, i.e. the emission intensity. Most of the standard semiconductors (Si, Ga, etc.) are affected by severe quenching of the luminescence at room temperature. It was shown by Favennec *et al.* [2] that the thermal quenching of erbium doped semiconductors decreases with increasing bandgap and that wide gap semiconductors are ideal hosts for the lanthanide ions. Among the wide gap semiconductors, GaN has turned out to be an ideal host candidate because of its high field transport characteristics, because it is chemically and thermally rugged and because it incorporates very well the RE ions. The emission from RE doped GaN is strong enough to be observable to the naked eye at room temperature.

Technological importance

The photoemission from RE in GaN covers the entire visible spectrum. In particular the light emission in the red (from Eu ions, 621 nm), green (Er, 537/558 nm) and blue (Tm, 477 nm) is very pure and matches quite well the CIE coordinates adopted by the National Television System Committee (NTSC) in the USA and by the European Broadcasting Union (EBU) in the European community. The success in doping GaN samples with RE ions (during growth or by implantation) has been exploited for the creation of novel multi colour and full colour (white) displays [3, 4]. Besides the primary colours obtained by GaN doped with Eu, Er and Tm, mixed colours and hues can be obtained using different RE. The combined emission is in fact perceived by the human eye as a single colour depending on the relative intensity of the RGB components. Fig. 1 represents a CIE x-y chromaticity diagram: all the colours within the triangle defined by the primary colours can be in principle obtained. This is a big advantage with respect to other commercial displays, where the phosphors for different colours have to be generated from different materials. RE doped GaN samples have been in fact successfully exploited for the realisation of flat panel displays (FLD), high contrast thick dielectric electroluminescent (TDEL) and thin film electroluminescent (TFEL) display devices. The displays can be developed with either multiple RE doping in a single layer or with more phosphor layers each doped with a different lanthanide. Construction schemes of the standard devices (both dc- and ac-biased) and their development, as well as the construction methods used to optimize and enhance their performances are reported in a review article of Steckl *et al.* [4]. Today's devices are characterised by high brightness and contrast (contrast ratio >40:1), outstanding durability (5% loss in brightness after 1000 hours in an environment with 40% humidity) and extremely long lifetime (<50.000 hours, i.e. an order of magnitude more than other commercial displays) due to the chemical stability of the phosphors. These performance are expected to be further improved in the next decade [5–7], where GaN:RE based devices will be the standard for flat-TVs and portable displays. Furthermore, the absence of polymeric materials, vacuum or gases

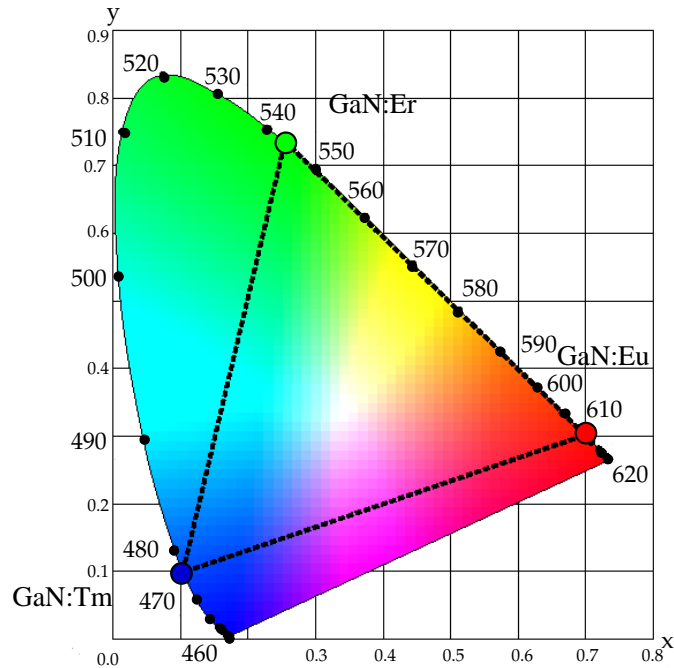


Figure 1: CIE chromaticity x - y diagram showing the location of the red, green and blue emission from rare earth doped. All the mixed colours within the marked triangle defined by the three primary colours as well as white light can be obtained mixing the RE.

in the device structure allows the usage of the displays in harsh environments like airplanes, hospitals and factories.

Rare earth doped GaN has other important applications in the field of telecommunications, especially in the area of optical fibers. This is a field in constant and explosive growth and evolution, driven mainly by the widespreading popularity of large bandwidth home networks. The standard wavelength of the signals traveling in optical fibers is $1.5 \mu\text{m}$ (and more rarely $1.3 \mu\text{m}$), because at this IR wavelength the dispersion and the loss are minimal. For this reason fiber optic sources and amplifiers have been developed doping different hosts with Er^{3+} and Pr^{3+} . The big advantage of GaN with respect to other hosts is again the absence of thermal quenching at room temperature. In other semiconductors like Si the emission is completely quenched already at 200 K. A consistent co-doping with oxygen improves the thermal properties of Si but at expense of a more complicated process and degraded electrical properties [8].

Experimental knowledge of rare earth doped GaN

Rare Earth compounds have been a long time puzzle. They show extremely interesting properties but are quite difficult to investigate both experimentally and from the theoretical point of view. Researchers realized that even a small amount of impurities or crystal disorder could dramatically affect the properties of relatively simple systems like RE monopnictides [9]. This was combined with the well known problems of chemically separating different rare earths. Nevertheless in the last five years the understanding of the microstructure of RE-doped III-nitrides has improved substantially, in part due to the intensive work of the Steckl group in Cincinnati [10] and of the RENiBEL (Rare Earth doped Nitrides for high Brightness Electroluminescent emitters) consortium, a network of university laboratories (including the Universität Paderborn) funded by the European Commission in a Fifth Framework Research Training Network [11, 12]. Implanted or *in situ* doped samples have been extensively investigated with different spectroscopic techniques in order to win informations

about the excitation paths, the lattice locations of the active sites and the sample preparation conditions which maximise the emission. Important informations about the RE preferred lattice site (90% of the RE are found to reside on Ga sites) and its geometry (C_{3v}) could be gained but some questions still remain open. The transfer of excitation from the band states of a semiconductor host to the inner electronic shell of RE ions, perhaps involving the mediation of host intrinsic defects and the migration and localisation of excitons, is itself not a well-understood process: this process may well favour the excitation of particular sites through some as yet undiscovered physical mechanisms. Besides, despite many efforts any luminescence band in RE doped nitrides could be definitively assigned to a particular lattice site. Another important issue in the process of maximising the emission is the idea of enhancing the luminescence efficiency by the addition of co-dopants (O, F and C), which may either act either locally, to influence the defect symmetry or non locally, as "sensitizers" of the luminescence. Till now there have been contradicting reports, among other Torvik *et al.* reported that co-doping with O led to a 20 times increase in the Er^{3+} related luminescence in GaN:Er [13] while Citrin *et al.* found no correlation between the Er^{3+} related luminescence in the same host and the presence of O [14]. The question of co-doping seems not to be settled. A last question of big importance regards the clustering of the lanthanide ions in the GaN host. Recently Katchkanov *et al.* [15] have shown by means of EXAFS analysis the tendency of the RE ion in implanted GaN to cluster. Does it negatively influence the RE emission or is this possibly causing the emission? Further details about the experimental knowledge of RE doped nitrides are reviewed in the first chapter.

Theory

The role of the theory is the development of models to help to reproduce and understand the results of experiments and predict the behaviour of the investigated systems. The study of strongly correlated systems like RE is in this sense a big challenge for theorists as it requires different techniques than the usual methods for the simulation of solid state systems. Many properties of the lanthanide elements depend on the strongly correlated behavior of their f -electrons. Unfortunately methods based on a standard mean-field DFT-LDA approach give qualitatively incorrect description of systems containing strongly localised orbitals [16], allowing far too much hybridisation with the environment. The study of such systems requires a more sophisticated theory than simple mean-field methods. Large scale configuration interaction based simulations instead are prohibitively demanding for the case of lanthanide ions in GaN, where dilute amount of dopants are used and huge cells are needed to represent the experimental system. Furthermore RE ions have atomic numbers of between 57 and 70, hence relativistic effects become important and have to be considered. Up to date there have been three major attempts to investigate the behaviour of lanthanides in III-V hosts. The Jones group in Exeter used the DFT approach to calculate energetic and electrical properties of Eu, Er and Tm in different hosts. The $4f$ -shell was treated as core state of pseudopotentials, which were generated assuming the trivalent configuration of the ions [17]. Svane *et al.* [18] used a DFT-based method including a correction for the self-interaction (SIC) error to investigate isolated RE_{Ga} in GaAs and GaN. More detailed reports of the results of the above cited investigations will be given in the following. Finally the Frauenheim group in Paderborn used LDA+ U [16] and pseudo-SIC techniques implemented in the spin-polarised density-functional based tight-binding (DFTB) to investigate RE point defects in GaN. This investigation is the subject of this work.

Objectives of this work

The main goal of the current research on lanthanide doped nitrides is, for both experimentalist and theoreticians, to optimise the emission from the RE. Given a multiplicity of sites, it may be possible to engineer the occupation statistic in order to maximise the rare earth emission intensity. The main question of the defect engineering approach is if the lanthanide emission is principally due to a majority site with a low oscillator strength or rather to a minority site of exceptionally high luminescence efficiency (called "magic site"). The main goal of this work is to identify and characterise

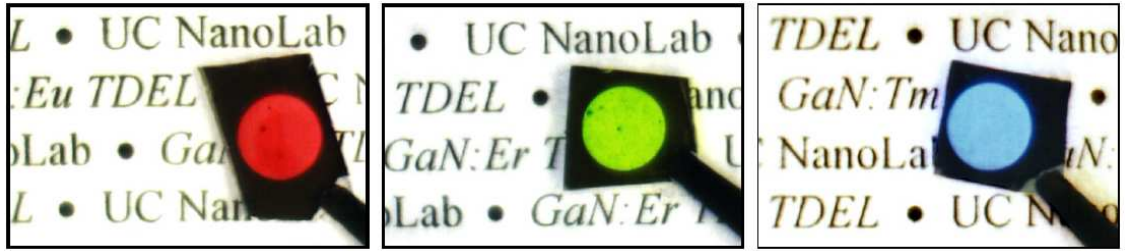


Figure 2: Single colour red, green, and blue GaN:RE TDEL devices obtained using Eu, Er and Tm as phosphors. The picture is taken from Ref. [3].

particular sites that could act as luminescence centers (they are called lumophores). This will be done with a systematic investigation of RE point defects, including isolated impurities and defect pairs. On the basis of the physical characteristics of the single sites (geometric characteristics like symmetry, lattice distortion etc. as well as electronic characteristics, like formation energy, introduction of localised states in the host etc.) we will be able to identify or exclude particular defect sites as responsible candidate for the observed emission. We will also address the problem of the co-doping, investigating which effect oxygen ions (representative for the whole class of donors) have on RE-doped GaN samples. The rare earth clustering in the GaN samples is not investigated in this work. The spectrum of theoretical methods for the investigation of atomic structures ranges from computationally very demanding high-accuracy techniques based on configuration interactions over post-Hartree Fock and density functional theory based methods to the computationally cheaper (semi-)empirical techniques. Each class of methods is best suited for certain types of application, defined by the number of atoms that can be handled at a desired level of accuracy. The density functional based tight-binding (DFTB) approach used in this work can be located among the medium-accuracy tools and is characterised by a favourable ratio between accuracy and efficiency. To pursue our goals we followed a plan made of four main steps. Firstly the formalism needed to conjugate the orbital dependent potentials in the framework of the tight-binding was developed and implemented in the so called DFTB+ software [19]. In a second phase the DFTB parameters for a selection of lanthanides, the host GaN and some common dopants (O, C) have been created and validated. The third step consisted in the simulation of different GaN intrinsic defects: this had the double purpose of testing the DFTB representation of the host and gain information about the nature of the defects itself, needed successively to understand the characteristic of those complexes formed by an intrinsic GaN defect and a RE impurities. Finally, the systematic simulation of the rare earth point defects was carried out, paying attention to the issue of co-doping. Bulk systems and point defects are today usually investigated with DFT-based calculation schemes, which guarantee an high accuracy at an affordable computational cost. The investigation of RE systems however goes far beyond a classical study of point defects because of the nature of the RE itself. DFTB offers a lot of advantages which make it one of the most suitable simulation packages for the simulation of RE systems. First of all, despite its simplicity (a two center only non-orthogonal Hamiltonian is used) the density functional based tight-binding (DFTB) method scheme has been proven to be accurate when applied to solid state [20], molecular or biological systems [21]. Materials like silicon [22], SiC [23], diamond [24], boron and boron nitride [25] and III-V semiconductors like GaN [26] and GaAs [27] have successfully been studied within the DFTB approach. Second, with a classic *ab initio* package it would be impossible to carry out an extensive sampling of RE defects in GaN¹. A thorough study of those systems in fact includes the investigation of an huge number of possible defect configurations which have to be considered in different charge states and spin configurations. Another problem related to the *ab initio* codes would be the generation of reliable pseudopotentials for RE ions, while in DFTB it is easier to create suitable parameters for the code. It is interesting to notice that also semiempirical methods have strong deficiencies in the

¹We use nonetheless different *ab initio* packages throughout this work to check the precision of DFTB on key systems and test systems.

simulation of RE systems and most of the commercial packages completely miss a set of parameter for the simulation of RE ions, due to the lack of known systems to use as fit system. This, again, is due to the nature of the ions we want to investigate. RE ions have atomic numbers between 57 and 70, hence relativistic effects begin to become important. Additionally, many properties of RE ions depend on the behavior of their $4f$ -electrons, which are strongly correlated. To study such cases requires a more sophisticated theory than simple LDA-like mean-field methods. To address this additional complexity in treating lanthanides, the DFTB method has been substantially extended. To treat strongly correlated systems, an LDA+ U like approach [28] and a SIC-like approach have been adopted. We would like to remark that (to our knowledge) DFTB contains the only TB implementation of an LDA+ U or SIC-like method. Combining DFTB methods and LDA+ U should allow handling highly correlated electrons for very large systems with a calculation quality close to the one of the *ab initio* methods. This is particularly interesting for the case of RE in GaN where dilute amount of RE are used. DFTB can easily handle the huge unit cell size that is necessary to represent the experimental system and properly reproduce the effect of the stress induced by RE doping in particular on the electronic structure. Finally, as we will show in the following chapter, the correct simulation of the band gap of the semiconductor host is a fundamental point in modeling RE defects. While *ab initio* simulations are affected from a known gap problem, DFTB is not² and is from this point of view well suited to simulate the behaviour of RE ions in GaN.

Outline

The first chapter is dedicated to the lanthanides, their emission spectra and the general problem related to the so called $4f$ -systems. We review the actual state of the research from a theoretical and from an experimental point of view, we show why rare earth systems are interesting from a scientific and from commercial point of view and why they are so difficult to simulate. Subject of the second chapter are the methods underlying our simulations. We show how we can extend the DFTB approach with orbital dependent potentials and tackle in this way the problem related to the $4f$ -systems. Some general aspects of point defects and their simulation are discussed there. In the third chapter we deal with the process of generation and test of the parameters needed by DFTB to model the host GaN and the RE ions. The generation process as well as various test calculations are reported. The fourth chapter deals with the host, GaN in its polytypes Zinc-blend and Wurtzite as well as with GaN intrinsic defects. It is in fact essential to know the behaviour of the intrinsic defects, if we want to investigate how do they couple with RE defects. The actual result of our simulations are then presented and discussed in chapter five to seven, while in the eighth and last chapter we summarise the main results of this work.

²This is due to the minimal basis set, which in many cases is a limitation to the accuracy of the methods but in this case reveals to be an advantage.

Contents

Abstract	iii
Kurzfassung	iv
Introduction	v
Contents	xiii
List of figures	xvi
List of tables	xvii
1 The Rare Earths	1
1.1 General properties of the RE	1
1.2 The f -electrons: screening from the outer shells	2
1.3 Conduction properties of RE-systems	3
1.4 Emission from Rare Earth ions	4
1.5 RE in GaN: Experiment	7
1.5.1 The samples	7
1.5.2 Electron emission channeling (EC)	8
1.5.3 X-ray absorption fine structure (XAFS)	9
1.5.4 Optical studies (PL, PLE, CL)	9
1.5.5 Other techniques	9
1.6 RE in GaN: Earlier theoretical works	10
1.7 Summary	10
2 Methods	11
2.1 The Density Functional Theory	11
2.1.1 The many body problem	11
2.1.2 Theoretical foundations of the DFT	12
2.1.3 The theorems of Hohenberg and Kohn	12
2.1.4 The Kohn-Sham equations	14
2.1.5 Spin Density Functional Theory	15
2.2 Calculation of the charge transition levels	16
2.2.1 Total energy differences	16
2.2.2 Janak's theory	17
2.3 Orbital dependent potentials	20
2.3.1 LDA+ U	21
2.4 <i>ab initio</i> methods	22
2.4.1 The pseudopotential approach	22
2.5 Density Functional based Tight Binding	23
2.5.1 The zeroth-order Hamiltonian	25
2.5.2 Fluctuation dependent contributions to the energy	27
2.5.3 The repulsive contribution	31
2.5.4 Total energy and potential	31
2.5.5 Determination of the constants τ_{Al} and W_{AlV}	32
2.5.6 Hamilton operator and self consistency	34

2.5.7	Calculation of the forces	35
2.5.8	An LDA+ U -like approach in DFTB	36
2.5.9	A pSIC-like approach in DFTB	36
2.5.10	Connection between LDA+ U and pSIC	37
2.6	Modeling defects	38
2.7	Summary and conclusions	39
3	Parameterization	41
3.1	Generation of the parameters	42
3.1.1	The electronic part	42
3.1.2	The atomic constants U_l and $W_{ll'}$	44
3.1.3	The repulsive part	48
3.2	Validation of the parameters	49
3.2.1	Ga-bulk	50
3.2.2	Diamond	52
3.2.3	Elemental RE	52
3.2.4	The O ₂ and N ₂ molecules	56
3.2.5	RE Nitrides	58
3.3	Summary and conclusions	65
4	The host: GaN	67
4.1	The group III-Nitrides	67
4.2	Brief history of GaN	68
4.3	Properties of GaN	69
4.3.1	Structural properties	69
4.3.2	Thermal and thermodynamic properties	71
4.3.3	Electrical properties	72
4.3.4	Optical properties	73
4.4	The simulation of GaN	75
4.5	Defects	76
4.5.1	Nitrogen vacancies	77
4.5.2	Gallium vacancies	80
4.5.3	Donors in GaN: the substitutional O _N	82
4.5.4	Acceptors in GaN: the substitutional C _N	84
4.6	GaN as host for the rare earths	85
4.7	Summary and discussion	86
5	Rare earth point defects in GaN	89
5.1	Substitutionals	90
5.1.1	The substitutional RE _{Ga}	90
5.1.2	Charge state and transition levels	95
5.1.3	Hybridisation of the f -orbitals	99
5.1.4	Error of the calculation	100
5.1.5	The substitutional RE _N	102
5.2	Interstitials	102
5.2.1	I _{RE} in hexagonal GaN	102
5.2.2	RE _{Ga} I _N in hexagonal GaN	104
5.3	Summary and conclusions	105
6	Rare earth defect complexes in GaN	107
6.1	Complexes with vacancies	108
6.1.1	RE _{Ga} V _N	108
6.1.2	RE _{Ga} +V _{Ga}	111
6.1.3	RE _N +vacancies	113
6.2	Antisites	114

6.2.1	$\text{RE}_{\text{Ga}}\text{Ga}_\text{N}$	114
6.3	Summary and conclusions	115
7	Co-doping with oxygen	117
7.0.1	Geometry	118
7.0.2	Energetics	120
7.0.3	Charge states	122
7.1	Summary and conclusions	124
8	Summary and discussion	127
A	Formation Energies	133
	Bibliography	135
	Publications	153
	Acknowledgements	155
	Colophon	157

List of Figures

1	CIE chromaticity x-y diagram	vi
2	Single colour red, green, and blue GaN:RE TDEL devices	viii
1.1	The $4f$ orbitals of the rare earths.	1
1.2	Screening of the $4f$ electrons by outer $5s$ and $5p$ shells.	2
1.3	Atomic chain: model system for LDA+ U	3
1.4	LDA and LDA+ U representation of an f -shell	4
1.5	Simplified energy diagram of the $4f$ levels of Pr, Eu, Er and Tm in GaN	6
1.6	Emission spectra of Eu, Er and Tm doped GaN films in GaN	7
1.7	Energy transfer mechanisms in RE doped GaN	8
2.1	Optical and charge transition levels	17
2.2	The exact total energy profile of a system of N electrons in the DFT	19
2.3	Pseudo atomic potentials and pseudo wave functions for Erbium	22
2.4	Cluster method for the simulation of point defects	38
2.5	Supercell method for the simulation of point defects	39
3.1	Band structure of elemental rare earths	45
3.2	Overlap integrals for the RE ions	47
3.3	The α -Ga structure	48
3.4	The electronic band structure of FCC-Ga	51
3.5	Rare earth lattices	54
3.6	Charge density difference between two N atoms and the N ₂ dimer	56
3.7	Energy levels of the atomic and molecular orbitals for O ₂ and N ₂	57
3.8	The molecular orbitals of N ₂	57
3.9	LDA band structure of the rare earth nitrides	60
3.10	Magnetization density in the (100) plane for FM ErN	63
3.11	Spin resolved band structure of rock-salt ErN	64
4.1	Room temperature bandgap energy vs lattice constants of common semiconductors	68
4.2	The α -GaN and the β -GaN phases	69
4.3	High symmetry sites in wurtzite GaN	72
4.4	Brillouin zone for cubic and hexagonal lattices	74
4.5	GaN band structure	76
4.6	Charge states for the isolated V _N in hexagonal GaN	78
4.7	Charge states for the isolated V _{Ga} in hexagonal GaN	80
4.8	The substitutional O _N in hexagonal GaN	82
4.9	Charge states for the substitutionals O _N and C _N	83
4.10	One particle levels for the substitutionals O _N and C _N	84
4.11	Formation energy of selected native point defects in GaN	85
5.1	RE _{Ga} substitutionals in hexagonal GaN	89
5.2	The band structure related to the Er _{Ga} substitutional in wurtzite GaN.	94

LIST OF FIGURES

5.3	Er _{Ga} : charge distribution	95
5.4	LDA band structure at the Γ point for RE _{Ga} substitutionals in wurtzite GaN	96
5.5	The DOS related to the Er _{Ga} substitutional in wurtzite GaN.	97
5.6	Location of the lowest $4f^n$ states of divalent and trivalent lanthanides in GaN.	98
5.7	Wave functions of localised and extended orbitals	99
5.8	Eu _{Ga} : determination of the $\epsilon(0/-)$ charge transition	100
5.9	Effect of the $+U$ potential on the induced gap levels at the Γ point.	101
5.10	RE _{Ga} interstitials in hexagonal GaN	103
5.11	Tm _{Ga} + I _N interstitials in hexagonal GaN	104
6.1	Complexes formed by RE _{Ga} substitutionals and V _N in hexagonal GaN	107
6.2	Formation energy of RE _{Ga} V _N pairs in hexagonal GaN for different values of the Fermi energy	109
6.3	Charge distribution around the Er _{Ga} V _N complex	110
6.4	Defect pairs formed by RE _{Ga} V _{Ga} in hexagonal GaN	111
6.5	Formation energy of RE _{Ga} +V _{Ga} pairs in hexagonal GaN for different values of the Fermi energy	113
6.6	Defect pairs formed by RE _{Ga} substitutionals and vacancies in hexagonal GaN	114
6.7	Complexes formed by RE _{Ga} substitutionals and the antisite Ga _N in hexagonal GaN	115
7.1	RE _{Ga} and O _N substitutionals in hexagonal GaN	117
7.2	The influence of the atomic rows and planes on the trajectories of energetic particles within the crystal	118
7.3	The three minima of the Er _{Ga} O _N axial pairs in hexagonal GaN	119
7.4	Binding energy of the Er-O pair as function of the Fermi energy	120
7.5	Fraction of bound oxygens in Er-O co-doped GaN	121
7.6	Cohesive energy per bond of the Er-O _x complexes	122
7.7	Charge density of Er _{Ga} O _N pairs in hexagonal GaN.	123
7.8	Charge density difference of Er _{Ga} O _N in hexagonal GaN.	124
7.9	Atomic levels of some used impurities in GaN	125
8.1	Possible excitation mechanism of the Er _{Ga} V _N pairs in GaN	131

List of Tables

1.1	Atomic properties of the selected lanthanides	2
1.2	Hubbard Us , experimental values	4
2.1	The atomic units used throughout this work	12
3.1	Orbital basis for the parameterised ions	42
3.2	Compression radii (in atomic units) used in this work	43
3.3	Hubbard Us	44
3.4	Spin coupling constants $W_{All'}$	46
3.5	Structural and electronic properties of α -Ga.	50
3.6	Structural and electronic properties of FCC-Ga.	52
3.7	Structural and electronic properties of diamond.	53
3.8	Structural and electronic properties of elemental RE	55
3.9	Structural and electronic properties of the N_2 and O_2 molecules.	58
3.10	Structural and electronic properties of RE nitrides	59
3.11	Lattice constants and elastic parameters of FM ErN	61
3.12	Heat of formation ΔH_f^0 for compounds of interest in this work.	62
4.1	Structural and electronic properties of zinc-blende GaN.	73
4.2	Structural and electronic properties of wurtzite GaN.	75
4.3	Charge transitions for some GaN intrinsic defect	79
4.4	Geometry of the Ga vacancies in GaN for different charge states.	81
5.1	Bond lengths around the RE_{Ga} substitutional	90
5.2	Calculated geometry of the RE_{Ga}^{3+} substitutionals.	91
5.3	Reference bond lengths of the RE_{Ga} substitutional in GaN.	92
5.4	f -shell occupation for the RE_{Ga}^{3+} substitutional in GaN.	93
6.1	Geometry and binding energy of the $RE_{Ga} V_N$ complex in hexagonal GaN.	108
6.2	Geometry of the $RE_{Ga}+V_{Ga}$ complex in hexagonal GaN.	112
7.1	Geometry of the complex Er-O in hexagonal GaN	119
7.2	Mulliken charges around the Er_{Ga} and $Er_{Ga} O_N$ complexes	123
8.1	Charge state transition of some rare earth defect in GaN	128
A.1	Chemical potential of the system of interest for this work.	134
A.2	md5sum of the parameter files	157

Chapter 1

The Rare Earths

In this chapter the general properties of the lanthanides and the problems related to the $4f$ -electrons are reviewed. In the second part of the chapter the actual knowledge about RE ions in GaN is reported, from the experimental as well as from the theoretical point of view.

1.1 General properties of the RE

The rare earth (RE) ions are the 14 lanthanide elements in group III-A of the periodic table, from cerium (Ce) to lutetium (Lu) and are characterised by the presence of the $4f$ -shell. The interesting and unusual physics of the lanthanides is due to their f -shell, pictured in Fig. 1.1. Despite their name, the RE elements are not especially rare. Each of them is more common than silver, gold or platinum. The name is rather due to difficult extraction of the elements and their late discovery. The elements were in fact discovered only in the 19th and 20th century and are available only recently in pure form. The properties of the lanthanides vary only slightly with the atomic number because the outer shells do not change within the group and this makes them difficult to distinguish from each other. RE metals have a high electrical conductivity, high melting and boiling points and share many common properties. With increasing atomic number the effective nuclear charge experienced by each $4f$ electron increases, causing a shrinking of the RE radii from Ce to Yb known as *lanthanide contraction*. Rare earths in general have the electronic configuration $[\text{Xe}]4f^n5d^06s^2$ with n varying from 1 (Ce) to 14 (Lu). In solids however they lose the three outer electrons (the two $6s$ electrons and one f or d electron) remaining with the configuration $(5s^25p^6)4f$. For this reason they are also named $4f$ -ions. All RE exist as trivalent cations (RE^{3+}). Cerium (Ce), praseodymium (Pr) and terbium (Tb) also exhibit +4, while samarium (Sm), europium (Eu), thulium (Tm) and ytterbium (Yb) can form compounds with a valence +2. Due to the weak coupling of the $4f^n$ electrons with the host lattice RE ions behave like free ions. Many lanthanides play an important role in various optoelectronic and photonic applications, ranging from emitting elements in solid-state lasers (using Nd) and phosphors for colour lamps and displays (for example Eu or Tb) to optical fiber telecommunications (using Er or Pr).

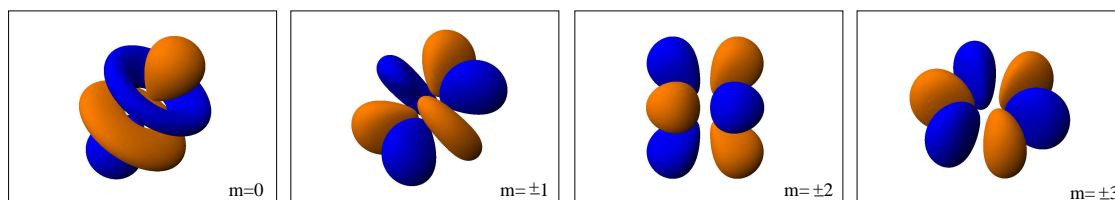


Figure 1.1: The $4f$ orbitals of the rare earths. The interesting and unusual physics of the lanthanides is due to the peculiar nature their f -shell.

Table 1.1: Fundamental atomic properties of the selected lanthanides. Rad. indicates the covalent radius and is expressed in Å, El. is the electronegativity after Pauling, 4f and 6s are the valence shell orbital radii and are expressed in Å. Data from www.webelements.com

RE	At. N.	Rad.	El. Conf.	At. Mass	El.	Str.	4f	6s
Pr	59	1.65	$4f^3 5d^0 6s^2 6p^0$	140.91	1.13	HCP	0.361	2.247
Eu	63	1.85	$4f^7 5d^0 6s^2 6p^0$	151.96	1.18	BCC	0.310	2.140
Gd	64	1.61	$4f^7 5d^1 6s^2 6p^0$	157.25	1.20	HCP	0.297	2.012
Er	68	1.58	$4f^{12} 5d^0 6s^2 6p^0$	167.26	1.24	HCP	0.268	2.031
Tm	69	1.56	$4f^{13} 5d^0 6s^2 6p^0$	168.93	1.25	HCP	0.261	2.011

On the other side the technological relevance of the RE is not limited to advanced photoelectronic devices. Just to cite some application, Pr can be found in the pyrophoric stones of cigarette lighters, La in camera lenses, Sm in ceramics and with Nd the strongest known magnets can be created. In this work we will consider only a selection of lanthanides, namely Pr, Eu, Gd, Er and Tm. The simulation of each rare earth would be not only extremely time consuming, but probably also not necessary. All lanthanides behave in fact similarly and a few ions are enough to individuate trends along the RE series. Some of the properties which we will use in the following are listed in Tab. 1.1.

1.2 The f -electrons: screening from the outer shells

Fig. 1.2 shows the partially filled 4f-orbitals of the RE, located relatively close to the nucleus and shielded very efficiently by the outer 5s, 5p and 6s electrons. The valence shell radii of the 4f and 6s-orbitals are reported in Tab. 1.1. This shielding has different effects: from one side it makes it impossible for the f -electrons to largely hybridise with other states and makes the shell nearly inert. Due to this shielding, the intra $4f^n$ shell transitions result in very sharp optical emissions at wavelengths from the ultraviolet (UV) to the infrared (IR). The wavelengths of these emissions are determined by the energy of the transition between the 4f states of the RE and are relatively independent of the host material. On the other side this screening is not complete and much of the interesting and unusual physics of rare earth systems, such as heavy-fermion behavior, mixed valency, and Kondo screening, is due to the f^n shell not being completely inert. For a completely inert f^n shell, the occupation number fluctuation on that particular site vanishes leading to a reduction of Coulomb energy. The contraction of the 4f-shell determines also the conduction properties of the RE systems, as explained in the following section.

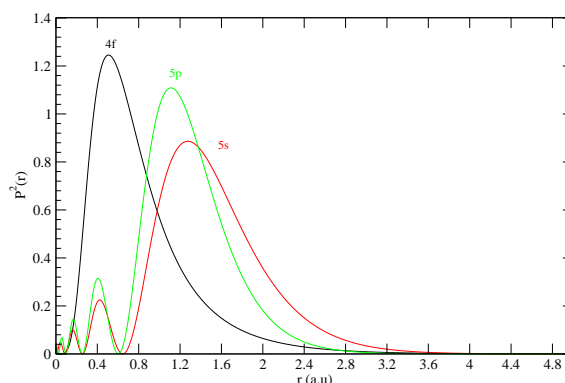


Figure 1.2: Screening of the 4f electrons by outer 5s and 5p shells for erbium ions. The 6s orbital, not reported here, is even more extended. Here the Er orbitals used in the DFTB calculations are plotted.

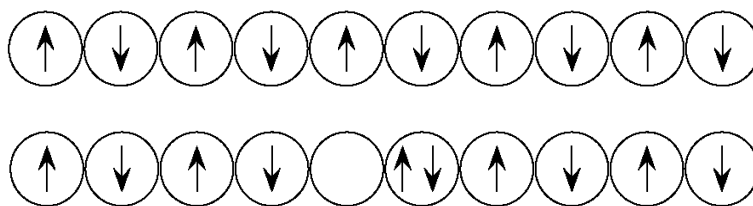


Figure 1.3: The one dimensional system we choose to illustrate the effect of the strong correlated electrons on the conduction properties of the solids

1.3 Conduction properties of RE-systems

Many lanthanide compounds might be expected to be metallic, as they have partially filled d or f -bands. Experimentally they are instead known to be insulators or semiconductors. This apparently strange behaviour is due to the electron-electron repulsion, which localises electrons that should be available for the conduction on single atoms, strongly reducing or compromising the electrical conductivity of the material. This happens when the overlap between atomic orbitals is small and consequently the width of the resulting energy band is small. We can understand it with a simple model. A full treatment of the electron-electron repulsion in solids is extremely complicated, for this reason we use the approximation done in the Hubbard theory, that is, the only important electron-electron repulsion happens between electrons on the same atom. We consider a one dimensional line of atoms, which, for simplicity is assumed to have only a s -orbital and one electron per orbital. In this model, the s -band will be half full and the material a metal. If the orbital overlap between neighbouring atoms is very small however, it will be energetically favourable to localise the electrons in their valence shell (as in Fig. 1.3) in order to reduce the Coulomb repulsion which arises when two electrons are forced to pair on the same atom, as happens when an electron moves through the solid via the s -band. In this case the solid, which we thought to be metallic, will instead be insulating. The half-filled band ends up being divided into two sub-bands (empty upper Hubbard band and occupied lower Hubbard band) separated by an energetic gap, as shown in Fig. 1.4. With this simple model, we can also predict if a solid will be insulating or a metal. The energy needed to subtract an electron from an atom is the ionisation energy I . The energy win we have when we put an isolated electron in an atom with an half filled orbital is the electron affinity (A_e) of this atom. So the energy needed to move the electron from an atom to another one (called *Mott-Hubbard splitting* or *Hubbard U*) is:

$$U = I - A_e$$

and can be interpreted as the repulsion energy between two electrons in the same atom. As discussed above, metallic conductivity only occurs, when the atomic overlap is big enough, so that the width W of the resulting energy band is bigger then the value of U . If instead $U > W$ the electronic repulsion prevails and the solid is insulating. The $4f$ -orbitals of the lanthanides are extremely contracted and interact to a very small extent with the surrounding ligands in lanthanide compounds. A further consequence of this contraction is that the overlap of the $4f$ orbitals in lanthanides compounds (for example RE-nitrides or elemental RE solids) is very small and the $4f$ band widths are very small (typically about 0.1 eV). In the solid state elemental rare earths are nonetheless metals, but only because of the $5d$ and $6s$ orbitals, which overlap to a greater extent. Tab. 1.2 shows that the conductivity of the elemental RE solids cannot be due to the $4f$ -electrons.

The extreme high values for Eu and Gd are easily explained. Let us remain in the case of the elemental RE solids: each ion contributes with three electrons to the band structure and this leads Gd to have the configuration $[\text{Xe}]f^7$ which is particularly stable because of the half filled f -shell (which means filled f sub-shell). This stability is lost when an electron is added to make the $[\text{Xe}]f^8$ configuration, hence U is very high. The $[\text{Xe}]f^7$ configuration is so favourable that is adopted also from Eu, which then contributes to the metallic bonding and band structure with only two electrons. This fact is reflected in the bigger atomic volume for Eu than for the other RE (except Yb, which is similar to Eu)

Table 1.2: Data experimentally determined [29] using solid state X-ray photoelectron spectroscopy (XPS) and bremsstrahlung isochromat spectroscopy (BIS). For each rare earth ion the value of U is much greater than 0.1 eV. All the values are expressed in eV, the error is ± 0.3 eV

RE	Ce	Pr	Nd	Pm	Sm	Eu	Gd	Tb	Dy	Ho	Er	Tm
U	5.39	5.47	6.37		5.53	10.14	11.48	4.99	5.68	6.82	6.86	5.67

1.4 Emission from Rare Earth ions

The Russell Saunders coupling scheme

The atomic states of the lanthanides are generally labeled with symbols following the Russell-Saunders (RS) coupling scheme. Each electron in an orbital is, as generally known, characterised by four quantum numbers: the principal quantum number n , the orbital quantum number l , the magnetic quantum number m_l and the spin quantum number m_s . There are many different ways in which the angular momenta associated with the orbital and spin motions in many-electron-atoms can be combined together. The RS scheme is only one possible coupling scheme, based on the concepts of atomic spin S , atomic angular momentum L , atomic total angular momentum J .

- S is the resultant spin quantum number for a system of electrons. The overall spin S arises from adding the individual m_s together.
- L , the total orbital angular momentum quantum number defines the energy state for a system of electrons. These states or term letters are represented as follows: S=0, P=1, D=2, F=3, H=4, I=5 and so on.
- Coupling occurs between the resultant spin and orbital momenta of an electron which gives rise to J , the total angular momentum quantum number. J is the sum of L and S and permissible values of J fall between $|L + S|$ and $|L - S|$.

The Russell Saunders term symbol that results from these considerations is

$$^{2S+1}L_J$$

with term multiplicity $2S+1$ and total angular momentum J . For example a f^2 state $S=(1/2+1/2)=1$ and $2s+1=5$, $L=5=H$ and the Russell-Saunders term symbol is 5H . Each term symbol labels a degenerate group (multiplet) of $2J + 1$ states, which may be split by an external field (e.g. crystal field splitting of the Russell-Saunders terms).

The correct ordering of the energy levels is provided (in most cases) by the Hund's rules:

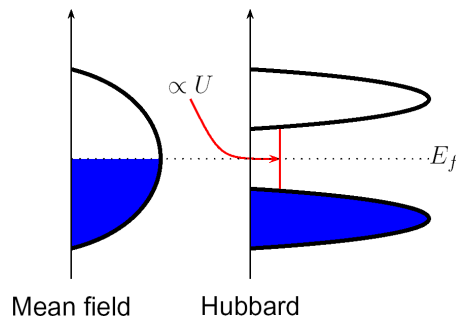


Figure 1.4: One half filled shell appears in a mean field theory as DFT-LDA like an half-filled band, which could take part to the conduction process. Because of the localised nature of the shell it is however better represented by two sub-bands (an empty one and an occupied one) separated by an energetic gap.

- The ground term will have the maximum multiplicity
- If there is more than one term with maximum multiplicity, then the ground term will have the largest value of L .

Since the $4f$ shell is strongly localised and distinct from the states of the surrounding crystal it is customary to label the states considering only multiplets of the $4f$ manifold.

Selection Rules

A selection rule is a condition constraining the physical properties of the initial system and the final system that is necessary for a process, in our case the photon emission, to occur with a nonzero probability. In the process of emission the emitted particle (photon) carries away an angular momentum from the system. Considering that the total angular momentum and the parity have to be conserved during the transition leads to two rules for allowed transitions:

- $S = 0$ (Spin rule)
This rule says that allowed transitions involve the promotion of electrons without a change in their spin.
- $l = \pm 1$ (Orbital or Laporte rule)
This rule says that transitions within a given set of orbitals (i.e. those which only involve a redistribution of electrons within a given sub-shell) are forbidden if the molecule has a centre of symmetry.

The expression forbidden transitions is often used even if this does not mean that these transitions cannot occur but rather that they are electric-dipole forbidden. These transitions are perfectly possible, but occur at a lower rate. For example an allowed transition will have as rule of thumb an intensity 10^4 greater than a transition spin and Laporte forbidden. J. H. van Vleck pointed out as first that in the free ions the $4f \rightarrow 4f$ transitions are forbidden, as the RE luminescence comes from dipole transitions and the operator for these is of odd parity, i. e. they violate the Laporte selection rule [30]. Relaxation of the selection rules can anyway occur because of different factors like vibronic coupling, symmetry breaking and orbital mixing in molecules and solids (so transitions are no longer purely $4f \rightarrow 4f$). Ofelt [31] proposed that for RE in a host the crystal field could produce mixed states containing contributions from more configurations of electrons (generally $4f^n$ mixing with $4f^{n-1}5d$), if the ion's environment lacks inversion symmetry. The RE_{Ga} substitutional site in GaN has C_{3v} symmetry, which is not centrosymmetric and the Laporte rule is so relaxed that a photon emission can happen with a finite probability. This consideration also invalidates the practice of labeling the $4f$ -states of the lanthanide in a host like GaN with the free atom term symbols. Different symbolisms exists, which also keep in account the crystal- and ligand-field interactions (Stark splitting, which depend on the local symmetry of the RE surroundings) to label the resulting states. Many of these notations are quite usual (Racah irreducible representation and Mulliken point group symbols), other are, though precise, arcane and complicated. In any case, lacking informations about the RE site-symmetry or being the main goal the comparison of different sites, the inaccurate but familiar term symbols give labels that are at least a first approximation of the states involved. The RE $4f$ states and their transitions in different hosts have been investigated theoretically and experimentally in the 1950s and 60s, culminating with the work of Dieke [32], who gave a consistent picture of energy levels for trivalent lanthanides. The resulting set of levels (known as Dieke's diagram) is till today useful, as the energies of RE multiplets vary only fractionally between different hosts. The electronic transitions of interest for this work are schematically reported in Fig. 1.5.

Light emission mechanisms

The light emission from RE doped GaN samples has been observed by photoluminescence (PL), cathodoluminescence (CL) and electroluminescence (EL). The main mechanisms underlying the emission are reported in Fig. 1.7. In PL the electron-hole pairs are generated by above band-gap

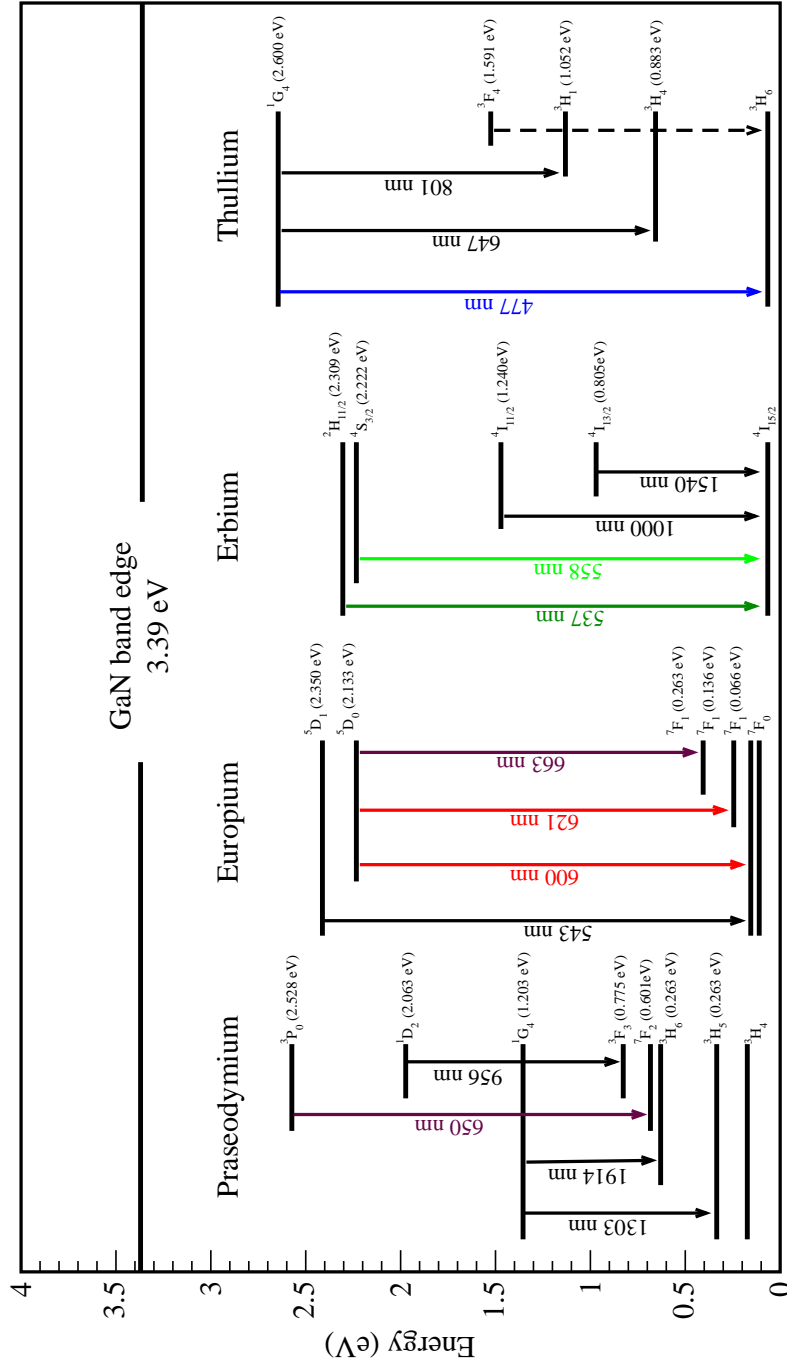


Figure 1.5: Simplified energy diagram of the 4f levels of Pr, Eu, Er and Tm in GaN as reported in [3]. Only transitions which have been exploited for the creation of displays are coloured. For further details and a discussion of the single transitions see the reference.

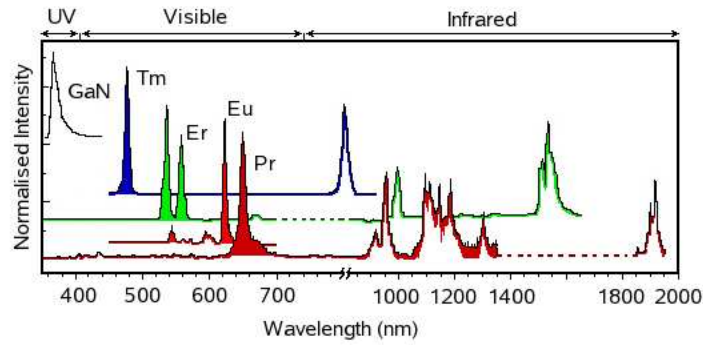


Figure 1.6: Emission spectra of Pr (dark red), Eu (red), Er (green) and Tm (blue) doped GaN films from UV to IR [4]. Spectra are normalised to their highest value and therefore not directly comparable.

photon absorption, in CL the charge carrier generation is provided by high energy electron beams and finally in EL the carrier injection occurs by applying a bias to the electrical contacts on the GaN layer. In any case the charge carrier is transferred to the RE ion by impact excitation of hot carriers or as consequence of a nearby hole-electron recombination. The RE may then relax with a non-radiative process (multi-phonon emission or Auger electron excitation) or with a radiative process, which is the desired one, as it results in the photoemission exploited in electroluminescent displays. The relative strength of the radiative relaxation (i.e. the emission intensity) is a complex function of the host crystalline quality and RE concentration. A crystal of good quality reduces the probability of a non-radiative process, but at the same time a good crystallinity is achieved under conditions which are not compatible with the optimum incorporation of RE. For a review of the parameters used to maximise the emission see [4].

1.5 RE in GaN: Experiment

We review here briefly the experimental knowledge of RE doped GaN, especially the results of recent experiments. The experimental techniques used to investigate rare earth doped GaN samples are not described in detail. For such a description we remand the reader to the references.

1.5.1 The samples

There are principally two ways of doping GaN with RE, *in situ* i.e. by doping during MBE growth or *ex situ*, by ion implantation into previously grown materials. The advantages of the first method is the possibility to obtain thicker and more heavily doped samples, while the second method is useful for certain purposes. Implanted samples are doped only on a thin layer (typically about 100 nm) where the crystal lattice is in part disrupted and annealing is required after the implantation to repair lattice damage. In RE implanted GaN samples luminescence is activated only after annealing. This has two kinds of consequences. The first is that only these defect complexes which are stable enough to endure the annealing process¹ can be addressed as possible candidate for the luminescence. The second is that something during the annealing leads to the luminescence. Two processes which may enhance the RE emission are the removal of non-radiative recombination centers and the formation of specifically efficient RE-containing lumophores. Additionally, if a specific lattice location for the RE ions is required to produce efficient luminescence, annealing may allow diffusion of the ions to occur. Doping GaN during the growth is possible to avoid the lattice damage induced by ion implantation and most of all it is possible to carefully control the concentration of dopants. Surprisingly it has be found that structurally good samples show rather

¹Using AlN caps GaN samples can be annealed after implantation at temperatures which exceed the template growth temperature, as reported in [36–38].

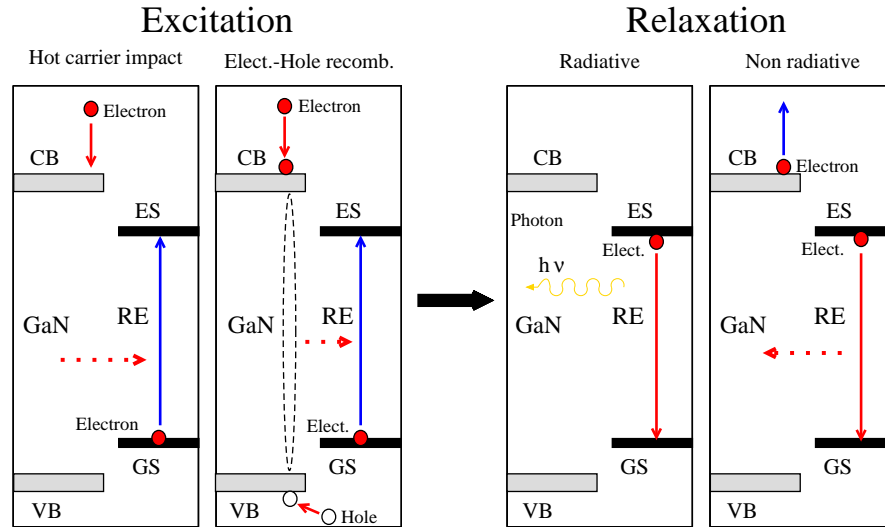


Figure 1.7: Energy transfer mechanisms in RE doped GaN: the RE dopant excitation and consequent relaxation in the GaN host. In the diagram red circles are electrons and white circles holes. Conduction and valence band edges are called CB and VB, while excited and ground states for RE transitions are called ES and GS respectively. The box on the right (relaxation) represent the radiative emission (photon in yellow) and the non-radiative Auger de-excitation. The non-radiative phonon emission is not represented here.

poor luminescence [33, 34]. It was demonstrated that best luminescence results are not correlated with the crystalline quality of the sample: this has lead to the conclusion that some unidentified effects are involved in the energy transfer from the host matrix (GaN) to the RE-ions [35]. Details about the preparation of lanthanide doped crystals can be found in the references [39–41].

1.5.2 Electron emission channeling (EC)

While conventional channeling techniques based on the use of probe ion beams like the Rutherford Backscattering Spectroscopy/Channeling (RBS/C) or the Particle-Induced X-ray Emission (PIXE) require the presence of a large amount of impurities in the material, the Electron-emission Channeling (EC) can be used to investigate low concentrations of isolated impurities. As a large impurity concentration normally also introduces unwanted effects like impurity clustering or crystal damage (if implantation is used to introduce foreign elements), good samples are normally those with low impurity concentration. The goal of EC investigations is to determine the sites occupied by implanted radioactive ions measuring the angular distribution (with respect to major crystal axes) of β - or conversion-electrons that are emitted by the implanted nuclei during their radioactive decay. The majority (50-95%) of Pr, Nd, Eu, Gd and Er ions implanted in GaN occupies lattice sites that appear to be slightly displaced from the ideal substitutional RE_{Ga} , with a nearly isotropic root mean square (rms) displacement of the order of 0.10-0.25 Å. The displacement is however too large to be explained in terms of lattice vibrations. The rest of the implanted ions reside in on low-symmetry sites or lattice sites with more disordered surroundings [42, 43]. After high-temperature annealing the substitutional fraction stays nearly constant while the rms displacement decreases, indicating that the displacement are mostly likely related to the presence of randomly distributed defect complexes introduced during the implantation. The fact that the displacements are observed for all investigated RE, and that none of them shows perfect incorporation in the host until annealing at 1200 °C indicates that the formation of lanthanide defect complexes is an universal process in GaN and the corresponding binding energies must be fairly large. This explains two issues, the lattice site multiplicity observed in luminescence experiments (see following) and the high annealing temperature needed to activate implanted dopants, even if the majority of them are already on-site

in the as implanted samples. The natural candidates for the enhancing defects are the N vacancies in the nearest neighbour shell of the substitutional RE, Ga vacancies in the second neighbour shell or Ga interstitial between first and third neighbour shells.

1.5.3 X-ray absorption fine structure (XAFS)

XAFS spectroscopy is used to determine the lattice sites occupied by dopants or native defects in crystalline solids [44]. A Fourier Transform of the so called XAFS yields the radial distribution function (RDF) of the ions neighbouring a particular target atom. XAFS studies clearly reveal impurity aggregation effects as one would expect in heavily doped samples [45] as well as for rather low levels of doping. Let us keep Tm here as example: Tm atoms are found only in substitutional Ga sites for very low concentration samples (≤ 0.5 at %). Increasing the Tm concentration to 1-2 at % Tm is found again at the Ga place surrounded by four nitrogen atoms, but the presence of a substantial number of Tm ions in the second coordination sphere indicates the beginning of dopant clustering. In more heavily doped samples a phase decomposition can be observed: a sizeable portion of the Tm ions find themselves in a TmN environment. The formation of pure TmN clusters was found in an *in situ* doped sample with a dopant concentration as low as 3.4%. In contrast to EC, XAFS is not sensitive to a random displacement of a target atom from its ideal lattice position, so that it cannot be easily determined if RE ions remain on-site or not. A good review of XAFS results obtained to date can be found in [46, 47] and can be summarised as follows: all RE atoms have been found to reside on Ga substitutional sites, independently of the doping method. RE in GaN have (in contrast to In) a strong tendency to agglomerate. When the RE concentration increases over a certain threshold clusters with high RE content are observed. The lowest concentration at which RE clustering was observed is 0.17% and 1.2% for Er and Tm respectively, at higher concentration pure REN phases are observed.

1.5.4 Optical studies (PL, PLE, CL)

The most common techniques used to obtain spectroscopic signatures of particular RE ions are photoluminescence (PL) and cathodoluminescence (CL). While the former is spectrally selective, depending on the photon energy of excitation, the latter tends to "excite everything" that the high-energy electron beam encounters, even if the penetration of the electron beam can be restricted by limiting its energy. Photoluminescence excitation (PLE) spectroscopy monitors a single PL emission feature, as the exciting light is swept through a range of higher photon energy. Both PL and CL can be performed in time-resolved (TR) mode: when the sample excitation is removed, the luminescence signal decreases towards zero as the excited state population return to its equilibrium value. Luminescence spectroscopy of RE-doped group III-N samples offers clear evidence for the coexistence of different sites with distinctive excitation and emission signature. In a recent work [48] combined excitation emission spectra (CEES) spectroscopy was used to study Er MBE-doped samples: two "majority" and up to four different signatures were found, in agreement with previous works [49, 50]. These observations concern internal RE transitions below the host band-gap in terms of photon energy, even if at the same time the sites are observed to interact differently with the host. Similarly Eu implanted GaN samples [7] were recently investigated by PL and PLE spectroscopy, revealing the existence of at least four luminescent sites [12, 51–53]. Finally there is experimental (PL and PLE studies) evidence that in Er doped samples different types of defects can be excited [54]. Some sites can be excited selectively by carefully choosing the excitation wavelength below band-gap.

1.5.5 Other techniques

A number of other investigation techniques has been used for the characterisation of RE doped samples and from each of them a lot of information can be gained. The surface morphology of the samples is investigated using scanning electron microscopy (SEM) or by high resolution transmission electron microscopy (HRTEM) [55]. The implantation damage and its recovery is monitored by Raman spectroscopy, while the doping concentrations are accurately measured using

Wavelength Dispersive X-Ray (WDX) and Rutherford back-scattering (RBS) spectroscopy. Deep level transient spectroscopy (DLTS) of implanted and annealed GaN samples shows a level at $E_C - 0.2$ eV, independent from the implanted impurity. Other levels were observed in the band gap at 0.19, 0.22, 0.26 and 0.65 eV below the conduction band. The last two levels are found essentially in all of the investigated samples, suggesting that they are host-related, while the first two appear exclusively in the random implanted and channeled implanted samples respectively, suggesting a relation with the implantation geometry [56].

1.6 RE in GaN: Earlier theoretical works

Because of the difficulties represented by the simulation of systems containing rare earths (which we will explain in some detail in the next chapter), our theoretical knowledge of the behaviour of RE ions in GaN is behind the experimental one. The first attempt to study RE ions in GaN from the theoretical point of view is due to the Jones' group in Exeter [17, 57]. They used the density functional theory to investigate the stable Er, Eu and Tm defects and their electronic properties in hexagonal GaN. In their approach the f -electrons have been treated like core states, assuming the trivalent configuration. RE_{Ga} substitutionals were found to be electrically and optically inert, while substitutional-vacancy defects are found to have a bound energy of 1.0, 0.8 and 0.7 eV for Eu, Er and Tm respectively and to introduce localised levels in the GaN band gap. Interstitials-complexes and RE-O complexes were also investigated, with the conclusion that they probably do not play any role in high energy fluorescent transitions. Successively the Svane's and Temmerman's groups in Aahraus and Daresbury investigated the electronic structure of substitutional RE impurities in cubic GaN by means of the self interaction corrected local spin density approximation (SIC-LSDA) [18]. For an analytical description of the SIC method see the following chapter. They investigated different configurations of the $4f$ -shells for the substitutionals of the whole RE series to reveal trends in the magnetic and electronic properties. An acceptor level $\epsilon(0/-)$ was found within the GaN band gap for different RE including the Eu_{Ga} substitutional. Finally we mention a work of Dorembo and van der Kolk [58], who used the knowledge from lanthanide spectroscopy to understand and predict optical and electronic properties of the lanthanides in GaN. They proposed a scheme for the localisation of the $4f$ -states with respect to the conduction and valence bands of GaN and demonstrate that the luminescence efficiency of Pr^{3+} , Eu^{3+} , Tb^{3+} and Yb^{3+} depends on the location on the lanthanide levels.

1.7 Summary

In this chapter we introduced the rare earth ions, reviewing their peculiar behaviour, which can be attributed to the particular nature of the f -orbitals. The unique conduction and emission properties of RE ions, could also be related and interpreted in term of non-classical behaviour of the localised f -electrons. At the end of the chapter the experimental and theoretical work done up to date to investigate RE ions in GaN was briefly summarised. From experimental studies we know that Er ions in GaN prefer the Ga position [42], occur in 3+ valence state [13] and posses C_{3v} symmetry [59] with relatively short distances to the surrounding N-ligands [46]. Clustering of RE is observed and REN phase segregation is observed when the RE concentration increases over a certain threshold, estimated in 0.17% and 1.2% for Er and Tm respectively [47]. The question of co-doping of RE in order to improve and enhance the luminescence seems not to be settled, as different opinions (see for example [13] and [14] in the case of Er) can be found in the literature. Concerning the association of the luminescence with a particular defect or complex it is know that (at least in the case of Eu and Er) a multiplicity of sites can be excited [12], but the luminescence could not be definitively assigned to a particular lattice site. Theoretical investigations seems to agree that RE_{Ga} substitutionals are favoured with respect to RE_{N} substitutionals, happen in the 3+ charge state and do not cause an important lattice distortion [18, 57]. No agreement could be found instead about the optical and electrical activity of the RE_{Ga} substitutionals.

Chapter 2

Methods

This chapter is divided in two parts, the first dealing with the Density Functional Theory (DFT) and its extensions concerning the Janak formalism and the orbital dependent potentials, and the second with its approximation used throughout this work, the Density Functional based Tight Binding (DFTB). While in the first part the DFT is only briefly reviewed (to the extent needed to understand and derive the DFTB formalism), in the second part the theory underlying the DFTB formalism is discussed in some detail and a rigorous mathematical formulation is given. This chapter is structured in order to highlight the aspects which are peculiar to this work, which are the LDA+ U approach and its connections with the Janak formalism, while the DFTB method, which has been discussed and in other works, is presented at the end of the chapter.

2.1 The Density Functional Theory

2.1.1 The many body problem

The Schrödinger equation describing the stationary state of a system of M ions in the coordinate space has the form:

$$\hat{H}_{\text{tot}}(\{\mathbf{R}_I\}, \{\mathbf{r}_i\}) \Psi_{\text{tot}}(\{\mathbf{R}_I\}, \{\mathbf{r}_i\}) = E' \Psi_{\text{tot}}(\{\mathbf{R}_I\}, \{\mathbf{r}_i\}) \quad (2.1)$$

where \hat{H}_{tot} is the Hamilton operator of the whole system (electrons + nuclei), Ψ_{tot} is the wave function and E_0 the energy eigenvalue. The position of the nuclei and of the electrons are given through the position vectors $\{\mathbf{R}_I\}$ and $\{\mathbf{r}_i\}$ respectively.

In the Born-Oppenheimer approximation [60] the fast motion of the electrons is separated from the relatively "slow" motion of the nuclei, allowing the separate solution of one Schrödinger equation for the electrons and one for the nuclei. The wave function $\Psi_{\text{tot}}(\{\mathbf{R}_I\}, \{\mathbf{r}_i\})$ of the system is then represented by the product of two terms, the first being related to the electrons and the second to the nuclei (Product-Ansatz). The nuclear coordinates appear as parameter in the electron wave functions. This parametric dependence will not be explicitly indicated in the following, i.e.

$$\Psi(\{r_i\}) = \Psi_{\text{el.}}(\{r_i\}, \{R_I\})$$

The Hamilton operator of the whole system can be separated into an electronic and one nuclear part, just like the wave function:

$$\hat{H}_{\text{tot}}(\{\mathbf{R}_I\}, \{\mathbf{r}_i\}) = \underbrace{\hat{T}_{\text{nucl.}} + \hat{v}_{\text{nucl.}}}_{\hat{H}_{\text{nucl.}}(\{\mathbf{R}_I\})} + \underbrace{\hat{T}_{\text{el.}} + \hat{v}_{\text{el.}} + \hat{v}_{\text{el.-nucl.}}}_{\hat{H}_{\text{el.}}(\{\mathbf{r}_i\})} \quad (2.2)$$

where \hat{T} and \hat{v} are the operators for the kinetic and potential energy. The coupling between electrons and nuclei is included in $\hat{v}_{\text{el.-nucl.}}$. The electronic Hamilton operator $\hat{H}_{\text{el.}}(\{\mathbf{r}_i\})$ contains again implicitly the nuclear coordinates as parameter: these will appear again in the coupling potential

Table 2.1: *The atomic units used throughout this work*

Length	Bohr	\hbar^2/m_e^2	$0.529177 \cdot 10^{-10}$ m
Energy	Hartree	m_e^4/\hbar	27.2114 eV
Mass	El. rest mass	m_e	$9.10 \cdot 10^{-31}$ Kg
Charge	El. charge	e	$1.6022 \cdot 10^{-19}$ coul.

$\hat{v}_{\text{el.,-nucl.}}$. Applying the Product-Ansatz for the wave functions and separating the operator as in Eq. 2.2 one gets from the Eq. 2.1 two separate Schrödinger equations for the electrons

$$\hat{H}_{\text{el.}} \Psi(\{\mathbf{r}_i\}) = E_{\text{el.}} \Psi(\{\mathbf{r}_i\}) \quad (2.3)$$

and for the nuclei:

$$\hat{H}_{\text{nucl.}} \Psi_{\text{nucl.}} = \left(\hat{T}_{\text{nucl.}} + \hat{V}_{\text{nucl.}} + E_{\text{el.}} \right) \Psi_{\text{nucl.}} = E' \Psi_{\text{nucl.}} \quad (2.4)$$

In this work we will consider the nuclei as classical particles, coupled with the electrons only by Coulomb interactions. The electrons will then move in the potential generated by the nuclei. In this way the original quantum mechanical problem is reduced to the solution of the electronic Schrödinger equation.

$$\hat{H} \Psi(\{\mathbf{r}_i\}) = E \Psi(\{\mathbf{r}_i\}) \quad (2.5)$$

Here we drop all the labels referring to the electrons as no more confusion is possible. The wave function Ψ , which is the eigenfunction of the Hamilton operator \hat{H} to the eigenvalue E , has to be normalised to the unity. The Hamilton operator in the equation above is still the one of the many body problem. All electrons are coupled through the Coulomb interaction and an exact, analytic solution is no more possible. Many different approximated methods have been developed to solve this problem, the most famous being the Hartree-Fock method [61] and a lot of its derivations, called post Hartree-Fock [61] methods. Among them the by far most successful and widespread is the Density Functional Theory or DFT, which is the starting point of the methods used throughout this work.

2.1.2 Theoretical foundations of the DFT

Most scientists see the principle of the DFT already in the Thomas-Fermi theory [62, 63], which is an attempt to describe atoms in a statistic way. In its today's form the DFT is however quite different: fundamental deficits of the Thomas-Fermi theory were removed and the theory itself was further improved. The common point of the two theories is, that the role of the fundamental quantity is not played by the many body wave functions like in HF and its derivations but by the electronic density. In the following the basics of the DFT are reviewed. Throughout this chapter we will use atomic units, which are listed in Tab. 2.1.

2.1.3 The theorems of Hohenberg and Kohn

We consider a Hamilton operator of the form:

$$\hat{H} = \hat{T} + \hat{v} + \hat{v}_{\text{ext.}} \quad (2.6)$$

where

$$\hat{v} = \frac{1}{|r - r'|}$$

is the operator for the Coulomb interaction between electrons in atomic units (see Tab. 2.1), \hat{T} is the operator for the kinetic energy and $\hat{v}_{\text{ext.}}$ an external potential like for example the electron-nuclei

interaction. This operator will be the basis for the derivation of the following theory. The external potential and the total number N of electrons in the system univocally determine the Hamilton operator and, with it, the wave functions Ψ solution of the Schrödinger Equation. The electronic density $n(\mathbf{r})$ is given from the diagonal elements

$$n(\mathbf{r}) = \gamma(\mathbf{r}, \mathbf{r})$$

of the one-particle density matrix:

$$\gamma(\mathbf{r}, \mathbf{r}') = N \int \dots \int \Psi(\mathbf{r}, \mathbf{r}_2, \dots, \mathbf{r}_N) \Psi^*(\mathbf{r}', \mathbf{r}_2, \dots, \mathbf{r}_N) d\mathbf{r}_2 \dots d\mathbf{r}_N \quad (2.7)$$

and as the wave functions Ψ are normalised, from the electronic density one can derive back the total number of electrons:

$$N = \int n(\mathbf{r}) d\mathbf{r}$$

The DFT is based on the theorems of Hohenberg and Kohn [64], which we cite here without demonstration. The first theorem legitimates the choice of the charge density as central quantity of the theory:

Theorem 1

The external potential v_{ext} is a definite functional of the ground state charge density n_0

In this way the charge density, together with the number of electrons N , suffices to determine the wave functions Ψ univocally. For the total energy expressed as functional of the charge density we have:

$$\begin{aligned} E[n(\mathbf{r})] &= T[n(\mathbf{r})] + V[n(\mathbf{r})] + V_{\text{ext.}}[n(\mathbf{r})] \\ &= T[n(\mathbf{r})] + \int v_{\text{ext.}} n(\mathbf{r}) d\mathbf{r} \end{aligned}$$

where $T[n]$ is the functional of the kinetic energy, $V[n]$ is the electronic potential energy and $V_{\text{ext.}}[n(\mathbf{r})]$ is the potential energy part due to the external potential. The Hohenberg-Kohn density functional is defined [62] as:

$$F_{HK}[n] = E[n] - \int v_{\text{ext.}} n(\mathbf{r}) d\mathbf{r}. \quad (2.8)$$

The second theorem of Hohenberg Kohn assures the following variational principle

Theorem 2

The density functional

$$E[n] = F_{HK}[n] + \int v_{\text{ext}} n(\mathbf{r}) d\mathbf{r}$$

has a minimum for the ground state charge density n_0 .

Changing from the wave functions $\Psi(\mathbf{r}_i)$ (which depend from $3N$ electronic coordinates) to the electronic density $n(\mathbf{r})$ (which depends on only three coordinates) the complexity of the equations to solve is strongly reduced. This is one central point of the DFT: the reduction of the degrees of freedom makes the treatment of big systems possible. Both theorems can be demonstrated for non degenerate as well as for degenerate ground states [62]. An extension to the excited states is also possible, if one considers only one possible electronic geometry [65]. If the theorems are extended to the excited states the electronic density has to satisfy more requests which can be derived from the definition of the density functional itself. A thorough discussion about this theme can be found for example in [62, 63].

2.1.4 The Kohn-Sham equations

The functional of the electronic density $F_{\text{HK}}[n]$ we introduced in the previous section is unfortunately unknown. Specifically, the functional $T[n]$ of the kinetic energy is a complex term which cannot be easily approximated or handled with classical physics. We have therefore to introduce some sophisticated approximations: this was firstly done in a work of Kohn and Sham [66], which was the key to the analytic formulation of the density functional theory and led to the Kohn-Sham equations. At first we consider a system of N non interacting electrons. The wave function $\Psi(\mathbf{r}_i)$ of such a system is as usual represented by a determinant of one-particle orbitals $\psi_i(\mathbf{r})$ with occupations n_i . The electronic density is then given through:

$$n(r) = \sum_i^N n_i |\psi_i(r)|^2 \quad (2.9)$$

In the case of non interacting particles the expression for the kinetic energy as function of the orbitals $\psi_i(\mathbf{r})$ is known:

$$t = \sum_i^N n_i \langle \psi_i | \hat{t} | \psi_i \rangle = \sum_i^N n_i \langle \psi_i | -\frac{1}{2} \Delta | \psi_i \rangle \quad (2.10)$$

and, following the definition, the functional $F_{\text{HK}}[n]$ takes the form (see Eq. 2.8):

$$F_{\text{HK}} = t = \sum_i^N n_i \langle \psi_i | -\frac{1}{2} \Delta | \psi_i \rangle \quad (2.11)$$

For an interacting electron system this situation is not true any more, in particular the representation of the total wave function Ψ through a determinant is in general no more possible. Kohn and Sham suggested to consider a reference system of not interacting electrons, with exactly the same charge density of the system of interacting electrons. Using the variational principle one can then get a one-particle Schrödinger equation for the one-particle orbitals ψ_i :

$$\hat{h}\psi_i = (\hat{t} + V_{\text{eff}}) \psi_i = \varepsilon_i \psi_i \quad (2.12)$$

The wave function of the ground state of the non interacting electrons reference system is given as the determinant of the energy lowest lying orbitals ψ_i . They are eigenfunctions of the Hamilton operator to the eigenvalues ε_i . The eigenvalues are used as Lagrange multipliers: in their physical interpretation they do not correspond to the one-particle energies. The effective potential $v_{ee}(\mathbf{r})$ contains the classic electron-electron Coulomb interaction:

$$v_{ee}(\mathbf{r}) = \int \frac{n(\mathbf{r}')}{|\mathbf{r} - \mathbf{r}'|} d\mathbf{r}'$$

as well as the external potential v_{ext} and a new potential, called *exchange-correlation potential* v_{xc} .

$$v_{\text{eff}} = v_{ee} + v_{\text{ext}} + v_{xc} \quad (2.13)$$

which is connected with the so called *exchange-correlation energy functional* $E_{xc}[n]$ through:

$$v_{xc}(\mathbf{r}) = \frac{\delta E_{xc}[n(\mathbf{r})]}{\delta n(\mathbf{r})}$$

which is on turn connected with the Hohenberg-Kohn density functional $F_{\text{HK}}[n]$ through:

$$E_{xc}[n] = F_{\text{HK}}[n] - t[n] - V_{ee}[n] = T[n] + V[n] - t[n] - V_{ee}[n] \quad (2.14)$$

here is

$$V_{ee}[n] = \int v_{ee}(\mathbf{r}) n(\mathbf{r}) d\mathbf{r}$$

the electronic Coulomb energy. The exchange-correlation energy E_{xc} introduced from Kohn and Sham contains on one side the corrections to the kinetic energy of the considered reference system of non interacting electrons and on the other side the non classic parts of the electron-electron interaction (both merged in the concept of electronic correlation) and the exchange interaction. In the Kohn-Sham formalism of the DFT the Coulomb and kinetic part of the energy of a system of non interacting electrons can now be calculated. Being $F_{\text{HK}}[n]$ is unknown, also $E_{xc}[n]$ is unknown. For the latter however different approximations and some properties the exact functional has to satisfy are known. In [67] an overview about these issues can be found. As approximation of the exchange-correlation potential can be used, in the simplest case (in analogy with the Coulomb interaction potential v_{ee}):

$$v_{\chi\alpha} = -\frac{3}{2}\alpha \left(\frac{3}{\pi}n(\mathbf{r}) \right)^{\frac{1}{3}}. \quad (2.15)$$

This is the so called $\chi\alpha$ -approximation, where a considerable part of the correlation effects is neglected. Normally α is considered as parameter which can range between $2/3$ and 1 . Starting from the homogeneous electron gas one gets the expression for the Local Density Approximation (LDA) which uses the exchange-correlation energy of this model-system and explicitly contains the correlations effects. Beyond LDA are different approximation which contain gradient corrections to the homogeneous case, like the Generalised Gradient Approximation (GGA). These functionals reach a very good precision if compared for example with the $\chi\alpha$ -approximation or with simple Hartree-Fock [63, 68], even if the analytic expressions become more and more complex. The effective potential in the Kohn-Sham equation (Eq. 2.12) depends on the electronic density of the ground state which has to be calculated. The equation has then to be solved self-consistently: starting from a "good guess" for the start potential the equation is solved, a new charge density can be calculated with the solution, which is on turn used to generate a new effective potential. This iterative process is repeated as long as the potential (or the charge density) does not change considerably anymore from an iteration to the successive. The electronic total energy E_{KS} is calculated after a self consistent solution of the Kohn-Sham equations as:

$$E_{\text{tot}}^{\text{KS}} = \sum_{i=1}^{\text{occ.}} \langle \psi_i | -\frac{1}{2}\Delta | \psi_i \rangle + \frac{1}{2} \iint \frac{n(\mathbf{r})n(\mathbf{r}')}{|\mathbf{r}-\mathbf{r}'|} d\mathbf{r}d\mathbf{r}' + \int v_{\text{ext}}(\mathbf{r})n(\mathbf{r})d\mathbf{r} + E_{xc}[n]. \quad (2.16)$$

Allowed charge densities in the Kohn-Sham DFT are the densities allowed in the Hohenberg-Kohn theorems.

2.1.5 Spin Density Functional Theory

The derivation of the theory done in the previous section can be generalised for external potentials that are not scalar, like the nuclear potential, but vectorial, like for example the interaction with an external magnetic field [62]. In particular this has been done for spin dependent potentials [69], leading to the so called *spin-DFT*, in which for example the interaction with intrinsic magnetic fields can be described (ferromagnets or radical molecules are examples). While in the previously presented theory the main variable was the electronic density $n(\mathbf{r})$, in the easiest form of the spin-DFT¹ the densities of electrons with spin up $n_{\uparrow}(\mathbf{r})$, and spin down $n_{\downarrow}(\mathbf{r})$ are considered. In this case the quantisation direction is the direction of the external magnetic field. Alternatively one can choose as variables the total electronic density:

$$n(\mathbf{r}) = n_{\uparrow}(\mathbf{r}) + n_{\downarrow}(\mathbf{r}) \quad (2.17)$$

together with the magnetisation density:

$$m(\mathbf{r}) = n_{\uparrow}(\mathbf{r}) - n_{\downarrow}(\mathbf{r}) \quad (2.18)$$

¹This is the collinear version of the spin-DFT, which means the electronic spin are either considered parallel or antiparallel to the quantisation direction. Non collinear spin versions of the theory can be found for example in [240].

because they are a linear combination of the spin up and spin down magnetisation densities. The Kohn-Sham equations are then generalised as:

$$\begin{aligned} \left(\frac{1}{2}\Delta + v_{ee} + v_{\text{ext.}} + v_{xc}^\uparrow\right) \psi_{i\uparrow} &= \varepsilon_{i\uparrow} \psi_{i\uparrow} \\ \left(\frac{1}{2}\Delta + v_{ee} + v_{\text{ext.}} + v_{xc}^\downarrow\right) \psi_{i\downarrow} &= \varepsilon_{i\downarrow} \psi_{i\downarrow} \end{aligned} \quad (2.19)$$

where (from now on we use the notation $\sigma = \uparrow$ or \downarrow) v_{xc}^σ is the spin dependent exchange correlation potential:

$$v_{xc}^\sigma(\mathbf{r}) = \frac{\delta E_{xc}[n_\uparrow(\mathbf{r}), n_\downarrow(\mathbf{r})]}{\delta n_\sigma(\mathbf{r})} \quad (2.20)$$

which in turn derives from E_{xc} (see for example [62, 63]). The Kohn-Sham spin-orbitals $\psi_{i\sigma}$ to the eigenvalues $\varepsilon_{i\sigma}$ are correlated in the traditional way to the spin densities.

$$n_\sigma = \sum_i^N n_{i\sigma} |\psi_{i\sigma}|^2 \quad (2.21)$$

The spatial distribution and with them the spatial behaviour of the $\psi_{i\sigma}$ can be different for spin up and spin down electrons. Also in the spin polarised case one can derive a spin dependent version of the Janak's theorem [70]:

$$\varepsilon_{i\sigma} = \frac{\partial E_{\text{KS}}^{\text{tot}}}{\partial n_{i\sigma}}. \quad (2.22)$$

With this connection the Kohn-Sham eigenvalues are related to the first derivatives of the total energy with respect to the occupation numbers $n_{i\sigma}$. The Janak theorem is the starting point for the calculation of charge state transitions by means of the Janak-formalism, which is illustrated in the next section.

2.2 Calculation of the charge transition levels

Point defects and impurities usually introduce localised levels within the band gap of the host. These levels can be experimentally detected and can be therefore used to identify the defect or impurities present in the sample. For this reason it is of great importance to have a model which allows the calculation of these levels, even if the calculation itself presents some difficulty. The levels that can be determined experimentally involve transitions between the charge states of the defect or impurity. The one-particle levels deriving from a band structure calculation of the system have a position depending from the charge state (i.e. from their occupation) and cannot be identified with any levels which are experimentally relevant. We define therefore the thermodynamic transition $\epsilon(q_1/q_2)$ as the position of the Fermi-level at which the charge state q_2 becomes favoured over q_1 . This kind of levels can be observed with deep-level transient spectroscopy (DLTS) or derived from an analysis of the temperature-dependent Hall data². Charge transition levels should not be confused with optical levels, which can be detected for example with photoluminescence experiments.

2.2.1 Total energy differences

A first method to calculate the position of the transition level E^T between the two charge states q_1 and q_2 of a center X is to apply the definition of charge transition: when the Fermi energy E^F is equal to E^T , none of the two charge states is favoured with respect to the other, i.e. they have the same formation energy³:

²In the case of shallow centers in fact the level corresponds to the thermal ionisation energy.

³Formation energies and their calculations are discussed in the Appendix A

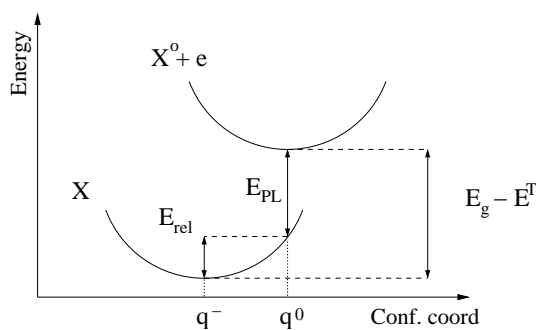


Figure 2.1: Configuration coordinate diagram illustrating the difference between charge transition and optical levels. For a discussion of this diagram see the text.

$$E_X^f[q_2](E^f = E^T) = E_X^f[q_1]$$

and from the definition of formation energy, neglecting the corrections needed to align the reference potential in the defect supercell with that of the bulk:

$$E^T = E_X^f[q_2](E^f = 0) - E_X^f[q_1] = E^{\text{tot}}[q_2] - E^{\text{tot}}[q_1]$$

where in each charge state the atomic structure is relaxed to its equilibrium configuration. The equilibrium structures of the same defect center may considerably differ for two charge states: this is the difference between thermodynamic charge transition levels and optical levels. Optical levels are defined like the charge transitions but the energy of the defect in the charge state q_2 is calculated with the geometry of the charge state q_1 . Indeed optical levels are revealed by techniques like photoluminescence (PL), where the center in the final charge state cannot relax to its equilibrium configuration. We illustrate this concept with an example. Let us suppose that the charge state q_2 and q_1 are the negative and neutral charge states of the defect center X respectively. The exciting light in a PL experiment will create electron-hole pairs. The negatively charged X^- centers can trap holes, becoming X^0 centers. If e is an electron at the bottom of the conduction band, the equilibrium configuration of the $X^0 + e$ state is $E_g - E^T$ higher than the equilibrium configuration of X^- , where E_g is the energy of the band gap. Electrons in the conduction band can now recombine with the trapped hole, leaving the defect center in the negative charge state but with the structure of the neutral charge state. The recombination leads to the emission of a photon with energy E_{PL} . The difference between this configuration and that of the equilibrium configuration X^- is the relaxation energy E_{rel} , also called Franck-Condon shift.

2.2.2 Janak's theory

Another way to calculate the charge transition levels is given by the Janak transition state formalism, which is an extension of the density functional theory which holds for the DFT as well as for the DFTB calculation scheme we are going to introduce. According the Janak theorem the Kohn-Sham eigenvalues of the density functional theory can be calculated as the derivative of the total energy with respect to the occupation number of the related Kohn-Sham orbital [70]

$$\frac{\partial E[N]}{\partial \eta_i} = \epsilon_i. \quad (2.23)$$

Here E is the DFT total energy, ϵ_i the Kohn-Sham eigenvalue of the i^{th} orbital and η_i its occupation number ($0 < \eta_i < 1$), so that the total number of electrons becomes $N = \sum_i \eta_i$. By integrating Eq. 2.23 it becomes possible to calculate the change in the total energy when we introduce one electron in the lowest unoccupied level of a system with N electrons, that of course for the system

with $N + \eta$ electrons becomes the highest occupied orbital:

$$E^{N+1} - E^N = \int_0^1 \epsilon_H(\eta) d\eta. \quad (2.24)$$

If the Kohn-Sham eigenvalue ϵ_H is at least a linear function of the occupation number (which is often assumed in practical applications), we obtain

$$(N/N + 1) = E^{N+1} - E^N = \epsilon_H(1/2) \quad (2.25)$$

which defines the Slater-Janak (SL) transition state. If we want the SL transition state to be rigorously taken into account $\epsilon_H(1/2)$ has to be calculated in a self-consistent calculation with a 1/2 occupation of the highest occupied orbital that is affected by the charge transition.

However, making again use of an assumed linearity of ϵ_H one can also write

$$\epsilon_H(1/2) \approx \frac{1}{2} [\epsilon_H^{N+1}(0) + \epsilon_H^{N+1}(1)] = \frac{1}{2} [\epsilon_L^N(0) + \epsilon_H^{N+1}(1)] \quad (2.26)$$

In other words, a good estimate for $\epsilon_H(1/2)$ is obtained by averaging the eigenvalues of the lowest unoccupied orbital in the N -electron system and the highest occupied orbital in the system containing $N + 1$ electrons. In the work of Göransson *et al.* [71] a thorough investigation of the validity of this approach using LDA for selected examples can be found. It gives a very good estimate of the position of the transition level as long as the Franck-Condon shift, which is due to the lattice relaxation as consequence of the charge change of the defect, is negligible. However, a remaining problem of the approach remains in the correct description of ϵ_i for the general case. It is well known, that in LDA the HOMO-LUMO gap between occupied and unoccupied orbitals is not well described, inducing in critical cases also some uncertainties into the energetic position of the KS levels. In addition, the assumption of the linearity of the ϵ_i is not ensured for strongly localised electrons. In the following we show that both problems can be coped with the use of orbital dependent functionals beyond LDA, e.g. by a LDA+ U approach. This approach will be presented in detail in the following sections, we anticipate here the main idea of the method to discuss how it improves, in connection with the Janak formalism, the description of the charge transition states.

The exact total energy $E[N]$ is a piecewise linear function of the total number of the electrons. As stated by Eschrig [72] and Cococcioni [73] this linearity is never provided in actual realisations of the theory (DFT-LDA or DFT-GGA). In LDA or GGA the incorrect treatment of the partially occupied Kohn-Sham orbitals gives a non linear contribution to the total energy, resulting in an unphysical curvature of $E[N]$, as reported in Fig. 2.2. The linearity is hardly verified for strongly correlated electrons like the ones in the strongly localised d - or f -shells of transition metals and rare earths. Here, the application of the $+U$ potentials largely recovers the piecewise linear behaviour of the exact ground state energy as function of the occupations [73]. In the LDA+ U approach also the slope of the KS eigenvalues can be improved considerably. This guarantees that the assumption behind the Janak transition state model, i.e. that the eigenvalues are linear functions of the occupation number, is automatically verified, even in the case of solids, where fractional occupations of the orbitals could occur as consequence of the hybridisation between atomic-like orbitals and environment. If the total energy functional $E[N]$ is, as it should, a linear function of the total number of electrons N , then the one-particle energies are not only linear in the occupation numbers η_i but also piecewise constant (with jumps at integer values N):

$$\epsilon_i = \frac{\partial E[N]}{\partial \eta_i} = \frac{\partial N}{\partial \eta_i} \cdot \frac{\partial E[N]}{\partial N} = \frac{\partial E[N]}{\partial N} = \text{const.} \quad (2.27)$$

In other words, if we would have an ideal U , i.e. a value which perfectly recovers the piecewise linearity of $E[N]$ then the Kohn-Sham levels, defined as the first derivative of this functional with respect to the occupation numbers, would be *piecewise constant* and independent from the occupation numbers itself. The independence of the KS-orbitals from their occupation numbers is for sure verified (also in DFT-LDA) in the case of extended orbitals, corresponding to the vanishing U for

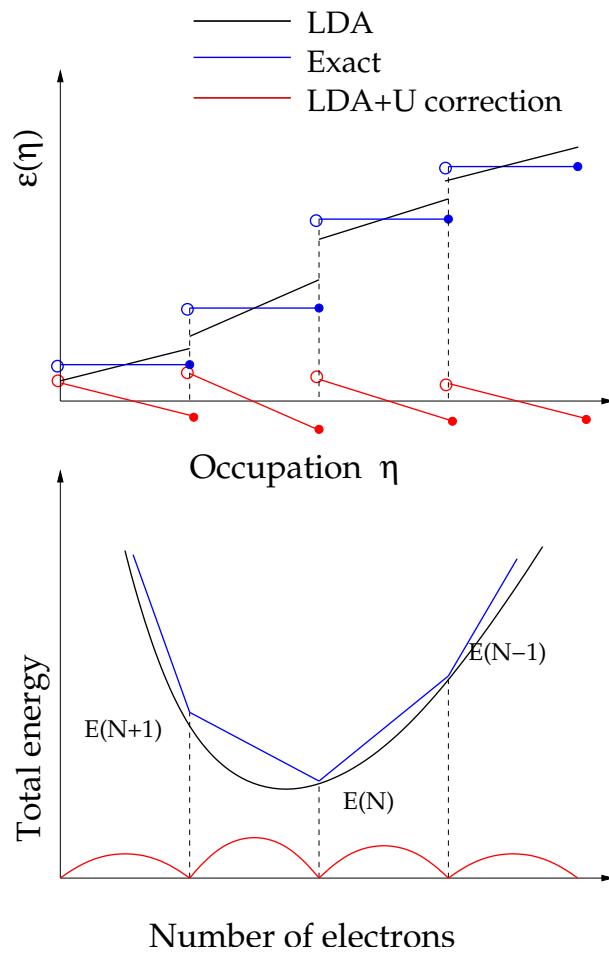


Figure 2.2: Lower part: The exact total energy profile of a system of N electrons as a piecewise linear curve, never provided in actual DFT implementations like LDA/GGA, where a spurious curvature is a consequence of the incorrect treatment of the self interaction. The bottom curve is the difference between the other two. Upper part: The LDA/GGA eigenvalue depend roughly linearly from the occupation numbers. The LDA+ U corrections (red) are also a linear function of the occupation number. The resulting LDA+ U eigenvalues are in the best case constant (for the ideal U value).

delocalised electrons (e.g. the band structure of an ideal solid does in fact not change adding or subtracting electrons). In the case of localised states the situation is of course different: an additional charge in the orbital will cause a change in the form (wavefunction) of the orbital, but in the ideal case not in its energy. The total energy of a system of N electrons is corrected in LDA+ U adding an Hubbard-like term which properly takes in account the coulomb energy of the N_M correlated electrons to the LDA total-energy functional and subtracting the coulomb interaction as given by LDA for the same electrons:

$$E = E_{\text{LDA}} - \sum_{\mathcal{M}} \left[\frac{1}{2} \overline{U_{\mathcal{M}}} N_{\mathcal{M}} (N_{\mathcal{M}} - 1) - \frac{1}{2} \sum_{i \neq j \in \mathcal{M}} U_{ij} \eta_i \eta_j \right]$$

with $U_{ij} = \langle i, j | V_{ee} | i, j \rangle$

(2.28)

$$\overline{U_{\mathcal{M}}} = \frac{1}{N_{\mathcal{M}}^2} \sum_{i, j \in \mathcal{M}} U_{ij} = \frac{1}{(2l+1)^2} \sum_{i, j \in \mathcal{M}} U_{ij} = F^0$$
(2.29)

whereby the U_{ij} vanish if i and j are belonging to different localised manifolds \mathcal{M} , containing $N_{\mathcal{M}} = 2l + 1$ strongly interacting electronic orbitals. As a consequence, each Kohn-Sham level is corrected by an amount:

$$\epsilon_i = \frac{\partial E_{\text{LDA}+U}}{\partial \eta_i} = \epsilon_{i\text{LDA}} + U_{ii} \left(\frac{1}{2} - \eta_i \right)$$
(2.30)

i.e. an orbital-dependent linear correction $U_{ii} (\frac{1}{2} - \eta_i)$ is provided that is able to recover the constant one-particle levels from the linear dependent regime in the case of LDA as sketched in the upper part of Fig. 2.2. In summary we have shown analytically, that the LDA+ U formalism the perfect recover of the constance of the one-particle levels is provided by a set of perfect U -values. This holds also in the case of strongly correlated electrons, as we will show numerically in the chapter 5. The description of the LDA+ U approach is the topic of the next section while its implementation in the DFTB calculation scheme will be the topic of the following one.

2.3 Orbital dependent potentials

In the density functional theory (DFT) the exchange-correlation potential is often approximated by using the exchange-correlation present in a homogeneous electron gas (LDA), which has been proven to be very successful for solids even if not all systems are equally well described. Materials with strongly correlated electrons however are examples where this mean field approach most strikingly fails. LDA is in fact an one-electron method with an orbitally independent potential and applying it to a system containing transition metals (TM) or rare earths (RE) with partially filled d - or f -shells gives results consistent with a metallic electronic structure and itinerant d - or f -electrons, which is definitely wrong for most RE compounds and several examples of TM systems (NiO being the classic example). Other choices for the exchange correlation such as generalised gradient (GGA) can also be applied, but as with LDA this is a mean-field correction for the non-interacting system, so suffers from the same pathology. In the strongly correlated systems the d - or f -electrons are often strongly localised and there is a noticeable energy difference between occupied and unoccupied states with strong d or f character, which are called *lower* and *upper* Hubbard bands, in analogy with the Hubbard Hamiltonian approach. There have been a number of attempts to go beyond the LDA and make it possible to account for strong electron-electron correlation in such systems. The full self interaction corrected (SIC) approach [74] can reproduce the the localised nature of d and f electrons in TM and RE compounds as well as the total energy of these systems but is not intended to reproduce the one-electron energies, additionally SIC is known to over-correct many properties [75]. As discussed in section 2.5.9 there have also been several recent attempts to approximate the effects of the SIC method with (semi-)local corrections. An alternative correction, the LDA+ U approach, is conceptually similar to the Hubbard Hamiltonian approach: the non-local and energy dependent self energy is approximated by a frequency independent but non-local screened Coulomb potential.

2.3.1 LDA+U

As discussed by Anisimov *et al.* [16], it is natural to separate electrons into localised d - or f -electrons and delocalised s - and p -electrons. While for the latter an orbitally independent one-electron potential (as in LDA) will suffice, a Hartree-Fock like interaction better describes the local interactions of the strongly localised d - or f -electrons. This is of the form $\frac{1}{2} \sum_{i \neq j} n_i n_j$, where n_i are the occupancies of the localised shells. If we assume that the Coulomb energy of the electron-electron interaction as a function of the total number of electrons $N = \sum n_i$ is well represented by LDA (even if it gives wrong single-particle energies), then LDA already contains part of this energy. This must be subtracted from the total energy and instead replaced with a Hubbard model-like term. As a result we get the functional [76, 77]:

$$E = E_{\text{LDA}} - \frac{1}{2} U N(N-1) + \frac{U}{2} \sum_{i \neq j} n_i n_j = E_{\text{LDA}} + \Delta E_{\text{LDA}+U} \quad (2.31)$$

Strictly speaking, the process of subtracting the double-counting of the electron-electron interaction of strongly correlated electrons from the LDA total energy and substituting it with a Hubbard Hamiltonian-like term is not without ambiguity. The electron-electron interactions have already been taken into account in a mean field way with LDA, while the Hubbard Hamiltonian also incorporates a large part of the total Coulomb energy of the system. One can try to identify those parts of the DFT total energy corresponding to the interactions included with the Hubbard Hamiltonian in order to subtract them. This is not trivial, because while the Kohn-Sham Hamiltonian is written in terms of the total density, the Hubbard Hamiltonian is written in terms of orbital occupation numbers, and a direct link between the two is not straightforward. Secondly, even if it were possible to exactly remove the on-site Coulombic contribution in the LDA and Hartree contributions, it would be undesirable, as the spatial variation of the Coulomb and exchange-correlation potential is important and better described in DFT than in the Hubbard approach. It is instead better to try and identify a mean-field part of the Hubbard Hamiltonian and subtract that, leaving only a correction to the LDA solution. In the limit of uniform occupancy (all occupations equal to the average value in that shell) the corrections for total energy and potential can be written in terms of on-site occupation matrices (n) as [78]:

$$\Delta E^{AMF} = -\frac{1}{2} \sum_a \sum_{l \in a} (U - J)_l \sum_{\sigma} \sum_{\mu\nu} (\delta n_{\mu\nu}^{\sigma} \cdot \delta n_{\nu\mu}^{\sigma})_{\nu\mu \in l} \quad (2.32)$$

$$\Delta V_{\mu\nu}^{\sigma} = -(U - J) \delta n_{\nu\mu}^{\sigma} \quad (2.33)$$

where U is the spherically averaged Hubbard repulsion and J is the intra-atomic exchange. δn , the orbital occupation matrix, is given by

$$\delta n_{\mu\nu}^{\sigma} = n_{\mu\nu}^{\sigma} - \bar{n}_{\mu\nu}^{\sigma} \delta_{\mu\nu}$$

Here, $\delta_{\mu\nu}$ “masks out” elements off the diagonal of the average occupation matrix $\bar{n}_{\mu\nu}^{\sigma}$, the effect being to return a matrix shifted by the average occupation. In the “around mean field” (AMF) limit the LDA+U correction to the electronic potential averaged over all occupied states in a given shell is zero, this is a possible way to define a mean field. For strongly correlated systems (or in the presence of a crystal/ligand field) the limit of uniform occupancy is not correct and the AFM functional leads to rather unrealistic results for strongly localised electrons. This has led to the suggestion of another correction which produces the correct behavior in the fully localised limit (FLL) where the eigenvalues of $n_{\mu\nu}^{\sigma}$ are either 0 or 1.

$$\Delta E^{FLL} = -\frac{1}{2} (U - J) \sum_{\sigma} \sum_A \sum_{\mu\nu} ((n_{\mu\nu}^{\sigma})^2 - n_{\mu\mu}^{\sigma})_{\mu\nu \in l \in A} \quad (2.34)$$

$$\Delta V_{\mu\nu}^{\sigma} = -(U - J) \left(n_{\mu\nu}^{\sigma} - \frac{1}{2} \delta_{\mu\nu} \right)_{\mu\nu \in l \in A} \quad (2.35)$$

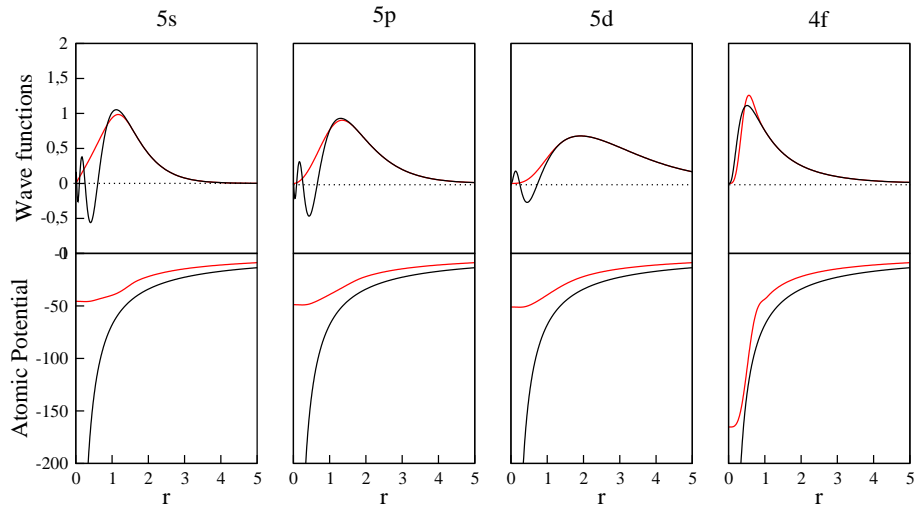


Figure 2.3: Pseudo atomic potentials and pseudo wave functions for Erbium. Each column represent a shell, up are reported the all electron (black) and pseudo (red) wave functions and down the atomic potential Z/r (black) and the pseudo potential (red). All quantities are expressed in atomic units. 5s and 5p electrons (reported here) are considered semi-core electrons, while 4f, 5d, 6s and 6p are proper valence electrons.

AMF and FLL correct the mean field double-counting if the occupation numbers are respectively all equal or only 0 or 1. Most of the modern LDA+ U calculations rely on one of these two functionals, although in real materials the occupation numbers should lie between these two limits, hence neither AMF nor FLL are strictly speaking correct for real systems, one should therefore use an interpolation between the two limits [78]. However, AMF and FLL will bracket the correct values.

2.4 *ab initio* methods

2.4.1 The pseudopotential approach

Even if the main tool for the investigation of the RE-defects in this work is DFTB, a number of calculation was done with other *ab initio* programs, used as reference and validation. For this reason in this session the pseudopotential approach is introduced briefly. In this short introduction we do not discuss any of the arising problems like singularities in potentials, ghost states [79, 80], relativistic effects for heavier atoms and the transferability of pseudopotentials. Further details about this topics and about the different possibilities one has for the practical realisation of the pseudopotential can be found in more specific literature [81–83]. In the practical realisation of the DFT methods the orbitals $\psi(\mathbf{r})$ in Eq. 2.16 are normally expanded in a superposition of plane waves (PW), Gaussian orbitals or other functions. Inside the atomic core the electronic wave functions oscillate quite strongly and a huge number of PW is required for a correct description of the wave function itself. As result, full-potential all-electrons calculations are computationally very demanding and not feasible for most systems of interest.

A way out from this problem is found introducing some considerations which reduce the computational complexity of our problem: firstly, the bonding between atoms in solids is predominantly governed by their valence electrons. The core electrons of the closed inner shells basically behave like in an isolated atom and create a screening effective potential. The idea is then to only consider the valence electrons when self-consistently calculating the electron density. The remaining core electrons as well as the electrostatic potential of the nuclei are included in a new effective potential, the so called pseudopotential $v_{ps}(r)$, which basically represents the potential created by all ions. The number of electrons, and with this the number of orthogonal wavefunctions to be included explicitly in the self-consistent calculation of the total energy is then reduced dramatically. Re-

ducing the number of electrons in the system also reduces the error of the calculation. Comparing all-electron energies of similar systems might in fact lead to relatively large errors, since two large numbers are subtracted. This error is of course smaller if only the valence electrons contribute to the difference in energy. The pseudopotential reproduces the correct eigenenergies and eigenfunctions for the valence electrons outside the core region. Inside the core the valence pseudo-wavefunctions are smooth and nodeless but reproduce the correct electron density inside the core. The overall effective potential in the Schrödinger equation becomes:

$$v_{\text{eff}}[n^V(\mathbf{r})] = v^{ps}(\mathbf{r}) + \int \frac{n^V(\mathbf{r}')}{|\mathbf{r} - \mathbf{r}'|} d\mathbf{r}' + v_{xc}[n^V(\mathbf{r})] \quad (2.36)$$

where $n^V(\mathbf{r})$ is the valence electron density. The pseudopotential $v^{ps}(\mathbf{r})$ is given as the superposition of all single ionic pseudopotentials:

$$v^{ps}(\mathbf{r}) = \sum_{j=1}^M v_j^{ps}(\mathbf{r} - \mathbf{R}_j)$$

where \mathbf{R}_j are the nuclear coordinates. To obtain the ionic pseudopotential $v_j^{ps}(\mathbf{r})$ one starts with the effective all-electron potential of a neutral atom $v_j^{eff}(\mathbf{r})$. Stripping off the valence electron contribution yields:

$$v_j^{ps}(\mathbf{r}) = v_j^{eff}(\mathbf{r}) - \int \frac{n_j^V(\mathbf{r}')}{|\mathbf{r} - \mathbf{r}'|} d\mathbf{r}' - v_{xc}[n_j^V(\mathbf{r})] \quad (2.37)$$

There are several recipes how to construct pseudopotentials in detail. In this work we only use pseudopotentials generated with the scheme of Hartwigsen-Goedecker-Hütter described in [84]. We don't go through the exact construction of these particular pseudopotentials in this section, for a detailed review see the given reference.

Non linear core correction

We have seen that the ionic pseudopotentials are determined subtracting from the effective ionic potential the Hartree and exchange-correlation contributions due to the valence electrons. The term $v_{xc}[n_j^V(\mathbf{r})]$ in Eq. 2.37 refers to the the exchange-correlation interaction between the valence electrons themselves. The exchange-correlation interaction between the valence and the core electrons is included in the pseudopotential, as a term that depends linearly on the valence charge density $n^V(\mathbf{r})$. Although E_{xc} is a non linear functional of the total electron density $n(\mathbf{r})$, the linearity is often assumed and used within LDA and GGA. However in some case the explicit account of the non-linearity is required to have good description of the system. This is done by restoring the non-linear dependence of $E_{xc}[n]$ on the total electron density. In practice, it suffices to add a partial core density $n_{\text{core}}(\mathbf{r})$, as suggested by Louie *et al.* [85]. The form of this charge will not be discussed here. The resulting nonlinear core-valence exchange-correlation scheme uses the redefined ionic pseudopotentials

$$v_j^{ps}(\mathbf{r}) = v_j^{eff}(\mathbf{r}) - v_j^H[n_j^V(\mathbf{r})] - v_{xc}[n_j^V(\mathbf{r}) + n_j^{\text{core}}(\mathbf{r})] \quad (2.38)$$

The non-linear exchange-correlation is normally important for the description of alkali metals and with increasing atomic numbers, i.e. the farther the upper core orbitals extend into the tails of the valence density, as in the case of the lanthanides.

2.5 Density Functional based Tight Binding

The Kohn-Sham equations (Eq. 2.16) has to be solved self-consistently. In particular in each step new potentials have to be calculated from the electronic density, which is a very demanding task because of the integrals one has to solve. To avoid this effort and nonetheless get results with a quality and precision similar to the ones of a fully self consistent DFT calculation the

Density Functional-based Tight Binding method (DFTB) was developed [86]. The method was then extended [87] to include charge self consistency (SCC), to handle spin polarised systems [88, 89] and finally to handle the so called strongly correlated systems [28]. In this section the DFTB formulation appears as found in [90] and implemented in the DFTB⁺ code [19]. For an alternative formulation and a historical review of the method see [19]. The already derived expression for the total energy of a system of M atoms with nuclear charge Z in the Kohn-Sham formulation of the spin DFT is:

$$\begin{aligned}
 E_{\text{tot}}^{\text{KS}} = & \sum_{\sigma=\downarrow,\uparrow} \sum_i^{\text{occ.}} n_{i\sigma} \left\{ \langle \psi_{i\sigma} | -\frac{\Delta}{2} + v_{\text{ext}} + \frac{1}{2} \int \frac{n(\mathbf{r}')}{|\mathbf{r}-\mathbf{r}'|} |\psi_{i\sigma}\rangle \right\} \\
 & + E_{xc}[n(\mathbf{r}), m(\mathbf{r})] + \underbrace{\frac{1}{2} \sum_{I,J}^M \frac{Z_I Z_J}{|\mathbf{R}_I - \mathbf{R}_J|}}_{E_{NN}}
 \end{aligned} \tag{2.39}$$

where Z_I represents the atomic number of each of the M ions of the system. The summation over the KS spin-orbital $\psi_{i\sigma}$ runs over the occupied orbitals. The electronic coordinates are indicated with the vector \mathbf{r} and the nuclear coordinates with \mathbf{R} , $n(\mathbf{r})$ is the charge density of the electron with coordinates \mathbf{r} . The basic DFTB approximation⁴ is to expand the charge density around a reference charge density of $n_0(\mathbf{r})$:

$$n(\mathbf{r}) = \sum_{\sigma=\uparrow,\downarrow} \sum_i^N n_{i,\sigma} |\psi_{i,\sigma}|^2 = n_0(\mathbf{r}) + \delta n(\mathbf{r}) \tag{2.40}$$

with $\delta n(\mathbf{r})$ being the difference between the reference charge density used in parameterisation and the actual ground state of the system. The system magnetisation is also expanded, but the reference chosen is the spin unpolarised atom case, which has (per definition) a magnetisation density of zero⁵:

$$m(\mathbf{r}) = m_0(\mathbf{r}) + \delta m(\mathbf{r}), \quad \text{with } m_0 = 0 \tag{2.41}$$

Now, introducing the abbreviations n , n_0 , δn and δm for $n(\mathbf{r})$, $n_0(\mathbf{r})$, $\delta n(\mathbf{r})$ and $\delta m(\mathbf{r})$, as well as n' , n'_0 , $\delta n'$ and $\delta m'$ for $n(\mathbf{r}')$, $n_0(\mathbf{r}')$, $\delta n(\mathbf{r}')$ and $\delta m(\mathbf{r}')$ and with a little algebra the expression for the total energy of the system (Eq. 2.39) can be written as:

$$\begin{aligned}
 E_{\text{tot}} = & \sum_{\sigma=\downarrow,\uparrow} \sum_i^{\text{occ.}} n_{i\sigma} \langle \psi_{i\sigma} | -\frac{\Delta}{2} + v_{\text{ext}} + \int \frac{n'_0}{|\mathbf{r}-\mathbf{r}'|} d\mathbf{r}' + v_{xc}[n_0, m_0] |\psi_{i\sigma}\rangle \\
 & - \frac{1}{2} \iint \frac{n'_0(n_0 + \delta n)}{|\mathbf{r}-\mathbf{r}'|} d\mathbf{r} d\mathbf{r}' - \int v_{xc}[n_0, m_0](n_0 + \delta n) d\mathbf{r} \\
 & + \frac{1}{2} \iint \frac{\delta n'(n_0 + \delta n)}{|\mathbf{r}-\mathbf{r}'|} d\mathbf{r} d\mathbf{r}' + E_{xc}[n_0 + \delta n, m_0 + \delta m] + E_{NN}
 \end{aligned} \tag{2.42}$$

where we just added zeros and grouped together the terms depending n_0 and those depending on δn . Following the same principle the exchange-correlation term, too, is expanded in a Taylor-series to the second order in δn and δm .

⁴This is the so called Foulkes-Haydock Ansatz [91]. In the work of Foulkes and Haydock is shown that the resulting expression for the energy is not variational but stationary for changes in the charge fluctuation. For a more specific discussion on this theme see [92].

⁵As seen in the section dedicated to the spin-DFT, it would be possible to choose n_\uparrow and n_\downarrow instead of n and m as main quantities for the development of the theory, though one would not come to expressions which correspond to the ones in the spin unpolarised DFTB method. In particular the first derivatives would not vanish.

$$\begin{aligned}
 E_{xc}[n, m] &= E_{xc}[n_0, 0] + \int \frac{\delta E_{xc}}{\delta n} \Big|_{n_0, 0} \delta n d\mathbf{r} + \int \frac{\delta E_{xc}}{\delta m} \Big|_{n_0, 0} \delta m d\mathbf{r} + \\
 &+ \iint \frac{\delta^2 E_{xc}}{\delta n(\mathbf{r}) \delta m(\mathbf{r}')} \Big|_{n_0, 0} \delta n(\mathbf{r}) \delta m(\mathbf{r}') d\mathbf{r} d\mathbf{r}' + \\
 &+ \frac{1}{2} \iint \frac{\delta^2 E_{xc}}{\delta n(\mathbf{r}) \delta n(\mathbf{r}')} \Big|_{n_0, 0} \delta n(\mathbf{r}) \delta n(\mathbf{r}') d\mathbf{r} d\mathbf{r}' + \\
 &+ \frac{1}{2} \iint \frac{\delta^2 E_{xc}}{\delta m(\mathbf{r}) \delta m(\mathbf{r}')} \Big|_{n_0, 0} \delta m(\mathbf{r}) \delta m(\mathbf{r}') d\mathbf{r} d\mathbf{r}' \quad (2.43)
 \end{aligned}$$

For exchange-correlation functionals that do not contain any spin-orbit coupling $E_{xc}[n, m] = E_{xc}[n, -m]$ holds. For this reason the third and fourth term at the right side in Eq. 2.43 must vanish, as the first derivative in $m = 0$ vanishes too. Furthermore, considering that any non local (i.e. depending at the same time from both \mathbf{r} and from \mathbf{r}') density functional is known, the sixth term in Eq. 2.43 can be simplified to:

$$\frac{1}{2} \iint \frac{\delta^2 E_{xc}}{\delta m(\mathbf{r}) \delta m(\mathbf{r}')} \Big|_{n_0, 0} \delta m(\mathbf{r}) \delta m(\mathbf{r}') d\mathbf{r} d\mathbf{r}' = \frac{1}{2} \iint \frac{\delta^2 E_{xc}}{\delta m(\mathbf{r})^2} \Big|_{n_0, 0} \delta m(\mathbf{r})^2 d\mathbf{r}$$

Inserting the Eq. 2.43 in Eq. 2.42 results in the following approximated expression for the total energy:

$$\begin{aligned}
 E_{tot} &= \sum_{\sigma=\downarrow, \uparrow} \sum_i^{occ.} n_{i\sigma} \langle \psi_{i\sigma} | \underbrace{-\frac{\Delta}{2} + v_{ext} + \int \frac{n'_0}{|\mathbf{r} - \mathbf{r}'|} d^3 r' + v_{xc}[n_0, 0]}_{\hat{H}_0[n_0, 0]} | \psi_{i\sigma} \rangle \quad (2.44) \\
 &+ \underbrace{E_{NN} + E_{xc}[n_0, 0] - \int v_{xc}[n_0, 0] n_0 d^3 r - \frac{1}{2} \iint \frac{n_0 n'_0}{|\mathbf{r} - \mathbf{r}'|} d^3 r d^3 r'}_{E_{rep}} \\
 &+ \underbrace{\frac{1}{2} \iint \left(\frac{1}{|\mathbf{r} - \mathbf{r}'|} + \frac{\delta E_{xc}}{\delta n \delta n'} \Big|_{n_0, 0} \right) \delta n \delta n' d^3 r d^3 r'}_{E_{\delta n}} + \underbrace{\frac{1}{2} \int \frac{\delta^2 E_{xc}}{\delta m^2} \Big|_{n_0, 0} \delta m^2 d^3 r}_{E_{\delta m}}
 \end{aligned}$$

This equation only contains two types of terms, the first only depending on the reference density ($\hat{H}_0[n_0, 0]$, and E_{rep}), and the second including fluctuations of the charge and magnetisation densities compared to the reference ($E_{\delta n}$ and $E_{\delta m}$). In the following will be shown how each of these terms can be inserted in the framework of an efficient Tight-Binding calculation scheme.

2.5.1 The zeroth-order Hamiltonian

We now discuss the zeroth-order Hamiltonian contribution to this expression ($\hat{H}_0[n_0, 0]$). Before we start to calculate the elements of the Hamiltonian matrix we need a basis for the representation of the one-particle wave functions $\psi_{i\sigma}$.

Basis functions

We expand the spin orbitals as a linear combination of Slater type orbitals (LCSTO):

$$|\psi_{i\sigma}\rangle = \sum_{\nu} c_{\nu i\sigma} |\varphi_{\nu}(\mathbf{r} - \mathbf{R}_{\mathbf{A}})\rangle, \quad A = A(\nu). \quad (2.45)$$

The basis function $\varphi_\nu(\mathbf{r} - \mathbf{R}_A)$ is centered on the atomic nucleus A , with position \mathbf{R}_A . The spin is included in the coefficients $c_{\nu\sigma}$ of the expansion. The basis functions $\phi_\nu(\mathbf{r})$ are themselves a linear combination of single Slater orbitals:

$$\varphi_\nu(\mathbf{r}) = \left(\sum_{j=1} \left(\sum_{n=0} a_{jn} \mathbf{r}^{l_\nu+n} \right) e^{-\alpha_j \mathbf{r}} \right) Y_{l_\nu m_\nu} \quad (2.46)$$

The angular and magnetic quantum numbers are indicated with l_ν and m_ν . $Y_{l_\nu m_\nu}$ is the corresponding real spherical harmonic. For the choice of the exponents α_j and of the optimal number of terms in the expansion see the work of Eschrig *et al.* [93]. The coefficients a_{jn} are determined with fully self consistent DFT calculations on neutral, not spin polarised and spherically symmetric so called *pseudo atoms*. The KS equation for the determination of the a_{ij} and with them $\varphi_\nu(\mathbf{r})$ is:

$$(\hat{t} + v_{\text{psat}})|\varphi_\nu(\mathbf{r})\rangle = \varepsilon_\nu|\varphi_\nu(\mathbf{r})\rangle \quad (2.47)$$

$$v_{\text{psat}} = v_{ee} + v_{\text{ext}} + v_{xc} + v_{\text{add}}(\mathbf{r}) \quad (2.48)$$

An additional harmonic confining potential is applied to the *pseudo-atom*, of the form:

$$v_{\text{add}} = \left(\frac{r}{r_0} \right)^m \quad (2.49)$$

to localise the orbitals for a more crystal/molecule like environment. This potential forces the wave functions to avoid areas far from the nucleus, resulting in an electron density that is compressed in comparison to the free atoms and is then suitable for modeling condensed systems [93, 94]. Adding a confining potential can also be interpreted as the attempt to include part of the effects of a fully self-consistent DFT treatment. This is reasonable, bearing in mind that in the calculation of the zeroth-order matrix elements \hat{H}_0 no self consistency is considered. In all recent DFTB works and in this work, too, a quadratic potential ($m = 2$) is used. The parameter r_0 in Eq. 2.49 is usually set to $r_0 = 1.85 \cdot r_{\text{cov}}$, where r_{cov} is the covalent radius of the considered atom. r_0 can be considered as a parameter which can be tuned for an optimal representation of the system. A more detailed discussion can be found in the chapter dedicated to the parameter generation. Electrons in heavy ions move with a speed which is not negligible if compared to the light speed and relativistic effects become important, causing for example the contraction of the atomic orbitals and lowering the energy of the outer electrons. It is then essential to consider somehow the relativistic effects in the simulation of heavy ions. As the DFTB method itself is a non relativistic method, the relativistic effects have to be included at the moment of generating the wave functions of the pseudo atoms. This can be done substituting the Schrödinger equation for the description of an electron in the pseudo-atom with its relativistic counterpart, the Dirac equation:

$$\hat{H}_D|\varphi(\mathbf{r})\rangle = \left(E + \frac{1}{2}c^2 \right) |\varphi(\mathbf{r})\rangle \quad (2.50)$$

where c is the light speed (in atomic units $c = 264.08$) and the Dirac Hamiltonian can be expressed as a matrix operator:

$$\hat{H}_D = c^2\beta + c\tau\sigma\hat{p} + V(\mathbf{r}) \quad (2.51)$$

where τ , σ and β are Pauli spin matrices and $V(\mathbf{r})$ is a potential containing the usual Hartree and exchange-correlation contributions in local form. For a thorough discussion see the work of Heera *et al.* [95].

Reference densities and matrix elements

Solving the Dirac equation one obtains the basis functions and the atomic electronic charges n_0^A for each atom type. Inserting Eq. 2.45 into Eq. 2.44 we have:

$$\langle \psi_{i\sigma} | \hat{H}_0[n_0, 0] | \psi_{i\sigma} \rangle = \sum_{\mu, \nu} c_{\mu i\sigma}^* c_{\nu i\sigma} \langle \varphi_\mu | \hat{H}_{\mu\nu}^0[n_0, 0] | \varphi_\nu \rangle = \sum_{\mu, \nu} c_{\mu i\sigma}^* c_{\nu i\sigma} \hat{H}_{\mu\nu}^0[n_0, 0] \quad (2.52)$$

In the spirit of the two center approximation the matrix elements are calculated neglecting all the terms which do not come from the atoms φ_μ and φ_ν are centered at. If φ_μ and φ_ν are centered at the same atom one gets the eigenvalues ε_ν of the Dirac equation of the pseudo atom. In praxis though the eigenvalues $\varepsilon_\nu^{\text{free atom}}$ of a free atom (without contracting potential) are used to recover the right dissociation limit. Neglecting all the contributions which were not explicitly considered before:

$$H_{\mu\nu}^0 = \begin{cases} \varepsilon_\mu^{\text{free atom}} & \text{if } \mu = \nu \text{ and } A = B \\ \langle \phi_\mu^A | T + V_A^0 + V_B^0 | \phi_\nu^B \rangle & \text{if } A \neq B \\ 0 & r > r_{\text{cutoff}} \end{cases} \quad (2.53)$$

where $V_{A,B}$ is the effective Kohn-Sham potential (Coulomb plus exchange-correlation) for atoms A and B . These matrix elements are calculated without further self consistent cycles from the basis functions and the atomic charge densities. In the DFTB approximation two contributions to the potential, which normally are included in fully self consistent calculations, are neglected: the crystal field and the three center terms. The former is given when two basis functions centered on the same atom interact with the potential coming from another atom, the latter is given when two basis functions centered on different atoms interact with the potential coming from a third atom.

All the electronic states can be simulated with this calculation scheme. However, increasing the total number of electrons in the system results in an even faster increasing of the basis functions φ_ν . For this reason the so called core-electrons, which do not really contribute to the bond, are neglected, similarly to a pseudopotential scheme [88, 94]. The choice of the electrons we consider as valence or core is a matter discussed in the section dedicated to the parameter creation. The Hamiltonian matrix elements are then calculated only for the valence electrons, which are the only ones which explicitly appear in the calculation. Because of the neglecting of the crystal-field and three-center terms the wave function $\psi_{i\sigma}$ of the valence electrons do not have to be orthogonalised against the wave functions of the core electrons [94]. For the explained calculation a basis function φ_ν is assigned to each combination (l, m) present in the valence shell. This is known as minimal basis. The Hamiltonian $\hat{H}_{\mu\nu}^0$ and overlap matrix elements ($S_{\mu\nu} = \langle \phi_\mu | \phi_\nu \rangle$) are calculated only once and tabulated as function of the interatomic distance between A and B . Since the basis functions decay in space, above a certain distance (r_{cutoff}) they give rise to matrix elements smaller than a reasonable tolerance, which are then discarded. Note that the potential in Eq. 2.53 is a superposition of the atomic potentials. Another possibility is to express it as the potential generated by the superposition of the charge densities of A and B , as is used instead in some DFTB parameterisations [21]. Then by following the method of Slater and Koster [96] and its extension to the f -shell [97, 98] this potential is used to generate the two-centre H^0 . The values of the matrix elements in each particular calculation are computed by interpolating the tabulated data, this is one of the DFTB features which make the computational scheme particularly efficient. Unlike empirical tight-binding however, since an explicit basis set is used in the generation of parameters, it is for example possible to plot spacial dependence of the resulting single-particle wavefunctions in a real calculation.

2.5.2 Fluctuation dependent contributions to the energy

The terms grouped in the last line of Eq. 2.44 depend on the charge density fluctuation δn and on the magnetisation density fluctuation δm . Let us firstly discuss the part depending from δn .

Charge density fluctuations

The charge density fluctuation in the term

$$E_{\delta n} = \frac{1}{2} \iint \left(\frac{1}{|\mathbf{r} - \mathbf{r}'|} + \left. \frac{\delta^2 E_{xc}}{\delta n \delta n'} \right|_{n_0,0} \right) \delta n \delta n' d\mathbf{r} d\mathbf{r}' \quad (2.54)$$

of the total energy can be written in analogy to the reference charge density as sum of atomic contributions, even if we have now to consider the angular momentum (l) dependence.

$$\delta n = \sum_A \sum_{l \in A}^M \delta n^{Al} \quad (2.55)$$

These atomic contribution can be on turn expressed in terms of spheric functions Y_{LM} with coefficients $c_{L,M}$:

$$\delta n^{Al} = \sum_{L,M} c_{L,M}^{Al} F_{L,M}^{Al}(|\mathbf{r} - \mathbf{R}_A|) Y_{L,M} \quad (2.56)$$

where the radial parts are given in terms of the unknown functions $F_{L,M}$. We define the normalisation factor $Y_{00} = 1/\sqrt{4p}$. In the spirit of a monopole approximation we neglect now all the terms with $L > 0$ in the sum. The monopole approximation is legitimate from the consideration that one electronic shell of an atom in a context with fully spheric symmetry like the pseudo-atom we are considering will give rise to a spheric charge distribution. The coefficients $c_{L,M}^{Al}$ can be identified with the so called *Mulliken charges* q_{Al} [99]. These are given subtracting for each orbital the number of valence electrons q_0^{Al}

$$q_{Al} = \left(\sum_{\sigma=\uparrow,\downarrow} p_{Al\sigma} \right) - q_0^{Al} \quad (2.57)$$

from the spin-dependent *Mulliken populations*:

$$p_{Al\sigma} = \frac{1}{2} \sum_{i=1}^{occ.} n_{i\sigma} \sum_{\mu \in A,l} \sum_{\nu} (c_{\mu i \sigma}^* c_{\nu i \sigma} S_{\mu\nu} + c_{\nu i \sigma}^* c_{\mu i \sigma} S_{\nu\mu}) \quad (2.58)$$

of the same orbital. The sum over μ comprehends all the basis function centered on atom A needed for the description of the orbital l . The sum over ν is extended to all the basis functions. Inserting the expression derived for the charge density fluctuation into Eq. 2.54 leads to the expression:

$$E_{\delta n} = \frac{1}{2} \sum_A^M \sum_B^M \sum_{l \in A} \sum_{l' \in B} \iint \left(\frac{1}{|\mathbf{r} - \mathbf{r}'|} + \left. \frac{\delta^2 E_{xc}}{\delta n \delta n'} \right|_{n_0,0} \right) \times \frac{F_{00}^{Al}(|\mathbf{r} - \mathbf{R}_A|) F_{00}^{Bl'}(|\mathbf{r} - \mathbf{R}_B|)}{4\pi} q_{Al} q_{Bl'} d\mathbf{r} d\mathbf{r}' \quad (2.59)$$

The integral consists of two parts, the first (proportional to $1/|\mathbf{r} - \mathbf{R}_A|$) being long ranged, the second being more complex. For the exchange-correlation part we have to distinguish two cases. The radial functions F_{00}^{Al} and $F_{00}^{Bl'}$ drop off with the charge density of the atom they belong.

- If they are centered on different atoms ($A \neq B$) their overlap is small. The derivative of the exchange-correlation functional is always evaluated in $(n_0, 0)$ and brings always the same contribution.
- If they are centered on the same atom ($A = B$) the overlap is maximal and the so the exchange-correlation contributions to the total energy. The latter are called *on-site contributions* in this case.

To calculate the double integral in Eq. 2.59 we neglect at first the exchange correlation contribution and evaluate the long ranging part (proportional to $1/|\mathbf{r} - \mathbf{R}_A|$):

$$\gamma_{Al,B'l'} = \iint \frac{1}{|\mathbf{r} - \mathbf{r}'|} \frac{F_{00}^{Al}(|\mathbf{r} - \mathbf{R}_A|) F_{00}^{B'l'}(|\mathbf{r} - \mathbf{R}_B|)}{4\pi} d\mathbf{r} d\mathbf{r}' \quad (2.60)$$

For the radial function we use the ansatz:

$$F_{00}^{Al}(|\mathbf{r} - \mathbf{R}_A|) = \frac{\tau_{Al}^3}{4\sqrt{\pi}} e^{-\tau_{Al}|\mathbf{r} - \mathbf{R}_A|} \quad (2.61)$$

where τ_{Al} is a parameter we still have to determine. The exponential term drops off like a Slater-type basis function. Calculating the integral for $R = |\mathbf{R}_A - \mathbf{R}_B| \neq 0$ then gives⁶ [100]:

$$\gamma_{Al,B'l'} = \begin{cases} \frac{1}{R} - e^{-\tau_{Al}R} \Gamma(\tau_{Al}, \tau_{B'l'}, R) - e^{-\tau_{B'l'}R} \Gamma(\tau_{B'l'}, \tau_{Al}, R) & \text{if } \tau_{Al} \neq \tau_{B'l'} \\ \frac{1}{R} - e^{-\tau_{Al}R} \left(\frac{1}{R} + \frac{11\tau_{Al}}{16} + \frac{3\tau_{Al}^2 R}{16} + \frac{\tau_{Al}^3 R^2}{48} \right) & \text{if } \tau_{Al} = \tau_{B'l'} \end{cases} \quad (2.62)$$

Here we used the abbreviation:

$$\Gamma(a, b, R) = \left(\frac{b^4 a}{2(a^2 - b^2)^2} - \frac{b^6 - 3b^4 a^2}{(a^2 - b^2)^3 R} \right)$$

We can again distinguish two cases:

$R \rightarrow \infty$ In the case of very big atomic distances ($R \rightarrow \infty$) the expression 2.62 drops off like $1/R$. For this reason this part can be interpreted (neglecting the exchange correlation part of Eq. 2.54) as Coulomb interaction between the Mulliken charges q_{Al} of the atomic shells.

$R \rightarrow 0$ In the limit case of $R \rightarrow 0$ on the other side is given [99] by:

$$\gamma_{Al,B'l'} = \frac{\tau_{Al}\tau_{B'l'}}{2(\tau_{Al} + \tau_{B'l'})^3} ((\tau_{Al} + \tau_{B'l'})^2 + \tau_{Al}\tau_{B'l'}) + O(R) \quad (2.63)$$

And in particular for the atomic case $A = B$ we have:

$$\gamma_{Al,A'l'} = \frac{\tau_{Al}\tau_{A'l'}}{2(\tau_{Al} + \tau_{A'l'})} \left(1 + \frac{\tau_{Al}\tau_{A'l'}}{(\tau_{Al} + \tau_{A'l'})^2} \right) \quad (2.64)$$

as well as we have for the same atomic shell $l = l'$:

$$\gamma_{Al,Al} = \frac{5}{16} \tau_{Al} \quad (2.65)$$

here is $\gamma_{Al,Al}$ proportional to the parameter τ_{Al} . This is a constant specific for the electron of angular momentum l of each atomic type. We will show in one of the following sections that in the DFTB approximation the parameter τ_{Al} is identified with (and replaced by) the Hubbard U of the free atom, which also contains exchange-correlation contributions. Considering the exchange-correlation part of the integral 2.54 as not long-ranging, one only has in first approximation to consider the Hubbard U .

⁶In the reference the calculation is shown for a model in which all the atomic quantities do not depend on the angular momentum l but only on the atom A . This does not affect the evaluation of the integral, which being a mathematical operation can be obtained adding the opportune labels indicating each atomic shell. Dropping the angular momentum index the integral evaluation perfectly mirrors the one of the reference. This model was used in the earliest DFTB implementations then abandoned and finally re-adopted for the latter day DFTB implementations.

The coupling between shells with different angular momentum of the same atom is given by Eq. 2.64, depends also on the τ_{Al} of the single shells. The second term in the bracket can be in a rough approximation considered being unitary.

$$\gamma_{Al,A'l'} \approx \frac{1}{4} \left(\frac{2\tau_{Al}\tau_{A'l'}}{(\tau_{Al} + \tau_{A'l'})} \right) \quad (2.66)$$

The term in the bracket has the form of an harmonic medium between the τ_{Al} . Summarising, the term $E_{\delta n}$ depending from the charge fluctuation in Eq. 2.44) can be approximated with the expression:

$$E_{\delta n} = \frac{1}{2} \sum_A^M \sum_B^M \sum_{l \in A} \sum_{l' \in B} q_{Al} q_{B'l'} \gamma_{Al,B'l'} \quad (2.67)$$

where $\gamma_{Al,B'l'}$ is an analytical [21] function of the interatomic distance and of the Mulliken charges (which depends in turn on the tabulated elements of the overlap matrix and on the wave function coefficients) which approximates the Hartree and (spin unpolarised) exchange correlation contributions from the charge fluctuations. In this expression no integration appears anymore.

Magnetisation density fluctuations

The part of the total energy depending from the magnetisation density fluctuations differs from its charge density fluctuation dependent counterpart (Eq. 2.54) because it only contains exchange-correlation contributions.

$$E_{\delta m} = \frac{1}{2} \int \frac{\delta^2 E_{xc}}{\delta m^2} \Big|_{n_0,0} \delta m^2 d\mathbf{r} \quad (2.68)$$

In the evaluation of the latter we considered the exchange-correlation parts of it short ranged and therefore neglected it at first, even if at least part of the exchange and correlation is considered in the formalism through the atomic constants τ_{Al} . We have also seen (Eq. 2.62 to 2.66) that they are only important, when the charge density fluctuation in the integral 2.59 belong to the same atom. The exchange-correlation contributions in the charge density fluctuation dependent part of the total energy have also on-site character, even if they formally depend on two coordinates, \mathbf{r} and \mathbf{r}' . On the basis of similar considerations we assume that also the exchange-correlation contribution in the magnetisation density fluctuation dependent part of the total energy has a local character, i.e. it only depends on one position coordinate. In the framework of the on-site picture it is then correct to consider two spin densities of two different atoms not to be coupled through the integral 2.68. Following the schema of the previous section, we expand the magnetisation density fluctuations δm in the monopole approximation into a sum of atomic contributions:

$$\delta m(\mathbf{r}) = \sum_A^M \sum_{l \in A} p_{Al} f_{Al}(|\mathbf{r} - \mathbf{R}_A|) \quad (2.69)$$

Unlike the F_{00}^{Al} the radial functions f_{Al} are considered to be not overlapping. The coefficients p_{Al} are again labeled with the atomic index A and the angular momentum index l , which of course runs over all the angular momenta of the atom A . Proceeding in analogy with the previous section, the coefficients p_{Al} are identified with the differences between spin up and spin down Mulliken populations (see Eq. 2.58)

$$p_{Al} = q_{Al\uparrow} - q_{Al\downarrow} \quad (2.70)$$

Unfortunately, for the radial functions f_{Al} an ansatz similar to the one done for the F_{00}^{Al} (which were approximated by the expression 2.61) is not possible, because the magnetisation density can change its sign. Anyway, considering that the radial function do not overlap, inserting expression 2.69 in Eq. 2.68 leads to the expression:

$$E_{\delta m} = \frac{1}{2} \sum_A^M \sum_{l \in A} \sum_{l' \in A} p_{Al} p_{Al'} \int f_{Al} \left. \frac{\delta^2 E_{xc}}{\delta m^2} \right|_{n_0,0} f_{Al'} d\mathbf{r}. \quad (2.71)$$

As in this expression all the quantities are centered on the atom A , it arises the chance to identify the integral with an atomic constant $W_{Al'}$, which will be thoroughly discussed later in this chapter. Finally, we can express the magnetisation density fluctuation dependent contributions of the total energy as:

$$E_{\delta m} = \frac{1}{2} \sum_A \sum_{l \in A} \sum_{l' \in A} p_{Al} p_{Al'} W_{Al'} \quad (2.72)$$

In the spirit of the one-centre approximation in this expression are coupled the spin population on one atom A . Also in this expression do not appear any integrals.

2.5.3 The repulsive contribution

With the transformations and approximations introduced in the previous sections the total energy in the spin polarised DFTB method can be expressed as:

$$E_{\text{tot}} = \underbrace{\sum_{\sigma=\uparrow,\downarrow} \langle \psi_{i\sigma} | \hat{H}_0[n_0, 0] | \psi_{i\sigma} \rangle}_{E_{el.}^{\text{DFTB}}} + E_{\delta n} + E_{\delta m} + \quad (2.73)$$

$$E_{NN} + E_{xc}[n_0, 0] - \int v_{xc}[n_0, 0] n_0 d\mathbf{r} - \frac{1}{2} \iint \frac{n_0 n'_0}{|\mathbf{r} - \mathbf{r}'|} \quad (2.74)$$

We still have to evaluate the terms in the second row, which are the ionic repulsion and other contributions depending only from the reference charge density. These terms, collected together as E_{rep} are not calculated separately, although this would be possible knowing the reference charge density, but merged into one repulsive pair potential $U_{\text{rep}}(|\mathbf{R}_A - \mathbf{R}_B|)$, like in empirical tight-binding [88, 101]. This potential only depends on atomic separation and species, and is evaluated as the difference between the Kohn-Sham DFT total energy and the electronic part of the DFTB energy. For each chemical combination of atom pairs in our system of M atoms we have:

$$U_{\text{rep}}(|\mathbf{R}_A - \mathbf{R}_B|) = E_{\text{tot}}^{\text{KS}}(|\mathbf{R}_A - \mathbf{R}_B|) - E_{el.}^{\text{DFTB}}(|\mathbf{R}_A - \mathbf{R}_B|) \quad (2.75)$$

and the sum over all the atom pairs in the system gives the repulsive part of the energy:

$$E_{\text{rep}}(\{\mathbf{R}_I\}) = \sum_{A,B}^M U_{\text{rep}}(|\mathbf{R}_A - \mathbf{R}_B|) \quad (2.76)$$

For each combination of atomic species the pair repulsive potential $U_{\text{rep}}(|\mathbf{R}_A - \mathbf{R}_B|)$ is calculated (as $E_{\text{rep}} = E_{\text{tot}} - E_{el.}^{\text{DFTB}}$) for a fit system in a chosen interval of interatomic separations and tabulated. Thereby E_{tot} is identified with the DFT $E_{\text{tot}}^{\text{KS}}$ or alternatively calculated with a state equation for the system of interest if experimental parameters are available. A discussion about the features of the repulsive potential and the choice of the fit system can be found in the chapter dedicated to the parameter generation.

2.5.4 Total energy and potential

Now that we have described all of the parts of the Eq. 2.44, we can write the expression for the total energy within the spin polarised DFTB approximation as sum of four contributions:

$$\begin{aligned}
 E_{\text{tot}} &= \sum_{\sigma=\downarrow,\uparrow} \sum_i^{\text{occ.}} n_{i\sigma} \langle \psi_{i\sigma} | \hat{H}_0[n_0, 0] | \psi_{i\sigma} \rangle + E_{\delta n} + E_{\delta m} + E_{\text{rep}} = \\
 &\sum_{\sigma=\uparrow,\downarrow} \langle \psi_{i\sigma} | \hat{H}_0[n_0, 0] | \psi_{i\sigma} \rangle + \frac{1}{2} \sum_A^M \sum_B^M \sum_{l \in A} \sum_{l' \in B} q_{Al} q_{Bl'} \gamma_{Al} \gamma_{Bl'} + \\
 &+ \frac{1}{2} \sum_A \sum_{l \in A} \sum_{l' \in A} p_{Al} p_{Al'} W_{All'} + E_{\text{rep}} \tag{2.77}
 \end{aligned}$$

Practically we have replaced the charge density fluctuations with the Mulliken charges and the magnetisation density charges with the difference of the Mulliken spin populations. They are easily determined, as the overlap matrix elements are tabulated. The zeroth-order Hamilton operator depends now only from the reference charge density, the Mulliken charges q_{Al} enter in the second term while the third term gives the energy dependence from the spin polarisation through the Mulliken spin-populations. The fourth term, the repulsive potential, only depends on the ionic coordinates. Neglecting both fluctuation dependent terms one gets an expression which only depends on the reference charge density and which corresponds to the traditional tight binding calculation schemes. However, it fails in the correct description of systems with important charge transfer and the possibility of considering spin-polarisation effects is lost.

2.5.5 Determination of the constants τ_{Al} and $W_{All'}$

In the expression 2.77 for the total energy the constants τ_{Al} which appear in the algebraic functions $\gamma_{Al,Bl'}$ and the spin $W_{All'}$ constants for the the calculation of the spin polarisation energy have not been determined yet. This can be done starting from the atomic case, for which the total energy is:

$$\begin{aligned}
 E_{\text{tot}} &= \sum_{\sigma=\downarrow,\uparrow} \sum_i^{\text{occ.}} n_{i\sigma} \langle \psi_{i\sigma} | \hat{H}_0[n_0, 0] | \psi_{i\sigma} \rangle + \frac{1}{2} \sum_{l \in A} \sum_{l' \in A} q_{Al} q_{Al'} \gamma_{Al} \gamma_{Al'} + \\
 &+ \frac{1}{2} \sum_{l \in A} \sum_{l' \in A} p_{Al} p_{Al'} W_{All'} \tag{2.78}
 \end{aligned}$$

The constants τ_{Al} of the charge density fluctuation

From Eq. 2.64 and Eq. 2.65 follows that the constants τ_{Al} have to be determinate for every shell with different angular momentum of each different atom type, to generate the functions $\gamma_{Al,Bl'}$. At first though we will address some particular issues about the Mulliken charges q_{Al} and the Mulliken spin populations p_{Al} in the atomic case. A differentiation with respect to the variables q_{Al} can be replaced by a differentiation with respect to the total Mulliken population ($p_{Al\uparrow} + p_{Al\downarrow}$): they will only differ by an additive constant (see Eq. 2.57). The overlap matrix $S_{\mu\nu}$ is a diagonal matrix, whose entries are given through the Kronecker-Symbol $\delta_{\mu\nu}$. The basis functions are determined as eigenvectors of the pseudo-atomic problem (see Eq. 2.47) and the eigenvalues to the angular momentum l are $(2l + 1)$ time degenerated. The degeneration does not matter here and in the following, because in the calculation of the Mulliken population the sum runs over all degenerate orbitals. Therefore we can substitute the index i with the angular momentum label l in the eigenvalues of the Eq. 2.47. With this consideration the whole Mulliken spin population is then equal to the corresponding occupation number:

$$p_{Al\sigma} = n_{i\sigma} \quad \text{and} \quad p_{Al\uparrow} + p_{Al\downarrow} = n_{i\uparrow} + n_{i\downarrow} = n_i \tag{2.79}$$

The spin polarisation will not matter in the following, as our starting point are not spin polarised pseudo atoms. The $n_{i\sigma}$ are then all the same and their sum can be replaced by an occupation number n_i . Differentiating twice the Eq. 2.78 respect to q_{Al} and considering the Eq. 2.65:

$$\frac{\partial E_{\text{tot}}^A}{\partial q_{Al}^2} = \frac{\partial E_{\text{tot}}^A}{\partial n_i^2} = \gamma_{Al,Al} = \frac{5}{16} \tau_{Al} \quad (2.80)$$

On the other hand, Janak's theorem [70] says that differentiating the DFT $E_{\text{KS}}^{\text{tot}}$ with respect to the occupation numbers gives:

$$\frac{\partial E_{\text{tot}}^{\text{KS},A}}{\partial n_i^2} = \frac{\partial \varepsilon_i}{\partial n_i} \quad (2.81)$$

If we now consider⁷ the *highest occupied molecular orbital* (HOMO), we have:

$$\frac{\partial \varepsilon_{\text{HOMO}}}{\partial n_{\text{HOMO}}} \approx U_A = I_A - A_A \quad (2.82)$$

which is the so called Hubbard- U of the atom. This is also the *chemical hardness* of the atom, defined as the difference between ionisation potential I and electronic affinity A [63]. It can be also be interpreted as the energy used to extract an electron from the atom (and put it elsewhere). The concept of Hubbard U should be now generalised for the shells of each angular momentum:

$$U_{Al} = \frac{\partial \varepsilon_l}{\partial n_l} \quad (2.83)$$

As before, it was considered that the index i of the eigenvalues can be substituted by the angular momentum label l if the degeneration of the magnetic quantum number does not play any role. Inserting Eq. 2.80 in Eq. 2.81

$$\gamma_{Al,Al} = \frac{5}{16} \tau_{Al} = \frac{\partial \varepsilon_l}{\partial n_l} = U_{Al} \quad (2.84)$$

As we used the atomic KS DFT total energy for the determination of the τ_{Al} , atomic exchange-correlation contributions are kept in account. For this reason neglecting the exchange-correlation contributions in Eq. 2.59 only has a relative meaning.

The constants $W_{Al'}$ of the magnetisation density fluctuation

Also the spin constants $W_{Al'}$ can be determined differentiating the atomic DFT total energy and using the expression 2.78. However it is convenient to operate a variable change, from the set of independent variables charge density and magnetisation density $\{n(\mathbf{r}), m(\mathbf{r})\}$ to the set of independent variables spin up and spin down electronic densities $\{n_{\uparrow}(\mathbf{r}), n_{\downarrow}(\mathbf{r})\}$. Keeping in mind the considerations of the previous section about the atomic case, this variable change means a change in the occupation numbers from $\{(n_{i\uparrow} + n_{i\downarrow}), (n_{i\uparrow} - n_{i\downarrow})\}$ to $\{n_{i\uparrow}, n_{i\downarrow}\}$. Furthermore we have to consider that all the elements and not only the ones of the shell of some angular momentum have to be determined. Differentiation leads to:

$$\frac{\partial^2 E_{\text{tot}}^A}{\partial p_{Al} \partial p_{Al'}} = \frac{1}{4} \left(\frac{\partial^2}{\partial n_{l\uparrow} \partial n_{l'\uparrow}} \frac{\partial^2}{\partial n_{l\downarrow} \partial n_{l'\downarrow}} \frac{\partial^2}{\partial n_{l\uparrow} \partial n_{l'\downarrow}} \frac{\partial^2}{\partial n_{l\downarrow} \partial n_{l'\uparrow}} \right) E_{\text{tot}}^A = W_{Al'} \quad (2.85)$$

And using the spin-polarised version of the Janak's theorem, differentiating the KS DFT atomic total energy leads to:

$$\begin{aligned} \frac{1}{4} \left(\frac{\partial^2}{\partial n_{l\uparrow} \partial n_{l'\uparrow}} \frac{\partial^2}{\partial n_{l\downarrow} \partial n_{l'\downarrow}} \frac{\partial^2}{\partial n_{l\uparrow} \partial n_{l'\downarrow}} \frac{\partial^2}{\partial n_{l\downarrow} \partial n_{l'\uparrow}} \right) E_{\text{tot}}^{\text{KS},A} = \\ \frac{1}{4} \left(\frac{\partial \varepsilon_{l\uparrow}}{\partial \varepsilon_{l'\uparrow}} + \frac{\partial \varepsilon_{l\downarrow}}{\partial \varepsilon_{l'\downarrow}} - \frac{\partial \varepsilon_{l\downarrow}}{\partial \varepsilon_{l'\uparrow}} - \frac{\partial \varepsilon_{l\uparrow}}{\partial \varepsilon_{l'\downarrow}} \right) = \frac{1}{2} \left(\frac{\partial \varepsilon_{l\uparrow}}{\partial \varepsilon_{l'\uparrow}} - \frac{\partial \varepsilon_{l\downarrow}}{\partial \varepsilon_{l'\downarrow}} \right) \end{aligned} \quad (2.86)$$

⁷We are of course considering atoms and not molecules. For the sake of simplicity we use in this work the denomination of HOMO for the highest occupied atomic orbital, as today is usual in the literature.

Where the last transformation is based on the symmetry of both spin states at the moment of the choice of the not spin polarised System as reference. Inserting Eq. 2.85 in Eq. 2.86 leads to the expression for the determination of the $W_{ll'}$:

$$W_{ll'} = \frac{1}{2} \left(\frac{\partial \varepsilon_{l\uparrow}}{\partial \varepsilon_{l'\uparrow}} - \frac{\partial \varepsilon_{l\downarrow}}{\partial \varepsilon_{l'\downarrow}} \right) \quad (2.87)$$

A further discussion about the determination of the U_{Al} and $W_{ll'}$ can be found in the chapter dedicated to the parameter generation.

2.5.6 Hamilton operator and self consistency

Applying the variational principle, the total energy expression 2.77 is differentiated with respect to the wave function coefficients $c_{\mu i \sigma}^*$ [24, 87]) The particle-conservation is kept in account by the Lagrange multipliers $\varepsilon_{i\sigma}$:

$$\frac{\delta}{\delta c_{\mu i \sigma}^*} \left(E_{tot} - \varepsilon_{i\sigma} \left(N_{\sigma} - \sum_i \frac{occ.}{2} n_{i\sigma} \sum_{\zeta} \sum_{\eta} (c_{\zeta i \sigma}^* c_{\eta i \sigma} S_{\zeta \eta} + c_{\zeta i \sigma} c_{\eta i \sigma}^* S_{\eta \zeta}) \right) \right) = 0 \quad (2.88)$$

where N_{σ} is the number of electrons with spin σ . We get a secular equation for the coefficients $c_{\nu i \sigma}$ of the wave functions:

$$\sum_{\nu} c_{\nu i \sigma} \left(\hat{H}_{\mu \nu \sigma} - \varepsilon_{i\sigma} S_{\mu \nu} \right) = 0 \quad (2.89)$$

with Hamiltonian matrix elements:

$$\begin{aligned} \hat{H}_{\mu \nu \sigma} = & \hat{H}_{\mu \nu}^0 + \frac{1}{2} S_{\mu \nu} \sum_C \sum_{l' \in C}^M (\gamma_{A(\mu)l(\mu), Cl'} + \gamma_{B(\nu)l(\nu), Cl'}) q_{cl'} + \\ & + \delta_{\sigma} \frac{1}{2} S_{\mu \nu} \left(\sum_{l' \in B(\mu)} W_{B(\mu)l(\mu)l'} P_{B(\mu)l'} + \sum_{l' \in B(\nu)} W_{B(\nu)l(\nu)l'} P_{B(\nu)l'} \right) \end{aligned} \quad (2.90)$$

and overlap matrix elements:

$$S_{\mu \nu} = \langle \varphi_{\mu} | \varphi_{\nu} \rangle \quad (2.91)$$

We have used the symbol $\delta_{\sigma} = \pm 1$. The sign + has to be used for spin up electrons and the sign - for spin down electrons. The Hamiltonian matrix consists like the total energy of three parts:

- The matrix elements of the 0th-order Hamilton operator $\hat{H}^0[n_0, 0]$ are stored in dedicated tables.
- With the second term on the right side of the 2.90 the effects of the charge density fluctuation are considered: the intra-atomic as well as the inter-atomic matrix elements are influenced. All the Coulomb interactions are considered through the sum over all the atoms (C) of the system with $A(\mu)$ and $B(\nu)$, weighted with the overlap matrix $S_{\mu \nu}$ and added as correction to the zeroth-order matrix elements.
- The spin polarisation part of Eq. 2.90 couples magnetisation densities of different atoms together. Unlike the correction due to the charge density fluctuations here only the terms on both atoms $A(\mu)$ and $B(\nu)$ are considered. The corrections to the zeroth-order matrix elements are likewise weighted with the overlap matrix. The magnetisation density fluctuation corrections differ from the charge density fluctuation corrections because one atom each time is considered and not all together (in the second term of the right side of 2.90 there is a

double sum which runs over all atoms while in the third term there is a single sum). This has a damping effect on the interactions in comparison to the charge density case⁸.

Note that this expression, which is the one used throughout this work, slightly differs from the one reported in the work of Frauenheim *et al.* [88], as the one center spin approximation in the potential has been dropped. In that work applying the one-center approximation at 2.90 the Hamilton operator:

$$\begin{aligned} \hat{H}_{\mu\nu} = & \hat{H}_{\mu\nu}^0 + \frac{1}{2} S_{\mu\nu} \sum_C^M \sum_{l'' \in C} (\gamma_{A(\mu)l(\mu),Cl''} + \gamma_{B(\nu)l(\nu),Cl''}) q_{cl''} + \\ & + \delta_\sigma \delta_{\mu\nu} \sum_{l'' \in A(\mu)} W_{A(\mu)l(\mu)l''} p_{Al''} \end{aligned} \quad (2.92)$$

was proposed. This operator was also derived starting from the Eq. 2.59 and considering spin densities of different atoms not overlapping and therefore non interacting. This operator has the advantage to be (especially in the case of periodic boundary conditions) easy to implement, as the spin-dependent correction do affect only diagonal matrix elements (because of the Kronecker delta $\delta_{\mu\nu}$). The Hamiltonian matrix elements in the Eq. 2.90 depends through the Mulliken spin population on the wave function coefficients $c_{\nu i \sigma}$, which have to be determinate with Eq. 2.89. Therefore the problem must be solved self consistently: starting from a "good guess" the secular equation is solved, new Mulliken populations are calculated and with them a new Hamiltonian matrix constructed. The latter is introduced in turn on the secular equation and the process is repeated as long as the solution does not change considerably anymore, i.e. self consistency is reached. Like in the spin-DFT two sets of secular equations have to be solved, one for the spin up and one for the spin down electrons, which lead to different coefficients for spin up and spin down wave functions. This has the consequence that the spin up and spin down could be spatially different. This increases the number of freedom degrees and lowers the total energy. Similarly there will be a different potential for spin up and spin down electrons, which leads to the splitting of the one particle levels for spin up and spin down electrons.

2.5.7 Calculation of the forces

It is possible to calculate the force F_C acting on the atom C analytically. To derive the analytical expression of the force it is necessary to differentiate the expression 2.77 for the total energy with respect to the ionic coordinates R_C . As not only Hamilton and overlap matrix elements depend on the ionic coordinates, but also the wave function coefficients, it is necessary to impose the charge conservation as auxiliary constraint. This is done like in Eq. 2.88 introducing the Lagrange multipliers⁹ $\varepsilon_{i\sigma}$:

$$F_C = -\frac{\partial}{\partial \mathbf{R}_C} \left(E_{tot} - \sum_{\sigma=\downarrow,\uparrow} \sum_i^{occ.} \frac{1}{2} n_{i\sigma} \varepsilon_{i\sigma} \left(\sum_{\mu} \sum_{\nu} (c_{\mu i \sigma}^* c_{\nu i \sigma} S_{\mu\nu} + c_{\mu i \sigma} c_{\nu i \sigma}^* S_{\mu\nu}) - 1 \right) \right) \quad (2.93)$$

And with a little algebra:

⁸In the case of transition metals for example the overlap matrix elements of the d -electrons (which bear the atomic spin moment) at equilibrium distance of the order of magnitude of 10^{-2} . This is an order of magnitude smaller than for s -electrons. Furthermore the constants $W_{Al'}$ are an order of magnitude smaller than the τ_{Al} .

⁹Considering the secular equation 2.89 the wave function coefficients will vanish. This can be interpreted as consequence of the fact that Eq. 2.88 guarantees the presence of an extremum. Any dependence of the occupation number from the atomic coordinates is neglected, which is correct for systems with a non-zero band gap and without extreme Fermi-smearing of the occupation numbers when coupled with an external thermic bath.

$$\begin{aligned}
 F_C = & - \sum_{\sigma=\downarrow,\uparrow} \sum_i^{occ.} n_{i\sigma} n_{i\sigma} \sum_{\mu\nu} \left(\frac{\partial H_{\mu\nu}^0}{\partial \mathbf{R}_C} + \frac{1}{2} \frac{\partial S_{\mu\nu}}{\partial \mathbf{R}_C} \sum_B \sum_{l' \in B} (\gamma_{A(\mu)l(\mu),Bl'} + \gamma_{A(\nu)l(\nu),Bl'}) q_{Bl'} + \right. \\
 & \left. + \frac{1}{2} \delta_\sigma \frac{\partial S_{\mu\nu}}{\partial \mathbf{R}_C} \left(\sum_{l \in A(\mu)} W_{A(\mu)ll'(\mu)} P_{A(\mu)l} + \sum_{l \in A(\nu)} W_{A(\nu)ll'(\nu)} P_{A(\nu)l} \right) - \varepsilon_{i\sigma} \frac{\partial S_{\mu\nu}}{\partial \mathbf{R}_C} \right) + \\
 & - \sum_{l \in C} q_{Cl} \sum_B \sum_{l'} q_{Bl'} - \frac{\partial \gamma_{Cl,Bl'}}{\partial \mathbf{R}_C} - \frac{\partial E_{rep}}{\partial \mathbf{R}_C}
 \end{aligned} \tag{2.94}$$

2.5.8 An LDA+ U -like approach in DFTB

While it has previously been suggested that for *empirical* tight-binding the effects of on-site correlation can be mimicked by an empirical adjustment of symmetry resolved on-site energies [102], this is problematic for example for low symmetry d electron systems, or for f manifolds. In the RE ions of interest here, the so-called fully localised limit should be achieved (i.e. the orbital occupations of states localised within the $4f$ manifold should be either be 0 or 1 [76, 77]). However we also wish to test the AFM-like limit as well. In the simplest rotationally invariant form of LDA+ U [103] the correction to the LDA potential is of the form:

$$\Delta V_{\mu\nu}^\sigma = -(U - J)_l (n_{\mu\nu}^\sigma - DC[n_{\mu\nu}^\sigma])_{\mu\nu \in l} \tag{2.95}$$

Where n^σ is the local spin occupation matrix within a given atomic manifold, and $(U - J)$ is the screened and spherically averaged electron-electron interaction. $DC[n]$ is the double counting term, and the two limiting cases FLL and AMF are

$$\begin{aligned}
 DC_{\mu\nu}^\sigma[n]^{FLL} &= \frac{1}{2} \delta_{\mu\nu} \\
 DC_{\mu\nu}^\sigma[n]^{AMF} &= \frac{Tr(n_{\mu\nu})}{2l + 1} \delta_{\mu\nu}
 \end{aligned}$$

Where l is the angular quantum number. $(U - J)$ is usually taken to be either an adjustable parameter or from a constrained DFT calculation. We instead present a prescription for choosing U and J from atomic calculations. Since the DFTB energy aims to be a reasonable approximation to the LDA energy it seems sensible to adopt the form of the LDA+ U energy correction unchanged for DFTB. There is then the issue of how to choose the on-site occupation matrix [104] for a non-orthogonal basis. In the on-site case the modification to the total energy and the DFTB Hamiltonian can be written in terms of atomic sub-blocks of the single-particle density matrix ($\rho_{\mu\nu \in l \in A}$), while for the dual basis case, the occupation matrix takes the form of a generalisation of Mulliken charges:

$$n_{\mu \in l \in A, \nu \in l \in A}^\sigma = \frac{1}{2} \sum_B \sum_{\tau \in B} (S_{\mu\tau} \rho_{\tau\nu} + \rho_{\mu\tau} S_{\tau\nu}) \tag{2.96}$$

where the diagonal of the resulting occupation matrices are then basis-function resolved Mulliken charges.

2.5.9 A pSIC-like approach in DFTB

Full self-interaction corrected (SIC) LDA is relatively expensive, hence several cheaper approximations have appeared. In DFTB we adopt an approximation of the full SIC based on the method proposed by Vogl [105] and its recent refinements [106, 107], which is referred to as pseudo-SIC (or pSIC) as it only includes contributions near to atoms. Since the majority of the self-interaction

error, in the case of interest, is local in character this hopefully captures the majority of the error. To ensure that for single electrons the Coulomb and exchange-correlation terms are canceled out exactly, the exchange-correlation potential is modified by subtracting off the local self-interaction in this basis:

$$\Delta V_{\mu,\text{pSIC}}^{\sigma} = -\alpha V_{\mu,\text{H+XC}}^{\sigma}[n_{\mu}(\mathbf{r}), m_{\mu}(\mathbf{r})] \quad (2.97)$$

To make calculations of the potential tractable $V_{\text{H+XC}}$ is approximated as that for a single, fully occupied and completely spin-polarised state $V_{\text{H+XC}}^{\sigma}[n(\mathbf{r}), m(\mathbf{r})] = V_{\text{H+XC}}^{\sigma}[1, 1]$. The pre-factor α allows an additional scaling of the potential for example to account for electronic relaxation on electron removal ($\alpha = \frac{1}{2}$ in the work of Filippetti and Spaldin, however this is incorrect for a system with a single electron [107]). As yet, no energy expression related by variational principle to the potential is available [106, 107], hence no expression for inter-atomic forces has been derived. In the following we will derive such an expression from similarities between the LDA+ U and pSIC formalism. Eq. 2.97 is not invariant to unitary transforms, however, similar to the original LDA+ U formalism [108], this can be achieved by using the density matrix formulation.

$$\Delta V_{\text{pSIC}\mu\nu}^{\sigma} = -\alpha V_{\text{H+XC}}^{\sigma}[1, 1] n_{\mu\nu}^{\sigma} \quad (2.98)$$

Due to the similarity in the functional of the potential to LDA+ U , we can write an energy expression in matrix form (which *is* directly connected to the potential) as:

$$\Delta E^{\text{pSIC}} = -\alpha \sum_{\sigma} V_{\text{H+XC}}^{\sigma}[1, 1] \text{Tr}(n^{\sigma} \cdot n^{\sigma}) \quad (2.99)$$

In these approximations, pSIC is written as a type of non-double counted LDA+ U (i.e. $DC[n]$ is absent from Eq. 2.95), without ambiguity in the choice of (U - J) since the pre-factor comes from the exchange-correlation potential. Additionally, atomic forces can be derived [104]. This has some similarity to the Atomic Self Interaction Correction (ASIC) form of Pemmaraju *et al.* [107], however they do not provide a variationally connected energy.

2.5.10 Connection between LDA+ U and pSIC

In the following we will discuss a connection between LDA+ U in its FLL-version and pSIC that allows a further simplification of the latter approach in a tight-binding scheme. The starting point of this discussion is Eq. 44 of Anisimov *et al.* [16] relating the atomic Slater integral F^0 and the exchange J , to the LDA potential for an atomic state as:

$$V_{\text{H+XC}}^{\sigma} = F^0 N - \frac{1}{2} (F^0 - J) - J N_{\sigma}. \quad (2.100)$$

Thus for the orbital occupation choices for which $V_{\text{H+XC}}$ is needed in pSIC ($V_{\text{H+XC}}[1, 1]$, i.e., $N = N_{\sigma} = 1$) the spherically symmetric part of the exchange-correlation potential is given by:

$$V_{\text{H+XC}}^{\sigma}[1, 1] = \frac{F^0 - J}{2}.$$

In DFTB, we use U in the SCC-DFTB correction (section 2.5.2) that is related to the screened F^0 Slater integral [16]. If we moreover assume in the zeroth limit that screening in the isolated atom, for which U is calculated, is small, F^0 can be substituted by U . Similarly the diagonal part of the spin coupling matrix, $W_{ll'}\delta_{ll'}$, given in section 2.5.2, is equivalent to J_l . We thus obtain for the basis that is used to expand the local states in pSIC:

$$V_{\text{H+XC}}^{\sigma}[1, 1] \approx \frac{(U - J)_{\text{atomic}}}{2}. \quad (2.101)$$

In this approximation, pSIC then gives a contribution to the potential of:

$$(\text{pSIC}) \Delta V_{\mu\nu}^{\sigma} = -\alpha \frac{(U - J)_{\text{atomic}}}{2} n_{\mu\nu}^{\sigma}. \quad (2.102)$$

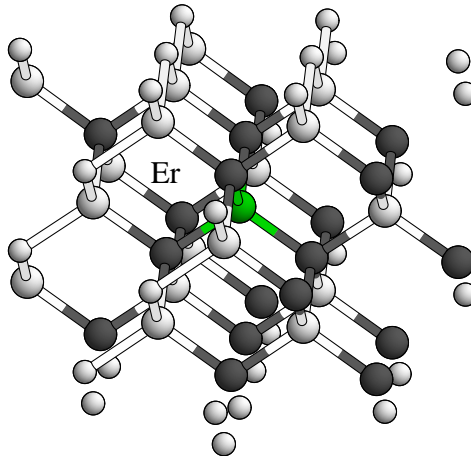


Figure 2.4: Simulating a defect (the erbium atom in green) within a cluster of the host material whose surfaces (in the picture only top and bottom) are passivated with pseudo-hydrogens.

For a system with a Hubbard gap, the relaxation corrected form of pSIC ($\alpha = \frac{1}{2}$) would apply the same potential to the lower Hubbard band as obtained by a FLL-LDA+ U contribution of:

$$\text{(FLL)} \quad \Delta V_{\mu\nu}^{\sigma} = -\frac{(U - J)_{\text{atomic}}}{2} \left(n^{\sigma} - \frac{1}{2} \right), \quad (2.103)$$

since the eigenvalues of the n^{σ} matrix are either 0 or 1, so the occupied states in the local manifold experience a net downward shift of:

$$-\frac{(U - J)_{\text{atomic}}}{4}.$$

This suggests, in comparison with Eq. 2.35, that the LDA+ U and relaxation-corrected pSIC have the same effect on the occupied band-structure, and that

$$(U - J) = \frac{(U - J)_{\text{atomic}}}{2}$$

is a sensible first choice for the parameters in LDA+ U . This agrees with the (empirical) choice of $\approx 0.5 \times (U - J)_{\text{atomic}}$ being suitable for many LDA+ U applications [16, 78]. Since there are different potentials for unoccupied states in pSIC and FLL-LDA+ U these methods give different gaps [107] and different total energy corrections (compare Eq. 2.34 and 2.99). All of the above corrections share the feature that they are semi-local (decaying on the length scale of the overlap matrix in the dual basis form), hence they can not fully address non-local effects such as the derivative discontinuity in Kohn-Sham theory [109, 110].

2.6 Modeling defects

Goal of the defect physics is to simulate how the presence of a defect influences the physical properties of the host. The system to study is then a single defect embedded in the host, an ideal crystal, which is an ordered array of atoms periodically repeated in the space. Now, the number of atoms in a real crystal is far too big to be simulated with usual atomistic simulation, which can only deal with a certain number of atoms, this number depending from the available calculation power and calculation schemes. Only a limited region around the defect can be described, and this is done mainly with two different strategies.

The first way is to use a cluster consisting of a part of the lattice containing the defect whose surfaces are passivated by pseudo-hydrogen atoms (see Fig. 2.4). The passivation is necessary to

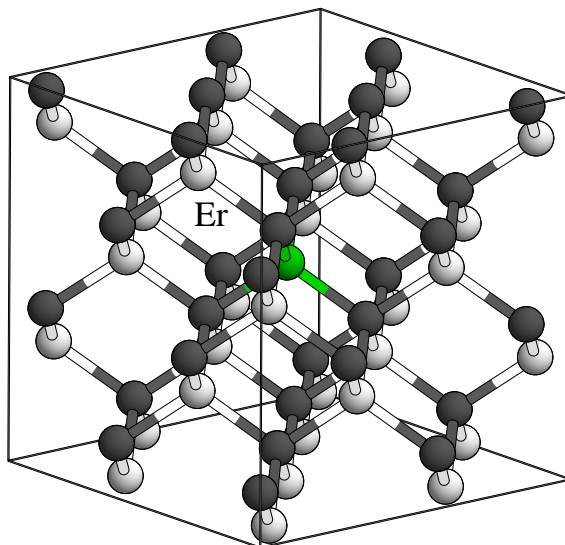


Figure 2.5: *Simulating a defect (the erbium atom in green) with the supercell method, results in a super-lattice of defects, which can interact if the supercell is not chosen big enough.*

avoid the dangling bonds in the surface atoms. Position and charge of the pseudo-hydrogens are chosen in order to reproduce the same environment that the outer atoms of the cluster would have in the bulk. The used cluster should be quite big and possibly have spherical form in order to minimise the ratio of volume-surface and the surface effects. Nonetheless the result of the simulation depends on the position of the defect within the cluster and on the symmetry of the cluster itself. Changes of the cluster form and in the distance of the defect from the passivated surface, which can happen during the relaxation, are often important sources of error. Increasing the dimensions of the cluster reduces these geometrical effects but increases the calculation time and the surface effects. The second method arises from the consideration that for the description of an isolated defect the simulation of an infinitely extended crystal would come closer to real conditions. Infinite perfect crystals can be simulated with periodic boundaries. This is achieved by the use of supercells, a finite array of atoms repeated in the space. Practically it is assumed that the margin atoms of the supercell are neighbours of the margin atoms on the opposite side of the supercell and can interact with them. When we now put a defect in the supercell we can simulate it without fearing artificial interactions with surfaces. The problem is that in this way we are no longer simulating an isolated defect, because when the supercell is repeated in the space the defect and its images in neighbouring cells form a super-lattice of defects, with a geometry and a "lattice constant" given from the supercell vectors. If the cell is not big enough spurious interaction of the defect with its periodic image may arise, whose effect and correction is still argument of debate. In small cells also the form of the cell may influence the result. Increasing the dimension of the supercell makes the error induced from this effects negligible, but as increasing the number of atoms in the system increases the computational power required, one has to find a good compromise between time invested and precision. One big advantage of the DFTB approach is that it allows the handling of very big cells and makes the spurious interactions of one charged defect with its periodic images really negligible. In this work we will use mainly 512 and 256-atoms supercells, where the defects in two neighbouring cells are separated by 17.5 Å and their interactions can be considered negligible.

2.7 Summary and conclusions

We presented an efficient calculation scheme in framework of the SCC-DFTB for the simulation of strongly correlated electrons and discussed its new extensions to include orbital dependent po-

tentials. The implementation of LDA+ U and pSIC methods in the DFTB code is certainly an important advance for many problems where DFT-like methods fail to reproduce the experimental observations. This implementation is essential for problems involving some transition metal oxides or rare earths. Combining DFTB methods and LDA+ U allows handling highly correlated electrons for very large systems with a calculation quality close to the one of DFT. This is particularly interesting for the case of lanthanides in GaN where dilute amount of RE are used. DFTB can easily handle the huge unit cell size that is necessary to represent the experimental system and properly reproduce the effect of the stress induced by rare earth doping in particular on the electronic structure. Concluding, the capability of the method to carry out spin polarised calculations as well as its capability to treat strong correlated systems in a proper way with an LDA+ U like approach make DFTB a powerful tool for the systematic study of the RE defects and defect complexes in GaN. In the last part of this chapter reviewed the Janak transition state formalism for the calculation of charge transition states on the basis of the one particle levels. The formalism has been proven to work within the DFTB framework and in particular in connection with LDA+ U , which guarantees that the requirements for the applicability of the formalism are satisfied.

Chapter 3

Parameterization

In the previous chapter the LDA+ U and pSIC approaches have been adapted to the tight-binding formalism and implemented in the simulation package DFTB. The next step of our study on rare earth impurities in GaN is the creation of the DFTB parameters for the RE ions and for the host. The issue of the parameter generation is a central point in the DFTB approach, because in this phase the precision of the method is determined. It can be affirmed indeed, that the method is as good as the parameters are. The process of parameterisation can be in principle lead back to the classic problem of minimizing the value of a function in a multi-parameter space. In the actual realisation of a parameter set many complications may occur which introduce errors and uncertainty. We try in this phase to eliminate or minimise every source of error. The latter is mainly due to three factors:

- approximation in the methods
- bad reference data
- incomplete optimization

The first type of error is an intrinsic error which cannot be eliminated but can be minimised. For example, choosing as fit system for a particular interaction a system which is known to be a pitfall for DFTB (e.g. high coordinated bulks) will negatively affect the quality of the created parameter. The second typology of error is due to uncertainties in the data used to fit the parameters: it can be an error in the measurement of some physical characteristic of a reference system as well as an error due to bad pseudopotentials in the *ab initio* calculations we take as reference. The third factor of error is present when too few fit systems are considered, or if the optimisation is only done with respect to one particular parameter only. This source of error can be completely removed in the parameterisation process. Apart from these three factors, there is no room for other error sources. Coming to the particular case of the RE, the main problem is the lack of reliable reference data. For this reason different semi-empiric methods (e.g. MOPAC) cannot be used for the simulation of RE compounds: the parameter for these ions have never been created. The advantage of DFTB is that only few, possibly well chosen systems are needed to create the parameters. In DFTB fit systems can also be purely ideal systems, if they are chemically acceptable and can be described with an *ab initio* approach. What we would like to have are parameters which allow the correct description of as many systems as possible, i.e. we would like to have portable parameters. Good parameters have to work without restrictions. This is unluckily not always possible. If a parameter is created using a fit system of a certain type, it would be hardly correctly describe systems which are very different from the fit system. In our work we paid particular attention in the generation of parameters which are reliable in the description of solid state systems and for defect physics. In this chapter we show the process of generation of a set of DFTB parameters for the modeling of RE in GaN. After showing how this has been done we propose a validation of the parameters, i.e. we report the results of the reliability tests that created parameters have to pass.

Table 3.1: Orbitals treated as valence orbitals in the parameterisation of the studied elements. Including more orbitals in the valence makes each calculation more accurate but more computationally demanding. Covalent radii are listed here in Å and used as reference for the following discussions.

Ion	Cov. radius (Å)	El. configuration	Basis
H	0.37	$1s^1$	$1s$
C	0.77	$[He]2s^2 2p^2$	$2s 2p$
N	0.75	$[He]2s^2 2p^3$	$2s 2p$
O	0.73	$[He]2s^2 2p^4$	$2s 2p$
Ga	1.26	$[Ar]3d^{10} 4s^2 4p^1$	$4s 4p (3d)$
Pr	1.65	$[Xe]4f^3 6s^2$	$6s 6p 5d 4f$
Eu	1.85	$[Xe]4f^7 6s^2$	$6s 6p 5d 4f$
Gd	1.61	$[Xe]4f^7 5d^1 6s^2$	$6s 6p 5d 4f$
Er	1.57	$[Xe]4f^{12} 6s^2$	$6s 6p 5d 4f$
Tm	1.56	$[Xe]4f^{13} 6s^2$	$6s 6p 5d 4f$

3.1 Generation of the parameters

In this work we elaborate a set of DFTB parameters for the modeling of RE in GaN. It includes the interactions needed for the simulation of GaN and its "classical" dopants (C and O) as well as those lanthanides which are known for their peculiar emission spectra (Pr, Eu, Er, Tm) or which have been exploited for the realisation of spintronic devices (Eu, Gd) because of their magnetic properties.

3.1.1 The electronic part

The DFTB parameters are divided in three sections: a header, containing atomic informations like on-site energies, Hubbard- U and valence charge, a body, containing the proper SK-tables (20 columns for the Hamiltonian and 20 columns for the overlap matrix elements) and a spline for the storage of the repulsive potential. The first two parts contain informations needed for the calculation of the DFTB electronic energy (also called band-structure energy), while the third part is needed for the calculation of the repulsive energy (Eq. 2.76). We firstly report information about the creation of the electronic part of the parameters.

Electronic configuration

Before we start the generation of the Slater-Koster tables necessary to the DFTB method, we have to make some basic decision, the first of them being the electronic configuration of the chosen elements. More precisely we have to decide which orbitals we consider as core and which are instead valence, i.e. we determine the orbital basis (see Eq. 2.47 and 2.50) used in all the future calculations. The choice of the electrons we treat as valence states influences the accuracy of the method but also the speed of the calculation. Even if it is possible to create parameter for ions in different electronic configurations, we choose to parameterise all the elements, including the lanthanides, in their atomic ground state. This choice is consistent with the experimental evidence that RE ions behave in GaN host as isolated ions. The f -shell has been treated as a valence shell and can be therefore depleted (if f -electrons are promoted to other states) or occupied with extra electrons. The orbitals treated as valence for each atomic species are listed in Tab. 3.1.

In the case of gallium ions it arises the issue whether the $3d$ electrons have to be included in the valence or not. From one side it has been shown at the beginning of the last decade that the Ga- $3d$ electrons despite of their localisation do not behave as proper core electrons and even undergo a hybridisation with the N- $2s$ orbitals in the LDA representation [111]. Later on it was shown that this hybridisation is an artificial feature of the LDA functional and is not observed experimentally [105]. Whether the *ab initio* description of Ga and Ga-compounds is qualitatively

Table 3.2: Compression radii (in atomic units) for the confining potential used for each atomic type considered in this work. The criterion for the choice of the following values is the consistency with previous DFTB works (H, C, N, O and Ga) or the band structure (reported in Fig. 3.1) of the bulk-phase (RE).

Ion	s-orbital	p-orbital	d-orbital	f-orbital
H	1.30	–	–	–
C	2.78	2.78	–	–
N	2.71	2.71	–	–
O	2.60	2.60	–	–
Ga	4.55	4.55	4.55	–
Pr	5.00	5.00	6.00	6.00
Eu	5.00	5.00	6.00	6.00
Gd	5.00	5.00	6.00	6.00
Er	5.00	5.00	6.00	6.00
Tm	5.00	5.00	6.00	6.00

improved by considering the $3d$ orbitals valence orbitals is still argument of debate. Many scientists believe that not including this shell in the valence will not change the physics of the Ga-compounds, as the Ga- $3d$ on-site energy is about 10 eV lower than the Ga p -shell. Other scientists argument instead that the lattice parameters and the electronic structure of Ga-compounds calculated treating the $3d$ -electrons as valence are closer to the experimental values. Sure is the fact, that including these orbitals in the valence implies we have to include ten additional electrons for Ga atom in the calculation, which, in a supercell of 512 atoms means more than 2500 additional electrons. We created a parameter set with the $3d$ electrons explicitly included in the valence and one with the Ga $3d$ orbitals treated as core. The decision about which one we will use in this work for the investigation of GaN defects is postponed to the next chapter, where we discuss the influence of the particular treatment of the d -shell in the description of GaN and the extent of an eventual interaction with the RE f -shells.

Atomic reference calculation

Once the electronic configuration has been chosen, it is important to perform reference atomic calculations, to check the atomic energy and the on-site energy of the valence orbitals. This energy gives in fact the DFTB atomic energy in the case of isolated atoms (see Eq. 2.53). Values calculated with RLCAO have been compared with the atomic reference calculations published by the American National Institute of Standards and Technology (NIST Database) [112], finding an overall good agreement.

Choice of the compression radii

The second decision we have to make is the value of the compression radius (see Eq. 2.49) for each valence orbital of each ion. If we use the superposition of atomic potentials as parameterisation method we only have to choose a value for the compression of the wave functions, while if we use the superposition of atomic charges we have to choose a compression for the charge densities and another compression for the wave functions [90]. We parameterise all the ions with the potential superposition method and only need a value for the compression of the wave functions. The usual choice for the compression radius is

$$r_c \approx 2r_{\text{cov}}$$

where r_{cov} is the covalent radius of the parameterised atom [93]. For elements of the second row like N, C and O it is usual to use a single value for the compression f -shells with different angular momentum. Because of the very different localisation of the s , p and d , f orbitals, we use angular momentum dependent compression radii. The value of $r_c = 2r_{\text{cov}}$ is only a starting point and can

Table 3.3: Atomic parameters: the Hubbard U s calculated for the studied elements. We note that for the first row elements (C, N and O) the Hubbard U s relative to s - and p -shells are very similar, while for the rare earths the Hubbard U values of the f -shells are quite different from the values of the other shells. The same happens to the d -shells of the transition metals like Ni. That is due to the strong localisation of the f (or d) shells of such so called strong correlated systems. All the given values are in atomic units.

	H	C	N	O	Ga	Pr	Eu	Gd	Er	Tm
U_s	0.41	0.39	0.49	0.49	0.38	0.21	0.21	0.29	0.21	0.22
U_p	–	0.36	0.49	0.52	0.35	0.18	0.19	0.27	0.23	0.24
U_d	–	–	–	–	0.63	0.26	0.26	0.26	0.26	0.27
U_f	–	–	–	–	–	0.45	0.54	0.56	0.51	0.57

be changed in order to improve the description of particular aspects. We choose, starting from this first guess, the value of the compression using the band structure of the elements in their solid state as criterion. The band structures of the elemental RE calculated with the chosen compression radius using the experimental values of the lattice parameters are reported in Fig. 3.1 (left side). At this stage, in absence of a repulsive potential, bulk calculations can only be performed using the experimental lattice parameters. The DFTB band structure of the elemental RE has been compared with the band structure calculated with the *ab initio* all electron program Wien2K [113], which we also report in Fig. 3.1 (right side). Goal of this comparison is not to have the correct simulation of the experimental band structure itself, but to have a good agreement between the DFTB and DFT. For this reason we do not compare the bands calculated with orbital dependent potentials, but the bands calculated with the LDA approach. We found that the DFTB band structure are in good agreement with the Wien2K ones for values of the compression radii between 5.0 and 6.0 atomic units. Even if the band structures are not extremely sensible to the choice of the compression, outside this range DFTB and Wien2K calculations do not show a good agreement. The compression used in this work are consistent with the values that can be found in the literature concerning previous DFTB publications [90, 99, 100], yet only for the elements N,C,O and Ga. RE ions have been parameterised for the first time in this work and we do not have further terms of comparison. The compression radii used for the atomic species parameterised in this work are given in Tab. 3.2.

Changing the compression radius of the wave function also influence the form of the DFTB electronic energy curve and the cohesive energy of bulk systems. These can also be used as criterion for the choice of the compression. This is not the case of this work, where the band structures were the only criterion. A discussion about the effects of different compressions on the bulk properties is beyond the goal of this section, which is to present the parameter set we created. For further details about this issue see for example Ref. [93, 114]. Like almost all recent DFTB works we use a quadratic potential ($m = 2$) for the confining potential (Eq. 2.49). In connection with peculiar systems, like those containing for example $3d$ -transition metals or noble metals also other values have been chosen. A different choice for the exponent of the potential has been used for example in Ref. [90].

3.1.2 The atomic constants U_l and W_{ll}

Apart from the on-site energy, the atomic mass and the valence charges, two other atomic constants must be included in the parameters needed by DFTB: the U_l , which can be considered to be a generalisation of the *Hubbard-Us* for each shell and the spin constants W_{ll} . Both have been defined in the previous chapter with the Eq. 2.83 and Eq. 2.87 respectively. The values used in this work for each atom type and are reported in the Tab. 3.1.1 and Tab. 3.1.2. To calculate the U_l -constants the program RLCAO has been used. This is the program we used to calculate the integral tables and which is able to perform relativistic atomic calculations. The values are

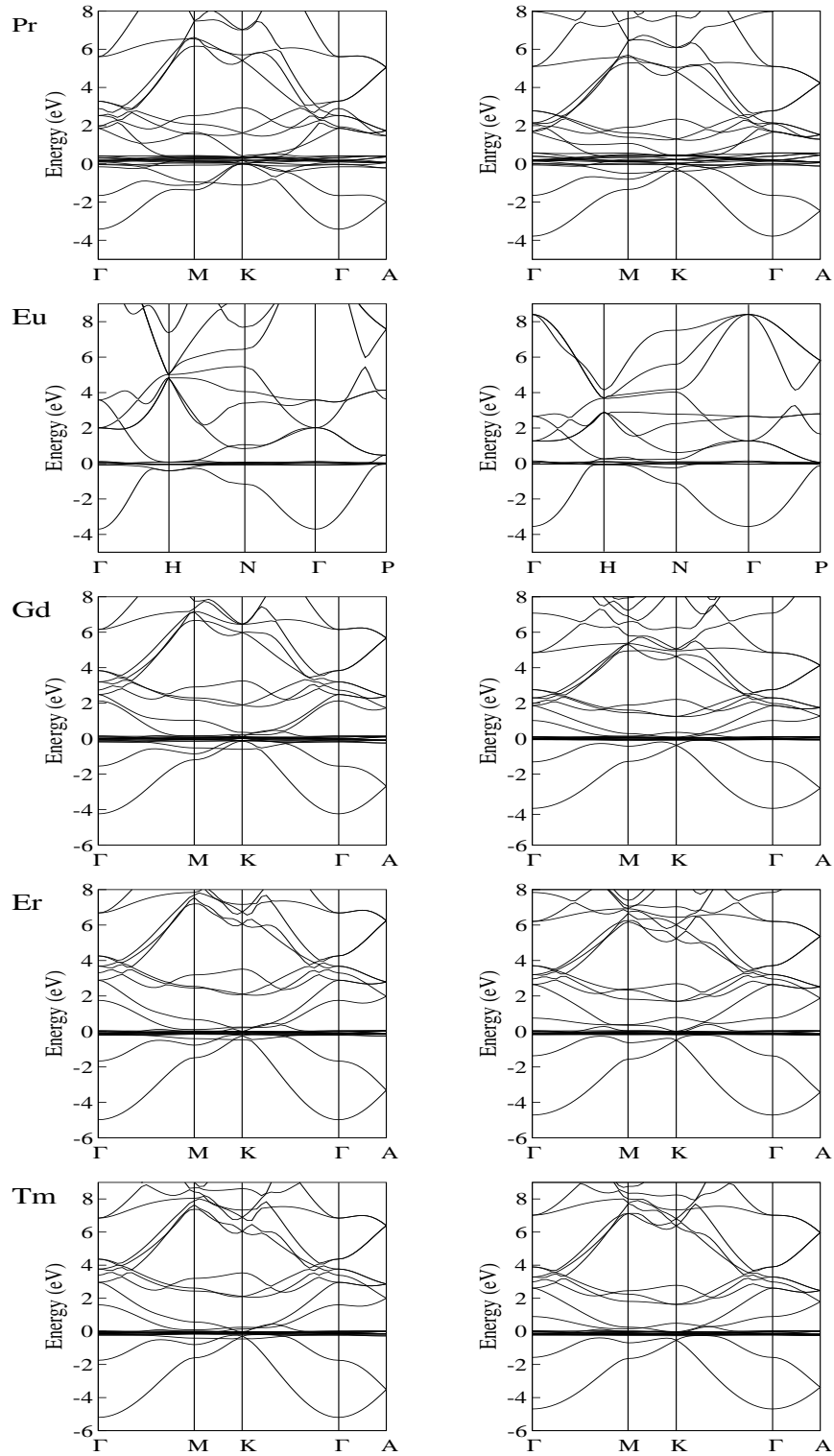


Figure 3.1: LDA band structure of the elemental rare earths calculated with DFTB (left column) and Wien2K (right column): in each case the the Fermi level was chosen as zero of the energy scale. The k-points are labeled after the bulk structure they refer to, that is BCC for Eu and HCP for all the other elements.

3.1. GENERATION OF THE PARAMETERS

Table 3.4: Atomic parameters: the spin coupling constants $W_{AU'}$ calculated for each of the studied elements. All the values in atomic units. The spin coupling constants are expected to be symmetric against index exchange: $W_{U'} = W_{U'1}$. This is verified in our calculations to the given precision.

	H	C	N	O	Ga	Pr	Eu	Gd	Er	Tm
W_{ss}	-0.0640	-0.0279	-0.0303	-0.0323	-0.0174	-0.0078	-0.0084	-0.0083	-0.0089	-0.0089
W_{sp}	—	-0.0240	-0.0262	-0.0282	-0.0129	-0.0061	-0.0063	-0.0064	-0.0066	-0.0066
W_{sd}	—	—	—	—	-0.0030	-0.0053	-0.0058	-0.0052	-0.0065	-0.0058
W_{sf}	—	—	—	—	—	-0.0007	-0.0005	-0.0004	-0.0004	-0.0004
W_{ps}	—	-0.0240	-0.0262	-0.0282	-0.0129	-0.0061	-0.0064	-0.0064	-0.0066	-0.0067
W_{pp}	—	-0.0238	-0.0248	-0.0271	-0.0134	-0.0067	-0.0070	-0.0072	-0.0074	-0.0075
W_{pd}	—	—	—	—	-0.0011	-0.0029	-0.0032	-0.0027	-0.0037	-0.0031
W_{pf}	—	—	—	—	—	-0.0003	-0.0002	-0.0002	-0.0002	-0.0002
W_{ds}	—	—	—	—	-0.0030	-0.0053	-0.0058	-0.0052	-0.0065	-0.0058
W_{dp}	—	—	—	—	-0.0011	-0.0029	-0.0032	-0.0027	-0.0037	-0.0030
W_{dd}	—	—	—	—	-0.0213	-0.0077	-0.0078	-0.0083	-0.0077	-0.0085
W_{df}	—	—	—	—	—	-0.0021	-0.0016	-0.0017	-0.0011	-0.0014
W_{fs}	—	—	—	—	—	-0.0007	-0.0005	-0.0004	-0.0004	-0.0004
W_{fp}	—	—	—	—	—	-0.0003	-0.0002	-0.0002	-0.0002	-0.0002
W_{fd}	—	—	—	—	—	-0.0021	-0.0016	-0.0017	-0.0011	-0.0014
W_{ff}	—	—	—	—	—	-0.0115	-0.0128	-0.0141	-0.0139	-0.0150

calculated as numeric derivative of the atomic eigenvalues with respect to the occupation number¹. All the calculations were executed with spin-unpolarised pseudo-atoms and the electrically neutral spin-unpolarised pseudo-atom was the reference. One common approximation in the DFTB spirit is to use the same value of the Hubbard- U s for all the shells of a given atom. This approximation does not introduce any noticeable errors in calculations involving element of the second row (H,C,N and O), for which the Hubbard- U of the $2s$ -shell is not really different from the value of the $2p$ -shell. In the case of transition metals (like Ga) or lanthanides however the difference between delocalised s - and p -shells and strongly localised d - and f -shells is noticeable, so that we chose to use the calculated value of the Hubbard- U for each shell. To calculate the $W_{U'}$ -constants instead the software SCFATOM has been used, which is the atomic part of TWOCENT, another code used to calculate the DFTB integral tables. This code is not able to perform relativistic atomic calculations and this may introduce some error in the calculation of the parameters of heavy elements like the rare earths. We think however that this is only a minor error: DFTB itself is not a relativistic method and the relativistic effects are kept in account only through the calculation (relativistic) of the SK tables. For this reason a possible inaccurateness in the estimation of the $W_{U'}$ would be in any case overwhelmed by other error sources. From symmetry considerations the coupling constants $W_{U'}$ are expected to be symmetric for an index exchange: this has been verified within the numerical precision of the code. SCFATOM offers the possibility to calculate the spin constants both with the LDA and GGA functional and this has also been done. The values calculated with the two different exchange-correlation functionals do not differ noticeably ($\approx 1\%$ of the value itself): we used in this work LDA values.

Calculation of the SK tables

Once all the possible decisions have been made, the Slater-Koster tables of Hamiltonian $H_{\mu\nu}^0$ and overlap $S_{\mu\nu}$ elements can be calculated in the spirit of the two centers approximation (Eq. 2.53). These integrals are indeed calculated immediately following the pseudo-atom calculations and are tabulated as a function of the distance between the two atoms involved.

Hamiltonian and overlap matrix elements have been calculated with a step of 0.04 atomic units for distances between 0 and ≈ 15 a.u. Due to symmetry reasons, only 20 integrals between basis functions remain nonzero. Their sequence as tabulated in the parameter files is, in standard molecular orbital notation:

¹For the numeric derivative a step of 0.01 electrons was used. In case of fully occupied or completely empty shells single-edge differences were used.

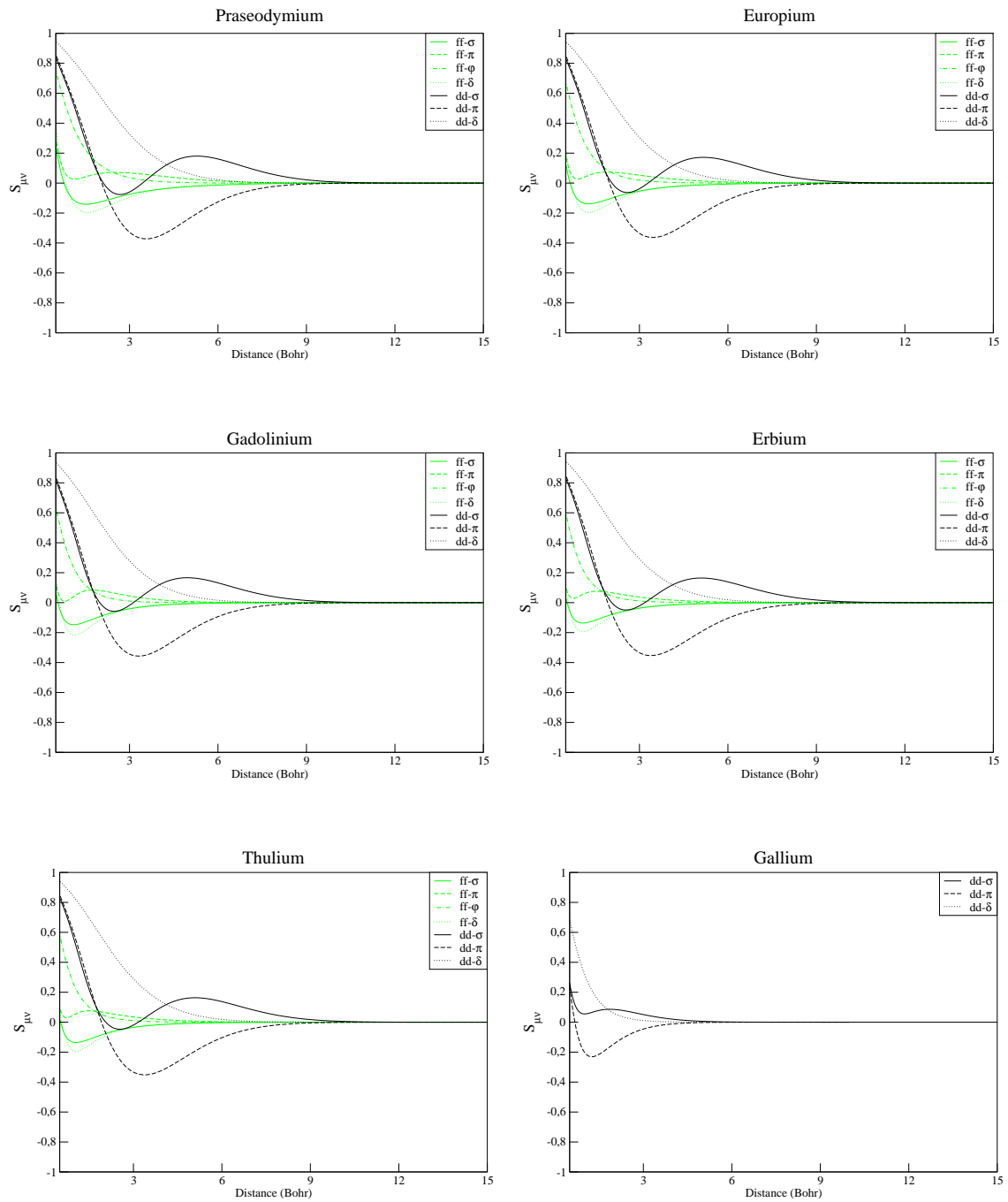


Figure 3.2: *Overlap integrals of the f- (in green) and d-orbitals (in black) for the parameterised ions. The localisation of the RE 4f-electrons and Ga 3d-electrons is evident. The overlap of s- and p-orbitals begins even before the overlap of the d-orbitals.*

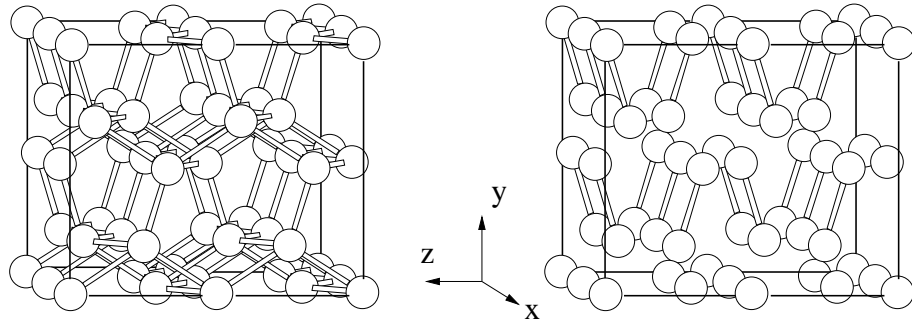


Figure 3.3: The α -Ga structure. On the right hand side the bond factor in the graphic representation has been lowered to evidence the the first neighbours and the molecular nature of the crystal, which can be thought as constituted of Ga_2 dimers.

ff σ ff π ff δ ff φ df δ df π df σ dd σ dd π dd δ pf σ pf π pd σ pd π pp σ pp π sf σ sd σ sp σ ss σ

In Fig. 3.2 the overlap elements $S_{\mu\nu}$ of the f - and d -orbitals are plotted for the RE-ions and Ga. It can be observed that the overlap and consequently the interaction between $4f$ -orbitals begins at atomic distances for which the $5d$ -shells already have an important overlap. $6s$ - and $6p$ -orbitals (not reported here) are even more extended and begin to interact even earlier. From the overlap table we can obtain informations about the localised nature of the f -electrons which has as consequence the previously discussed screening effects.

3.1.3 The repulsive part

The second step of the parameter generation procedure is the fitting of the repulsive potentials introduced with the Eq. 2.76, calculated as energy difference between the total energy of a reference (fit) system and the DFTB band-structure energy (Eq. 2.75). The determination of the repulsive pair potential is the most time consuming step of the whole parameterisation, because of the DFT calculations which have to be executed for all pairs of atom type. The choice of the fit system is essentially free and determines the portability of the parameter set. A good description of the fitting process can be found in Ref. [114]. We have to create repulsive potentials for the interaction of each used element with itself and with all other. Let us start with the homonuclear lanthanide parameters. The choice of the fit system influences the description of the the systems to simulate and the portability of the parameters. In general one has a good description of systems whose bond nature is similar to the one of the fit system, while normally the description of systems which are chemically very different from the fit-system is not optimal. Of course important exceptions to this general trend exist and are known. We think that a reasonable reference for the RE-RE interaction in the study of RE defects in GaN is given by the metallic bulk phase of the single lanthanides. For organic molecules it is an established procedure to use different fit systems, mainly dimers, for different regions of the atomic distances, in order to correctly reproduce the bond nature in these regions². In the case of metals like the elemental RE this is not possible, from one side because dimers are systems which are very different from bulk RE from the other because complexes of RE and H would be created which would change the nature of the RE-RE bond [115–117]. This kind of processes have been illustrated and discussed in other DFTB studies [90]. Apart from this, it does not make sense to speak about single and double bonds if our goal is to correctly reproduce the metallic bond of the bulk-RE.

We have to choose a system where all the bonds have the same nature and the position of the second neighbours is not close to the first neighbours. Otherwise the bonds which we are going

²This can be easily done for example using dimers of an atomic specie decorated with a different number of hydrogen atoms. The hydrogen atoms saturate the dimer's electrons and can be used to control the bond type (simple, double or triple) between the atoms of the dimer.

to parameterise would not be well defined and the fit system cannot be considered a good fit system. One possibility is to use the so called platonic geometries (Tetraheder, Cube, Octaheder, Icosaheder) where all bond lengths are the same. The problem of this structures is that the smaller they are the bigger difference from the bulk system they show. On the other side the use of very big clusters as fit systems makes the process of fitting very time consuming, as the total energy for each bond length has to be calculated in some way. Different clusters are of course characterised by a different coordination number. Another possibility is to use the RE bulk-phases as fit system. Apart from Europium, all selected RE crystallise in the hexagonal close packed (HCP) crystal structure, which is not an ideal fit system, as each atom has two types of inequivalent neighbours. These neighbours are at distances which differ by 0.04% and can be thus considered, in first approximation, equivalent. The advantage of using bulk systems is that any total energy calculation has to be done³, as the total energy can be easily derived by means of a state equation, like the Birch-Murnaghan equation [118, 119], if the experimental values of the bulk modulus B and its first pressure derivative B' are known.

$$E(V) = \frac{V_0 B_0}{B'_0} \left[\frac{1}{B'_0 - 1} + \left(\frac{V_0}{V} \right)^{B'_0 - 1} + \frac{V}{V_0} \right] + E(V_0) \quad (3.1)$$

The values of B and B' for bulk Pr, Eu, Gd, Er and Tm can be found in the literature [120] and have been used for the estimation of the total energy of the RE bulk via Murnaghan equation. Fitting the repulsive potential on bulk systems simplifies the choice of the range of the potential itself. It is sufficient to fit the repulsive curve for a range of $\pm 10\%$ of the equilibrium bond length. It is important that the repulsive potential begins at a distance shorter than the first neighbour distance and ends at a distance shorter than the second neighbour distance. In this way the tight-binding approach is supposed to work properly. Coming to the other homo-atomic interaction (Ga-Ga, C-C, N-N and O-O), we adapted the repulsive potentials used in previous DFTB works [20] to our electronic part. The interaction RE-N and RE-O were parameterised by means of the RE nitrides and oxides, RE-C with a dimer and RE-Ga with an hypothetical ideal crystal with HCP structure. In all these cases the total energies have been estimated with spin unpolarised DFT-LDA calculations [121]. We do not report here the details of each single calculation and limit us to say that the calculations were carried on on primitive cells with k -point mesh and plane waves cutoff energy chosen after thorough convergence tests. The question how good the parameters we created actually are is answered in the next section.

3.2 Validation of the parameters

Before we start the investigation of RE defects in GaN with the parameter we created, we have to check thoroughly the parameters itself. This process, called validation of the parameters consists in a series of tests which will give an idea of the accuracy of the combination of the DFTB method and the created parameters. We test out the DFTB representation against experimental results and against other theoretical investigations, namely DFT-LDA or DFT-GGA works. Our validation is strongly oriented on the solid state physics, i.e. we test the parameters mainly on bulk system and check the aspects of relevance in this field, i.e. lattice parameters, elasticity properties, cohesive energy and electronic structure. We do not carry out studies on molecules or small clusters containing lanthanide ions. This section is organised as follows: at first the bulk phases of Ga (α -Ga and FCC-Ga), N (HCP), C (diamond) and of the metallic RE are investigated. Then we briefly analyse the gas phases of N and O and finally the RE-nitrides. The interaction between Ga and N, governing the behaviour of the host, GaN, is of particular importance and deserves a chapter on its own. The DFTB representation of the semiconductor GaN will be the subject of the next chapter.

³This is a double advantage: on one side a lot of time is saved, on the other side problems due to the DFT-LDA simulation of strongly correlated systems are avoided.

Table 3.5: Structural and electronic properties of α -Ga. All the distances are expressed in Å, the energies in eV and bulk moduli in Kbar. Elasticity properties are calculated in this work by means of the Murnaghan equation.

Reference	Method	Basis	a	b/a	c/a	B	B'	E_{coh}
This work	DFTB	s, p	4.803	0.962	1.839	707	3.89	-3.574
This work	DFTB	s, p, d	4.742	0.987	1.795	767	4.01	-3.674
[122]	DFT-LDA	s, p	4.389	1.001	1.695	669	4.93	
[123]	DFT-LDA	s, p	4.44	0.997	1.691			-3.46
[123]	DFT-GGA	s, p	4.51	0.997	1.691			-2.60
[124]	DFT-LDA	s, p, d	4.437	0.999	1.687			-3.484
[124]	DFT-GGA	s, p, d	4.596	0.992	1.696			-2.796
[125, 126]	Exp.		4.511	1.001	1.695	613		-2.81

3.2.1 Ga-bulk

Gallium is a trivalent metal with a quite complicated phase diagram with a lot of stable and metastable crystalline phases very close in energy. The stable phase at low pressure is an unusual orthorhombic structure called α -Ga, while two other phases called Ga-II and Ga-III are stable at higher pressures. A lot of metastable phases, called β -Ga, γ -Ga, δ -Ga, ϵ -Ga as well as the FCC phase have been identified at atmospheric pressure [122]. In this work we check the DFTB description of the α -Ga and FCC phases. The first one is the crystal which would grow at the MBE conditions used to grow RE-doped samples object of this work and is therefore of interest here.

α -Ga

The α -Ga structure, with space group $Cmca$ and crystal number 64 is described by a four atom base-centered orthorhombic cell with the following primitive vectors:

$$\text{Primitive vectors: } \begin{cases} \mathbf{t}_1 = \frac{1}{2}a, \frac{1}{2}b, 0 \\ \mathbf{t}_2 = -\frac{1}{2}a, \frac{1}{2}b, 0 \\ \mathbf{t}_3 = 0, 0, c \end{cases}$$

and basis:

$$\text{Basis vectors: } \begin{cases} \mathbf{d}_1 = 0, & bu, & cv & (\text{Ga}) \\ \mathbf{d}_2 = 0, & -bu, & -cv & (\text{Ga}) \\ \mathbf{d}_3 = 0, & \left(\frac{1}{2} + u\right)b, & \left(\frac{1}{2} - v\right)c & (\text{Ga}) \\ \mathbf{d}_4 = 0, & \left(\frac{1}{2} - u\right)b, & \left(\frac{1}{2} + v\right)c & (\text{Ga}) \end{cases}$$

Note that this cell is different from the one used in the works [122–124, 127] we use later on as reference. There an eight-atom orthorhombic supercell oriented in another direction but still consistent with the $Cmca$ space group is used. Our smaller cell is, of course, more efficient for electronic structure calculations. The α -Ga structure is depicted in Fig. 3.3. A peculiar feature of this structure is that each atom has only one first neighbour (at 2.44 Å, which is a fairly short distance for a normal metallic bond) and two second, third and fourth neighbours 0.27, 0.30 and 0.39 Å further apart. The crystal can also be viewed as molecular crystal of Ga₂ dimers, an unique case among metals. This structure is characteristic for the non metallic Cl₂, Br₂ and I₂ and is very different from that of Ga-isoelectronic elements like Al. This is probably due to the incomplete screening of the nucleus by the shallow 3d core states which yields an anomalous spatial contraction

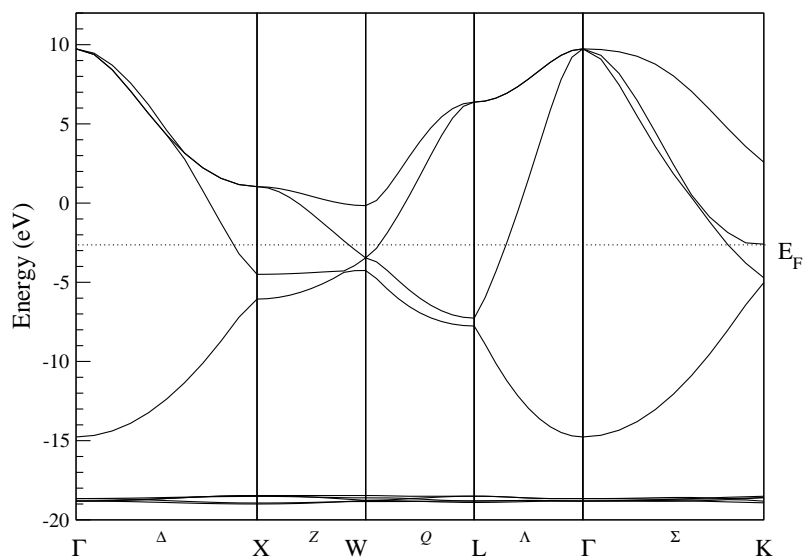


Figure 3.4: Electronic band structure of FCC-Ga. The high-symmetry point within the Brillouin zone are labeled after Papaconstantopoulos. E_F indicate the position of the Fermi level. The free electron like band structure reveals the metallic nature of FCC-Ga.

of the valence charge. On turn this favours covalency over metallicity in Ga as though it were a much lighter element. In other words, among group-III elements Ga is closer to B than to Al. A thorough discussion about the double nature (metallic-covalent) of the Ga-bond in solid Ga can be found in [122]. In the Tab. 3.5 are shown calculated and experimental properties of the material. DFTB calculations are executed with a primitive cell of α -Ga and a $12 \times 12 \times 12$ MP k -point mesh [128]. We observe that lattice parameters as well as the cohesive energy of the solid are slightly overestimated in DFTB. This could be due to two effects: firstly, for the sake of the computational effort the internal parameter are fixed to the experimental values [122] of $u = 0.1525$ and $v = 0.0785$ and not relaxed, and second, the inclusion of the Ga-3d electrons in the valence band leads to a more accurate description of the bonds and consequently of the properties of the solid (second row of Tab. 3.5). The DFTB description of the α -Ga phase can be anyway considered satisfactory for our purposes.

FCC Ga

A phase transition from the Ga-II structure to the Ga-FCC phase at the pressure of 145 Kbar has been predicted by Bernasconi *et al.* [122]. This region of the Ga phase diagram has not been yet explored experimentally, so that we only have other theoretical result to test our parameters. As predicted in the mentioned work FCC-Ga is a proper metal: in the Fig. 3.4 we report the band-structure of the FCC phase of Ga calculated with DFTB including the 3d in the valence. It can be compared for example with the band structure reported in Ref. [122, 129]. We observe that the agreement between the electronic bands calculated in this work and the bands calculated in the given references is very good. The *free-electron* like band structure reveals the metallic nature of FCC-Ga, the 3d-related bands are on the bottom of the picture. Other structural and electronic properties of solid Ga in the FCC phase are reported in Tab. 3.6. All the calculations have been carried on with the FCC-Ga primitive cell and a $12 \times 12 \times 12$ MP k -point mesh. The agreement between DFTB and DFT can still be considered satisfactory, apart from the surprisingly high value of the DFTB bulk modulus calculated including the Ga-3d electrons in the valence shell.

Table 3.6: *Structural and electronic properties of FCC-Ga. All the distances are expressed in Å, the energies in eV and bulk moduli in Kbar. Elasticity properties are calculated in this work by means of the Murnaghan equation.*

Reference	Method	Basis	a	B	B'	E_{coh}
This work	DFTB	s, p	4.380	756	3.145	$E_{\text{coh}}(\alpha\text{-Ga})+0.081$
This work	DFTB	s, p, d	4.261	1070	3.751	$E_{\text{coh}}(\alpha\text{-Ga})+0.038$
[122]	DFT-LDA	s, p	4.015	676	4.633	$E_{\text{coh}}(\alpha\text{-Ga})+0.073$
[129]	TB	s, p, d	4.143			

3.2.2 Diamond

Carbon is of interest in this work because of the role it can play in co-doped GaN samples. Carbon is one of the most versatile chemical element. Its ability to form single, double and triple bonds leads to several crystal structures with completely different properties. For the same reason, carbon is also the basis of organic compounds. The two most important pure forms of carbon are graphite and diamond, both of which have been known for at least two thousand years. We analyse here quickly only the DFTB representation of bulk carbon in the diamond structure. The crystal structure of diamond is the prototype-lattice for many tetravalent semiconductors. It is a face centered cubic lattice with a two-atoms basis: each carbon atom is surrounded tetrahedrally by four neighbours. Electronic and structural properties of diamond calculated with DFTB are reported in Tab. 3.7. Lattice parameters reproduce the experimental data within an error of 0.3% and the cohesive (or binding) energy per atom is less overestimated than in other theoretical works [130]. We notice that also the bulk modulus is reproduced with a almost negligible deviation from the experiment [131, 132].

3.2.3 Elemental RE

We report here for the sake of completeness and because of their importance in commercially important applications⁴ the structural and electronic properties of the elemental rare earths in their metallic phase calculated with DFTB. We advise the reader that the investigation of the stablest structure in each case is not a significative test for our approach nor has been done with validation intent. The bulk of the stablest phases of the RE themselves were indeed used as fit system for the generation of the repulsive potentials and are certainly well reproduced in DFTB. However the other metallic phases (like the FCC phase) are interesting benchmarks. Rare earth metals represent a family of solids with very similar chemical and physical properties. This family is often divided in two sub-groups, the light rare earths and the heavy rare earths, depending from the occupancy of the f -shell (1 to 7 for the light RE and 8 to 14 for the heavy RE). Each sub-group has elements which show anomalies in some property with respect to the other elements (namely Ce, Pr and Eu, Yb) because of particular f -shell occupations (completely empty, half filled and completely filled) or proper peculiarities. Most of the trivalent RE metals undergo a dramatic transformation of their physical properties under pressure. The most known of these changes is the so called *volume collapse* [133], which can cause a volume reduction up to 15% and is probably due to a change in the correlation of the $4f$ -electrons. More precisely the f -electrons seem not to take part to the crystal bonding at larger volumes (high-correlation regime) while they do participate to the bond in the compressed crystal (weakly correlated regime). The nature of the f -electrons in these regimes is commonly defined as localised and itinerant. For increasing pressure the RE metals undergo many

⁴Metallic RE were once scientific curiosities and object of studies from a purely academic point of view. As the RE have very similar chemical and physical properties it was in the past almost impossible (and is difficult still today!) to separate the single RE from a raw crystal. With the modern techniques of separation RE metals have been investigated and have found a lot of commercial applications. They are used among others in the automobile industry, in electronic devices, in light bulbs, in the glass and ceramic industry, in optoelectronic devices and as permanent magnets.

Table 3.7: *Structural and electronic properties of diamond. All the distances are expressed in Å, the energies in eV and bulk moduli in GPa. Elasticity properties are calculated in this work by means of the Murnaghan equation.*

Reference	Method	a	B	B'	E _{coh}
This work	DFTB	3.575	440	3.98	8.986
[114]	DFTB	3.562	541		9.278
[130]	DFT-LDA	3.527	461	3.67	9.032
[131, 132]	Exp.	3.567	442	≈ 4	

structural phase transitions, involving in general the structures hexagonal close packed (HCP), double hexagonal close packed (D-HCP), face centered cubic (FCC) and distorted face centered cubic (DFCC), which can be all considered polytypes of the close packed structure. The mentioned structures are represented in Fig. 3.5. In this work we simulate many different structures for each lanthanide, including the FCC phase, which is the simplest close packed structure that approximates the real structure, and the stable structure at standard pressure and temperature, which is the hexagonal close packed except for Eu, which crystallises in the BCC structure. Another peculiar aspect of metallic Eu is its valency: Eu is (with Yb) the only RE metal to be divalent, while the other RE metals are all trivalent, i.e. a $4f$ electron is promoted to the conduction band. Even if there have been some attempts to investigate metallic RE within the DFT-LDA approach [134], this theory does not take properly in account the limited spatial extent of the f -orbitals and leads to a too large energy dispersion when the $4f$ -electrons are treated as band-like valence states. On the other hand treating the $4f$ orbitals as core states results in a very poor approximation as much of the interesting and unusual physics of the RE systems is due to the fact that the $4f$ -shell is not completely inert. A satisfactory description of the ground state properties of the elemental RE can only be achieved with calculation schemes involving orbital dependent potentials (see chapter 1). In the following we investigate RE-metals in their ferromagnetic phase with the LDA, LSDA and LSDA+ U (FLL) approach as implemented in DFTB. In this way the differences between the different approaches can be remarked.

Computational details

All the results reported in the following were obtained from calculations on primitive cells (see Fig. 3.5) with a Monkhorst-Pack $12 \times 12 \times 12$ k -point mesh [128]. In the case of LSDA and LDA+ U (FLL) calculations the spin configuration was determined by total energy comparisons. For the FLL calculations the value of the U - J parameter was chosen to be 0.23 H for Pr, 0.27 H for Eu, 0.32 H for Gd and 0.28 H for Er and Tm. This choice is thoroughly discussed and justified in the following chapters and will not be discussed here. The DFTB representation of band structures of the stablest phase of each lanthanide has been shown previously and compared with other DFT calculations (Fig. 3.1) and will not be discussed again. Concerning the structural and energetic properties, the calculated values are reported in Tab. 3.8, together with experimental values and other theoretical data for comparison.

Discussion

The lattice parameters of all the lanthanides are in qualitative agreement with experimental data and other simulations for all the investigated crystalline phases. We observe that in general the DFTB-LDA approach suffices for a satisfactory description of lattice parameters and that the DFTB-FLL approach leads to a substantial improvement of the simulation, i.e. the lattice parameters as well as the cohesive energies are closer to the measured values than within the DFTB-LDA or DFTB-LSDA approach. Summarising, DFTB-FLL gives in general a satisfactory description of the geometries and of the cohesive energies of each investigated structure. Averaging over all the investigated rare earths the DFTB-FLL mean deviation from the experiment is of 2.7% in the lattice

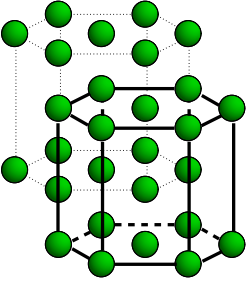
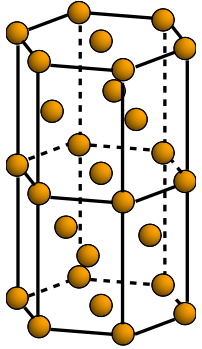
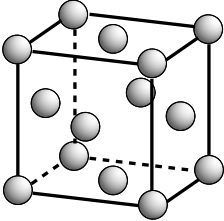
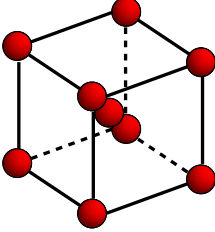
<p>HCP Primitive Vectors:</p> $\begin{cases} \mathbf{t}_1 = \frac{1}{2}a, & \frac{\sqrt{b}}{2}b, & 0 \\ \mathbf{t}_2 = -\frac{1}{2}a, & \frac{\sqrt{b}}{2}b, & 0 \\ \mathbf{t}_3 = 0, & 0, & c \end{cases}$ <p>Basis Vectors:</p> $\begin{cases} \mathbf{d}_1 = \frac{1}{2}a, & \frac{1}{2\sqrt{3}}a, & \frac{1}{4}c & (\text{Er}) \\ \mathbf{d}_2 = \frac{1}{2}a, & -\frac{1}{2\sqrt{3}}a, & \frac{3}{4}c & (\text{Er}) \end{cases}$	
<p>D-HCP Primitive Vectors:</p> $\begin{cases} \mathbf{t}_1 = \frac{1}{2}a, & \frac{\sqrt{b}}{2}b, & 0 \\ \mathbf{t}_2 = -\frac{1}{2}a, & \frac{\sqrt{b}}{2}b, & 0 \\ \mathbf{t}_3 = 0, & 0, & c \end{cases}$ <p>Basis Vectors:</p> $\begin{cases} \mathbf{d}_1 = 0, & 0, & 0 & (\text{Pr}) \\ \mathbf{d}_2 = 0, & 0, & \frac{1}{2}c & (\text{Pr}) \\ \mathbf{d}_3 = \frac{1}{2}a, & \frac{1}{2\sqrt{3}}a, & \frac{1}{4}c & (\text{Pr}) \\ \mathbf{d}_4 = \frac{1}{2}a, & -\frac{1}{2\sqrt{3}}a, & \frac{3}{4}c & (\text{Pr}) \end{cases}$	
<p>FCC Primitive Vectors:</p> $\begin{cases} \mathbf{t}_1 = 0, & \frac{1}{2}a, & \frac{1}{2}a \\ \mathbf{t}_2 = \frac{1}{2}a, & 0, & \frac{1}{2}a \\ \mathbf{t}_3 = \frac{1}{2}a, & \frac{1}{2}a, & 0 \end{cases}$ <p>Basis Vectors:</p> $\{ \mathbf{d}_1 = 0, 0, 0 \quad (\text{Ga})$	
<p>BCC Primitive Vectors:</p> $\begin{cases} \mathbf{t}_1 = -\frac{1}{2}a, & \frac{1}{2}a, & \frac{1}{2}a \\ \mathbf{t}_2 = \frac{1}{2}a, & -\frac{1}{2}a, & \frac{1}{2}a \\ \mathbf{t}_3 = \frac{1}{2}a, & \frac{1}{2}a, & -\frac{1}{2}a \end{cases}$ <p>Basis Vectors:</p> $\{ \mathbf{d}_1 = 0, 0, 0 \quad (\text{Eu})$	

Figure 3.5: Most rare earths (including Gd, Er and Tm) crystallise at standard temperature and pressure in the HCP structure, a few (including Pr) in the D-HCP structure, Eu in the BCC and Yb in the CCP structure. Among the metastable phases are the FCC structure, the Sm-structure and the distorted phases of all the mentioned structures.

Table 3.8: *Structural and electronic properties of elemental RE. All the distances are expressed in \AA , the energies in eV and bulk moduli in GPa. Elasticity properties are calculated in this work by means of the Murnaghan equation. Calculations of Ref. [134] refer to the paramagnetic phase of metallic RE and were done treating the f -shells as core state. Related data is derived from the pictures. For details about the experimental techniques or the computational approach see the single references.*

	Reference	Method	a	c	B	B'	E_{coh}
Pr	(HCP) This work	DFTB-LDA	3.570	5.760	61	3.3	5.65
	(HCP) This work	DFTB-LSDA	3.727	6.013	46	4.0	4.49
	(HCP) This work	DFTB-FLL	3.962	6.393	44	3.2	3.72
	(HCP) [120, 126, 135]	Exp.	3.669	5.920	28	2.9	3.7
	(FCC) This work	DFTB-LDA	5.273	-	59	3.4	5.10
	(FCC) This work	DFTB-LSDA	5.488	-	47	2.8	4.12
	(FCC) This work	DFTB-FLL	5.327	-	64	3.0	3.09
	(FCC) [134]	DFT-LDA	-	-	45	-	3.5
	(D-HCP) This work	DFTB-LDA	3.567	11.493	61	4.0	5.67
	(D-HCP) This work	DFTB-LSDA	3.731	12.022	48	8.6	4.50
	(D-HCP) This work	DFTB-FLL	3.671	11.829	-	-	4.13
	(D-HCP) [136]	DFT-SIC	3.672	11.832	29	2.0	-
	(D-HCP) [137]	Exp.	3.673	11.835	-	-	-
	Eu	(BCC) This work	DFTB-LDA	4.315	-	138	6.2
(BCC) This work		DFTB-LSDA	4.462	-	91	8.1	3.24
(BCC) This work		DFTB-FLL	4.494	-	91	6.7	3.09
(BCC) [134]		DFT-LDA	-	-	20	-	2.50
(BCC) [120, 126, 135]		Exp.	4.581	-	17	2.9	-
(BCC) [137]		Exp.	4.606	-	-	-	-
Gd	(HCP) This work	DFTB-LDA	3.722	5.953	52	9.9	3.59
	(HCP) This work	DFTB-LSDA	3.745	5.990	66	3.5	3.82
	(HCP) This work	DFTB-FLL	3.690	5.902	79	9.9	2.79
	(HCP) [120, 126, 135]	Exp.	3.636	5.783	35	2.9	4.14
	(HCP) [137]	Exp.	3.636	5.723	-	-	-
	(FCC) This work	DFTB-LDA	5.398	-	56	4.5	3.32
	(FCC) This work	DFTB-LSDA	5.401	-	64	4.3	3.51
	(FCC) This work	DFTB-FLL	5.340	-	81	6.6	2.09
	(FCC) [134]	DFT-LDA	-	-	50	-	4.0
	(FCC) [138]	Exp.	5.40	-	-	-	-
	Er	(HCP) This work	DFTB-LDA	3.559	5.587	76	3.9
(HCP) This work		DFTB-LSDA	3.556	5.582	82	4.3	4.05
(HCP) This work		DFTB-FLL	3.672	5.764	71	3.6	3.47
(HCP) [120, 126, 135]		Exp.	3.559	5.587	44	2.9	3.29
(HCP) [137]		Exp.	3.559	5.587	-	-	-
(FCC) This work		DFTB-LDA	5.084	-	87	5.0	3.83
(FCC) This work		DFTB-LSDA	5.075	-	90	4.2	3.85
(FCC) This work		DFTB-FLL	5.199	-	78	4.8	3.34
(FCC) [134]		DFT-LDA	-	-	60	-	1.5
(FCC) [138]		Exp.	5.09	-	-	-	-
Tm		(HCP) This work	DFTB-LDA	3.596	5.646	43	5.2
	(HCP) This work	DFTB-LSDA	3.596	5.646	47	2.4	2.97
	(HCP) This work	DFTB-FLL	3.702	5.812	27	1.4	2.18
	(HCP) [120, 126, 135]	Exp.	3.538	5.555	46	2.9	-
	(HCP) [137]	Exp.	3.538	5.555	-	-	-
	(FCC) This work	DFTB-LDA	5.185	-	52	2.6	2.75
	(FCC) This work	DFTB-LSDA	5.182	-	54	3.2	2.76
	(FCC) This work	DFTB-FLL	5.180	-	56	4.4	2.70
	(FCC) [134]	DFT-LDA	-	-	55	-	1.0
	(FCC) [138]	Exp.	5.06	-	-	-	-

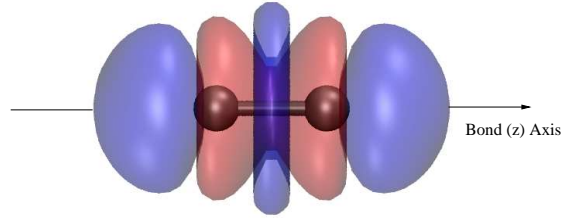


Figure 3.6: Charge density difference between two N atoms and the N_2 dimer. Electronic charge is taken from the region around the atoms and accumulated between the atoms, as expected for a covalent bond.

parameters, the cohesive energies are generally overestimated by some tenth of eV and the bulk moduli are generally overestimated by 10-50 GPa, depending from the lanthanide. These errors are of the typical order of magnitude for a DFTB calculation. The value of the bulk moduli and their first pressure derivative, which are delicate parameters for the tight-binding approach, can be considered a satisfactory approximation of the DFT values. We notice that the parameters have a problem in the simulation of the Eu bulk-modulus. This will not affect our future investigation, as we will only simulate a single Eu atom in our supercells. The correctness of the DFTB bulk modulus is particularly important for the investigation of the clustering properties of lanthanide dopants in GaN, which is not the object of this work. Comparing the cohesive energies of the different phases it can be observed that the most stable phase in our calculations is also the most stable phase as revealed by experiments [126]. This is in particular interesting for metallic Pr, which crystallises in two similar structures D-HCP and HCP very close in energy (with the first slightly favoured) besides the FCC. In each of the used approaches LDA, LSDA and FLL-LDA+ U as implemented in DFTB the favoured phase is the D-HCP, followed by HCP and FCC, in agreement with the experimental knowledge of this material.

3.2.4 The O_2 and N_2 molecules

In this paragraph we test the DFTB parameters on dimers of oxygen and nitrogen, underlining their differences. At standard temperature and pressure oxygen and nitrogen exist as diatomic molecules, characterised by a covalent bond. The bond distance is almost perfectly the sum of the covalent radii of the atoms (0.60 Å and 1.207 Å for oxygen and 0.65 Å and 1.10 Å for nitrogen). In Fig. 3.6 the charge density difference between two N atoms and the N_2 dimer calculated with DFTB is reported. Electronic charge is taken from the region around the atoms (in red) and accumulated between the two atoms, as expected for a covalent bond. In Fig. 3.7 the energy levels of the atomic and molecular orbitals and their occupation are plotted. The order of these levels is the same predicted by the molecular orbital theory. Combining two $2s$ and $2p$ (black levels on the side) results in four σ and four π orbitals (central red levels), which are then filled following the Aufbau-rules. The form of the molecular orbitals calculated with DFTB for the N_2 dimer is plotted in Fig. 3.8. We notice first that the two π_p bonding and antibonding orbitals are degenerate. The corresponding wave functions are identical in the form and differ only in the orientation. In the case of very light atoms ($n < 5$) the energy difference between the $2s$ and $2p$ atomic orbitals is small enough to allow a certain interaction between the molecular σ_s^* and $\sigma_p(z)$ orbitals, which have the same symmetry with respect to the bond axis. As a consequence the energy of the molecular $\sigma_p(z)$ orbital is raised above the $\pi_{p(x,y)}$ energy level. The order of the energetic levels $\sigma_p(z)$ and $\pi_{p(x,y)}$ is the first difference between O_2 and N_2 dimers. The second is the big difference in the binding energy. While in N_2 only σ_p and π_p bonding orbitals are occupied, in O_2 the $\sigma_p^*(z)$ antibonding orbital is doubly occupied, which lowers the binding energy. The molecule is paramagnetic, i.e. its measured magnetic moment is related to the presence of two unpaired electrons. This is in agreement with the molecular orbital theory and with the DFTB calculation, in which the configuration with two unpaired electrons is favoured by 0.74 eV with respect to the configuration with no unpaired electron.

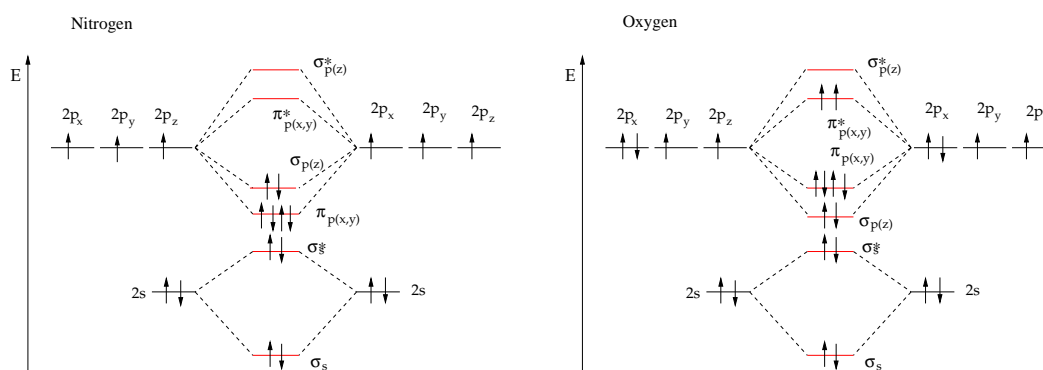


Figure 3.7: Energy levels and occupation of the atomic and molecular orbitals for the N_2 (left hand side) and O_2 (right hand side) dimers in their ground state. The atomic orbitals are black and the molecular red.

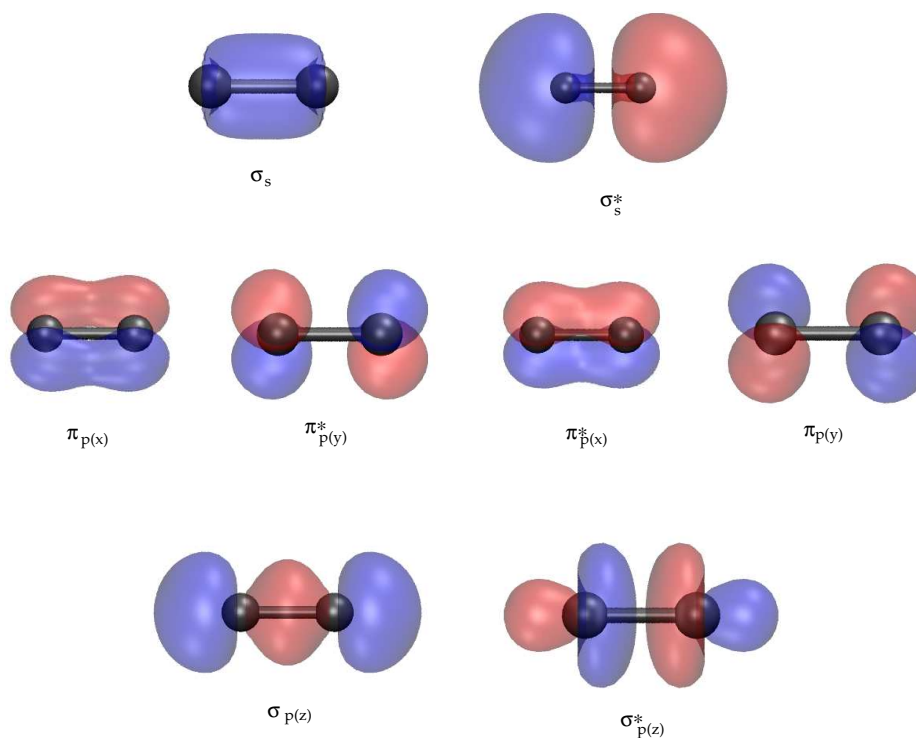


Figure 3.8: The wave function of the bonding and antibonding molecular orbitals of the N_2 dimer. In blue the regions where the wave function is positive and in red the regions where it is negative. Considering the z -axis as the bond axis, the atomic $2s$ and $2p_z$ orbitals give rise to molecular orbitals with cylindric symmetry, which are called, in analogy with the atomic s -orbitals, σ -orbitals. The other atomic $2p$ orbitals give rise to molecular orbitals without charge density along the bond axis and with antisymmetric wave function. For this reason they are called, in analogy with the atomic p -orbitals, π -orbitals.

3.2. VALIDATION OF THE PARAMETERS

Table 3.9: Structural and electronic properties of the N_2 and O_2 molecules. All the distances are expressed in \AA , the energies in eV and the vibration frequencies in cm^{-1} . The zero point vibration energy of the molecule has been considered only in the references [123, 127].

	Reference	Method	d	E_b	ω
N_2	This work	DFTB	1.121	-10.236	-
	[127]	DFT-LDA	1.09	-11.71	2363
	[127]	DFT-GGA	1.09	-10.66	2331
	[123]	DFT-LDA	1.08	-11.75	2385
	[123]	DFT-GGA	1.09	-10.69	2325
	[124]	DFT-LDA	1.107	-11.332	1549
	[124]	DFT-GGA	1.113	-10.558	1477
	[139]	Exp.	1.10	-9.82	2360
	[140]	Exp.	1.10	-9.9	1484
O_2	This work	DFTB	1.208	-7.341	-
	This work	B3LYP 6-31G*	1.216	-9.323	-
	[139]	Exp.	1.207	-5.166	-

The calculated bond energy together with other properties of these molecules is shown in Tab. 3.9. The binding energy is calculated as the energy difference between the dimer and the single atoms. In the case of N_2 , for example:

$$E_{\text{bind.}} = E_{\text{tot.}}^{\text{N}_2\text{-molecule}} - 2E_{\text{tot.}}^{\text{N-atom}}$$

The vibration frequency is calculated assuming the harmonic approximation. We observe that DFTB slightly overestimates the bond length of the dimer, and that in general DFTB results are less affected by over-binding problems than DFT-LDA.

3.2.5 RE Nitrides

We conclude the validation of the DFTB parameters with the simulation of the RE nitrides. Despite their simple rock-salt structures RE-nitrides have very different electronic and magnetic properties. We summarise here briefly terms and definitions used in the following:

PM Paramagnetic (PM) materials show permanent magnetic moments (dipoles) even in absence of an external field. This is normally due to the presence of unpaired electrons in the compound. As these dipoles are randomly oriented (because of the thermal agitation) and do not interact with each other there is no net magnetisation in absence of an external field. When an external field is applied, it aligns the magnetic dipoles resulting in a net magnetic moment in the field direction. To explain the origin of this alignment it is necessary to introduce the quantum mechanical properties of spin and angular momentum⁵. Macroscopically paramagnets are attracted to external fields but do not retain permanent magnetisation (like ferromagnets would). Paramagnetic behaviour is observed also in ferromagnets above the *Curie temperature* and in anti-ferromagnets above the *Néel temperature*.

FM Ferromagnetic materials (FM) show spontaneous magnetisation and a net magnetic moment in absence of an external field, in particular all magnetic ions add a positive contribution to the net magnetisation⁶. The origin of ferromagnetism can only be explained with the quantum-mechanic concepts of spin and Pauli exclusion principle. Ferromagnetism occurs

⁵If there is enough energy exchange between neighbouring dipoles, these will interact and spontaneously align (ferromagnetism) or anti-align (antiferromagnetism).

⁶If they are partially anti-aligned the compound is called ferrimagnetic and if they are completely anti-aligned, so that there is zero magnetisation despite the magnetic ordering, the material is called antiferromagnetic.

Table 3.10: *Structural and electronic properties of selected RE nitrides in the rock-salt structure. All the distances are expressed in Å, the energies in eV and bulk moduli in GPa. Elasticity properties are calculated in this work fitting the Murnaghan equation.*

Nitride	Method	a	B	B'	E _{coh}	Reference
PrN	DFTB LDA	5.034	139	3.7	9.417	This work
	DFTB LSDA	5.102	130	3.5	7.218	This work
	DFTB FLL	5.211	134	2.2	6.535	This work
	DFT LDA+U	5.29	140	-	-	[141]
	Exp.	5.155	-	-	-	[135]
EuN	DFTB LDA	5.269	268	3.9	8.496	This work
	DFTB LSDA	5.356	214	6.5	5.674	This work
	DFTB FLL	5.478	144	7.4	5.045	This work
	DFT LDA	4.91	179	-	-	Priv. Comm.
	DFT LDA+U	4.940	130	-	-	[142]
	DFT LDA+U	5.14	110	-	-	[141]
	Exp.	5.020	-	-	-	[135]
GdN	DFTB LDA	5.066	261	4.4	7.623	This work
	DFTB LSDA	5.100	269	4.3	6.486	This work
	DFTB FLL	5.101	281	2.8	6.111	This work
	DFT LDA	4.977	188.47	4.4	5.956	[150]
	DFT LDA+U	5.08	150	-	-	[141]
	Exp.	4.999	-	-	-	[135]
	Exp.	4.983	192±35	4	-	[143]
ErN	DFTB LDA	4.894	272	3.5	8.536	This work
	DFTB LSDA	4.915	271	3.7	7.071	This work
	DFTB FLL	4.942	274	3.9	6.712	This work
	DFT LDA	4.74	195	-	-	Priv. Comm.
	DFT LDA	4.789	220	4.3	4.452	[150]
	DFT LDA+U	5.00	160	-	-	[141]
	Exp.	4.839	-	-	-	[135]
TmN	DFTB LDA	4.811	245	2.2	7.966	This work
	DFTB LSDA	4.828	224	3.2	6.440	This work
	DFTB FLL	4.862	244	3.8	6.038	This work
	DFT LDA	4.70	201	-	-	Priv. Comm.
	DFT LDA+U	4.90	190	-	-	[141]
	Exp.	4.809	-	-	-	[135]

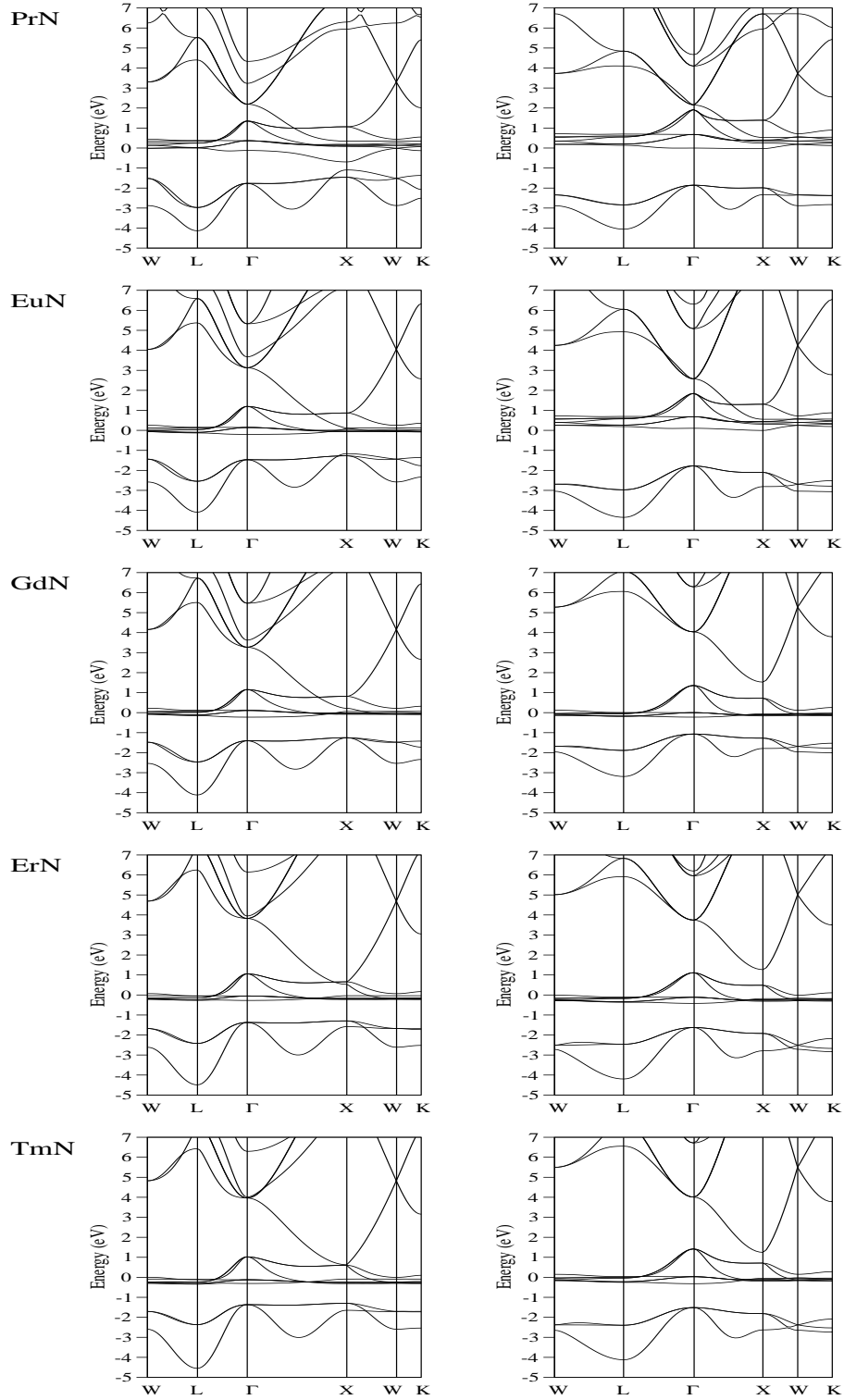


Figure 3.9: LDA band structure of the rare earth nitrides calculated with DFTB (left column) and Wien2K (right column): in each case the the Fermi level was chosen as zero of the energy scale. The k-points are labeled after the bulk structure they refer to, that is rock-salt for all the elements.

Table 3.11: Lattice constants and elastic parameters calculated with the different approaches implemented in DFTB for the FM phase of ErN. Dev. labels the deviation of the calculated values from the experimental ones.

Method	Lattice const. Å	Dev.	B (GPa)	B'
Exp.	4.839 [135]		220.25 [150]	4.3
DFTB	4.895	1.1 %	272.14	3.5
DFTB+ U FLL	4.969	2.7 %	231.40	4.7
DFTB+ U AMF	4.919	1.7 %	224.02	6.7
DFTB pSIC	4.892	1.1 %	264.20	3.0

in system with a lot of unpaired electrons (as in partially filled shells). Alignment effects occur only below a critical temperature, called *Curie temperature*. After this temperature the thermal agitation is too big and the system cannot maintain self-magnetisation anymore, even if it would paramagnetically respond to an external field. Ferromagnets are strongly attracted from magnetic fields.

AFM Antiferromagnets (AFM) are relatively uncommon materials in which the spins of the electrons align in a regular pattern with neighbouring spins pointing in opposite directions. Above a certain temperature, called *Néel temperature*, antiferromagnetic materials become paramagnetic. Below this temperature antiferromagnetic behaviour can result in diamagnetic or (more rarely) ferrimagnetic properties.

FiM In ferrimagnetic materials (FiM) spin moments on the atoms in different sublattices are anti-aligned as in antiferromagnets, however the opposing magnetic moments are not equal and a spontaneous magnetisation remains. Like ferromagnets, ferrimagnets show a spontaneous magnetisation below the Curie temperature and are paramagnets above⁷.

DM Diamagnets (DM) are materials which are repelled from an external magnetic field, as spin dipoles in it tend to align against the external field. Each material is diamagnetic, but the diamagnetic effects are normally overwhelmed by other forms of magnetism (ferromagnetism or antiferromagnetism) for most material, so that diamagnets are normally (but incorrectly) considered all the non magnetic materials like organic compounds and water.

RE-alloys cannot be classified on the basis of their conduction properties simply as metals, semiconductors and insulators, one needs to introduce the more sophisticated concepts of semi-metals and half-metals:

- Semimetals are materials with a negative, indirect band gap. This means that valence and conduction bands have a (mostly small) overlap, though the bottom of the conduction band and the top of the valence band are situated in different part of the momentum space. Unlike regular metals, semimetals have charge carriers of both types (holes and electrons), mostly in smaller amounts than in metals. Semimetals are normally metalloids or alloys.
- Half-Metals are ferromagnets whose density of state at the Fermi level is different from zero for only one spin channel. These materials are therefore metals for one spin and insulators for the other. Half metals are always compounds of more than one element and mostly oxides or Heusler alloys (ferromagnetic alloys whose constituents are not themselves ferromagnets).

Despite their simple rock-salt structure (common to all the RE nitrides), the RE-N compounds show interesting electric and magnetic properties [150], among others ferromagnetic behaviour, extremely low Curie and Néel temperature and an unusual (111) spin orientation. Apart from their properties, the fact that they can be grown epitaxially on semiconductor has made them

⁷Sometimes there is a temperature below the Curie temperature where the two sublattices have equal magnetic moments and the resulting magnetisation is zero. This is called compensation point.

3.2. VALIDATION OF THE PARAMETERS

Table 3.12: *The heat of formation ΔH_f^0 for compounds of interest in this work as calculated in DFTB and measured. As noticed in Ref. [145] there are no accessible data about measured values of ΔH_f^0 for the rare earth nitrides.*

System	Structure	DFTB (eV)	DFT [124]	Experiment
GaN	Zinc-blende	-2.084	-1.689	-1.145
GaN	Wurtzite	-2.084	-1.685	-1.08
PrN	Rock-salt	-4.976	-	
EuN	Rock-salt	-3.135	-	-2.25 ± 0.26 [146]
GdN	Rock-salt	-4.182	-	
ErN	Rock-salt	-5.113	-	
TmN	Rock-salt	-4.942	-	

interesting materials for the realisation of electronic devices. Despite this interest there have been only a few attempts to study such systems [144]. All the RE nitrides are experimentally found to be metals, half-metals or semi-metals [144, 150] characterised by a ionic bonding. Firstly we simulate the properties of all the RE nitrides in their stable rock-salt phase in general and in the DFTB representation, then we concentrate on a particular nitride, ErN, which we consider to be representative, and investigate it thoroughly with all of the approaches implemented in DFTB and in different structures. As term of comparison for the DFTB results we use experimental data and Wien2K [113] calculations. For simplicity we simulate all the rare earth nitrides in the ferromagnetic phase. As usual, primitive cells and a Monkhorst-Pack $12 \times 12 \times 12$ k -point mesh [128] are used. The DFTB-LDA band structures for the rare earth nitrides are reported in Fig. 3.9 and compared with the band structures calculated with LDA approach and the simulation package Wien2k. The LDA approach is not accurate enough to give a correct representation of the band structures and our goal is here only to verify the agreement between the two simulation packages. A qualitative and quantitative agreement is found. While in LDA the RE nitrides have a band gap, it is experimentally known that they are metals, semi-metals or half metals. The metallic or semi-metallic nature of RE nitrides causes them to be non-emitting systems. In overdoped GaN samples in fact (i.e where we try to increase the RE-dopants concentration in GaN above a specific value of the order of magnitude of 1-2%), we observe a RE-N phase segregation and the quenching of the emission. In order to study correctly the optical properties of RE-doped GaN it is therefore essential to simulate correctly the RE nitrides band structure. A proper investigation of the ErN band structure can be found in the following section. The results of our simulation of the geometric and energetic properties of the RE-nitrides are reported in Tab. 3.10. Similarly to the other investigated systems the error affecting the lattice parameters is of the order of magnitude of some percent and the cohesive energy is slightly overestimated, anyway the related error is still the typical precision of a DFTB calculation. Formation enthalpies of the RE nitrides are calculated and reported in Tab. 3.12: unfortunately there is no accessible experimental data concerning the formation enthalpies so that we do not have experimental data as terms of comparison.

ErN

ErN is a good test system for our methods because it is a standard representative of a class of materials (the RE-monopnictides) which have recently attracted much attention due to their peculiar characteristics. Unfortunately ErN has not been as extensively investigate as other Er pnictides (like ErAs) or other RE nitrides (like GdN), but there is a substantial set of experimental data in the literature (see [147, 148] and references there in) as well as several theoretical investigations [9, 144, 149–151] of this material. It is only recently [9, 144] that a consensus has been reached about its half-metallic character, i.e. ErN shows a finite density of states at the Fermi-level for one spin channel and a zero density of states for the other. In some earlier works [149] ErN was described as a metal while in others [150] it was found to be a semiconductor in both ferromag-

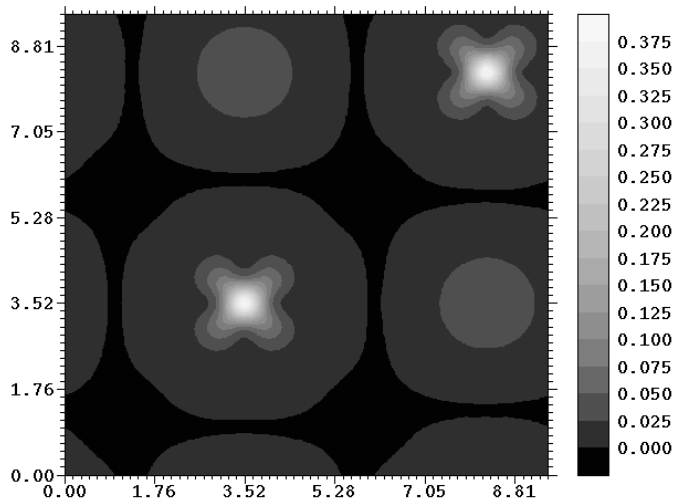


Figure 3.10: Volume slice of the magnetization density in the (100) plane of rock-salt ErN in the ferromagnetic phase. The axis labels are expressed in Å and the hue (in arbitrary units) represents the electronic density. The unpaired electrons are localized on the Er atoms.

netic and paramagnetic (PM) phases. Unlike the other Er-pnictides, in the ground state ErN is a ferromagnet with a magnetic transition at 3.4-6K [152, 153]. We investigated the FM and the PM magnetic phases. While it is clear that using a primitive ErN cell a spin-polarized calculation will be a sensible representation of the FM phase (or the saturation limit of the PM phase in a magnetic field), to simulate the PM phase we adopt a crude virtual crystal approximation. Following the considerations of Pethukov [150] we consider a non spin polarized calculation as representative of the paramagnetic phase. This is a very drastic approximation, a proper treatment of the PM phase would require the consideration of thermal fluctuation effects and knowledge of the magnetic phase diagram. However, this approximation will suffice for the goals of this work, which is to test our methods. We find the difference in the cohesive energy (defined as energy difference of free Er and N atoms in their spin polarized state) of the PM and FM phases to be, independently of the particular calculation approach, about 0.5 eV per atom, which is somewhat higher than the difference reported by Pethukov [150]. Like other RE nitrides ErN is [144, 150] characterized by ionic bonding, however the equilibrium distance (2.432 Å) [135] of Er and N in the compound is only 0.1 Å longer than the sum of the covalent radii of Er (1.57 Å) and N (0.75 Å). The Er ions in ErN are trivalent (existing in the +3 oxidation state), corresponding to an outer electronic configuration for the Er ions of [Xe] 4f¹¹, with a full *f*-semi-shell containing seven spin up electrons and a half filled *f*-semi-shell containing four spin down electrons. This was verified with all spin resolved approaches implemented in DFTB. The fact that 11 of 12 *f*-electrons remain strongly localised while the remaining one is lost is in agreement with the results of Temmerman *et al.* [154] who predict the existence of two kinds of *f*-electrons, localised and delocalised, whose relative numbers change depending on the RE. All ErN calculations in this work were performed using the rock-salt primitive cell and a 12×12×12 Monkhorst-Pack *k*-point mesh [128]. The *U*-value in the LDA+*U* approach is not considered as a free parameter. As discussed in the previous chapter we use half of the value of the atomic *U* and *J* values of the Er 4*f* shell, which was calculated for the atom using Janak's theorem, namely 7.6 eV. This value is consistent with that used in similar simulations [155] and will be used throughout this work for the Er *f*-electrons. The +*U* potentials are applied only to the *f*-shells. We start our ErN characterization with the determination of the lattice parameter. It is interesting to see how this is influenced by different methods. LDA is known to underestimate the band gap (if

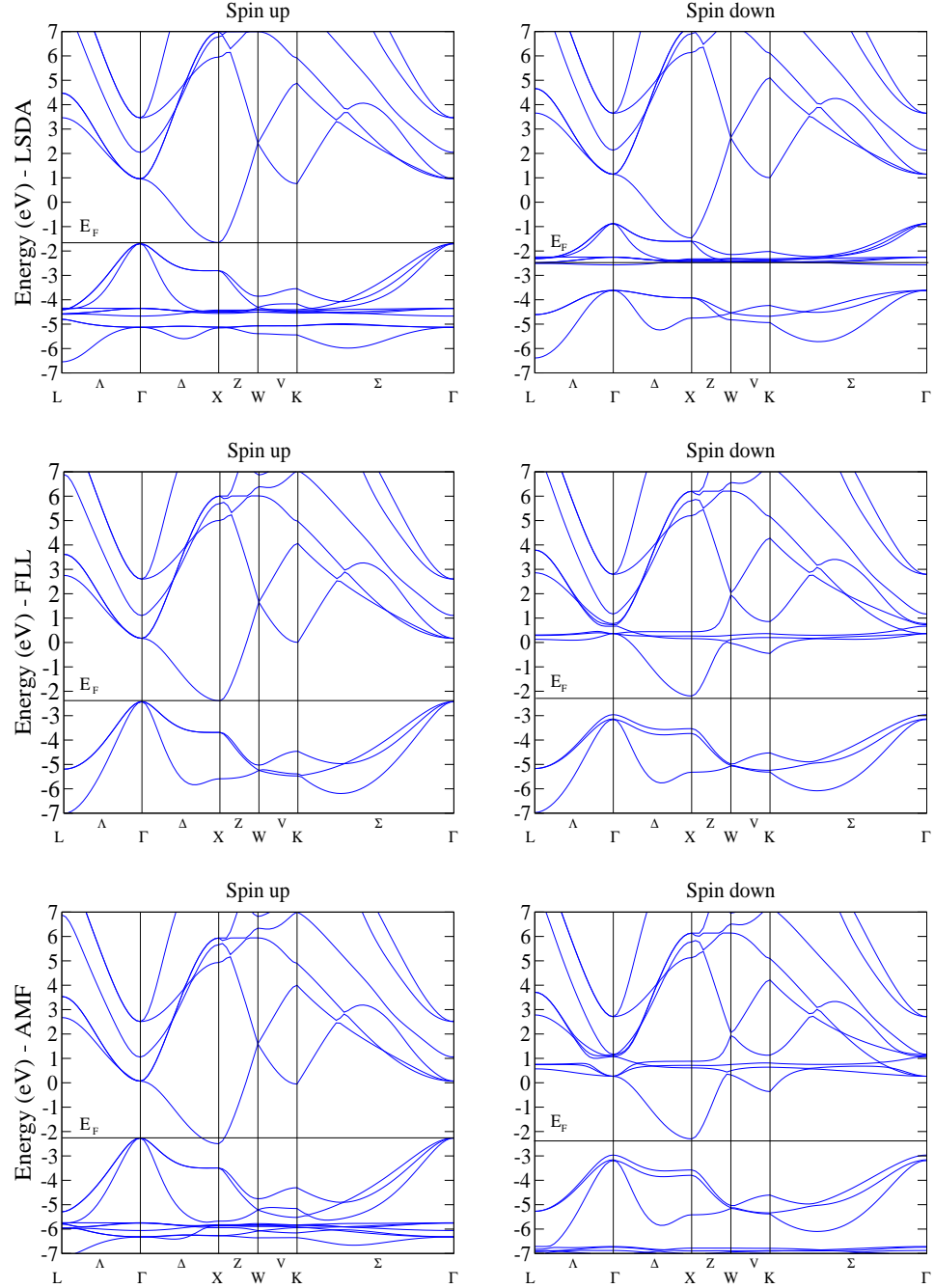


Figure 3.11: Spin resolved band structure of rock-salt ErN calculated with the DFTB-LSDA (first row), DFTB-FLL and DFTB-AMF (second and third row) approach.

present) and the inter-atomic distances of systems with strongly correlated electrons. The LDA+ U approach should improve the description of both. As the LDA-like approach in DFTB already gives relatively accurate results for ErN, one expects LDA+ U to overestimate the ErN lattice constant. This is verified, even if the difference between LDA and LDA+ U is only a few percent of the lattice constant (see Tab. 3.11). In the same table the values of the bulk moduli and their first derivative (with respect to the pressure) calculated with different approaches are reported. The values we have calculated are on average slightly larger than that calculated by Pethukov *et al.* [150] but still within the typical error of the DFTB method. We observe that the application of the AMF and FLL approaches leads to a great improvement in the description of the bulk modulus (and a small worsening in the description of the lattice constant) while the pSIC approach improves the description of the bulk modulus without loss of precision in the description of the lattice constant. The calculated values of the first derivative of the bulk modulus, which is a delicate parameter as well for the theoretical simulation as for the experiment, are around the experimental value for all the approaches. While the calculated values of the bulk modulus come closer to the experiment with the application of orbital dependent potentials, it does not seem to lead to major advantages in the description of B' . As already mentioned ErN is ferromagnetic in the ground state, and the results reported here are for this magnetic phase. The L(S)DA-like picture is not adequate for the simulation of ErN as it shows the narrow bands deriving from the f -states pinned at the Fermi level, which is incorrect for this material. Orbital dependent approaches like DFTB+ U (both in the AMF and FLL limits) instead find ErN in the FM phase to be a half metal, in agreement with Aerts *et al.* [144] and Duan *et al.* [151] (see Fig. 3.11). As in the previously mentioned works, the paramagnetic phase has been simulated by the spin unresolved LDA+ U approach: in this case in both the AMF and FLL limits, ErN is then a narrow-gap semiconductor. We do not report band structures calculated with pSIC here, as this approach is not expected to produce the correct band structure.

3.3 Summary and conclusions

In this chapter a parameterisation for the simulation of RE doping in GaN in the framework of the SCC-DFTB method was presented. The parameter set includes the atomic species necessary for the simulation of the host (Ga, N), of its classical acceptor and donor dopants (C, O) and of a selection of rare earths (Pr, Eu, Gd, Er and Tm) which have been exploited for the realisation of color displays or magnetic devices. In the first part of this chapter the parameterisation procedure is described and the decisions we come to, concerning electrons we consider as valence, compression radii etc., are justified and discussed. The proposed parameterisation was then tested on different systems including the metallic phase of gallium and of the rare earths in many different polytypes, the diamond structure of carbon, the gas phases of oxygen and nitrogen and finally the RE nitrides. Further data about GaN in the different crystalline phases can be found in the dedicated chapter, as well as simulations and discussions concerning the intrinsic defects and the “classical” GaN dopants. Properties like geometries, band structures and elasticity properties were tested against experimental measurements and DFT calculations showing a remarkable transferability and an overall good agreement between our simulations and existing data. We observe that in general DFTB results show a larger (some %) deviation from the experiment than DFT-LDA calculations in the geometric properties of the investigated systems but are less affected by overbinding problems. It can be concluded that the properties of the investigated systems show the same qualitative behaviour, but larger errors than those obtained with full *ab initio* methods. The accuracy of the parameters⁸ and the efficiency of the method allow the investigation of extended systems and the systematic sampling of many configurations for defect physics and chemistry.

⁸preliminary results obtained with our parameters have been also presented in Ref. [28].

Chapter 4

The host: GaN

If we want to understand the mechanisms underlying the RE-related emission from GaN samples, we need first of all a comprehensive knowledge of GaN itself. In this chapter we therefore review this semiconductor before we start the investigation of RE point defects in the next one. Firstly bulk properties such as lattice parameters and cohesive energies are calculated and compared to experimental values. Then intrinsic lattice defects are investigated. As the luminescence center in GaN could be related to complexes formed by RE impurities and GaN-defects, it is important to understand the physics of the latter. This chapter has two main goals, on one side it aims to give a review of the known properties of GaN (both from the experimental and from the theoretical point of view) and on the other side it wants to show that the investigated properties are well reproduced within the DFTB framework.

4.1 The group III-Nitrides

III-V semiconductors and in particular group III-Nitrides (AlN, GaN and InN) have been successfully employed for the realisation of devices already in the seventies [156] and are today still basic materials for optoelectronic devices. The reason for this big interest is due mainly to three factors:

- Group III-nitrides have direct bandgaps ranging from the 0.7 eV [157] for InN (this value is still argument of debate) to the 6.2 eV for AlN, thus covering part of the UV region, the whole visible spectrum and the IR region if alloyed (see Fig. 4.1). Together with their bond strength this property makes group III-nitrides suitable for devices such as full color displays, data storage devices and color printers.
- Due to their thermal stability group III-nitrides based devices can work properly at room temperature (in contrast with Si- or SiC-based devices), allowing the realisation of high-temperature transistors.
- Different group III-nitrides can be alloyed or epitaxially grown in layers as well as on common substrates, thus allowing band engineering. The direct band-gap of group III-nitrides increases the optical transition probability and therefore the adsorption or emission rate of photons by one order of magnitude compared with indirect band-gap semiconductors like SiC.

At standard temperature and pressure group III-Nitrides exist in two polytypes, the hexagonal α -phase (wurtzite structure) and the metastable cubic β -phase (zinc-blende structure). Nitrides in the β -phase have physical properties which are even more favourable with respect to the α -phase for some optoelectronic device applications such as higher electron mobility, easier cleavage and doping than the hexagonal phase [158]. Thus, cubic group III-Nitrides can be assumed as a promising material-system for future optoelectronic applications. Cubic materials can be realised by epitaxial growth on cubic substrates such as GaAs or SiC [159], In recent years, the use of nearly lattice matched, free standing high quality 3C-SiC (001) substrates has led to substantial improvements

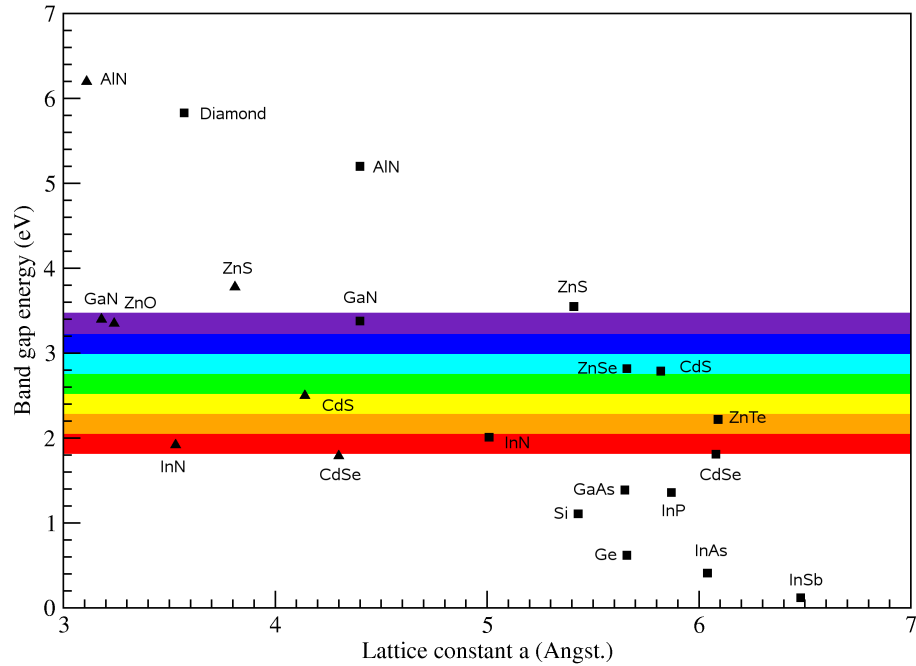


Figure 4.1: Room temperature bandgap energy versus lattice constants of common semiconductors. Triangles represent semiconductors with hexagonal structure, squares semiconductors with cubic structure. *C*, *Si* and *Ge* are the only materials in this picture with indirect band-gap, all other materials have direct band-gap.

of the crystal quality of cubic group-III nitrides [160]. For this reason both the α - and β -phases of GaN will be investigated in this work.

4.2 Brief history of GaN

GaN is by far the most extensively studied semiconductor of all the group III-nitrides, due to its very important technological applications. Because of the direct and large band-gap and its thermal and chemical stability already in the year 1970 GaN was considered a very promising material for the realisation of optoelectronic devices [156], nonetheless it took almost 25 years before scientists were able to produce the first commercial devices, green- and blue-light emitting diode created in the Nichia Labs. by the Nakamura group [161]. This delay was due in part to the difficulty to create good quality crystals and in part to the difficulty to grow *p*-type doped samples. Lasers and emitting diodes based on *pn*-junctions need in fact *p*-type as well as *n*-type materials. While it has never been a problem to produce *n*-type GaN (as-grown GaN is already *n*-type), in the '70 it was not known how to produce the *p*-type. The first problem was due to the lack of matched substrates: the widely used sapphire has a lattice constant 15% smaller than GaN and the lattice matched SiC was too expensive for the commercial production. Today it is possible to produce in a relatively convenient way hexagonal GaN, using developments of the two-steps process firstly proposed by Yoshida [162–164]. The problem of *p*-type doping was instead solved by Akasaki in the '80 [165] using Mg as dopant. The mechanisms underlying the *p*-type doping were successively explained by Neugebauer and Van de Walle [166], who showed how the hole concentration can be increased by co-doping with an acceptor (Mg) and a donor (H). During the following years, luminescent efficiencies improved drastically, which opened new markets for light-emitting devices, such as vehicle break lights, highway status signs and traffic control signs: this on turn pushed the research even further. Nowadays blue and ultraviolet (UV) laser emitting diodes (LEDs) have already been realised and commercialised. Other examples of modern GaN-based applications are UV detectors and microwave power and ultra-high power switches. Next-generation DVD players

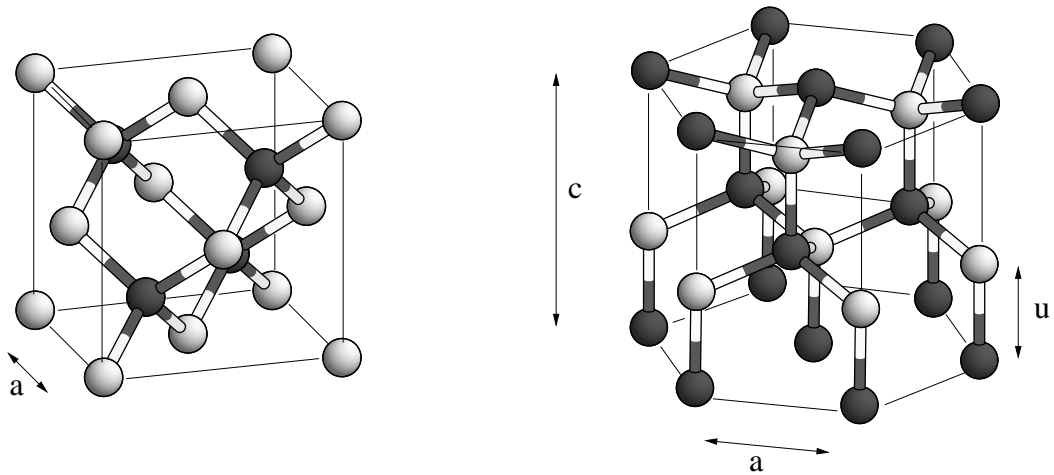


Figure 4.2: Conventional cells of β -GaN (zinc-blende structure) and α -GaN (wurtzite structure). a and c are the lattice parameters and u is the internal lattice parameter. In the pictures the Ga atoms are white and N atoms black.

and recorders as well as optical data-storage systems for computers will be GaN-based devices too. The change from currently available red or infrared (680-780 nm) laser diodes to the GaN-based lasers with a wavelength of 380-450 nm will significantly increase the optical-storage density up to six times the present capacity. Recently the rare earth ions became attractive candidates for optical GaN-based devices in the visible region, since these elements exhibit sharp optical emission lines (which are however almost independently from the host material). Moreover, due to the wide bandgap of GaN, luminescence is not quenched at room temperature as it happens for example in silicon. From the 1993, year of the first announcement of a GaN based LED, there has been a rapid increase in the Research and Development (R&D) field. In the 1999 the GaN-market had been grown from zero to \$ 400 million, by the year 2003 they were already \$ 1.35 billion and it is expected a further increase of \$ 400 billion to this year (2007) [167].

4.3 Properties of GaN

GaN is a semiconductor which crystallises in the wurtzite structure at ambient conditions. It is a tetrahedrally coordinated III-V compound characterised by a chemical bond which can be regarded as partially covalent and partially ionic. GaN possesses two unique properties: a large saturated electron drift velocity and a large direct band gap. In this section a brief overview of the most relevant structural, thermal, electrical and optical properties of GaN can be found. A more extended discussion can be found in the Ref. [161, 168].

4.3.1 Structural properties

As previously mentioned, the GaN stablest phase under ambient conditions is the hexagonal wurtzite structure, called α -GaN, space group C_{6v}^4 . The GaN cubic phase, called β -GaN has the zinc-blende structure with space group T_d^2 and is only slightly higher in energy [169, 170]. Both structures are represented in Fig. 4.2, the actual values of the lattice parameter can be found in the Tab. 4.1 and 4.2. Under high pressure conditions (50-70 GPa) GaN undergoes a structural phase transition to the rock-salt structure, which is favoured because of its high ionicity. No transition to the zinc-blend phase has been observed to date. In this work only the structures for which RE-related luminescence has been reported, i.e. the α - and β -phases are investigated. Wurtzite GaN is more common than the zinc-blende GaN as it is slightly more stable and easier to grow, but the latter has recently attracted a lot of attention due to its advantages with respect to hexagonal GaN,

namely a somewhat lower value of the bandgap and an even higher saturated electron drift velocity. Wurtzite GaN is anyway an excellent host for impurities: a defect density of 10^{10} cm^{-2} can be reached, which is extremely high if compared to other semiconductors like Si (10^2 cm^{-2}) or GaAs (10^4 cm^{-2}). At the same time the lattice location of the defects in wurtzite structure is quite complicate to investigate: this is due to the high number of possible interstitial site with different characteristics typic for the hexagonal environment. Some possible sites in β -GaN that should be considered in a simulation are indicated in Fig.4.3.

The wurtzite structure

The wurtzite structure (crystal number 168) is typical for GaN and many other semiconductors characterised by the sp^3 -hybridisation (III-V and II-VI). This structure can be thought as two interpenetrating hexagonal close packed (HCP) sub-lattices, each with one type of atoms (Ga or N), offset along the c -axis by $3/8$ of the cell height. The axis perpendicular to the basal planes is usually labeled as the c -axis (see Fig. 4.2). In each unit cell there are two atoms of each type: one possible description of the wurtzite structure is given through the lattice vectors:

$$\text{Primitive vectors: } \begin{cases} \mathbf{t}_1 = a \left(\frac{1}{2}, \frac{\sqrt{3}}{2}, 0 \right) \\ \mathbf{t}_2 = a \left(-\frac{1}{2}, \frac{\sqrt{3}}{2}, 0 \right) \\ \mathbf{t}_3 = c \left(0, 0, 1 \right) \end{cases}$$

$$\text{Basis vectors: } \begin{cases} \mathbf{d}_1 = \left(\frac{1}{2}a, \frac{1}{2\sqrt{3}}a, 0 \right) & (\text{Ga}) \\ \mathbf{d}_2 = \left(\frac{1}{2}a, -\frac{1}{2\sqrt{3}}a, \frac{c}{2} \right) & (\text{Ga}) \\ \mathbf{d}_3 = \left(\frac{1}{2}a, \frac{1}{2\sqrt{3}}a, uc \right) & (\text{N}) \\ \mathbf{d}_4 = \left(\frac{1}{2}a, -\frac{1}{2\sqrt{3}}a, \left(\frac{1}{2} + u\right)c \right) & (\text{N}) \end{cases}$$

The parameter a and c are the lattice constants, while u is a dimensionless internal lattice parameter. The basis vector \mathbf{d}_1 and \mathbf{d}_2 are occupied by an atom type while \mathbf{d}_3 and \mathbf{d}_4 by the other. Each atom is surrounded by an almost regular tetrahedron of atoms of the other type. This tetrahedron is regular if $\frac{c}{a} = \sqrt{\frac{8}{3}} = 1.633$ and $u = \frac{3}{8} = 0.375$. For β -GaN we have $c/a=1.625$ and $u = 0.375$.

The zinc-blende structure

The cubic counterpart of the wurtzite structure is the zinc-blende structure (space group $F43m$, crystal number 216), which is also typical for III-V and II-VI semiconductors with sp^3 -hybridisation. The zinc-blende structure can be thought as two interpenetrating FCC-lattices and is mathematically described as a cubic face centered lattice with a basis of two atoms:

$$\text{Primitive vectors: } \begin{cases} \mathbf{t}_1 = \frac{a}{2} \begin{pmatrix} 0 & 1 & 1 \end{pmatrix} \\ \mathbf{t}_2 = \frac{a}{2} \begin{pmatrix} 1 & 0 & 1 \end{pmatrix} \\ \mathbf{t}_3 = \frac{a}{2} \begin{pmatrix} 1 & 1 & 0 \end{pmatrix} \end{cases}$$

$$\text{Basis vectors: } \begin{cases} \mathbf{d}_1 &= \begin{pmatrix} 0 & 0 & 0 \end{pmatrix} & (\text{Ga}) \\ \mathbf{d}_2 &= \begin{pmatrix} \frac{a}{4} & \frac{a}{4} & \frac{a}{4} \end{pmatrix} & (\text{N}) \end{cases}$$

The lattice positions \mathbf{d}_1 and \mathbf{d}_2 are of course occupied by atoms of different type. The coordination number of the atoms in the zinc-blende structure is four, i.e. each atom is surrounded by four atoms of the other type in a tetrahedric configuration with the first neighbours at a distance of $a\frac{\sqrt{3}}{4}$. Note that if the basis is occupied by atoms of the same type one has the diamond structure examined in the previous chapter. The equilibrium structure of both wurtzite and zinc-blende GaN are obtained in this work by minimising the total energy with respect to the primitive cell volume V . As can be seen in the Tab. 4.1 and Tab. 4.2 the lattice parameters calculated in this work are in very good agreement with the measured ones (the deviation from the experiment is of 1.2% up to 2% depending on the basis set used) and are almost as precise as the DFT-LDA values (reported in the same tables).

4.3.2 Thermal and thermodynamic properties

The thermal properties of GaN (like thermal expansion) have not been investigated in this work and we limit ourself to report data from the literature. Moreover, thermodynamic properties like bulk modulus and cohesive energy have been calculated and are reported in the following. The thermal expansion of wurtzite GaN has been studied in the temperature range of 300-900 K by Maruska and Tietjen [171]. They reported a linear change with temperature for lattice constant a , with a mean coefficient of thermal expansion of $\Delta a/a = 5.59 \cdot 10^{-6} \text{ K}^{-1}$ across the entire temperature range. Meanwhile, the expansion of the lattice constant c shows a super-linear dependence on temperature. The mean coefficient of thermal expansion parallel to the c -axis is $\Delta c/c = 3.17 \cdot 10^{-6} \text{ K}^{-1}$ and $\Delta c/c = 7.75 \cdot 10^{-6} \text{ K}^{-1}$ for the temperature ranges 300-700 K and 700-900 K respectively. The Debye temperature (θ_D) of wurtzite GaN was calculated to be $\theta_D \gg 600 \text{ K}$ [172]. The bulk modulus is defined as:

$$B(T, P) = -V \left(\frac{\partial P}{\partial V} \right)_T \quad (4.1)$$

and its first derivative with respect to the pressure is defined as:

$$B' = -\frac{\partial}{\partial p} \left(V \frac{\partial}{\partial V} P(T, V) \right)_{T, P=0} \quad (4.2)$$

In this work they have been calculated for both GaN phases by fitting the energy-volume curves to the Murnaghan equation of state (Eq. 3.1). Calculated and measured values are reported in Tab. 4.1 and Tab. 4.2. The agreement of experimental and calculated data is surprisingly good, clearly beyond the standard DFTB accuracy in the calculation of elasticity properties [114]. The DFTB description of the GaN bulk modulus in both phases is as accurate as the DFT-LDA. The cohesive energy is by definition the energy necessary to separate the crystal in its constituent parts. This energy depends on what the constituent parts are considered to be. They are generally (and also in this work) taken to be the individual atoms of the chemical elements out of which the solid is composed:

$$E_{\text{coh.}}^{\text{GaN}} = E_{\text{tot.}}^{\text{GaN-Bulk}} - E_{\text{tot.}}^{\text{Ga-atom}} - E_{\text{tot.}}^{\text{N-atom}} \quad (4.3)$$

where $E_{\text{tot.}}^{\text{GaN-Bulk}}$, $E_{\text{tot.}}^{\text{Ga-atom}}$ and $E_{\text{tot.}}^{\text{N-atom}}$ are the total energies of GaN-bulk and of the Ga and N free atoms. The atomic spin-polarisation was explicitly included in the calculation of the cohesive energy: we used the values from Zoroddu [124], -2.89 eV for N and -0.134 eV for Ga. We observe that DFTB results are affected by over-binding problems like DFT-LDA (Tab. 4.1 and Tab. 4.2), almost

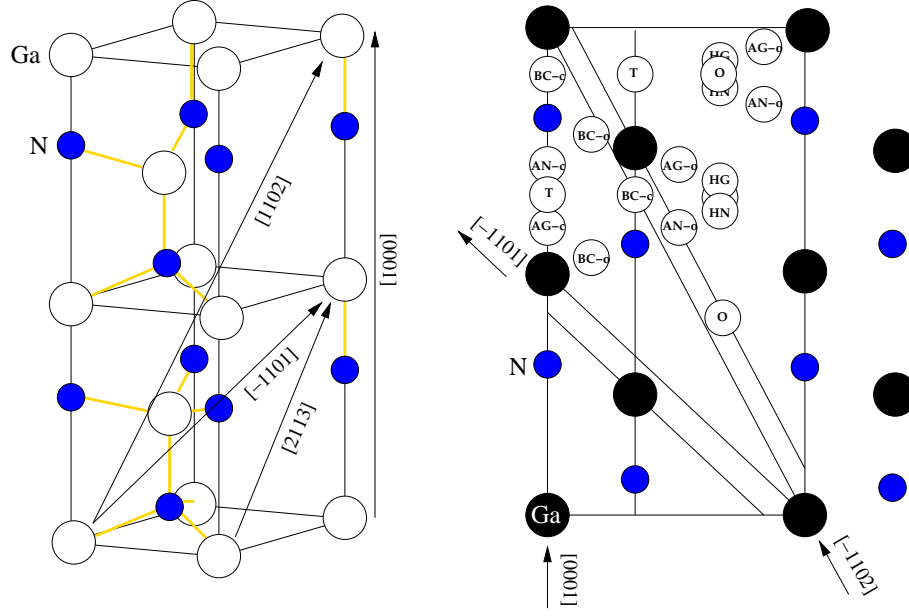


Figure 4.3: The most important high symmetry interstitial sites in α -GaN. Nitrogen atoms in the perfect crystal are represented by blue circles while gallium atoms are white (left hand side) or black (right hand side). Interstitial sites (white circles, right hand side), are labeled with their conventional names: BC-c and BC-o for bond center within and off the c-axis, AG-o, AG-c AN-o and AN-c are the Ga and N anti-bonding sites, HG and HN are the hexagonal sites, O stands for octahedral and T for tetrahedral. HG, HN and O sites are centered in the hexagon spanned by the Ga and N c-axis rows and posses trigonal symmetry (C_{3v}).

independently from the used basis. Experimentally the GaN hexagonal phase is found to be the most stable, while DFT-LDA calculations [173] reveal that the difference in energy between the two phases is less than 20 meV. This very small difference is within the intrinsic DFTB error, so that the two phases have to be considered energetically degenerate within the DFTB representation. We do not think that this negatively influences our simulation of RE point defects in GaN (see discussion at the end of this chapter).

When the constituent parts in Eq. 4.3 are considered the solid phases of Ga and N we have the formation enthalpy of the solid at $T=0$ K, defined as:

$$\Delta H_f^{T=0}(GaN) = E_{tot.}^{GaN-Bulk} - E_{tot.}^{Ga-bulk} - E_{tot.}^{N-bulk} \quad (4.4)$$

where $E_{tot.}^{GaN-bulk}$, $E_{tot.}^{Ga-bulk}$ and $E_{tot.}^{N-bulk}$ are the total energies of the bulk phases of GaN, Ga and N respectively. Calculated and experimental values can be found as usual in Tab. 4.1 and Tab. 4.2: even in this case DFTB turns out to be almost as precise as DFT-LDA calculations.

4.3.3 Electrical properties

The control of the electrical properties has been and remains the main obstacle for device fabrication. As-grown GaN samples have been observed to be n -type semiconductors with a relatively high electron concentration, even for the best samples without intentional doping. The big differences in the electrical characteristics of GaN reported in the literature reflect probably the crystal quality and purity of the materials used [174]. The high carrier concentration however implies the presence of donors even in as-grown samples. Since no impurities have been present in sufficient amounts to account for the carriers, this high concentration is generally believed to be caused by native defects and more specifically by nitrogen vacancies. Recently it was shown that N vacancies have large formation energies in n -type material [175]. This makes it of course unlikely that N vacancies are formed in the large quantities necessary to explain the observed carrier concentration. This issue

Table 4.1: *Structural and electronic properties of β -GaN (zinc-blende). All the distances are expressed in \AA , the energies in eV and bulk moduli in Mbar. Elasticity properties are calculated in this work fitting the Murnaghan equation.*

Reference	Method	Valence	a	Bandgap	B	B'	E_{coh}	$\Delta H_f^{T=0}$
This work	DFTB	s, p	4.43	4.21	1.73	4.8	-10.82	-2.06
This work	DFTB	s, p, d	4.55	4.06	1.71	3.7	-10.90	-
[176]	DFT-LDA	s, p, d	4.46	2.15	2.02	4.3	-	-
[170]	DFT-LDA	s, p	4.42	1.48	1.73	3.6	-	-
[124]	DFT-LDA	s, p, d	4.45	-	-	-	-10.98	-1.69
[124]	DFT-GGA	s, p, d	4.54	-	-	-	-9.25	-1.10
[169]	DFT-LDA	s, p	-	2.1	-	-	-	-
[169]	DFT-GW	-	-	3.1	-	-	-	-
[127]	DFT-LDA	s, p	4.38	2.35	1.97	4.5	-11.01	-0.50
[127]	DFT-LDA	s, p, d	4.52	1.76	1.88	4.4	-10.38	-1.22
[127]	DFT-GGA	s, p	4.43	2.01	2.13	4.4	-9.93	-1.28
[127]	DFT-GGA	s, p, d	4.60	1.39	1.66	4.1	-8.52	-0.62
[174]	Exp.	-	4.52	3.41	1.73	3.7	-8.96	-1.20

is shortly investigated in the following. Currently it is assumed that the carriers are provided by impurities like O or Si which contaminate the samples during the growth.

Electrical doping

The goal of electrical doping is to modify the conductivity of the semiconductor, by *dopant implantation* or *implantation isolation*. With the dopant implantation electrically active n - or p -type dopants are introduced to increase the free carrier concentration, while with the implantation isolation highly resistive layers are produced by implantation of various elements, which create mid-gap levels that trap electrons and holes. As seen in the introduction the production of n - or p -type GaN is necessary to produce pn -junctions. As grown GaN is typically n -type material with a high free carrier concentration, which makes the production of p -type GaN difficult. Different donor and acceptor dopants have been already used to achieve respectively n -type or p -type doping. Examples of donor impurities are Si [177] and O [178], while C [179], Mg [177], Be [180], Zn [180] and Ca [178, 180] are used as acceptor dopants.

4.3.4 Optical properties

Optical properties are probably the most investigated properties of GaN, because GaN shows its great potential specially as light emitter. The large direct bandgap allows efficient light emission and in the literature can be found many reports about luminescence from GaN-based samples. Maruska [171] was the first to accurately measure the bandgap energy at room temperature for the wurtzite structure. This transition is measured between the uppermost valence band states and the lowest conduction band minimum. The band gap of GaN in the native DFTB approximation is almost twice the experimental band gap, due to the minimal basis used in this approach. Of course, as one of our main goals is the description of the localised defect-related levels in the band gap we cannot find such a description of the band gap satisfactory. It is important to note here that also DFT-LDA calculations with a more expanded basis set suffer from a gap error, underestimating the band gap of semiconductors considerably (in the case of GaN a value typically around 2.2 eV is found instead of the experimental value of 3.5 eV). However, the at first view disadvantageous parameterisation needed in the DFTB approach allows here to correct the LDA gap error before the defect calculation: in this work we adjust the band gap to a value close to the experimental value by slightly modifying the on-site energy of the s -shells of nitrogen. This does not affect the description

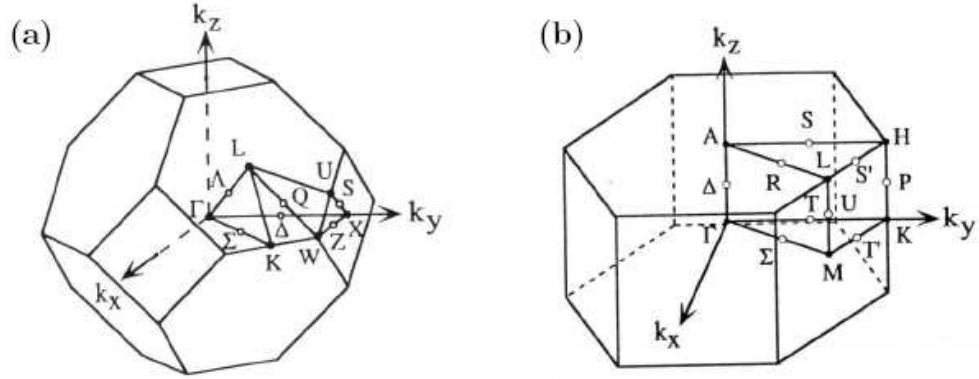


Figure 4.4: First Brillouin zones with the highest symmetry lines of (a) face-centered cubic (zinc-blende structure) and (b) hexagonal lattice.

of the other properties of GaN, as we show in the following. This correction is important, because the value of the band gap is crucial for correct description of the optical properties. The calculated band structure of wurtzite and zinc-blende GaN are shown in Fig. 4.5. Both phases have a direct band gap, with valence band maximum and conduction band minimum located at the Γ point of the Brillouin zone. The Brillouin zones for face-centered cubic (FCC) lattice and hexagonal lattice are shown in Fig. 4.4. The theoretical band gap is calculated using the energy difference between the highest occupied eigenvalue and the lowest unoccupied eigenvalue. In β -GaN there is a single conduction band with Γ_7 symmetry and three valence bands which are non-degenerate. The top of the valence band is split by the crystal field and by the spin-orbit coupling into three bands, two with Γ_7 symmetry (called light-hole and spin-orbit splitting band) and one with Γ_8 symmetry (called heavy-hole). In this calculation, we do not include spin-orbit coupling, therefore the spin-orbit splitting is not seen in the band structure. However, the splitting due to the crystal-field is found to be of few meV (this can be hardly distinguished in the picture). The experimental values lie in the range of 10-25 meV [174]. With a bandgap of about 3.5 eV, both wurtzite and zinc-blende GaN are situated in the UV region as can be observed from Fig. 4.1: on the left hand side of the same picture, can be found the more common semiconductors like Si, Ge and GaAs with a much lower bandgap energy.

Yellow luminescence

The general term "yellow luminescence" in GaN refers to a broad luminescence band centered around 2.2 eV. This band is a universal feature of GaN, as it has been observed as well from bulk GaN as from GaN-layers grown with different techniques. The intensity of the yellow luminescence varies from sample to sample and almost vanishes in samples with very good crystal quality. In order to explain the observed PL Ogino and Aoki [181] proposed a model in which the luminescence is due to a transition between a shallow donor and a deep acceptor level: this model has been confirmed by different experiments but is not clear which defects, impurities or complexes play the role of the shallow and deep levels. The origin of the yellow luminescence is still argument of debate, even if today gallium vacancies appear to be the most likely source, either in isolated form or in a complex with an impurity [182]. This issue is addressed later on in the section regarding Ga vacancies.

Red luminescence

Besides the yellow luminescence also red luminescence (a band centered at 1.8 eV) has been observed from C-doped (cubic) GaN [183] and Mg-doped GaN [184]. The red luminescence has been related

Table 4.2: *Structural and electronic properties of α -GaN (wurtzite). All the distances are expressed in \AA , the energies in eV and bulk moduli in Mbar. Lattice parameters and elasticity properties are calculated in this work fitting energy-volume curves to the Murnaghan equation of state.*

Reference	Method	Valence	a	c	Bandgap	B	B'	E_{coh}	$\Delta H_f^{\text{T}=0}$
This work	DFTB	s, p	3.142	5.105	4.27	1.71	5.1	-10.825	-2.06
This work	DFTB	s, p, d	3.226	5.242	4.16	1.69	3.6	-10.894	-
[169]	DFT-LDA	s, p	-	-	2.3	-	-	-	-
[169]	DFT-GW		-	-	3.5	-	-	-	-
[170]	DFT-LDA	s, p	3.126	5.119	1.63	1.90	2.9	-	-
[124]	DFT-LDA	s, p, d	3.131	5.104	-	-	-	-11.00	-1.69
[124]	DFT-GGA	s, p, d	3.199	5.227	-	-	-	-9.27	-1.12
[127]	DFT-LDA	s, p	3.133	5.179	2.20	2.17	5.9	-11.03	-1.80
[127]	DFT-LDA	s, p, d	3.196	5.213	1.60	1.87	5.4	-10.40	-1.25
[127]	DFT-GGA	s, p	3.191	5.211	1.90	1.84	4.8	-9.31	-1.15
[127]	DFT-GGA	s, p, d	3.252	5.298	1.27	1.62	4.1	-8.54	-0.64
[135]	Exp.		3.180	5.185	-	-	-	-	-
[174]	Exp.		3.189	5.179	3.45	1.88	4.3	-9.06	-1.15

to recombination processes involving the gallium vacancies and the (intentional or unintentional) doping with C or Mg.

Optical doping by RE-ion implantation

GaN is an ideal candidate as host for optical dopants because of its thermal stability and especially because of its large and direct bandgap. Pankove and co-workers [185] studied already in the 70s luminescence from 35 different species implanted in GaN, accurately reporting luminescence lines where present. They remarked that the implantation induced damage plays a crucial role, since it is detrimental for the luminescence. Numerous studies [186] have already been performed to investigate the influence of implantation damage from various elements on the luminescence of GaN. The group of elements which has recently caught the attention of many researchers are the rare earths, the main subject of this work. As seen in the first chapter, they are characterised by very sharp optical transitions in the visible and infrared regions, almost independent from the host material. This makes them extremely suitable for optoelectronic devices. Literature reports of the implantation of Ce [187], Pr [187–191], Nd [192, 193], Sm [194, 195], Eu [188, 196], Gd [197], Tb [198, 199], Dy [187, 200], Ho [194], Er [201–205], Tm [196, 200, 206], Lu [187] and Yb [207].

4.4 The simulation of GaN

The simulation of GaN is a challenge for theorists. The application of established calculations schemes like the local or gradient corrected density approximation (LDA/GGA) of the density functional theory to defects may be problematic. As discussed in Ref. [175], there are certain shortcomings which could become critical if describing intrinsic defects in GaN: DFT calculations suffer from an underestimation of the fundamental band gap. This leads to large uncertainties when interpreting the Kohn-Sham eigenvalues in the band gap as actual defect levels. Due to the drastic band gap error of more than one eV, the situation is specially critical in case of GaN. The Ga $3d$ electrons are an additional complication. It has been argued that the explicit treatment of these states in the valence is necessary for taking their hybridisation into account [111, 173]. On the other hand including the $3d$ in the valence means to consider ten more electrons per Ga-atom, which makes the calculations with supercells containing hundreds of Ga atoms much more demanding. Besides, LDA places the d states too high in energy (degenerate with the $2s$ band of the nitrogen atoms in contrast to their actual positions as determined by X-ray measurements [208]). This results in an

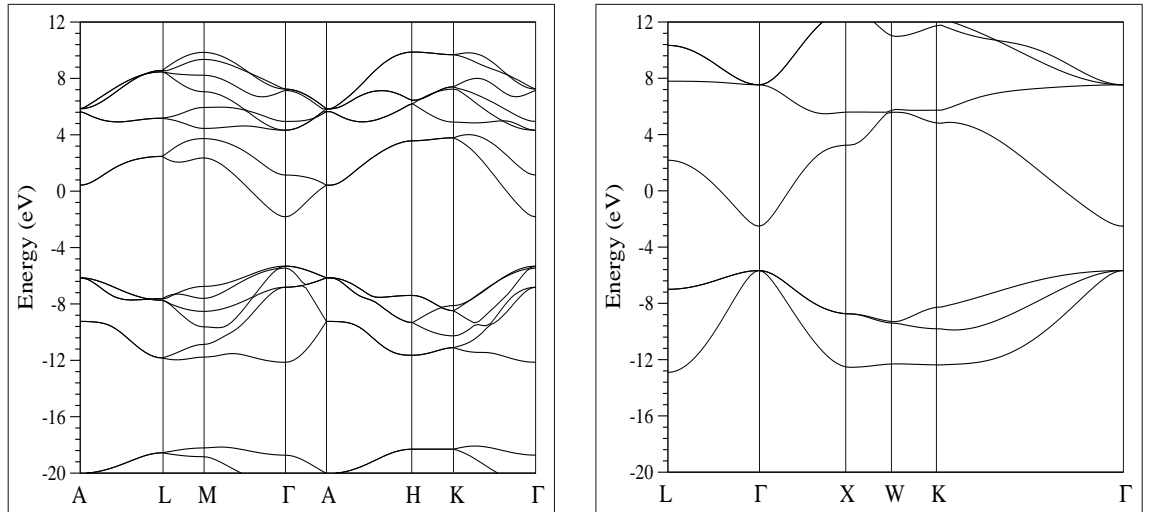


Figure 4.5: *Left: calculated band structure of hexagonal GaN. Right: Calculated band structure of cubic GaN. The band structure of the wurtzite GaN shows its typical features: starting from the top of the figure can be recognised the conduction band deriving from Ga p - and N s -electrons, the valence band with Ga s - and N p -character and, at the bottom, a band originating from the N $2s$ -states. The band structures were calculated at optimised geometries for both structures. For a comparison see [169].*

artificial hybridisation and pushes up the valence band maximum, further decreasing the already underestimated band gap. This effect can be clearly observed in the values reported in Tab. 4.1 and Tab. 4.2. It is thus of essential importance to consider the effect of band gap errors on the calculated GaN defect properties. This problem can be tackled in semi-empirical approaches adjusting the band gap to the experimental value like we did in this work (see Sec. 4.3.4). To decide whether the Ga- $3d$ shells have to be treated as core or valence states, we calculated structural and cohesive properties of bulk GaN using parameters treating Ga $3d$ as core and as valence states. We found that including the d -electrons in the atomic core does not substantially affect the DFTB description of GaN and therefore decided to treat only s and p orbitals as valence states. The band gap error is only one short-coming of DFT in the local density approximation and its gradient extensions. Another problem concerns the spurious self-interaction that becomes more critical with increasing electron localisation. This artificial self-interaction occurs partially also in hybrid functionals, due to the remaining local contribution to the exchange and correlation functional that amounts typically to about 75% [209]. Therefore, electrons in defect states may delocalise over too many atoms, in order to reduce the artificial Coulomb repulsion. In some cases this may lead to wrong structures with artificially enlarged symmetry.

4.5 Defects

Reference [175] provides a recent and comprehensive review of the state-of-the-art in first principles calculations of intrinsic and dopant defects in GaN. Several defects in GaN show properties which are strikingly different from more classic semiconductors like Si and GaAs. These properties can be explained with the big mismatch in the covalent radii of Ga and N. Among GaN intrinsic defects the vacancies are relatively known systems and are likely to be formed due to their stability (low formation energy) [210]. Self-interstitials and anti-sites are instead high-energy defects and thus, judging from pure formation energies, unlikely to occur during growth conditions near thermal equilibrium. However, they can be formed under non-equilibrium conditions, for instance by ion-implantation or electron irradiation. To check the DFTB representation of point defects in GaN we investigate in this section known systems like the isolated Ga and N vacancies in α - and β -GaN, which we consider representative for the class of intrinsic defects in GaN and C and O substitutionals, which we consider to be representative for the class of standard acceptor and

donor dopants respectively. All the results shown here were calculated with spin-polarized DFTB calculations. The spin configuration which minimizes the total energy was determined and used in each case. 512(256)-atom supercells of hexagonal GaN containing only one defect or impurity¹ were relaxed within the Γ -approximation till the residual forces were lower than 10^{-4} eV/Atom. At this distance defects in neighboring cells can be considered not interacting. The charge transition levels are calculated with the Janak-formalism described in the second chapter. For each investigated system the position of the highest occupied orbital was calculated for occupation numbers going from 0 to 1 with a step of 0.1, i.e. in 11 different points. The position of the transition levels is given with respect to the valence band maximum. Since the VB edge in a supercell approach is not easy to determine, an error bar of about 0.05 to 0.1 eV is induced. To analyse the linearity of the Kohn-Sham levels the *norm of the residuals* (or mean square deviation) between a linear fit and the calculated values is used:

$$\Delta = \frac{1}{n} \sqrt{\sum_{i=0}^n \{\varepsilon(x_i)^{\text{interpol.}} - \varepsilon(x_i)^{\text{calc.}}\}^2}$$

where $x_i = (0.0, 0.1, \dots, 1.0)$, $\varepsilon^{\text{calc.}}$ and $\varepsilon^{\text{interpol.}}$ are the calculated and interpolated positions of the one-particle levels. Since the mean square deviation depends on the magnitude of the eigenvalues, the Δ corresponding to different states are not readily comparable. We therefore introduce the deviation D

$$D = \frac{\Delta}{\alpha} \quad (4.5)$$

as measure of the linearity, where the norm of the residuals is divided by the slope α of the corresponding state.

4.5.1 Nitrogen vacancies

Nitrogen vacancies are a system which is still under debate at the time this work is being written. The electronic structure of such defects calculated by Jenkins *et al.* [211, 212] at the end of the 80s with a tight-binding approach has been widely used to interpret the experimentally observed defect levels. Successively, in the middle of the 90s, Neugebauer *et al.* stated that in n -type GaN the V_{Ga} dominate and the isolated V_{N} have such a high formation energy (4 eV) that cannot be formed in concentrations high enough to be responsible for the n -type doping (DFT-LDA) [182]. Recently Nieminen and co-workers found with a similar *ab initio* calculation scheme that N vacancies should be the dominant defect in GaN independently from the position of the Fermi energy within the band-gap [210]. In the following we give the DFTB representation of the isolated V_{N} both in hexagonal and cubic GaN.

Removing one N-atom from the lattice results in three electrons which are no more involved in the Ga-N bond and are distributed in a doubly occupied a_1 state and a t_2 state ($a_1 + e$) hosting one electron. Theoretically the V_{N} can be formed in all charge states between +3 and -5: the first case would happen when the three electrons are removed and the second when the t_2 state is completely filled with extra electrons. Practically not all of these states are allowed, because not all the created localised states lie in the band-gap of the ideal crystal. The nitrogen vacancy in GaN is discussed frequently in the literature as giving rise to negative- U transitions. Van de Walle *et al.* [175, 182] calculated a (3+/-) transition to take place around 0.5 eV, a value that based on increased supercell sizes was later corrected by the same authors to a value somewhat closer to the VB maximum (around 0.3 eV). Only recently, Nieminen and coworkers [210] claim the existence of transitions into negatively charged states. Accordingly, a (+/-) negative- U transition takes place 2.46 eV above the valence band edge. We simulate here all charge states between -5 and +3, both in wurtzite and zinc-blende GaN. The one-particle levels within the band gap are plotted at the Γ -point for all the charge states between +3 and -3 in Fig 4.6.

¹This corresponds to an impurity concentration of $\approx 0.4\%$ (0.8% for 256-atom supercells) or to a distance between defects in neighbouring cells of 17.5 Å.

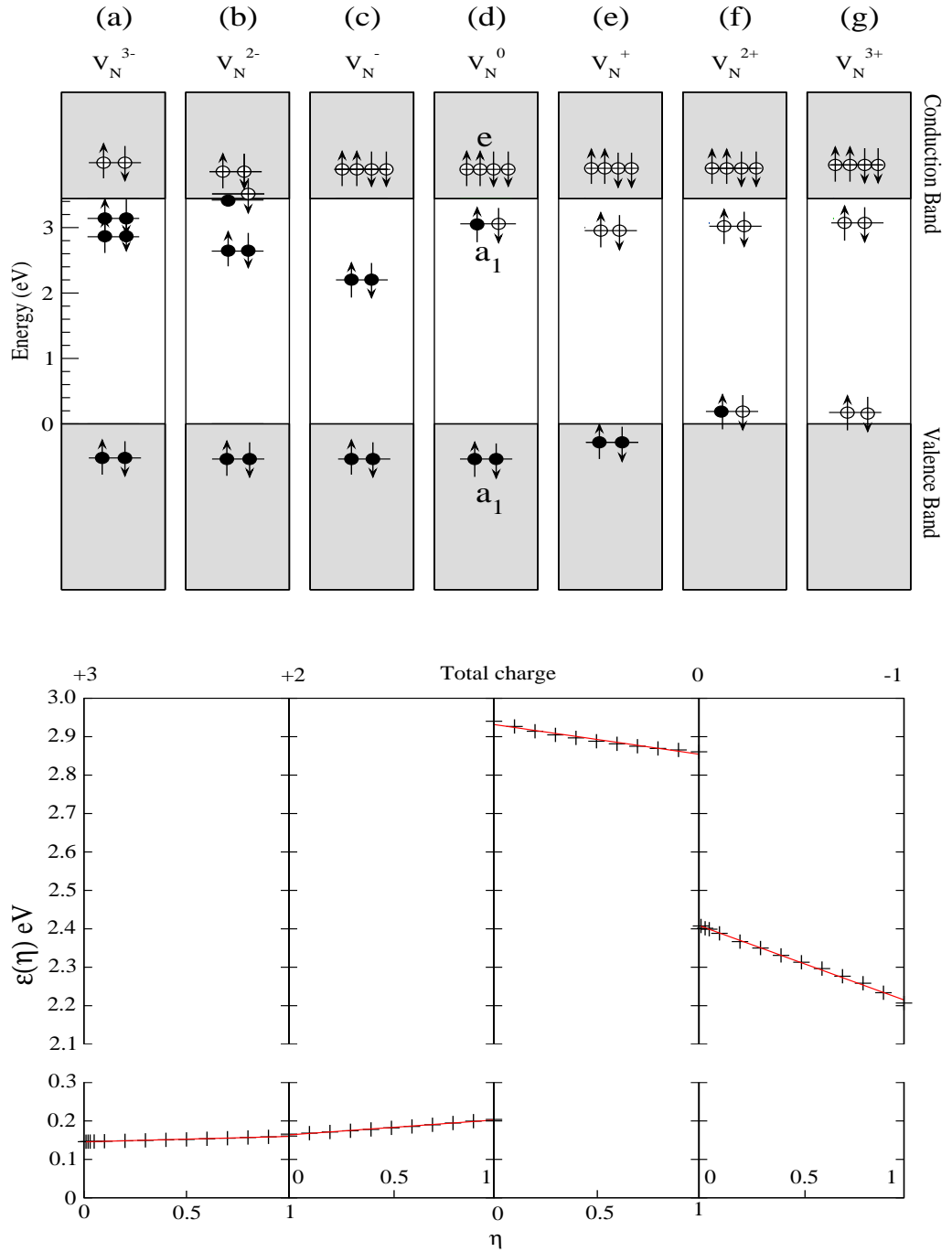


Figure 4.6: Upper part: possible charge states for the isolated V_N in hexagonal GaN, schematic representation of the one-particle levels in the band gap. Filled circles identify occupied states while unfilled circles identify empty states. Up and down arrows identify spin up and spin down electrons. Lower part: highest occupied one particle level as function of its occupation for the different charge states of the isolated V_N in hexagonal GaN. The lines are linear interpolations of the calculated points. Even if the charge transition $\epsilon(-2/-3)$ is in the band gap, when the vacancy is in the charge state -2 the highest occupied one particle level is in the conduction band, i.e. delocalised. For this reason we limit us to report the other charge transitions in this picture.

Table 4.3: Position of the charge transition and slopes of the function $\varepsilon(\eta) = \alpha\eta + \beta$ for different systems. All the transition are in eV above the valence band. The slope α (in eV) and the deviation D (defined by Eq. 4.5) have been calculated for the hexagonal phase.

Syst.	Method	Trans.	$\varepsilon(0.5)(hex)$	$\varepsilon(0.5)(cub)$	Slope	Deviation D
O _N	LSDA	(+/0)	3.35	3.35	-1.219	0.006
C _N	LSDA	(0/-)	0.32	0.34	0.103	0.009
V _N	LSDA	(0/-)	2.31	2.35	-0.194	0.005
V _N	LSDA	(+/0)	2.89	3.26	-0.077	0.017
V _N	LSDA	(2+/+)	0.18	0.07	0.039	0.009
V _N	LSDA	(3+/2+)	0.15	0.09	0.014	0.008

Let us start with the neutral charge state (Fig. 4.6 (d)): we have the fully occupied a_1 -state in the valence band and the t_2 state which is split in an half-occupied a_1 -state in the band gap and an e -state in the conduction band. The description of this charge states already presents difficulties within the DFT-LDA approach, because the localised gap-states reported in the picture are in the DFT-LDA representation already in the conduction band.

Adding an electron to the system the a_1 -level in the gap is filled, which lowers its energy (charge state -1, Fig. 4.6 (c)). This effect is not what one would expect from Coulombic considerations and is due to the relaxation effects. The relaxation energy of the system has a huge jump from 0.59 eV for the neutral charge state to 2.59 eV for the negative charge state. Such a important relaxation is normally associated with the so called negative- U effect, in which one charge state is bypassed.

Adding a second electron to the system (charge state -2, Fig. 4.6 (b)), it will occupy the empty e -state, which is split in two states that slide into the band gap. Consequently the a_1 -state which already was in the gap increases its energy (Coulombic effect). A third electron will finally fill the a_1 -state just below the conduction band edge (charge state -3, Fig. 4.6 (a)). It is not possible to further charge the vacancy, as the additional electrons would occupy the delocalised conduction band levels and won't stay localised on the vacancy.

Subtracting an electron from the neutral charge vacancy will result in an empty a_1 level in the band gap (charge state +1, Fig. 4.6 (e)). If we subtract further electrons from the system the occupied a_1 -state which was located in the valence band rises into the band gap (Fig. 4.6 (f) and (g)).

Let us now concentrate on the empty a_1 state in the band gap in Fig. 4.6 (e): adding an electron does not change its energy a lot (Fig. 4.6 (d)), while adding a second (Fig. 4.6 (c)) lowers its energy considerably. It is then energetically more favourable to charge this state directly with two electrons than with one. For this reason the neutral charge state, corresponding to the a_1 state occupied with only one electron is skipped. It is interesting to note that in this case the slope of the one particle level as function of its occupation becomes negative, as typical for negative- U transitions. The corresponding (+/-) transition can be easily calculated as the average of the charge transitions (+/0) and (0/-) resulting in a value of $(2.89+2.32)/2=2.61$ eV, in reasonable agreement with the value of 2.46 eV calculated by Nieminen. The remaining discrepancy may be due to the fact that our approach provides an empirically corrected gap, thus, leaving the one-particle level in question deep in the gap, whereas in the ab-initio calculation this level is found artificially close to the too low lying LDA conduction bands. A similar situation happens for the charge state -2 and the possible charge states for the nitrogen vacancy are, in the DFTB representation, +3, +2, +1, -1 and +3. The transition levels between these states are calculated at 0.015 eV ($\varepsilon(3+/2+)$), 0.018 eV, ($\varepsilon(2+/+)$) 2.61 eV ($\varepsilon(+/-)$), 3.20 eV ($\varepsilon(-1/-3)$). The charge states +3, +2 and +1 almost give rise to a negative- U system, as the vacancy in the charge state +2 only can be formed if the Fermi levels lies in an interval which is only 0.003 eV wide. We notice that if the vacancy is in the charge state -2 the highest occupied one particle level lays in the conduction band, i.e. it is delocalised. Even if the charge transition $\varepsilon(-2/-3)$ is in the GaN bandgap, the electron which has to be added to change from the charge state -1 to -2 is actually a conduction electron. For this reason we limit us to report the other charge transitions in the lower part of Fig. 4.6.

The structure of the nitrogen vacancy changes a lot with the charge states: while in the charge

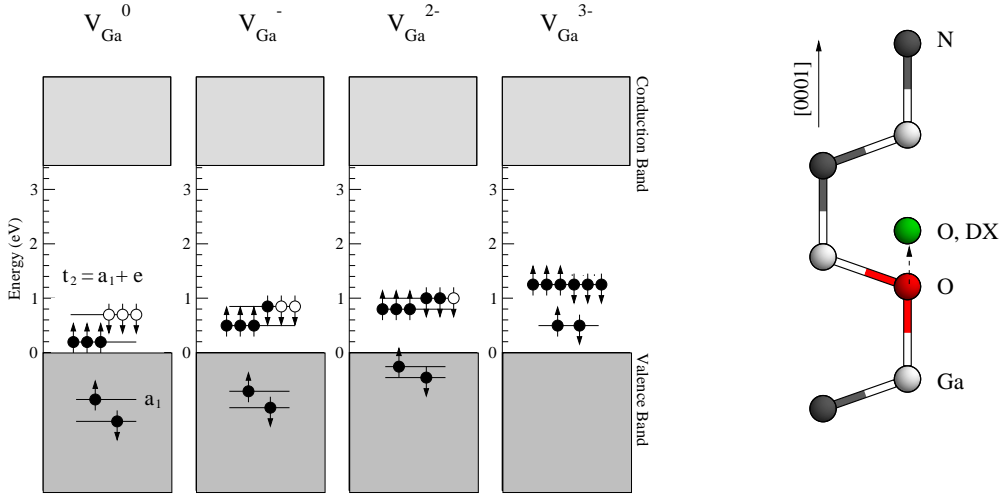


Figure 4.7: Left hand side: Possible charge states for the isolated V_{Ga} in hexagonal GaN: schematic representation of the defect levels in the band gap. Filled circles identify occupied states while unfilled circles identify empty states. Up arrows identify spin up electrons and down arrows identify spin down electrons, the spin separation is proportional to the unpaired electrons and is exaggerated in the picture for the sake of clearness. Right: Schematic illustration of the local environment of an oxygen impurity in the N-substitutional site and its migration (dotted line) to the DX-center.

state +1 the structure shows a (small) outward relaxation and the C_{3v} symmetry, in the charge states -1 and -3 the relaxation is inward (the effect is more pronounced for the -3 charge state) and the symmetry is D_{2d} , indicating a Jahn-Teller distortion. The distance between the Ga nearest neighbours is for the negative states very similar to the equilibrium Ga-Ga distance in bulk α -GaN and metallic-like Ga-Ga bonds have to be expected. The relaxation pattern calculated here is in perfect agreement with the one given in Ref. [210]. The relaxation energies calculated for the single charge states are: 3.11 eV (V_N^{3-}), 2.41 eV (V_N^{2-}), 2.48 eV (V_N^-), 0.59 eV (V_N^0), 0.21 eV (V_N^+), 0.20 eV (V_N^{2+}) and 2.2 eV (V_N^{3+}). Notice the two jumps for the charge states -3 and -1, corresponding to the negative- U transitions. The situation in zinc-blende GaN is similar and do not deserve a separate discussion here. The position of the charge transition and other informations concerning the Janak formalism are reported in Tab. 4.3.

4.5.2 Gallium vacancies

Removing a Ga atom from the ideal GaN lattice results in the lack of three electrons. The five N electrons which would form a bond with them (dangling bonds around the vacancy) are distributed in an a_1 state (originating from the s -states), filled and in the valence band, and a t_2 (originating from the p -states and divided in $a_1 + e$ by the hexagonal field) state with three electrons in the band gap. This state can host three further electrons and the V_{Ga} acts as a threefold acceptor. Charging the t_2 state increases the Coulombic repulsion and heightens the position of this level in the band gap. The transition states between these charge states calculated at 0.41 eV $\epsilon(0/-)$, 0.47 eV $\epsilon(-/2-)$ and 1.17 eV $\epsilon(2-/3-)$. The jump between $\epsilon(-/2-)$ and $\epsilon(2-/3-)$ can be explained with the fact that when the defect is triply charged, the a_1 state rises in the band gap, increasing the energy (see Fig. 4.7).

Allowing the V_{Ga} in the neutral charge state to relax from the ideal positions results in an outward relaxation of the structure, i.e. the N atoms get more distant from the position of the missing Ga than they would be in the ideal crystal. Charging the defect results in an inward relaxation (See Tab. 4.4). As revealed by the relatively low relaxation energies (0.66, 0.74, 1.04 and 1.58 eV for the charge state from 0 to -3) the relaxation effects are not particularly important and the vacancy does not induce a large amount of distortion in the lattice. The jump in the relaxation energy can again be explained with the presence of the a_1 state in the band-gap. In each charge state the

Table 4.4: Geometry of the isolated Ga vacancies in GaN for different charge states. Units are given in % with respect to the unrelaxed defect. r_{\parallel} is the distance from the vacancy center to the three equivalent neighbours, r_{\perp} the distance from the remaining neighbour.

	Reference	Method	Valence	-3	-2	-1	0	1	2	3
r_{\perp}	This work	DFTB	s, p	3.5	2.3	6.3	11.1	9.4	11.9	11.2
	[182]	DFT-LDA	s, p	10	8.3	6.3	3.7	4.1	5.9	7.1
r_{\parallel}	This work	DFTB	s, p	2.6	4.1	8.5	9.3	9.7	9.8	10.2
	[182]	DFT-LDA	s, p	4.7	5.2	5.0	3.5	4.1	6.1	7.3

vacancy has the symmetry C_{3v} , i.e. three equivalent nitrogen neighbours have the same distance from the vacancy center and the remaining is somehow further, directed along the crystal c -axis. It is interesting to notice that Neugebauer *et al.* [182] predict a different relaxation path when the defect is charged, namely an outward relaxation, independently from the sign of the charge. They explain this fact in terms of electrostatic effects: to reduce the electrostatic interaction the charged dangling-bonds within the vacancy will move outwards, in order to increase the distance between them. The dominance of electrostatic effects is consistent with the fact that the outward relaxation is independent from the sign of the charge: charging the V_{Ga} in either directions will result in an outward relaxation of the neighbouring atoms. Apart from the relaxation path, the DFT [175, 182, 210] and DFTB calculations are in agreement about the electronic configuration and the extent of the relaxation. In cubic GaN, Ga vacancies behave in a very similar way, the main difference is the symmetry of the defect, which remains T_d , consistent with the lattice symmetry. Similarly to V_{Ga} in hexagonal GaN the Ga vacancy is characterised by an outward relaxation, which is partially removed when the defect is negatively charged. The distance of the N-ligands from the vacancy center is for the charge state from 0 to -3 respectively 8.5%, 6.6%, 4.3% and 1.9% bigger than the equilibrium Ga-N distance. This corresponds to a relaxation energy of 0.55 eV, 0.64 eV, 0.98 eV and 1.64 eV respectively. The transition levels between the different charge states are again very similar to the ones found for hexagonal GaN and have been calculated at 0.67 eV $\epsilon(0/-)$, 0.95 eV $\epsilon(-/2-)$ and 1.20 eV $\epsilon(2-/3-)$. Concluding, there are only minor differences in the electronic and structural properties of the Ga vacancies in hexagonal and cubic GaN and they can be related to the different symmetry of the two crystal phases.

The charge transition $\epsilon(2-/3-)$ takes place at 1.17 eV (β -GaN) or 1.20 eV (α -GaN) above the valence band maximum. Optic transitions between this level and the conduction band or shallow levels would result in an emission at around 2.3 eV. For this reason the gallium vacancy has been indicated as responsible for the yellow luminescence from GaN. This issue is discussed in the following section.

V_{Ga} and yellow luminescence

Gallium vacancies have been related to the yellow luminescence in GaN as they could play the role of the deep acceptor (as isolated V_{Ga} [213] or as complex with O [214] or C [181] impurities) in the Aoki-model discussed in sec. 4.3.4. In the Ref [175] can be found a thorough discussion, which we summarise in the following, about the role of the V_{Ga} in the origin of the yellow luminescence. Different experimental and theoretical arguments are given to indicate V_{Ga} (either isolated or complexed) as the responsible for the yellow luminescence:

- It is known that V_{Ga} can form complexes with donor impurities (Si, O): while the $V_{\text{Ga}} \text{Si}_{\text{Ga}}$ pair has a small binding energy, the $V_{\text{Ga}} \text{O}_{\text{N}}$ pair has a fairly large formation energy (1.8 eV [214]) and can enhance the concentration of Ga vacancies. The electronic structure of this complex is similar to that of isolated V_{Ga} i.e. with a deep level at $E_{\text{CB}} + 1.1$ eV that could play the role of the deep acceptor in the Ogino/Aoki-model. The fact that presence of oxygen can enhance the concentration of Ga vacancies and therefore the yellow luminescence would be in agreement with the experimental observation luminescence increases in the neighbourhood of the sapphire substrate, where the oxygen concentration is higher [215].

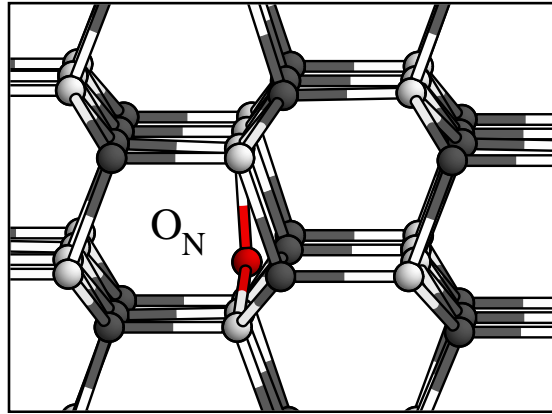


Figure 4.8: Geometry of the substitutional O_N in hexagonal GaN. The oxygen atom (in red) lays off-center.

- The presence of both isolated V_{Ga} and $V_{Ga} O_N$ pairs would cause a small shift in the transition energy and would explain the broadening of the luminescence line. Other factors which contribute to the width of the line could be strain, close extended defects and Coulomb effects in the recombination donor-acceptor pairs with varying separations.
- The most evident argument in the association of the V_{Ga} to the yellow luminescence is emerged from positron annihilation measurements [216], which can reveal the presence of Ga vacancies in the sample. It was found a direct relation between vacancies concentration and luminescence, providing direct evidence for the involvement of the V_{Ga} acceptor levels in the luminescence.
- Gallium vacancies are more likely to be formed in n -type than in p -type Ga (see the previous section). It was experimentally observed that the yellow luminescence is suppressed in p -type Ga [215], while an increase in n -type doping increases the intensity of the yellow luminescence [217]. These facts are in agreement with the V_{Ga} model.
- In Ga rich materials the concentration of Ga vacancies is of course very low. The fact that the yellow luminescence is suppressed in MOCVD-samples grown under high gallium flow rate [215] is another evidence of the fact that V_{Ga} are directly involved in the luminescence.

It is interesting to observe that the divacancy $V_N + V_{Ga}$ has attracted a lot of attention because of its high binding energy (≈ 2.34 eV) [210]. It is still under debate though, if this complex occurs in appreciable concentrations. While Mattila and Nieminen [210] find the formation energy of this complex to be lower than the one of isolated V_{Ga} independently from the position of the Fermi energy within the band gap, Van de Walle and Neugebauer [175] do not identify any condition where both V_N and V_{Ga} were favourable enough for the formation of the divacancy. This complex, though interesting, is not investigated here.

4.5.3 Donors in GaN: the substitutional O_N

We choose oxygen to be representative for the class of donor impurities in GaN for different reasons. Oxygen forms simple N substitutionals in GaN, where it acts as a single donor. Oxygen ions are not extremely different from the N ions they take the place of ($r_{cov.}^O = 0.73$ Å, $r_{cov.}^N = 0.75$ Å) and do not introduce a lot of distortion in the host lattice. However, according to the DFTB calculations, in the neutral charge state the oxygen ion does not lay on-site, but occupies an off-center position (see Fig. 4.8). More precisely it is displaced along the crystal c -axis by 0.59 Å in the direction of the three equivalent Ga-ligands. This configuration is 0.11 eV more favourable than the configuration with the oxygen laying on-site. In the positively charged state the oxygen impurity lays on-site

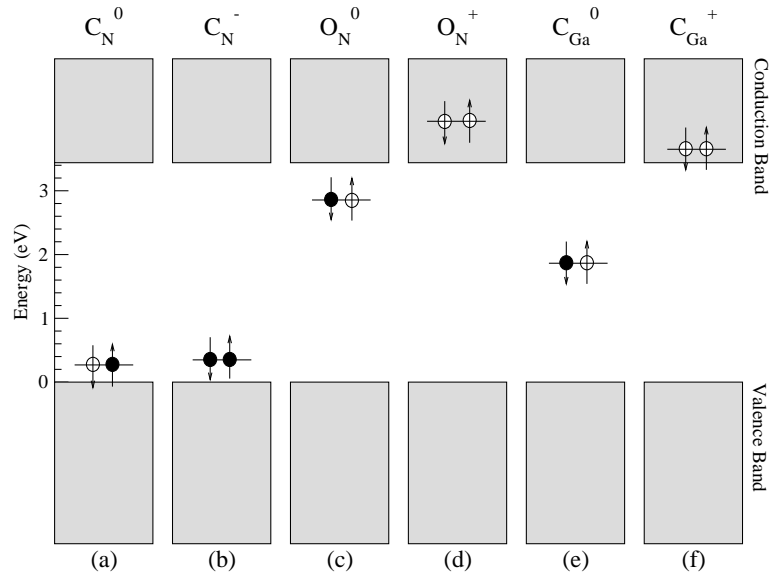


Figure 4.9: Schematic representation of the defect levels introduced in the GaN band gap by the substitutions O_N , C_{Ga} , and C_N . Filled circles identify occupied states while unfilled circles identify empty states. Up and down arrows identify spin up spin down electrons.

instead. Oxygen has one electron more than the nitrogen it substitutes in GaN and form thus a shallow donor state in the band gap. Besides of its intrinsic simplicity, which makes of it an easy system to simulate, O in GaN has also real applications in the growth of n -type samples. Oxygen is indeed, together with Si, an ideal donor in GaN. It has a relatively low formation energy in n -type GaN (around 2 eV in our calculation) and can be therefore readily incorporated in the host, as suggested by Neugebauer and Van de Walle [175]. Oxygen is also often present in GaN samples as unintentional impurity so that the n -type conductivity of bulk GaN has been attributed to unintentional oxygen incorporation.

In the Fig. 4.9 the possible charge states for the substitutional O_N are plotted. In Fig. 4.9 (c) we see that in the neutral charge state an half occupied localised state is introduced in the band gap (2.78 eV above the valence band), while in the ionised state (Fig. 4.9 (d)) this level is in the conduction band and the band gap is free from localised levels. This means that charging the level it lowers its energy, as characteristic for negative- U systems. Consequently the slope of the curve describing the position of this level depending from its occupation is negative. This is the classic behaviour of shallow donors. Summarising, as expected from a group VI element on a group V site it acts as a single donor. The transition $\epsilon(+/0)$ is calculated at 3.35 eV above the GaN valence band (see Tab. 4.3) so that the substitutional O_N is practically always positively charged. This is in agreement with all previous investigations. The ionised state does not introduce any major change in comparison with the isoelectronic substituted atom (see Fig. 4.9). For this reason O can be considered close to an ideal dopant. In Fig. 4.10 the linearity of the one particle-level with respect to the occupation is verified. As argued from the small difference of the covalent radii between substituted specie and dopant, O introduces only a small elastic strain around the defect. The calculated Ga-O bond distance is 1.94 Å both for the ionised charge state, which is only 1.8 % bigger than the equilibrium Ga-N bond distance. The Mulliken charges analysis reveals that the charge residing on the O-impurity is the same for the system in neutral and in the positive charge state, being the difference of $1.53 \cdot 10^{-3}$ eV. This is a confirmation of the fact that the extra electron is not bound, is not localised, does not take part to the bond and is a proper free carrier. The small relaxation energies (0.25 eV for O_N^0 and 0.26 eV for O_N^+) is an evidence for the easy incorporation of O in GaN. There is almost no difference between O_N substitutionals in wurtzite and zinc-blende GaN, as the magnitude of the relaxation and relaxation energy as well as the electronic structure are

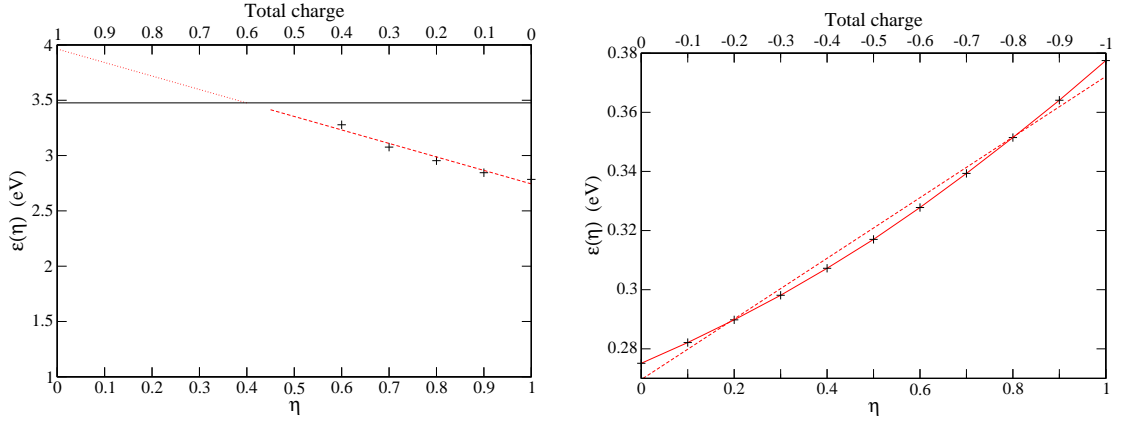


Figure 4.10: Highest occupied one particle level as function of its occupation for the O_N (left hand side) and C_N (right hand side) substitutionals in hexagonal GaN. The dotted lines are linear interpolations of the calculated points.

the same in both cases. These results are in agreement with previous theoretical studies [175, 218] and confirm the reliability of the DFTB approach in the simulation of point defects.

DX-center

Under high pressure the oxygen impurities leave the substitutional site and migrate to the off-center site (see Fig. 4.7, right side), called *DX*-center [219]. This has as consequence a large outward relaxation which induces a deep level in the band gap. The oxygen becomes negatively charged and acts as an acceptor. Once oxygen undergoes the *DX* transition it behaves as a deep acceptor, compensating the electrical activity of other donors in the sample and causing the so called freeze-out of the carriers in the samples under high-pressure. The *DX*-center though interesting, is not investigated here.

4.5.4 Acceptors in GaN: the substitutional C_N

Due to its small ionic radius ($r_{\text{cov.}}^{\text{C}} = 0.77 \text{ \AA}$, $r_{\text{cov.}}^{\text{N}} = 0.75 \text{ \AA}$), carbon fits quite well in the nitrogen site in GaN, where it forms a stable substitutional defect. Previous theoretical predictions found that in GaN the incorporation of C on a N site is preferred [218]. It has been suggested that doping with C ions could be a convenient way to increase the hole concentration in GaN [220]. Recent experimental studies suggested C in the nitrogen site (C_N) as an alternative way to Mg in cubic GaN [221], while its use would be discouraged in wurtzite GaN because of compensation effects caused by defect complexes such as carbon pairs [222]. From the theoretical point of view there are different investigations of C in GaN: with tight-binding simulations Jenkins [211, 212] found very shallow states or even levels resonant with the valence band. Neugebauer and Van de Walle [218] discussed carbon as the origin of the yellow luminescence from as-grown GaN, Boguslawski [223] and co-workers performed quantum molecular dynamics to determine the doping properties of carbon in hexagonal GaN and Gorczyca [224] and co-workers investigated the properties of the neutral carbon impurity in cubic GaN using LMTO-ASA Green function methods. Finally Ramos and co-workers [225] investigated carbon related shallow and deep levels in group III nitrides in huge supercells by means of DFT and particular ultrasoft pseudopotentials. All these studies agree that the substitutional C_N gives rise to a shallow acceptor levels, which we now investigate with the DFTB approach.

In Fig. 4.9 (right) the possible charge states for the substitutional C_N are reported: carbon is found as expected to be a single acceptor in GaN. The transition $\epsilon(0/-)$ is calculated at 0.32 eV (0.34 in cubic GaN), meaning that the impurity is practically for each position of the Fermi level within the band gap in the ionised state. In Fig. 4.10 the linearity of the one particle-level with respect to its

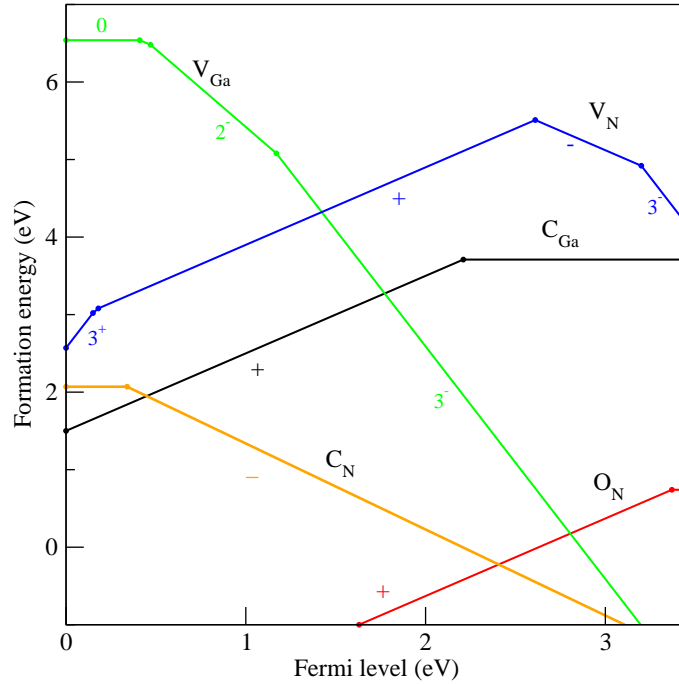


Figure 4.11: Formation energy of native point defects (V_N and V_{Ga}) and donor impurities (O_N and C_{Ga}) in GaN for different values of the Fermi energy. The conduction band maximum was chosen as zero of the energy scale. The slope of the curves indicates the charge state, while kink in the curves indicate transitions between different charge states. Nitrogen rich conditions and equilibrium with CN and NO gases are assumed.

occupation is verified: the small slope of the one particle level reveals its crystal-orbital nature. The strain introduced by the C_N substitutional in GaN is marginal: a small inward breathing relaxation is observed with the Ga-C bond only 0.58% smaller than the Ga-N bond distance in bulk GaN. The relaxation is the same for the neutral and for the negative charge state, evidence that the introduced hole is not localised on the C impurity. Relaxation energies are 0.14 eV and 0.17 eV for the two investigated charge states. The formation energy of the C_N substitutional in hexagonal GaN in N-rich conditions has been calculated to be 2.07 eV. This value is low compared to the formation energies of the other investigated defects and means that, if carbon is present during the crystal growth, it will be easily incorporated in the host. Once again no major difference is found between zinc-blende and wurtzite GaN. The results presented here are in overall good agreement with the values reported in the literature [218, 223, 224].

Carbon could in principle also act as a donor in GaN if incorporated at the Ga site. The formation energy for this configuration is anyway much higher than the formation energy of a nitrogen substitutional, where it acts as an acceptor and the Ga substitutional is very unlikely to happen: for a review about this defect see Ref. [218]. The donor behaviour of C in GaN is shortly investigated here (Fig. 4.9) the transition $\epsilon(+/0)$ is calculated at 2.21 eV.

4.6 GaN as host for the rare earths

The intra- f atomic transitions from the RE should be parity forbidden by the Laporte selection rule. It is empirically known that if the RE ions are incorporated in a (partially) ionic solid they prefer to occupy the cation site: if this cation site provides an uneven ligand field the selection rules are relaxed and the $4f \rightarrow 4f$ transition probability is different from zero. For this reason RE doped systems excited state lifetimes between 1 μ s and 1 ms are observable. In the specific case of wurtzite GaN, which has an important ionic bonding component, the big majority RE occupy

a Ga^{3+} cation site [42] where the lack of inversion symmetry produces strong ligand fields further increasing the $4f \rightarrow 4f$ transition probability. This is only one of the advantages of GaN as host for the rare earths. Even if the host material does not directly influence the wavelength of the $4f$ transitions, it does have a very strong influence on the radiative transition probability, i.e. the photoemission intensity. Conventional semiconductors like Si or GaAs doped with rare earth ions exhibit limited photoemission at room temperature due to low RE solubility and severe quenching of the luminescence at room temperature. As shown by Favennec *et al.* [2] comparing different host materials implanted with Er, the thermal quenching decreases with the bandgap energy of the semiconductor. Therefore, wide-bandgap semiconductors, such as GaN, are ideal candidates as host material for the rare earths. The intense light emission from RE doped GaN is at least partially a consequence of the GaN capability to incorporate a big number of (optically active) lanthanide ions, in contrast with other semiconductors like Si or GaAs, where high RE concentrations result in RE precipitation and consequent emission quenching. This capability is somehow surprising, because the size mismatch between RE and substituted cations (Ga^{3+}) is bigger in GaN than in other hosts, especially than in II-VI hosts like ZnO or ZnS. Despite this mismatch the RE-N bond in GaN is very strong: the very short bond length measured e.g. for GaN:Er (Er-N = 2.17Å [14]) is an evidence of the bond strength. In any other known solid the Er-N bond is so short. GaN can incorporate lanthanide ions without violating charge neutrality: doping with RE^{3+} in II-VI hosts like ZnS:Tb requires co-doping with O or F to satisfy charge neutrality and to achieve the luminescence. Concluding GaN can easily incorporate RE dopants, as attested by the dopant concentrations of 0.1-1% of the brightest ELDs. As all the lanthanides share the same outer shell ($5p^66s^2$) and therefore the RE-bonding in GaN is very similar. This enables the multicolor capability devices by simple co-doping with different RE and makes the GaN:RE technology so interesting. Considering that GaN has also excellent high field transport characteristics and is chemically and thermally rugged, it is evident that this host is an ideal candidate for the realisation of the displays cited in the introduction of this work. We do not repeat the effect of RE-dopants in GaN in this section: for this topic we invite the reader to have a look at the first chapter. The main difference between hexagonal and cubic GaN as host is the number of possible lattice site. In the hexagonal lattice there are, besides the substitutionals, various interstitial sites with different symmetry, while in cubic crystal the site multiplicity is not so pronounced.

4.7 Summary and discussion

In this chapter we reviewed the main properties of GaN both in the β - (zinc-blende) and in the α -phase (wurtzite), reporting data from the literature and performing calculations in the framework of the DFTB calculation scheme both for the bulk phases and for point defects. After having examined the structural, elastic, cohesive and energetic properties of bulk GaN (α - and β -phases) we can conclude that DFTB with carefully fitted parameters correctly describes these properties. Structural and elastic properties like lattice parameters and bulk modulus are reproduced in DFTB almost with the same accuracy of the more sophisticated DFT calculation scheme. In particular we found that including the Ga $3d$ electrons in the atomic core does not significantly affect the description of the material but decreases clearly the computational cost of each calculation. We therefore decided to treat the electrons in this shell as core electrons, without loss of accuracy. Cohesive energy and formation enthalpy in the DFTB representation are affected by the same problems which affect DFT-LDA calculations, namely we found the binding energy to be overestimated by ≈ 1 eV per atomic formula. One of the shortcomings of the DFTB representation of GaN is that the wurtzite and the zinc-blende phases appear to be degenerate in energy, because the energetic difference of the two phases is within the DFTB intrinsic error. This could be a problem if we would simulate reconstructions or extended defects but we do not think that it influences the description of RE point defects. Finally we investigated different point defects types, namely Ga and N vacancies as well as C and O substitutionals both in cubic and hexagonal GaN within the DFTB approach, and compared the results with recent theoretical simulations and experimental data finding an overall good agreement. Fig. 4.11 summarises the results of our investigation of native defects and impurities in GaN. In the picture the formation energy of the selected point

defects as a function of the Fermi level is shown. The conduction band maximum was chosen as zero of the energy scale. The slope of the curves indicates the charge state, while kink in the curves indicate transitions between different charge states. Nitrogen rich conditions and equilibrium with the two gases nitrogen monoxide (NO) and carbon monoxide (CN, also known as exhaust gas) are assumed. Throughout this work the formation energies are always estimated in N-rich conditions, because this is the growth condition which maximises the luminescence from RE-doped GaN samples. The picture can be compared with the values reported in the review article of C. Van de Walle and J. Neugebauer about point defects in GaN [175] or in the work of Nieminen and coworkers [210]. No major difference was found in the structural and electronic properties of the investigated defects and impurities between the wurtzite and zinc-blende structure. DFTB offers a satisfactory representation of bulk GaN in the α - and β -polytypes as well as of the intrinsic and impurities defects. This is the basic requisite for a correct simulation of RE dopants in GaN.

Chapter 5

Rare earth point defects in GaN

The main goal of this work is a systematic analysis of the rare earth defects in GaN. To understand which kind of defects may occur in the luminescent GaN samples we have to know how the rare earth impurities are introduced into the samples. There are mainly two ways to dope solids: *in situ* doping, where impurities are added during the crystal growth, and *ex situ* doping, where the impurities are introduced in the undoped samples after their growth. The advantages of the *in situ* doping are the possibility to control accurately the impurity concentration and the crystal quality of the doped samples in each phase of the crystal growth. *Ex situ* doping on the other hand offers other advantages, like the possibility to avoid surface segregation and residual contaminants as well as the possibility to introduce an impurity fluence which is higher than the solubility limit. In the process of ion implantation, the impinging ions will transfer kinetic energy to the host atoms in several collisions, resulting in the displacement of these atoms from their lattice site if sufficient energy is transferred. The recoiling atoms may displace other atoms, hence creating a cascade of atomic collisions. The most common defects caused by the impinging ions are vacancies, interstitials and extended defects such as dislocations or stacking faults. The damage concentration depends on the implantation temperature, on the structure of the host material but principally on the implanted ion mass and energy and is therefore supposed to be quite high in the case of the lanthanide implantation. We have therefore to investigate many different configurations involving RE impurities, even those which would not occur at equilibrium conditions. Rutherford backscattering and channeling spectrometry (RBS/C), transmission electron microscopy (TEM) and X-ray diffraction (XRD) are often used to investigate the crystalline quality, the defect formation and the lattice strain. These techniques revealed, as discussed in the first chapter, that the lanthanides prefer the Ga lattice site and that a number of different centers is responsible for the luminescence. Because of the cumbersome number of different defect structures which have to be investigated, we

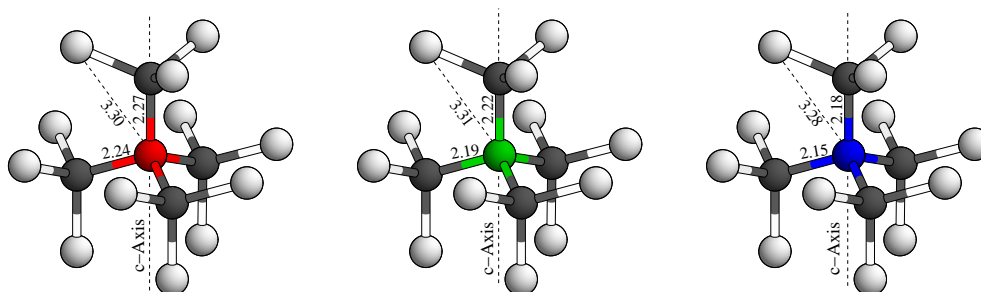


Figure 5.1: The RE_{Ga} substitutionals in hexagonal GaN. As usual Ga atoms are white, nitrogen atoms black, and Eu, Er and Tm are red, green and blue respectively. The numbers show the bond lengths in Å.

Table 5.1: Bond lengths in Å and local strain, around the C_{3v} RE_{Ga} substitutionals in GaN calculated with DFTB-FLL. The values in the bracket are DFTB-LSDA calculations. The local strain is the ratio between the length of the three equivalent RE-N and the corresponding bulk GaN bonds.

	RE-N ₁ (3 Bonds)	RE-N ₂ (1 Bond)	RE-Ga ₁ (9 Bonds)	RE-Ga ₂ (3 Bonds)	Strain
Pr	2.18(2.20)	2.17(2.18)	3.39(3.41)	3.26(3.35)	12.6%
Eu	2.27(2.29)	2.24(2.28)	3.45(3.39)	3.30(3.34)	16.2%
Gd	2.25(2.25)	2.24(2.23)	3.34(3.33)	3.28(3.28)	16.2%
Er	2.22(2.17)	2.19(2.16)	3.40(3.33)	3.31(3.30)	12.6%
Tm	2.18(2.15)	2.15(2.14)	3.37(3.33)	3.28(3.28)	10.6%

divide our study in three parts, reported here and in the next two chapters: these parts deal with RE defects involving only the RE impurity, complexes formed by the RE impurity and host-related intrinsic defects and finally complexes formed by the RE with other impurities. In this chapter we report the results of the investigation of the simplest rare earth defects, the substitutionals and the interstitials. Differences between defects in hexagonal and cubic GaN are examined and the role of the f -electrons in the structural and electronic properties of the system is discussed. For each substitutional and interstitial of each rare earth many different physical quantities are calculated and taken in account in order to get a well defined picture of the defect characteristics. Different charge states and spin configurations have been investigated: here we report only the characteristics of the favoured spin configuration for each charge state. The analysis of each defect is divided in two parts: one concerning its structure, i.e. its geometry, where symmetries and bond lengths in the neighbourhood of the RE are examined, and one concerning its energetic, where a collection of physical quantities like the band structure (BS), density of states (DOS), electronic configuration, formation energy, binding energy (of the RE with other defects), charge distribution and charge transition levels are examined. The calculated values are reported in tables where they are divided after RE. This allows a direct comparison of the different lanthanides and underlines their similarities and differences. The results obtained with our calculations are compared with experimental measurements and other *ab initio* calculations we carried out in order to check the validity and portability of our calculation scheme. At the end of each section the specific features of each defect or complex are examined and discussed, as well as the differences between the LDA, LSDA and LSDA+ U description of the defects. The easiest RE defects we can think about are the one involving the isolated RE, e.g. with the RE taking the place of an atom of the host (Ga or N) or placing itself between the atoms of the host, in a so called *interstitial position*.

5.1 Substitutionals

5.1.1 The substitutional RE_{Ga}

RE_{Ga} substitutionals are the simplest stable lanthanide defects in GaN and have been investigated experimentally and, in some extent, also theoretically [18, 57]. Because of its application in optical fiber communications the most studied rare earth is Erbium. Er:GaN based displays [13] have stimulated many experimental attempts to understand [14] the mechanisms underlying the emission from Er doped samples and to exploit [226–228] and improve [229, 230] the emission itself. From experimental studies we know that Er ions in GaN, prefer the Ga position [42], occur in 3+ valence state [13] and posses C_{3v} symmetry [59] with relatively short distances to the surrounding N-ligands [46]. The most interesting and puzzling rare earth is Europium. In the literature can be found contradicting reports about its valence state (even if Eu ions in GaN are mostly found to be trivalent like other RE (Eu^{3+}), in some work Eu is found to have charge state 2+), and its lattice position (Eu is indicated by RBS data [188] to be displaced from the ideal Ga lattice site).

Table 5.2: Bond lengths in Å and local strain around the C_{3v} $\text{Eu}_{\text{Ga}}^{3+}$ and $\text{Er}_{\text{Ga}}^{3+}$ substitutionals in hexagonal GaN. The local strain is defined as the ratio between the Er-N₂ bonds and the corresponding Ga-N bulk bonds. The DFTB-pSIC geometries are obtained minimising the total energy and not the forces. For further details see text and the individual references.

	Er-N ₁	Er-N ₂	Er-Ga ₁	Er-Ga ₂	Strain
DFT-AIMPRO [57]	2.14	2.11	-	-	-
DFT-ABINIT	2.39	2.31	3.23	3.31	-
Exp. [14]	2.17	2.17	3.26	3.26	-
DFTB	2.17	2.16	3.35	3.32	12.1%
DFTB+ <i>U</i> FLL	2.23	2.19	3.31	3.40	12.6%
DFTB+ <i>U</i> AMF	2.19	2.17	3.29	3.37	12.3%
pSIC DFTB	2.18	2.17	3.29	3.36	12.6%
	Eu-N ₁	Eu-N ₂	Eu-Ga ₁	Eu-Ga ₂	Strain
DFT-AIMPRO [57]	2.21	2.18	-	-	-
DFT-ABINIT	2.26	2.26	3.01	3.52	-
Exp. [231]	2.5	2.3	3.3	3.3	-
DFTB	2.29	2.28	3.34	3.39	18.3%
DFTB+ <i>U</i> FLL	2.27	2.24	3.30	3.45	16.2%
DFTB+ <i>U</i> AMF	2.29	2.27	3.32	3.40	17.4%
pSIC DFTB	2.29	2.25	3.32	3.40	17.4%

Geometry

We first discuss the geometry of the defect. Two DFTB-parameter sets have been created for the simulation of RE in GaN, in one the Ga-3*d* orbitals are treated as valence and in the other as core. We report here results obtained including the Ga-3*d* in the atomic core. Results obtained including the Ga-3*d* orbitals do not differ substantially and have been reported in a previous publication [232]. Supercells containing 256 atoms and a $4 \times 4 \times 4$ Monkhorst-Pack *k*-point sampling were used to calculate the data reported in the following. The supercells have been relaxed in different spin configurations to find out the one that minimises the total energy. In hexagonal GaN the charge neutral substitutional RE_{Ga} is found to have the C_{3v} symmetry. The rare earth is surrounded by four N atoms, the one along the crystal *c*-axis (identified by the label Er-N₁ in the Tab. 5.1) being slightly more distant from the rare earth than the other three (labeled by Er-N₂ in the Tab. 5.1). In agreement with the C_{3v} symmetry the RE second neighbours can be similarly divided into two groups (called Er-Ga₁ and Er-Ga₂ in Tab. 5.1). The symmetry is a particularly important parameter in the investigation of the RE defects, both because it can be measured experimentally and because it is known that the intensities of intra-*f* transitions are enhanced by lowering the symmetry. For example the symmetry difference between Eu and Tb substitutionals in wurtzite GaN is believed to be the cause of the higher relative luminescence intensity of Eu-doped GaN, as suggested by Bang *et al.* [233]. Charging the system with one additional electron introduces minor differences between the three equivalent RE-N bonds. All the studied RE substitutionals after geometry optimisation are on-site, even in the case of Eu, which was found, by RBS measurements to be displaced from the Ga site of 0.2 Å [188]. Our results agree with the suggestion of Filhol *et al.* [57], that the experimental data in case of Eu originate from some other defect complex. The calculated geometry (DFTB-FLL calculations) in the neighbourhood of the substitutional is reported in Tab. 5.1 together with experimental measurements and other theoretical results. The calculated values are in good agreement with the experimental measurements and the lattice distortion has values very close to previous pseudo-potential LDA calculations [57]. It is interesting to observe that in all the cases the RE-N bond is shortened, in average by 15-20%, compared to the corresponding RE-nitride. This is the shortest known RE-N bond length. The distortion of the host lattice can be simply explained with the size of the host atoms. All the RE ions are bigger (both in the neutral and in the +3 charge

Table 5.3: Reference bond lengths in Å and local strain (defined as before) around the C_{3v} RE_{Ga} substitutionals in hexagonal GaN. Experimental data from EXAFS measurements, for more details see the individual references. The measured distances refer to RE concentration similar to the one simulated with our calculations. To our knowledge no experiments have been performed to measure the bond distances in Pr-doped GaN.

	Method	RE-N ₁	RE-N ₂	RE-Ga ₁	RE-Ga ₂
Pr [234]	DFT	2.30	2.20	3.12	3.39
Eu [57]	DFT	2.21	2.18	-	-
Eu [231]	Exp.	2.3	2.5	3.3	3.3
Eu [234]	DFT	2.26	2.26	3.01	3.52
Gd [235]	Exp.	2.23	2.23	3.31	3.31
Er [234]	DFT	2.39	2.31	3.23	3.31
Er [57]	DFT	2.14	2.11	-	-
Er [14]	Exp.	2.17	2.17	3.26	3.26
Tm [234]	DFT	2.51	2.39	3.25	3.36
Tm [15]	Exp.	2.19	2.19	3.29	3.29
Tm [57]	DFT	2.15	2.12	-	-

state) than the Ga ion they take the place of and the proportion of the distortion caused by the substitutionals reflects the dimension of the dopants. Apart from the relatively small compressive stress in the neighborhood of the defect (for example Er is a bigger ion than Ga with covalent (3+ ionic) radii of 1.57 (1.03) and 1.26 (0.62) Å respectively) no other effect on the host geometry are observed. The compressive stress, estimated by the ratio between the RE-N bonds and the Ga-N bonds in the bulk, is reported in the last column of Tab. 5.1. We notice that in the case of Gd the DFTB-LSDA and DFTB-FLL geometries do not differ. Gd is in fact the lanthanide for which the LSDA description is less wrong. Investigating the Eu and Er substitutionals with different orbital-dependent calculation schemes we can affirm that these do not really influence the system geometry (see Tab. 5.2). Already the classic LDA formulation of the DFTB approach provides RE-N bond lengths in good agreement with experimental data. The LDA+ U like pSIC (data are reported here for Eu and Er) implementations lead to small changes only. In other words, relaxing the structure with or without the contributions of the orbital dependent potentials anyway does not substantially change the geometry of the system and influences only slightly the bond lengths: bond lengths calculated with and without the orbital dependent potentials differ at most by 0.05 Å (in the case of Erbium), corresponding to the 2% of the bond length (see Tab. 5.2). This effect is in general smaller than the effect due to the size of the supercells: RE-N bond lengths on 72-atoms supercells are found to be 1% to 2% smaller than in 256-atoms supercells, depending on the RE (data not reported here). Bond lengths calculated with bigger 512-atoms supercells were instead the same obtained with 256-atoms supercells. We notice that both implementation of the LDA+ U approach in DFTB+, AMF and FLL substantially lead to the same structure and differ in all the bond lengths by less than half percent. The pSIC structure was relaxed minimising the total energy and not the forces by means of the conjugate gradient algorithm, so that the error of the calculation is higher. Assuming the C_{3v} symmetry of the system the lengths of the three equivalent and of the not equivalent RE-N bonds were stretched by steps of 0.01 Å, calculating in each step the total energy. The minimum of the total energy, i.e. the relaxed structure is found by interpolation, as shown in Fig. 5.4. The formation energy of the RE_{Ga} substitutionals in the neutral charge state in N-rich¹ conditions has been calculated. Tm substitutionals have the lowest formation energy (4.71 eV), followed in order by Er (6.59 eV) and Eu (8.74 eV). This values and the order agree with the values reported by Svane *et al.* [18]. DFTB-LSDA and DFTB-FLL calculated value do not differ substantially.

¹In this work formation energies are always calculated in N-rich conditions. In slight N-rich conditions maximal luminescence intensity is achieved.

Table 5.4: f -shell occupation for the RE_{Ga} substitutional in the neutral charge state in GaN. The occupations are given in electronic units and are calculated with DFTB-FLL.

	Spin	Pr	Eu	Gd	Er	Tm
Wurtzite	Up	2.12	6.01	6.99	6.99	6.98
	Down	0.11	0.04	0.06	4.01	5.02
Zinc-blende	Up	2.11	5.99	6.99	6.98	6.98
	Down	0.11	0.06	0.06	4.01	5.02

Electronic band structure, charge states

In this section we report and discuss the results concerning electronic properties of the RE_{Ga} substitutionals. All the RE_{Ga} are found (both within the DFTB-LDA and the DFTB-LDA+ U approaches) to be trivalent, corresponding to an outer electronic configuration of $[Xe]4f^{n-1}$, if n is the number of f -electrons in the atomic configuration. This means that in neutral super-cells there is an effective 3+ charge on the RE ion. Generally (exception Gd) the $6s^2$ electrons and one of the $4f$ are promoted to the GaN lattice when the substitutional is formed. In the special case of Gd, which has a very stable half filled $4f$ shell, the $6s^2$ and one $5d^1$ electrons are promoted, i.e. the total number of f -electrons does not change.

Turning to the band structure of supercells containing a RE_{Ga} substitutional, we observe that the f -states at the Γ -point appear in DFTB-LDA like a bunch of narrow localised states within the GaN band gap and are situated close to the Fermi level, as plotted in Fig. 5.4. This is definitively a wrong description of the system, as many experiments reveal their localised nature as atomic multiplet over a broad range of energies [236]. The states in the picture are one-particle levels and should be not confused with the charge transition levels.

To show how LDA+ U influences the description of the system we examine the particular case of the Er_{Ga} substitutional. Concerning the DFTB-LDA+ U approach, from now on we report only results obtained with the DFTB-FLL implementation, as DFTB-AMF results are similar. The substitutional Er_{Ga} is a representative example, because all of the mid-series RE substitutionals behave in a similar way.

Band structure reference calculations were executed with the *ab initio* all electron code Wien2k [113]. In Fig. 5.2 the band structures of the substitutional Er_{Ga} calculated with DFTB-LSDA and DFTB-FLL (first row) and LDA/LDA+ U using Wien2k (second row) are reported. In LSDA (columns a and b) the size of the GaN original band gap (3.44 eV for DFTB-LSDA and 2.2 eV for Wien2K) is not modified by the presence of the substitutional, while in the middle of the gap appear very localised f -related levels in the spin-down channel (column b). An LSDA analysis reveals how the f -levels are occupied: 7 up electrons and 4 down in the Er case (2 and 0 for Pr, 6-0 for Eu, 7-0 for Gd and 7-5 for Tm). The occupations are reported in Tab. 5.4). No difference between the cubic and the hexagonal phase of GaN is observed.

Turning on the + U potentials (Fig. 5.2, columns c and d), the occupied f -states are pushed in the valence band and the empty ones in the conduction band, so that no localised levels are left in the gap. We notice that the agreement between DFTB-FLL and Wien2k-LDA+ U is very good. The Er oxidation state (+3, corresponding to an outer electronic configuration of $[Xe]4f^{11}$, with a full f -semi-shell containing 7 spin up and a half filled f -semi-shell containing 4 spin down electrons) was verified with all spin resolved approaches implemented in DFTB. The fact that 11 of the 12 f -electrons remain strongly localised while the remaining one is delocalised, is in agreement with the results of Temmerman *et al.* [154] who predict the existence of two kinds of f -electrons, localised and delocalised, whose relative numbers change depending on the RE. The density of state (DOS) of the same system is reported in Fig. 5.5, where the DFTB calculations appear on the upper part while the Wien2K reference calculations are reported for comparison in the lower part. Data reported in Fig. 5.2 and Fig. 5.5 were calculated using smaller 72-atoms supercells.

The changes in the DOS due to the application of the + U potentials are consistent with what is

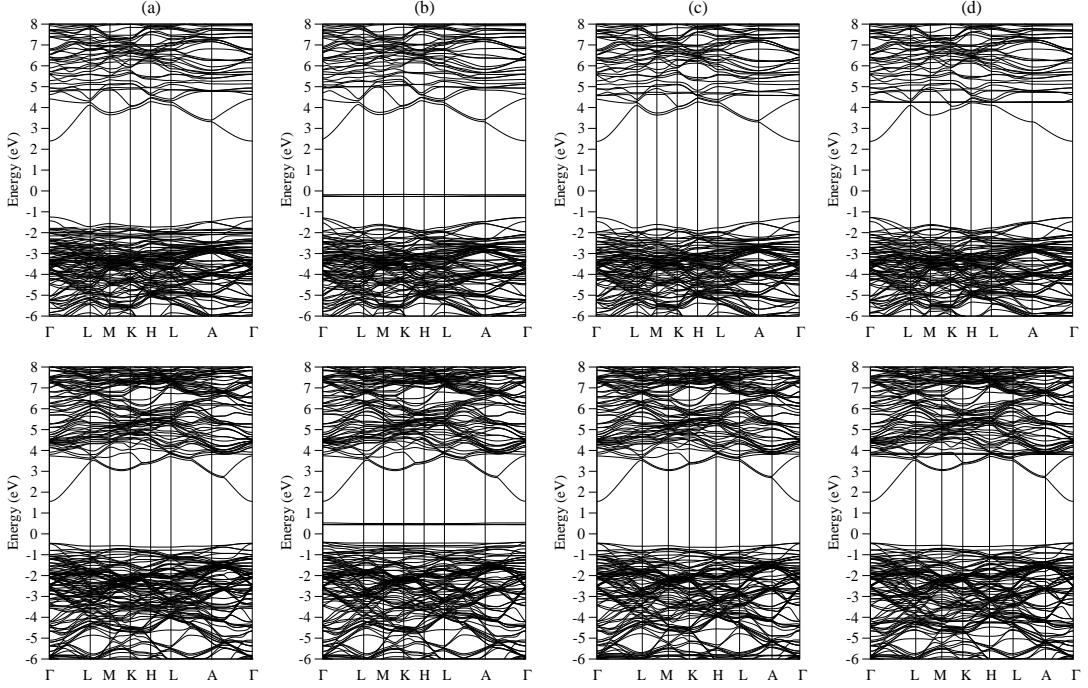


Figure 5.2: DFTB (first row) and Wien2K (second row, same computational parameters) simulations of the band structure of the substitutional Er_{Ga} in wurtzite GaN. Spin resolved (spin up (a) and (c), spin down in (b) and (d)) energy band structure are calculated with LSDA (a) and (b), and LSDA+U (c) and (d). For the LSDA+U calculations a value of $0.28 H$ for U - J is used.

observed for the band structure: the f -related peak in the band gap is split in two parts which are pushed in the valence and conduction band, leaving the GaN band gap free again. A detailed discussion about the interpretation of this clear gap can be found in Ref. [12] and references there in. As reported in Fig. 5.5 the DOS calculated with Wien2K and with DFTB are in very good agreement. In the neutral charge state a simple LDA-like approach where the f -electrons are treated as core like electrons produces the same results of a more sophisticated approach with a physical handling of the f -states. In Fig. 5.5 also the DOS calculated with the pSIC approach as implemented in DFTB is plotted. The pSIC potentials shift occupied states downwards but do not act on the empty ones. If we apply the pSIC potentials only on the f -shells (similarly to the usual LDA+ U treatment), the shift of the occupied f -states is the same as in FLL (as already expected by Eq. 2.102 and Eq. 2.103), whereas the position of the unoccupied states remain unchanged. However, SIC is usually applied to all occupied orbitals, as shown in the second box in Fig. 5.5. In this case, due to the interactions of all the SIC-corrected states, the splitting between occupied and unoccupied f -levels is reduced. Furthermore the unoccupied f -states are slightly shifted to higher energies. RE_{Ga} substitutionals are found not to influence the size of the GaN band gap, as expected from isoelectronic impurities. RE_{Ga} substitutionals do not introduce major changes in the charge distribution around the substituted atom. The Mulliken charges located on the four N-ligands are more or less the same observed in undoped GaN. The three equivalent ligands and the one inequivalent ligands show slightly smaller charge differences with respect to the bulk than the inequivalent ligand along the wurtzite c -axis. The differences, in electronic units, have been calculated to be 0.055 (0.065) for Pr, 0.076 (0.086) for Eu, 0.075 (0.080) for Er and 0.039 (0.041) for Tm. The charge differences are equally divided between the $2s$ - and $2p$ -orbitals of N and depend on the distance to the lanthanide. In the case where the difference with the bulk is more evident (inequivalent bond Eu-N) the charge difference with respect to the bulk represents only less than 1.5% of the total charge residing on the nitrogen atom. It can be concluded that the Mulliken charges on the ligands are not heavily affected by the presence of the lanthanide substitutionals. In Fig. 5.3 the the difference between the total charge of the relaxed supercell containing a Er_{Ga}

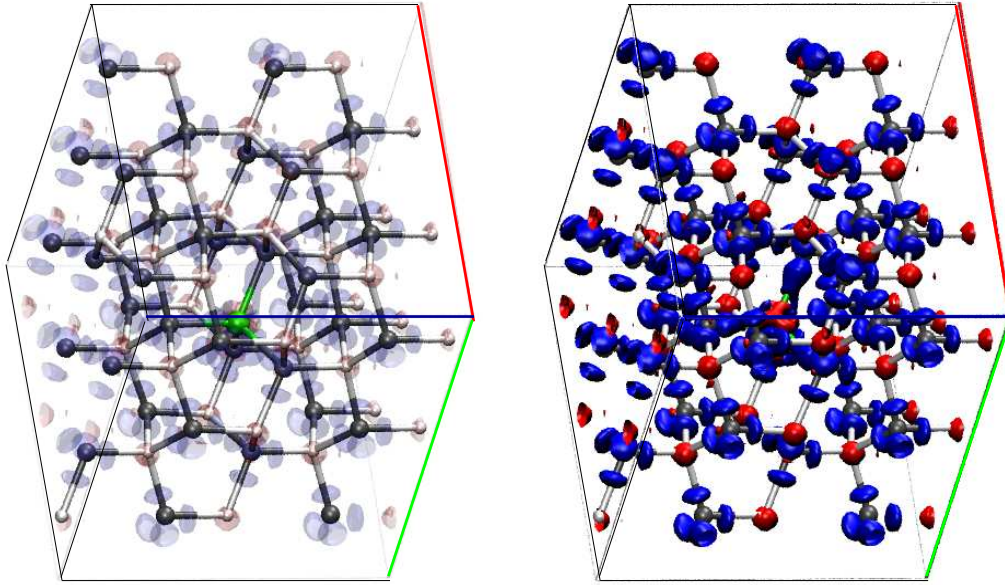


Figure 5.3: The Er_{Ga} substitutional. Both plots represent the difference between the total charge of the relaxed supercell and the overlap of single atomic charges. Blue isosurfaces represent regions where the electronic charges is accumulated while red ones the regions where the charge is taken from. In the left picture the charge isosurfaces are made transparent to show the atomic positions. As usual N atoms are in black, Ga in white and Er in green. The red, green and blue sides of the bounding box represent the direction of the t_1 , t_2 and t_3 wurtzite axes.

substitutional and the overlap of single atomic charges is plotted. This picture gives an idea of how the atomic charge is redistributed when the system is formed. The red isosurfaces, representing regions where charge is taken from, are localised on the Ga atoms, while blue regions, representing a charge accumulation are localised on the N atoms in a sp^3 configuration. It can be seen that a small amount of charge is localised between the atoms, as expected for a covalent solid with pronounced ionic fractions. A small charge accumulation along the Er-N bonds which is not present in the Ga-N bonds can be observed. This would indicate that the Er-N bonds have a more pronounced covalent nature than the Ga-N bonds and would also explain the shortness of the Er-N bonds in GaN:Er with respect to other solids like ErN. The sum of the covalent radii 0.56 \AA for N and 1.57 \AA for Er^{3+} matches quite well the Er-N bond distance in GaN:Er, suggesting the covalent nature of the Er-N bond in GaN. A thorough discussion about the nature of the Er-N bonds in GaN:Er and in other solids can be found in [14].

5.1.2 Charge state and transition levels

The luminescence from rare earth ions is well interpreted in terms of intra- f optic transitions (i.e. $f^n \rightarrow f^n$) in ionic models perturbed by the crystal field of the host. On the other side the charge transitions $f^n \rightarrow f^{n+1}$ are difficult to calculate because of the screening processes involved and cannot be simulated by simple LDA, except than in the case of Gd, where because of the half filled f -shell and the large exchange splitting already the LSDA provides a realistic description of the system. For this reason no agreement about the electric nature of the RE_{Ga} substitutionals in GaN could be achieved till now: in the simulations done by the group around Jones in Exeter these defects appear to be electrically inert [17], while in the works of Svane and Temmerman [18] an acceptor level was found for some lanthanide. In this paragraph we calculate the position of the divalent acceptor $\epsilon(0/-)$, corresponding to the addition of one electron to the f -shell, with DFTB-FLL by means of the Janak transition state explained in chap. 2.

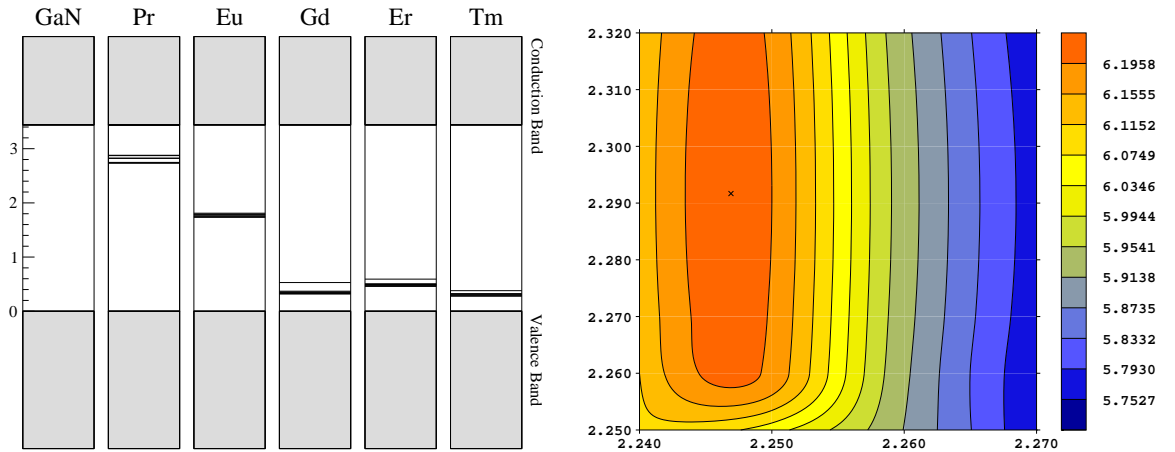


Figure 5.4: Left hand side: Band structure at the Γ point for the investigated RE_{Ga} substitutionals in wurtzite GaN, calculated with DFTB-LDA. The f -states appear in LDA like a bunch of narrow localised states within the GaN band gap and are situated close to the Fermi level. This is definitively a wrong description, as many experiments reveal their localised nature as atomic multiplet over a broad range of energies [236]. The states in the picture are one-particle levels and should be not confused with the charge transition levels. Right hand side: 3D-representation of the total energy (absolute value) calculated with DFTB-pSIC of a 256-atoms supercell containing one Eu_{Ga} substitutional as function of the Eu-N bond lengths. On the x-axis the length of the three equivalent Eu-N bond, in the y-axis the length of the Eu-N along the wurtzite c -axis. The \times indicates the position of the minimum.

We try at first to reproduce the results of the previous theoretical studies calculating the different charge states as described in each work. Jones [17] relaxed 72-atoms supercells within the LSDA approach including one lanthanide impurity in the hexagonal GaN lattice. The f -electrons were treated as core states for the generation of the pseudopotentials, assuming the valence state +3 and that the occupancy of the f -shell is not affected by the lattice site or by the chemical doping. To reproduce these results we generate a set of parameters for Eu and Er in which the f -orbitals are treated like core states, assuming the valence state +3. Using 72-atoms hexagonal cells we have investigated different charge states finding no localised states within the GaN band gap, independently from the lanthanide. DFTB, DFTB-FLL and DFTB-AMF do not lead to any difference. Treating the f -orbitals like core states leads to a description of the system where no localised states are introduced in the host gap by the substitutional RE_{Ga} , which can therefore only exist in the neutral charge state. We could reproduce the results of Ref. [17, 57] concerning the RE_{Ga} substitutionals in hexagonal GaN, i.e. that they are electrically inert. However we do not think that this is a satisfactory description of the system.

Svane *et. al.* [18] used cells of different sizes including one RE impurity in the cubic GaN lattice. The calculation scheme used (SIC) is more sophisticated than simple LSDA but the lattice positions were not allowed to relax. Using ideal 256 atoms supercells of cubic GaN containing one rare earth impurity, we calculated with DFTB-FLL the position of the acceptor level for Pr, Eu, Er and Tm, without relaxing the atomic positions. An acceptor like charge transition (0/-) was only found for Eu at 2.53 eV above the valence band and for Er on just below the conduction band edge (i.e. 3.3 eV above the valence band). No charge transition (0/-) was observed for Pr and Tm. This is in agreement with Svane who found a transition (0/-) only for Eu substitutionals at 2.44 eV above the valence band, even if no charge transition for Er was found. We additionally found a donor like charge transition (+/0) at 0.71 eV above the valence band for Pr substitutionals. Donor like charge transitions were not investigated by Svane.

As further (and last) test we calculate the position of the (0/-) transition in the case of Eu_{Ga} and Er_{Ga} substitutionals with the LDA+ U implementation of the LMTO-ASA simulation software described previously [237, 238] (and the same value of (U - J) used for the DFTB-FLL calculation) finding it to be located at 2.69 and 3.00 eV above the valence band. The error in the LMTO-ASA calculations can be estimated in ± 0.3 eV while the error affecting the DFTB-FLL calculations is

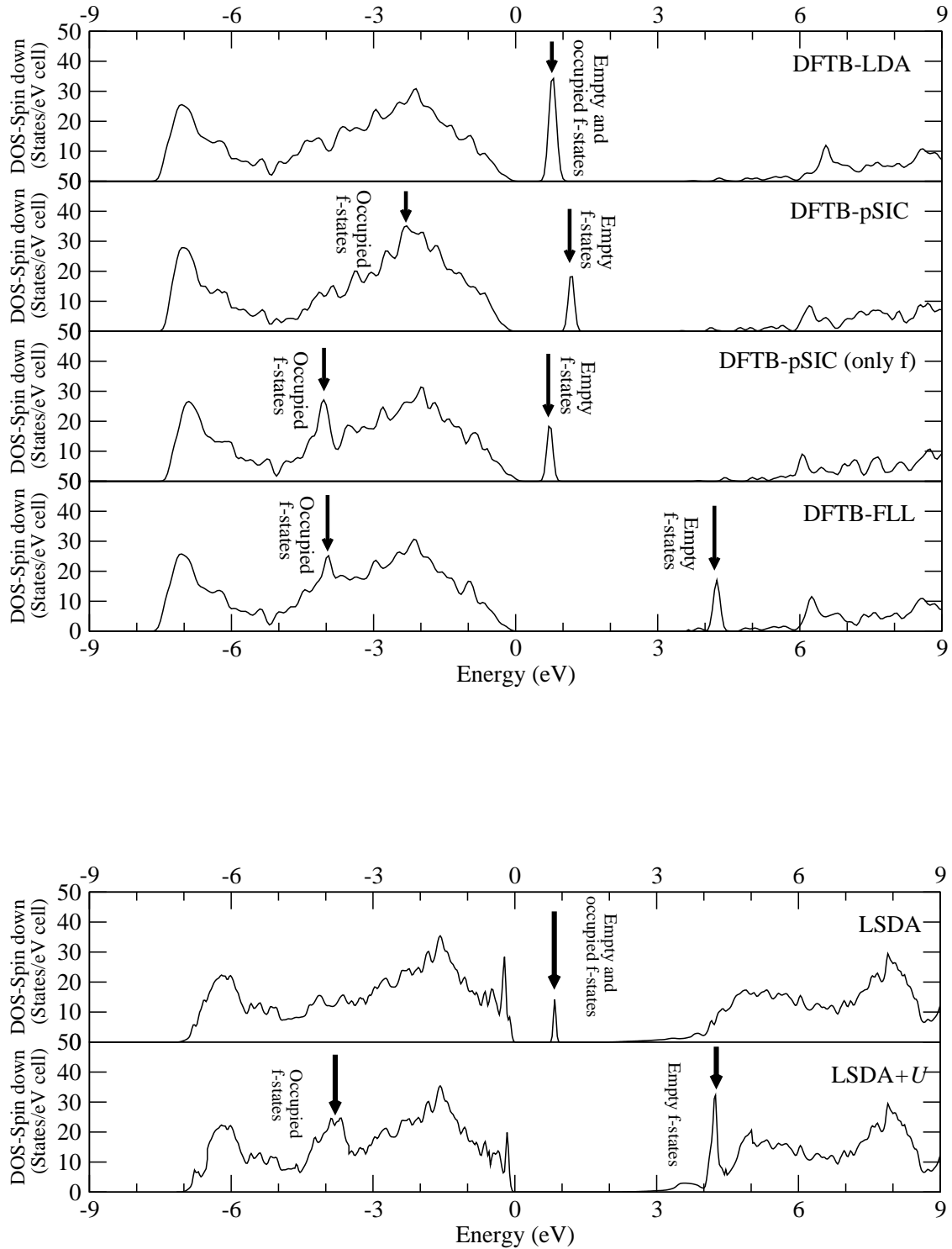


Figure 5.5: Er_{Ga} in the neutral charge state in wurtzite GaN. Spin resolved DOS calculated with the different approaches implemented in DFTB (upper box) and with LDA and LSDA+U as implemented in Wien2K (lower box). The arrows show the position of the f-related peaks. We only show the spin down electrons, as the spin up are occupied and included in the valence band. In the LDA+U and pSIC calculations the f-related peak visible in the band gap is split in two parts, the rest of the structure remains almost untouched. The valence band maximum was chosen in each case as zero of the energy scale.

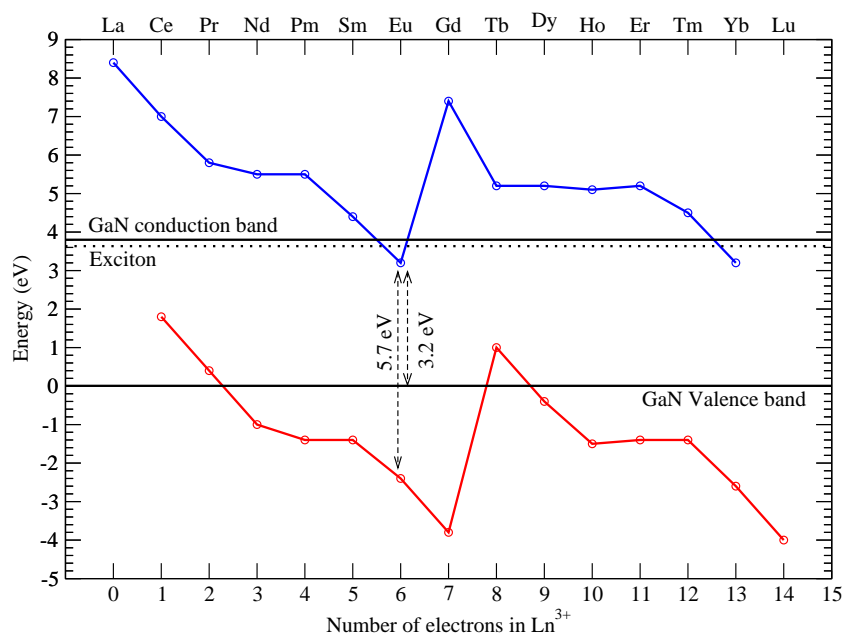


Figure 5.6: Location of the lowest $4f^n$ states of divalent and trivalent lanthanides in GaN proposed in Ref. [58]. The top of the valence band is chosen as zero of the energy scale. The GaN exciton state is at 3.48 eV and the conduction band bottom is estimated at 3.7 eV.

discussed later.

This picture changes anyway taking into account the geometry relaxation. While still no transition is observed for Pr_{Ga} substitutionals, Eu, Er and Tm have shown a (0/-) charge transition at 1.53, 2.01 and 2.10 eV respectively above the valence band. The (+/0) transition of Pr substitutionals too is shifted downwards by the relaxation and is calculated at 0.29 eV. Summarising, the effect of the geometry optimisation on the charge transition states cannot be neglected, as the position of the $\epsilon(0/-)$ level is shifted downwards by some tenth of eV. In the case of hexagonal GaN we find a very similar behaviour: (0/-) transition levels for the unrelaxed structure were found only for Eu, Er and Tm (at 2.40, 3.11 and 3.20 eV above the valence band respectively) and a (+/0) transition for Pr by 0.67 eV. Relaxing the structures Pr does again only show the (+/0) charge transition (at 0.27 eV) and Eu, Er and Tm the (0/-) transition levels at 1.28, 2.35 and 2.48 eV above the valence band respectively. We tested on the Eu_{Ga} substitutionals that the particular LDA+ U implementation used (FLL or AMF) does not change the results substantially. Our findings are in good agreement (i.e. within the error of the methods) with a simple scheme used to predict the position of the f -bands in lanthanide-doped wide-gap semiconductors. A few years ago Dorembo proposed an approximated way to predict the location of the $4f^n$ ground state energy of each divalent and trivalent lanthanide ion relative to the valence and conduction bands in GaN on the basis of lanthanide spectroscopic knowledge in wide gap inorganic compounds. The binding energy of the lowest $4f^n$ state in a Ln^{q+} ion, where n denotes the number of f electrons and q the ionic charge, has always a characteristic pattern. In Fig. 5.6 this pattern is shown for lanthanide in GaN (red and blue curve). The energy difference between the two curves depends on the host and in GaN is such that the Eu^{2+} and Eu^{3+} states are separated by 5.7 ± 0.3 eV. To place the GaN valence and conduction bands in this picture, the excitation spectrum of 622 nm red emission ${}^5\text{D}_0 \rightarrow {}^7\text{F}_2$ of Eu^{3+} in GaN is used. In this spectrum appears a broad (40 nm) but distinct excitation band at 388 nm. This band is due to the host to Eu^{3+} electron transfer. The charge transfer energy (called E^{CT}) is known to be 3.2 ± 0.3 eV, and measures the energy difference between the top of the valence band and the ground state of Eu^{3+} [239]. Using the knowledge of the exciton level in GaN (3.48 eV) the GaN conduction band can be placed and a scheme for the location of the f -bands in RE-doped GaN is complete (see Fig. 5.6). This scheme is affected by an error of approximately

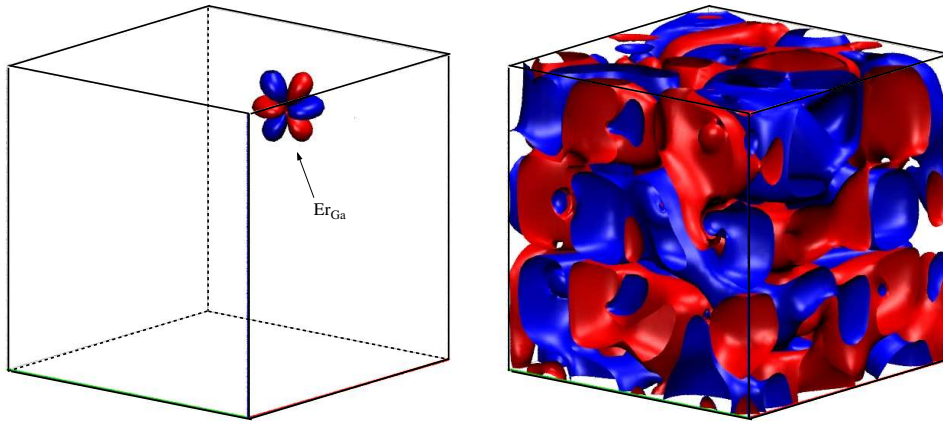


Figure 5.7: The substitutional Er_{Ga} in cubic GaN in the neutral charge state. Left hand side: wave function associated with one $4f$ -state: it is strongly localised and resembles atomic orbitals (LDA calculation, 72 atom cell, one single state is plotted). Right hand side: wave function associated with the extended conduction bands (on the plot the highest conduction band, LDA calculation). In the red parts wave functions are negative, in the blue ones positive.

0.5 eV and can be used to conclude that Eu^{3+} and Yb^{3+} can trap a free electron to form a stable divalent lanthanide. Ce^{3+} , Pr^{3+} and Tb^{3+} instead have their ground state in the forbidden region and can trap holes from the valence band to form tetravalent lanthanides. This is in agreement with our results concerning Pr and Eu and, considering the uncertainty of this scheme and of the DFTB methods, also in the cases of Er and Tm. We can conclude that the RE_{Ga} substitutionals are by no mean all electrical inert, confirming the results of Svane *et. al.* [18] and Dorembo *et. al.* [58]. The factors which affect the position of the calculated level are not the cell size nor the particular orbital-dependent potential used: only the geometry optimisation is found, despite of its small magnitude, to have an important influence on the position of the charge transfer level. The error affecting our results is discussed in the paragraph 5.1.4. The presence of a charge transition however is probably not related to the emission observed in photoluminescence experiments. The excitation mechanism is not straightforward and not all the rare earth impurities can be excited. A peculiarity of the photoluminescence effects in lanthanide doped GaN is that the created electron in the conduction band could recombine with the holes in the valence band without exciting the f -states. The process of charge carrier energy transfer can be in fact frustrated by the strong localisation of the f -shells or in the case in which the charge transition levels are deep in the gap. In this case an electron in the conduction band cannot occupy them directly because of the high energy mismatch. The energy transfer to the f -shell can be helped by a so called *assistant level*, a shallow transition-level introduced normally by another nearby defect. An electron from the conduction band can then in a first step occupy the assistant level and from this transfer its energy to the lanthanide f -states. For this reason we investigate complexes formed by lanthanide impurities and GaN native defects.

5.1.3 Hybridisation of the f -orbitals

The f -orbitals of the lanthanides have been described in this work as strongly localised. This does not mean that they are completely inert and not interacting with the host, but rather that their interaction with the host is very small. However much of the interesting physics of the rare earths is due to the f -electrons not being completely inert. For this reason the f -electrons can be divided in two groups, interacting and not interacting electrons. How can we demonstrate that the states which we consider non interacting are really not interacting? There are four main observations

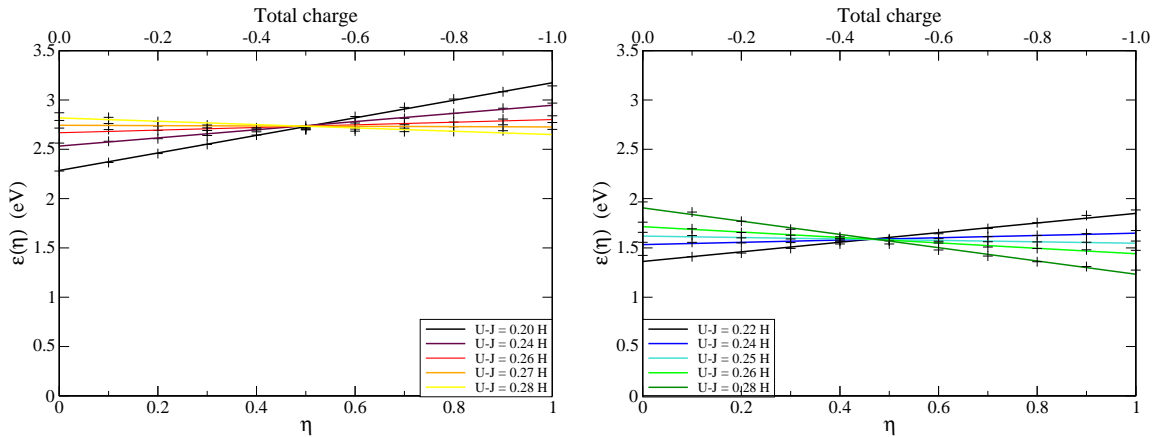


Figure 5.8: The substitutional Eu_{Ga} in cubic GaN. Position of the highest occupied state within the band gap for different occupations and different values of the U - J parameter. On the left hand side the structure is not relaxed while in the right hand side it is.

which let us deduct that such electrons are not interacting. At first we observe that the geometry of the studied defects does not really depend on the particular approach (LDA, LDA+ U or pSIC) we use to treat the f -electrons, from which we could guess that the f -electrons do not play a major role in the bond. This is also verified by the second observation: including all the f -states in the core does not substantially change the geometry of the defect. This is another evidence of the fact that these states do not enter the bond. Our third observation is that looking at the wave functions related to the f -states we observe not only a strong localisation but also that they keep their atomic-like form. In Fig. 5.7 the wave function associated with one f -state of an Er-ion in a GaN host are compared with a diffused conduction band. The form of the f -states is almost perfectly atomic-like, as can be seen in in Fig. 1.1. The last observation we make is that varying the value of the U - J parameter in the LDA+ U calculations the position of the f -states changes almost linearly, not only within the band gap but also in the valence and conduction bands, as shown in Fig. 5.9. This is another indicator that the f -states do not undergo any major hybridisation with the host levels.

5.1.4 Error of the calculation

In this paragraph we try to estimate the error affecting our calculations. Apart from the intrinsic DFTB error in fact there are three further possible error sources. These are the uncertainty in the choice of the U - J parameter for the LDA+ U calculations, the neglect of the spin-orbit coupling effects (which could be important for heavy ions like the rare earths) and of the Ga- $3d$ electrons. Let us examine these factors individually.

Dependence of the electronic transitions from the value of U - J

The position of the RE-related localised f -states is strongly dependent from the value of the U - J parameter. In contrast with this, neither the geometry nor the position of the charge transition levels are strongly dependent from this parameter. While the first is a consequence of the fact that the localised states are not largely involved in the bond and therefore do not deeply influence the geometry, the latter could be puzzling at first sight. However it must be considered that the + U corrections are maximal for empty states (which are pushed upwards) or occupied sates (which are pushed downwards) but are almost vanishing for half occupied states. As we use the Janak formalism involving half occupied states for the calculation of the charge transition levels, they are not really affected from the actual value of the LDA+ U correction. In principle the position of the highest occupied one-particle level with occupation 0.5 is not dependent from the value of U - J , but

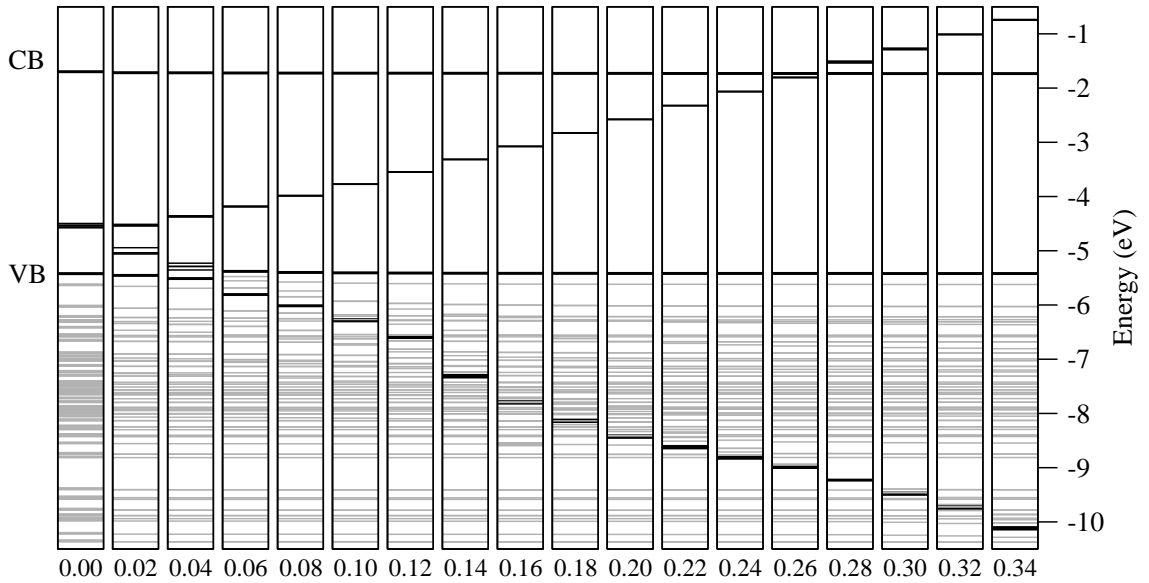


Figure 5.9: The substitutional Er_{Ga} in the neutral charge state in wurtzite GaN. Effect of the $+U$ potential on the induced gap levels at the Γ point, shown for different values of the parameter ($U-J$) from 0.00 H to 0.34 H (9.25 eV). The fact that the position of the f -related levels grows almost linearly with the $+U$ potential even within the valence and conduction bands suggests that the f -orbitals do not hybridise with the host orbitals.

small differences between different $U-J$ values could arise due to the self-consistency. This can be observed in Fig. 5.8, where the dependence of the highest occupied one-particle levels is reported as function of its occupation and of the $U-J$ value. The position of the half-occupied states varies by only some tenth of eV for a variation of 0.2 H (5.5 eV) of the $U-J$ parameter. The uncertainty in the determination of the $U-J$ parameter is then neither a big source of error in the calculation of the defect geometry nor in the evaluation of the charge transition levels. As explained in the section 2.2.2 the results reported in Fig. 5.8 can be used to determine the value of $U-J$ for which the piecewise linearity of the total energy functional is recovered.

Spin orbit coupling

In the above discussion as well as the following the effects of spin-orbit coupling are neglected. To estimate the error due to this neglect we have also carried on provisional calculations in the case of Er using the methodology outlined in Ref. [240] in addition to the LDA+ U -like treatment for DFTB. Using a $4f$ spin orbit constant of 2234 cm^{-1} , with the Er magnetic moment in the a plane [241], we find that the 7-fold degenerate localised gap levels shown in Fig. 5.9 in the gap are split into 4 filled and 3 empty non-degenerate levels which remain in the gap spanning a range of $\sim 700 \text{ meV}$. Applying the FLL-LDA+ U approach again ejects these states from the gap, demonstrating that in this case correlation has a larger effect than spin-orbit coupling. While the spin-orbit coupling does not considerably influence the description of the geometry of the system and the position of the charge transition states, it is the dominant factor concerning the optic effects. Neglecting it, we cannot calculate the optical properties of the investigated systems, but it will not influence the investigation of the microscopic characteristic of the defect centers, which is the goal of this work.

The role of the Ga 3d electrons

It has been argued in the previous chapter whether the Ga 3d orbitals are important for a correct description of GaN (and its interaction with the impurities) or not. We have verified that these orbitals are not indispensable for a qualitatively good simulation of the host, furthermore, being

the DFTB parameters the result of a fit with experimental data, eventual deficits in the simulation of the geometry caused by the absence of the d -shell are compensated in the fitting procedure. Concerning a possible interaction between RE f -states and Ga d -states, we could exclude it, having done a row of tests with parameters including and not including the Ga $3d$ -shell.

Furthermore we do not consider spurious interactions of charged defects in neighbouring supercells as an important source of errors, because the size of the used cells (256 or 512 atoms) should ensure that the Coulombic interaction caused by the finite size of the supercell is small. Summarizing, all the sources of errors in our calculation will affect our results with an error of some tenth of eV in the estimation of charge transitions levels but will not significantly affect the geometric description of the system. We can conclude that the uncertainty in our calculations is surely bigger than usual for standard *ab initio* calculations of "well behaved" system, nonetheless DFTB with its implementation (DFTB+ U and DFTB-pSIC) will give a qualitatively correct description of the investigated systems.

5.1.5 The substitutional RE_N

Our theoretical investigation confirms the experimental evidence of the fact that the rare earth ions prefer the Ga lattice site. RE_N substitutionals are a very instable configuration indeed, because the lanthanide tends to leave the N place, causing a serious lattice distortion in the host. This is probably due to the striking differences (in size and electronegativity first of all) between nitrogen and the rare earths. We have investigated the Eu_N, Er_N and Tm_N substitutionals, finding that in any case the RE does not stay on site. For each of the examined lanthanides the formation energy that the RE_N substitutional would lie at least 20 eV above the formation energy of the related RE_{Ga}, indicating that this kind of defect will not happen in significant concentrations, independently from its charge state. There is in fact no report in the literature (neither experimental nor theoretical study) regarding the existence RE_N substitutionals, which is in agreement with our findings. In the neutral charge state the lanthanides in the RE_N configuration are found not to lose any of their f -electrons and are therefore in the valence state +2, which was not observed experimentally. This is another hint about the evidence that RE_N substitutionals are not formed in significant concentrations and are most probably not related with the luminescence. For this reasons we do not further investigate this kind of defects, omitting the study of their band structure, density of state etc., and proceed with the inspection of another family of defects, the interstitials.

5.2 Interstitials

Another "simple" defect that could be created introducing rare earth ions in the GaN host is the RE-interstitial. In this configuration the impurity ions do not take the place of any host atoms, but rather occupy a lattice region between the host atoms (see Fig. 5.10, left hand side). Of course because of the different symmetry of hexagonal and cubic GaN some differences in the behaviour of RE interstitial in wurtzite and in zinc-blende GaN are expected. In particular in hexagonal GaN there is a multiplicity of interstitial sites with different symmetry, as discussed in the GaN-dedicated chapter (see Fig. 4.3). While there is no experimental evidence of the presence of interstitial RE ions in doped hexagonal GaN samples, the RE interstitial in cubic GaN has been proposed to be a stable defect. Glukhanyuk *et al.* [59] on the basis of a Stark-splitting analysis proposed a model in which the RE occupies an interstitial site with four Ga first neighbours and six octahedrally coordinated next neighbours N ions 15% further away.

5.2.1 I_{RE} in hexagonal GaN

We start our investigation with the lanthanide interstitials in wurtzite GaN. We only investigated the behaviour of the rare earths exploited for the fabrication of color displays, i.e. Eu, Er and Tm. Interstitials of these three ions in hexagonal GaN are found not to be stable defects: a configuration with the RE ion at the Ga place and the substituted Ga atom occupying an interstitial site is found to be energetically favoured for all the investigated rare earths (see Fig. 5.10, right hand side). In

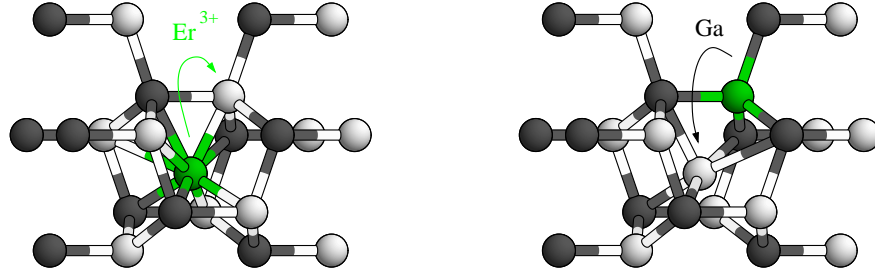


Figure 5.10: *The RE interstitials in hexagonal GaN. Rare earth ions will not stay in the interstitial configuration (left hand side) but will rather take the place of a neighbouring Ga atom, which is shifted in the interstitial site (right hand side). As usual N atoms are black, Ga white and Er green.*

other words interstitial RE defects are not stable against the formation of RE substitutionals and Ga interstitials:



The kick out process is favoured for all the investigated by more than 0.5 eV, with Eu showing the biggest differences. This is in agreement with the *ab initio* investigation of Filhol *et al.* [57].

This particular behaviour could be explained with the big size of the impurity ions. While very small impurity atoms like hydrogen in III-V semiconductors prefer the interstitial site [242, 243], big ions like the lanthanides do not fit in the space between the lattice sites and prefer lattice sites. This explains also why for bigger RE like Gd and Eu the kick out process is even more favourable than for Er and Tm. In general the intrinsic defects (substitutionals, vacancies, interstitials etc.) in GaN and in other hosts like GaAs or ZnO differ substantially, because the difference in size and electronegativity between the constituents (Ga and N) is much bigger than in other semiconductors [182]. RE interstitials do not seem to be an exception, as they have been observed in other RE-doped semiconductors like GaAs and Si [17] but not in GaN. Our results agree with these findings and cannot confirm the suggestion of Pellé *et al.* [50], who proposed to identify some emitting center in Er doped GaN with Er^{3+} ions in interstitial positions near defects created introducing the dopants into the lattice as observed for GaAs:Er³⁺. In the final configuration the RE has not the C_{3v} of the single substitutionals with one long and three short RE-N bonds, because the neighbouring Ga interstitial shortens one of the short bonds. The RE is displaced by 0.09 (Eu and Er) and 0.08 Å (Tm) in the direction of the Ga interstitial from the ideal lattice site of the substituted Ga. The substituted Ga atom occupies an interstitial site almost at the center of the hexagonal channel. This site has though a slightly different symmetry from the octahedral symmetry which would have a single I_{Ga} in hexagonal GaN [175]. This is due to the additional distortion introduced by the RE. The kick out of the Ga atom and relative substitution with the RE is a feature common to all the investigated RE (Eu, Gd, Er, Tm). Even if a Ga interstitial is more favorable than a RE interstitial it will nonetheless introduce a fairly large lattice relaxation. This is reflected in the large formation energies (26.24, 20.93 and 19.06 eV for Eu, Er and Tm in the neutral charge state). These formation energies however cannot be directly compared with the formation energies of the simple substitutionals. An important parameter in the study of isolated impurities and point defects is their binding energy (E_b), a parameter which measures the tendency of defects and impurities to agglomerate and form complexes. It is defined in terms of formation energies as :

$$E_b = E^f(RE_{Ga}) + E^f(I_{Ga}) - E^f(RE_{Ga} I_{Ga})$$

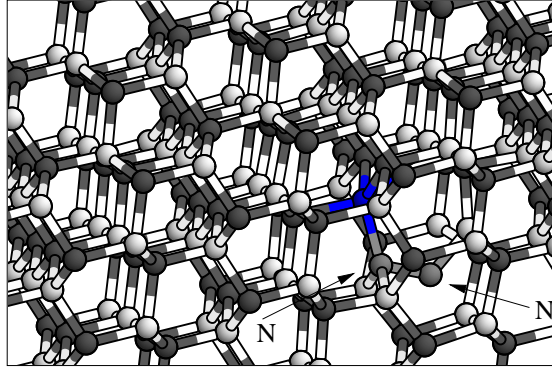


Figure 5.11: Complexes formed by RE substitutionals and N interstitials in hexagonal GaN will result in the so called N split interstitial configuration. In the picture in blue the Tm impurity occupying the Ga place. The arrows indicate the two N-atoms sharing a lattice site.

so that a positive binding energy corresponds to a stable bound complex². In the case of the RE substitutionals the calculated binding energy of 1.00 eV (Eu), 0.57 eV (Er) and 0.44 eV (Tm) is somehow higher (specially for Eu) than the values reported by Filhol *et al* [57] but anyway lower than the binding energy of other RE-defect complexes ($\text{RE}_{\text{Ga}} \text{V}_{\text{N}}$ or $\text{RE}_{\text{Ga}} \text{O}_{\text{N}}$), as we will show in the following chapters. In further agreement with the cited work we find the $\text{RE}_{\text{Ga}} \text{I}_{\text{Ga}}$ complex to possess deep gap levels. Unlike in the case of the simple RE_{Ga} substitutionals, where an electron from the *f*-shell is promoted to the lattice, the rare earths in the interstitial configuration do keep all their *f*-electrons like in the atomic configuration and can be thought in the neutral charge state as RE^{2+} ions. The fact that there is experimental signature of RE only in the trivalent state indicates that these complexes are not likely to occur in high concentrations. Because of its high formation energy the complex $\text{RE}_{\text{Ga}} \text{I}_{\text{Ga}}$ will hardly be formed under equilibrium conditions indeed. However it can be formed by non equilibrium processes like the ion implantation. In this investigation RE interstitials in zinc-blende GaN were not kept in account.

5.2.2 $\text{RE}_{\text{Ga}} \text{I}_{\text{N}}$ in hexagonal GaN

We only investigate complexes formed with Eu, Er and Tm lanthanides in hexagonal GaN in this paragraph. $\text{RE}_{\text{Ga}} \text{I}_{\text{N}}$ defect complexes present characteristics similar to the $\text{RE}_{\text{Ga}} \text{I}_{\text{Ga}}$ interstitials. The lanthanide ion is slightly displaced from the Ga site it occupies (by 0.15, 0.12 and 0.11 Å for Eu, Er and Tm respectively) and the I_{N} assumes the so called split interstitial configuration. It means that the interstitial nitrogen forms a N-N bond with one of the host nitrogen atoms with whom it shares the lattice site (see Fig. 5.11). In the neutral charge state the N-N distances are 1.551, 1.570 and 1.567 Å for Eu, Er and Tm respectively. This is well beyond the N-N distance in N_2 molecules (1.121 Å in DFTB) but shorter than the N-N distance in solid N (HCP structure, N-N distance 3.861 Å). The formation energy of these complexes (13.34, 11.54 and 9.95 eV for Eu, Er and Tm respectively, in the neutral charge state, LSDA calculation) is lower than the formation energy of the $\text{RE}_{\text{Ga}} \text{I}_{\text{Ga}}$ pairs. The calculated binding energy (1.33, 0.94 and 0.92 eV for Eu, Er and Tm respectively) is comparable with the binding energy of the $\text{RE}_{\text{Ga}} \text{I}_{\text{Ga}}$ complexes and again somehow higher than the values calculated by Filhol *et al.* [57]. Just like the $\text{RE}_{\text{Ga}} \text{I}_{\text{Ga}}$ complexes all investigated $\text{RE}_{\text{Ga}} \text{I}_{\text{N}}$ complexes can happen in different charge states and possess deep gap levels. The RE has valence +2 and does not lend any *f*-electron to the lattice, exactly like in the case of the related $\text{RE}_{\text{Ga}} \text{I}_{\text{Ga}}$ complexes, which probably excludes a role in high energy fluorescent transitions.

²A positive binding energy does not always imply that the complex will form, as the thermodynamics of the complex is ruled by the binding energy as well as by the configurational entropy [175].

5.3 Summary and conclusions

In this chapter we used the tight-binding simulation tool DFTB+ and different DFT simulation packages like Wien2k and ABINIT for the simulation of substitutionals and interstitials defects of rare earth ions in the GaN host. Both the hexagonal and cubic GaN phase have been examined. The DFTB+ tool showed, besides an outstanding efficiency also a noticeable reliability and is found to be in qualitative agreement with the other calculation schemes. Because of the efficiency of the code, a number of different geometric, spin and charge configurations could be investigated in big supercells and a self-consistent determination of the U - J value could be achieved. A qualitative agreement of our results is also found with existing experimental data and theoretical investigations. Summarising what we found about the RE substitutionals, we can affirm that they prefer the Ga lattice site and are always trivalent in their neutral charge state (RE^{3+}). This means they behave almost isoelectronically with Ga^{3+} in GaN. The presence of the $\text{RE}_{\text{Ga}}^{3+}$ substitutional does not noticeably influence the charge distribution around the substituted ion. The charge residing on the N-ligands differ at most by only 0.086 eV (in the case of Eu^{3+}) representing less than 1.5% of the charge localised on the atom. The $\text{RE}_{\text{Ga}}^{3+}$ substitutionals created by different lanthanides are characterised by the same properties and show only minor differences in the geometry. The latter are determined merely by the differences in the ionic radii of the investigated species. Bond lengths and band structures have been calculated with different approaches: the classical LDA and the more sophisticated LDA+ U approach predict the same structure, that is with the RE placed at the Ga site and tetrahedrally coordinated with C_{3v} symmetry, but qualitative different band structures. An acceptor like transition $\epsilon(0/-)$ is found at 1.28, 2.35 and 2.48 eV above the valence band (1.53, 2.01 2.10 eV in cubic GaN) for Eu, Er and Tm and a donor-like transition $\epsilon(+/0)$ is found at 0.27 eV above the valence band (0.29 eV in cubic GaN) for Pr. These transitions are probably not related with the lanthanide luminescence, as we discuss in the last chapter of this work. The $4f$ states of the rare earths are as expected strongly localised and play only a minor role in bonding. A consequence of this fact is that LDA+ U primary influences the energetics of the investigated systems and not the geometry. The RE_{Ga} substitutionals in both cubic and hexagonal GaN only induce a small lattice distortion, which we quantified with a parameter, called strain or stress, given by the ratio of the RE-N bond lengths and the corresponding Ga-N bond length in bulk GaN. Because of the small value of this parameter and because of the small changes in the charge distribution (with respect to undoped GaN) of the neighbouring N-atoms we can affirm that lanthanide impurities are easily incorporated at the Ga place in the GaN host. The small lattice distortion introduced by the substitutional rare earths is of importance for the realisation of luminescent devices. On the other hand lanthanide interstitials do introduce a fairly large lattice relaxation and are characterised by a high relaxation energy. RE interstitials do not take place, as the configuration with a RE_{Ga} substitutional and a I_{Ga} interstitial is energetically favoured. In the simple RE_{Ga} substitutionals the RE remains on site, while in interstitials it is slightly displaced from the ideal lattice site. The defect symmetry is C_{1h} , lower than the C_{3v} of the simple substitutionals. The lanthanides in the interstitial configuration can be considered RE^{+2} ions. Complexes formed with a RE_{Ga} substitutional and I_{N} interstitial share many similar characteristic with the $\text{RE}_{\text{Ga}} \text{I}_{\text{Ga}}$ complexes but are characterised by a slightly lower formation energy and binding energy. Because of their high formation energy and small binding energy all RE interstitials (or, more precisely, $\text{RE}_{\text{Ga}} \text{I}_{\text{Ga}}$ and $\text{RE}_{\text{Ga}} \text{I}_{\text{N}}$ complexes) are unlikely to be formed under equilibrium conditions, furthermore the presence of deep gap levels probably excludes a role in high energy fluorescent transitions. Instead the possibility that the simple RE_{Ga} play a role in the luminescence is discussed in the final chapter of this work.

Chapter 6

Rare earth defect complexes in GaN

The study of isolated rare earth ions is not enough to give a complete picture of lanthanide-doped sample. If implanted, the big and heavy impinging lanthanides produce a lot of damage in their path through the sample, which remains, almost partially, even after annealing. Instead, when a GaN sample is doped with lanthanides during the growth, intrinsic defects are likely to be formed and the rare earth ions can be bound by these defects. On the other side, in grown samples, voluntary or involuntary co-doping with non lanthanide impurities is often present and should be taken in account in the investigation of rare earth point defects. The complexes involving lanthanides and GaN intrinsic defects may have, of course, completely different physical properties than the RE simple substitutionals and should also be investigated in our simulations, in order to realise an exhaustive representation of the lanthanide-doping in GaN. Object of this chapter is the investigation of complexes formed by a rare earth impurity and intrinsic defects like vacancies or antisites, while the issue of co-doping is discussed in the next one. On the basis of the geometric, energetic and electronic characteristics of each investigated defect, its role in the mechanisms leading to the luminescence is discussed. Even if interesting on its own and in relation with the rare earth emission mechanisms, the issue of native defect-clustering is not tackled in this work. On the

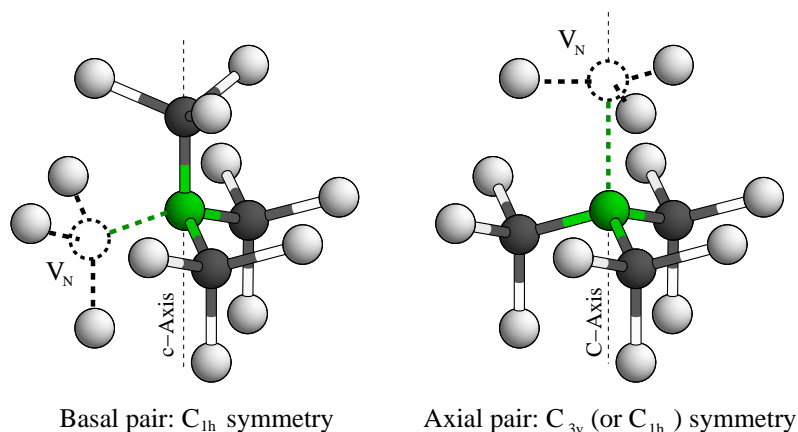


Figure 6.1: Defect pairs formed by RE_{Ga} substitutionals and V_N in hexagonal GaN. Because of the inequivalent N sites in hexagonal GaN (the Er-N bond along the c-axis is longer than the other three) the complexes can be formed in two configurations. The basal configuration (left hand side) has C_{1h} symmetry whereas the ideal axial configuration (right hand side) has the C_{3v} symmetry, or the C_{1h} if a Jahn-Teller distortion occurs.

Table 6.1: Geometry and binding energy of the $RE_{Ga} V_N$ complex in hexagonal GaN in the neutral and positively charged state. The bond distances are expressed in Å and the energies in eV. The data are calculated with DFTB-FLL (DFTB-LSDA data in parenthesis).

Charge	Symm.	RE- V_N		Displacement		$E^{bind.}$	
		0	+	0	+	0	+
Eu <i>basal</i>	C_{1h}	2×2.34 (2.32)	2×2.25 (2.31)	0.10 (0.10)	0.14 (0.18)	1.62 (1.67)	0.97 (1.00)
		1×2.30 (2.29)	1×2.29 (2.28)				
<i>axial</i>	C_{3v}	3×2.33 (2.30)	3×2.26 (2.28)	0.10 (0.09)	0.12 (0.13)	1.66 (1.69)	0.97 (0.93)
Er <i>basal</i>	C_{1h}	2×2.26 (2.20)	2×2.16 (2.16)	0.07 (0.05)	0.11 (0.08)	1.35 (1.04)	0.44 (0.27)
		1×2.21 (2.17)	1×2.23 (2.15)				
<i>axial</i>	C_{1h} (C_{3v})	2×2.25 (2.18)	2×2.19 (2.15)	0.01 (0.05)	0.07 (0.06)	1.42 (1.10)	0.53 (0.41)
		1×2.20 (2.18)	1×2.08 (2.15)				
Tm <i>basal</i>	C_{1h}	2×2.23 (2.17)	2× 2.12 (2.14)	0.11 (0.06)	0.10 (0.08)	1.14 (0.93)	0.33 (0.14)
		1×2.19 (2.14)	1× 2.15 (2.12)				
<i>axial</i>	C_{1h} (C_{3v})	2×2.19 (2.16)	2×2.13 (2.12)	0.04 (0.06)	0.04 (0.06)	1.15 (0.97)	0.33 (0.26)
		1×2.24 (2.16)	1×2.21 (2.12)				

same way we do not investigate these complexes with the rare earth neighbouring a native defect pair, like for example the $V_{Ga} V_N$ divacancies, which have been found to be very stable defects in GaN [210]. Unlike in the investigation of rare earth substitutionals we do not simulate all the possible configuration formed by Pr, Eu, Gd, Er and Tm in hexagonal and cubic GaN, but limit ourself to the investigation of complexes involving Eu, Er and Tm in hexagonal GaN. The choice of the host is motivated by the fact that wurtzite is the phase used in the vast majority of the experiments. The selection of the rare earths is due to their application in the realisation of colour displays.

6.1 Complexes with vacancies

Among all the rare earth point defects in GaN, particularly important are complexes formed by a rare earth substitutional and a vacancy. Gallium and nitrogen vacancies are in fact the dominating intrinsic point defects in GaN [210] and are likely to be present also in rare earth doped samples. If we imagine that during the growth of a RE-doped GaN sample a lanthanide takes the place of a Ga ion to form a RE_{Ga} substitutional, it will introduce some lattice strain. More precisely, as the RE occupies more space than the Ga would, it can be imagined that to recover the GaN-lattice constant, one of the neighbouring N or a Ga in the second neighbours shell ions could be let out. Furthermore Uedono *et. al* [244] put the luminescence from Eu samples in relation with the presence of $Eu-V_{Ga}$ pairs or Eu ions complexed with vacancy clusters. In this section complexes formed by lanthanide and neighbouring vacancies in hexagonal GaN are investigated. As usual, we carry out our investigation by means of the LDA+ U (FLL) implementation of DFTB, using 256-atoms supercells and a $4\times 4\times 4$ MP k -point mesh. The value of the U - J parameter is for each rare earth the same used and discussed in the previous chapters.

6.1.1 $RE_{Ga} V_N$

Because of the hexagonal symmetry of the host, the four lattice sites of the first neighbours of a RE substitutional are not equivalent. Around each RE ion there are three bonds of the same length and one, slightly longer, parallel to the crystal c -axis. When we create a RE substitutional plus a nitrogen vacancy, we can remove either an atom from one of the three equivalent positions or the one along the crystal c -axis. In the first case the $RE_{Ga} V_N$ complex is called basal pair and will have the C_{1h} symmetry, in the second case the complex is an axial pair and can have the higher “axial”

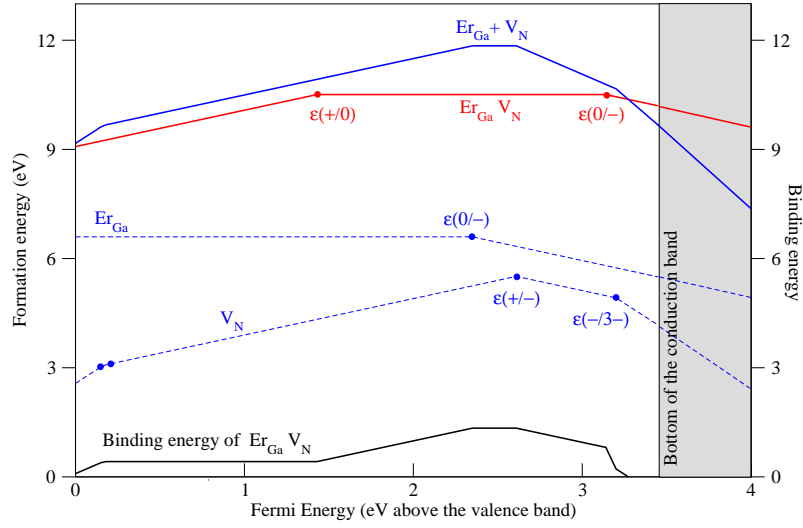


Figure 6.2: Formation and binding energy of the $RE_{Ga} V_N$ pair as function of the Fermi energy in hexagonal GaN. Dotted lines are the formation energies of the isolated Er_{Ga} and V_N , the blue line is their sum, the red line is the formation energy of the $Er_{Ga} V_N$ pair and the black line its binding energy, given as difference of the latter two curves.

C_{3v} symmetry or the C_{1h} symmetry if Jahn-Teller distortion occurs. We found the axial pairs to be energetically slightly favoured upon the basal pairs, with a formation energy in the neutral charge state lower by 0.04, 0.07 and 0.01 eV for Eu, Er and Tm respectively.

Geometry

In Tab. 6.1 we report the geometry and the binding energy of axial and basal pairs both in the neutral and in the positive charge state. Data refer to the stablest configuration (both axial and basal configurations have different minima). The differences are of the same order of magnitude of the method precision. Both in the case of the axial and basal pairs we observe that the relaxation of the structures is quite pronounced. The lanthanide is slightly displaced from the crystal c -axis. In the case of the axial pairs it means that the initial C_{3v} symmetry is distorted. The issue of the determination of the symmetry may be problematic both for the theoreticians and for the experimentalists. It is in fact not easy to find out how far rare earth atoms would have to be displaced off the c -axis in order to reveal a symmetry lower than the C_{3v} in luminescence experiments¹. Our DFTB-FLL calculations show that the axial configuration is slightly favoured with respect to the basal configuration for all investigated lanthanides in the investigated charge states. The displacement of the lanthanide from the Ga-site towards the vacancy in the neutral charge state is 0.10, 0.07 and 0.11 Å for Eu, Er and Tm basal pairs and 0.10, 0.01 and 0.04 Å for Eu, Er and Tm axial pairs. The displacement is more pronounced for Eu than for Er and Tm (see Tab. 6.1). The somewhat larger displacement of Eu was also found with the DFT-LDA calculations reported in Ref. [57], where the displacement is quantified in 0.23, 0.21 and 0.20 Å for Eu, Er and Tm for $RE_{Ga} V_N$ pairs which we assume to be in the axial configuration (see footnote 3). Assuming $RE V_N$ pairs as defect model, this could explain why previously Eu has been indicated to be the

¹Photoluminescence (PL) and cathodoluminescence (CL) are the most common techniques used to perform optical studies of particular rare earth ions. While PL is spectrally selective (the photon energy of the excitation can be tuned), CL tends to excite many different centers that the high energy electron beam encounters. A problem related to the CL optical studies that the experimentalists have to face assigning symmetry properties to the rare earth defect is therefore the following: while theoretical predictions from lattice sum calculations refer to single defect-centers, the informations in the CL spectra are due to the superimposition of different centers. Unfortunately EPR measurements, able to unambiguously distinguish between the symmetries are so far not available. Luminescence techniques are not sufficient to completely characterise the defect centers.

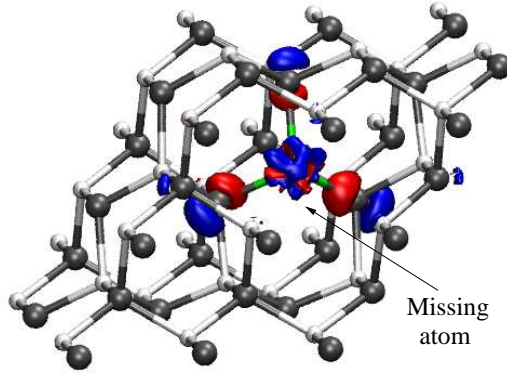


Figure 6.3: Total charge difference between the positive and neutral charge states of the $\text{Er}_{\text{Ga}} \text{V}_{\text{N}}$ axial pair. The electron is removed mainly from the neighbourhood of the Er-atom (blue region), while around the ligands polarisation effects can be observed. The changes in the charge distribution do not interest the vacancy region.

only rare earth to lay off-site [188, 233]. This structure was also related to the particularly strong intensity of the luminescence from Eu-doped GaN samples, which, on turn, was explained with the lower symmetry of the complex. As further test we carried out ABINIT [121, 234] calculations of the $\text{Er}_{\text{Ga}} \text{V}_{\text{N}}$ axial pair in the C_{3v} symmetry and in the neutral charge state. This are DFT-LDA calculations, which should give at least a satisfactory description of the system geometry. The $4f$ -electrons were treated as core state. After relaxation the C_{3v} symmetry is not lowered, the N-ligands are 2.38 \AA apart from the Er-ion, which is displaced by 0.18 \AA towards the nitrogen vacancy. This is in qualitative agreement with the analogue DFT-LDA calculations of Ref. [57].

Energetics, Charge states

Besides the geometry, in Tab. 6.1 the binding energy of the pairs (calculated as difference of the formation energy of the defect pair and of the isolated constituents for a given charge state) is reported. We observe that Eu complexes have the highest binding energy (1.66 eV in the neutral charge state). This can be explained with the dimension of the ion and the stress introduced in the structure. Eu is bigger than Er or Tm and it is even more energetically favourable to introduce a vacancy near the substitutional to recover some lattice distortion. In general nitrogen vacancies in the neutral charge state are more bound than positively charged vacancies. The number of vacancies which are effectively bound after annealing can be estimated with a simple model. If we assume that the lanthanide concentration c_{RE} is much bigger than the vacancy concentration $c_{\text{V}_{\text{N}}}$, the equilibrium concentration of the RE- V_{N} pairs is given by:

$$c_{\text{RE-V}_{\text{N}}} = \frac{c_{\text{RE}}}{c_{\text{RE}} + N e^{-\frac{E^b}{kT}}} \quad (6.1)$$

where, N is the density of Ga lattice sites, T is the temperature and k the Boltzmann constant. Considering c_{RE} to be like in our simulation and similarly to the real sample to be 0.78%, we find at 1000 K 80-99.% of the nitrogen vacancies to be bound with the rare earth. Eu complexes, which have the highest binding energy lead to the biggest concentration of such defects but also in the case of Er and Tm it can be affirmed that the vast majority of the vacancies are bound.

Strictly speaking the binding energy of the $\text{Er}_{\text{Ga}} \text{V}_{\text{N}}$ pair is a function of the position of the Fermi energy. In Fig. 6.2 we report the value of the binding energy for values of the Fermi energy within the GaN band gap. The pair is bound for moderately n -type doped GaN.

The formation energies of the $\text{RE}_{\text{Ga}} \text{V}_{\text{N}}$ complexes in the neutral charge state are 10.77, 10.51 and 9.127 eV for Eu, Er and Tm². The formation energy as function of the Fermi energy is reported

²The formation energy of these pairs cannot be directly compared with the formation energy of isolated defects

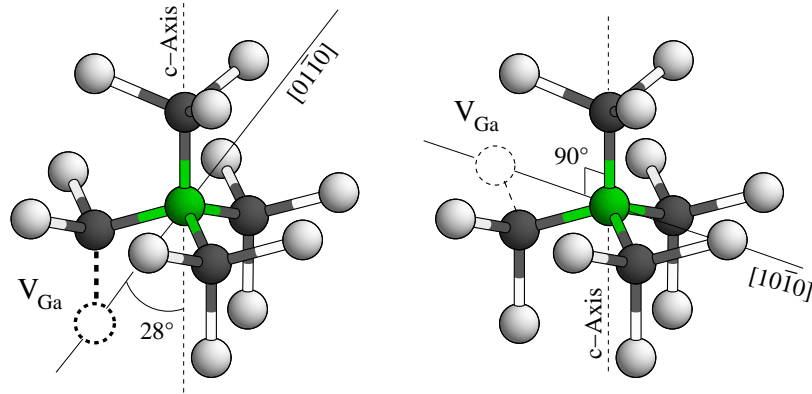


Figure 6.4: $RE_{Ga} V_{Ga}$ defect pairs in hexagonal GaN. Because of the inequivalent Ga sites in hexagonal GaN the complexes can have different symmetry. The configuration on the left hand side has the C_{1h} symmetry while the configuration on the right hand side the C_1 .

in Fig. 6.2. A charge transition $\epsilon(0/-)$ close to the valence band was found for all the investigated rare earths by means of the Janak Transition state. The transition takes place at 3.14, 3.14 and 3.15 eV above the valence band for Eu, Er and Tm respectively. Another charge transition $\epsilon(+/0)$ was calculated at 0.27, 1.43 and 1.59 eV above the valence band for Eu, Er and Tm respectively. In not strongly n -type GaN the $RE_{Ga} V_N$ pairs are therefore neutral or positively charged. In the positive charge state the lanthanide ion behaves iso-electronically with the substituted Ga, i.e. can be considered in the valence state +3. Like in the case of the single RE_{Ga} substitutionals two $6s$ and one $4f$ electron are promoted to the host. In the neutral charge state the lanthanide in the $RE_{Ga} V_N$ pair does not behave iso-electronically with the substituted Ga and has the valence state +2. The difference between the two charge states can be seen in the right hand side of Fig. 6.3. It is clear that in the positive charge state one electron is subtracted from the lanthanide (Er, in the picture) which becomes isovalent with Ga. Our result seems to be in qualitative agreement with Filhol *et al.*, which found a charge transition for Eu, Er and Tm for the $RE_{Ga} V_N$ complex within the C_{1h} symmetry 0.2 eV below the conduction band and suggested that the charge transitions of the complex can be considered as the perturbed transition of the isolated V_N vacancy³.

6.1.2 $RE_{Ga} + V_{Ga}$

Uedono *et al.* [244] have recently investigated Eu and Tb doped GaN samples by means of positron annihilation, showing the presence of Ga vacancies defect, which may take part to the luminescence. They suggested that vacancy-clusters consisting of two or more vacancies are the dominant defect in Eu-implanted GaN samples. In this section we investigate defect pairs formed by Eu, Er and Tm substitutionals and V_{Ga} vacancies in hexagonal GaN. Vacancy-clusters on the contrary are not object of this work and remain for future investigations. A single RE_{Ga} substitutional in hexagonal GaN is surrounded by a first shell of four nitrogen neighbours, which have, on turn, each three gallium neighbours. Each RE_{Ga} substitutional has 12 second neighbours, placed at a distance of 3.0 to 3.5 Å, depending on the rare earth. Removing one of these second neighbours originates a $RE_{Ga} + V_{Ga}$ complex, as reported in Fig. 6.4. Not all of these vacancies are equivalent, because of the presence of inequivalent sites in GaN. If the vacancy lies in the plane defined by the position of the lanthanide, the ligand along the c -axis and another ligand, the pair has symmetry C_{1h} (like in the right hand side of Fig. 6.4) otherwise it has symmetry C_1 . According to the DFTB calculations however, these configurations differ by an energy (0.003 eV) which is lower than the intrinsic error

but only with the formation energy of other pairs. Another parameter which we use to quantify the stability of the pair is the binding energy.

³In this work however no distinction between axial and basal pairs is made and the authors only refer to pairs with C_{1h} or with C_{3v} symmetry.

Table 6.2: Characteristics of the $RE_{Ga}+V_{Ga}$ complex in hexagonal GaN (DFTB-LSDA calculations). Displacement labels the displacement of the lanthanide from the Ga-site, $RE-V_{Ga}$ the distance of the lanthanide from the gallium vacancy, $RE-N$ in $RE-V_{Ga}$ the mean distance of the ligands from the lanthanide in RE -vacancy pairs and finally $RE-N$ in RE_{Ga} the mean distance of the ligands from the lanthanide in isolated RE_{Ga} substitutionals. All the lengths in Å.

Complex	Displacement	$RE-V_{Ga}$	$RE-N$ in $RE-V_{Ga}$	$RE-N$ in RE_{Ga}
Eu- V_{Ga}	0.51	2.59	2.29	2.28
Er- V_{Ga}	0.29	2.85	2.14	2.16
Tm- V_{Ga}	0.25	2.89	2.12	2.14

of the method and can be considered energetically degenerate. We will present therefore only the results of one configuration, i.e. of that where the missing Ga atom is the RE second neighbour along the $[01\bar{1}0]$ axis⁴. The presence of the vacancy causes a sizable relaxation of the neighbourhood of the complex: the N-ligand close to the vacancy moves towards the missing atom and the rare earth moves along the symmetry plane⁵ in almost the same direction, maintaining a similar distance from all N-ligands. The displacement of the RE atoms from the Ga-site is of 0.51, 0.29 and 0.25 Å for Eu, Er and Tm respectively. This effect is more pronounced for bigger rare earths, as reported in Tab. 6.2. As reported in Tab. 6.2 the distance of the rare earth from the vacancy center is only 20-30% bigger than the distance of the rare earths from V_N vacancies. The geometry optimisation is accompanied by a huge relaxation energy of as high as 6-10 eV, depending on the lanthanide. The third column of the table reports the mean distance of the nitrogen ligands to the rare earth in the $RE_{Ga}+V_{Ga}$ complexes. This is a parameter which has been considered important in the luminescence process [244]. It is well established that the intra- f transitions originating the luminescence are intrinsically forbidden and are enhanced by lowering the coordination symmetry. Uedono *et al.* [244] suggested that in the case of Eu doped GaN the presence of Eu- V_{Ga} complexes would stretch the lengths of Eu-N bonds and therefore enhance the transition rate of its 4 f -electrons. Our calculations reveal that even if the lanthanide is displaced from the Ga-lattice site and its environment undergoes a heavy relaxation, the mean RE-N bond length is substantially not different from that of the single RE_{Ga} substitutionals, as reported in Tab. 6.2.

The lanthanide near the Ga-vacancies have, independently from charge state, the valence state +3, which is the valence state of the lanthanide participating to the luminescence. This means that, like in the case of the RE_{Ga} substitutional the number of f -electrons of Eu, Er and Tm is 6, 11 and 12 respectively. In chapter 4 it has been shown that isolated V_{Ga} in GaN behave as triple acceptors, with the acceptor levels localised around 1 eV above the valence band. Because of the presence of these levels makes the participation of these defects in the 3 eV (412 nm) Er-related fluorescence very improbable [57]. In the DFTB-FLL approach also $Er_{Ga}+V_{Ga}$ pairs behave as triple acceptors, with charge transitions $\epsilon(0/-)$, $\epsilon(-/2-)$ and $\epsilon(2-/3-)$ at 0.45, 0.64 and 1.15 eV above the valence band in the case of erbium. We observe that these charge transition are very close to the charge transitions of the isolated V_{Ga} in hexagonal GaN. Being the components of the $Er_{Ga}+V_{Ga}$ pair an acceptor and a triple acceptor we investigate the possibility of a further charge transition to the charge state -4 for the pair. We found however this transition at 3.67 eV above the valence band, i.e. outside the band gap (see Fig. 6.5). In the neutral charge state the formation energy is slightly higher than the formation energy of $RE_{Ga} V_N$. The DFTB-LSDA calculated formation energies for Eu, Er and Tm complexes in N-rich conditions and in the neutral charge state are 13.23, 11.44 and 10.09 eV. However, unlike $RE_{Ga} V_N$ pairs, rare earths and gallium vacancies are bound for every position of the Fermi energy within the band gap (see Fig. 6.5). Unlike the defects investigated till now, $RE_{Ga}+V_{Ga}$ vacancies do not involve directly neighbouring lattice sites but rather a lattice site and its second neighbours. This does not mean however, that the complex is not bound, or that the binding energy is particularly low. This is due to the strong coupling

⁴This is the axis forming an angle of 28.0 with the $[0001]$ (or c) axis (see Fig. 6.4).

⁵For this reason the symmetry of the pair remains C_{1h} .

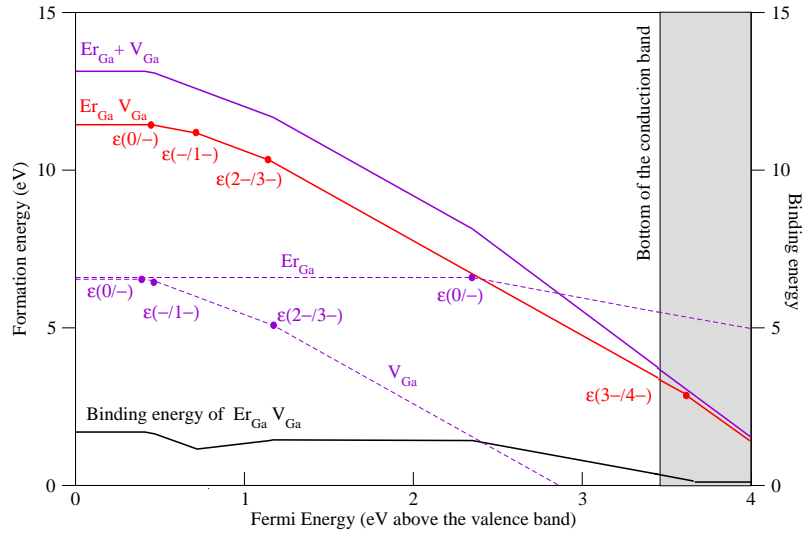


Figure 6.5: Formation and binding energy of the $RE_{Ga} + V_{Ga}$ pair as function of the Fermi energy in hexagonal GaN. Dotted lines are the formation energies of the isolated Er_{Ga} and V_{Ga} , the violet line is their sum, the red line is the formation energy of the $Er_{Ga} + V_N$ pair and the black line its binding energy, given as difference of the latter two curves.

between Er_{Ga} and V_{Ga} , mediated by the displaced N-ligand. Their binding energy makes of these pairs one of the dominant defects pairs in GaN.

6.1.3 $RE_N + \text{vacancies}$

In chapter 5 we have calculated that isolated RE_N substitutionals are defect states which are unlikely to be formed. They are characterised by a very high formation energy and large lattice distortion. In other words the lanthanide tends to avoid the nitrogen site. In the DFTB-LSDA approach we found RE_N substitutionals by far more unlikely to be formed in appreciable concentrations (high formation energy) and to be considered relevant for the luminescence (see sec. 5.1.5).

$RE_N + V_N$

We restrict therefore the investigation of the $RE_N + V_N$ pairs on the DFTB-LSDA calculations and we only calculate $Er_N V_N$ pairs with C_{1h} symmetry⁶. The structure is characterised by a large lattice relaxation. The lanthanide ions is strongly displaced from the on-site position (0.28, 0.41 and 0.98 Å for Eu, Er and Tm respectively) and the region around the lanthanide strongly distorted. In particular the Ga-ligand closest to the V_N vacancy is pushed away from the lanthanide in the direction of the vacancy. The formation energy of the pairs in the neutral charge state is more than 10 eV higher than the formation energy of any other investigated pair for all the investigated rare earths. We can therefore conclude that $RE_N + V_N$ pairs are not expected to be formed in appreciable concentrations or to play an important role in the observed luminescence.

$RE_N V_{Ga}$

Like in the case of the $RE_N + V_N$ pairs, we restrict the investigation of the $RE_N V_{Ga}$ pairs to DFTB-LSDA approach. Because of the inequivalent lattice sites in hexagonal GaN, these pairs should occur in the axial or basal configuration (see for example the analogue $RE_{Ga} V_N$ pairs in Fig. 6.4). However, independently on the starting configuration (axial or basal), we observe that these pairs are not formed at all. The rare earth in fact leaves the N-site moving into the V_{Ga}

⁶Like $RE_{Ga} + V_{Ga}$ distant pairs, also the $RE_N + V_N$ pairs can occur with the C_{1h} or C_1 symmetry (see Fig. 6.4).

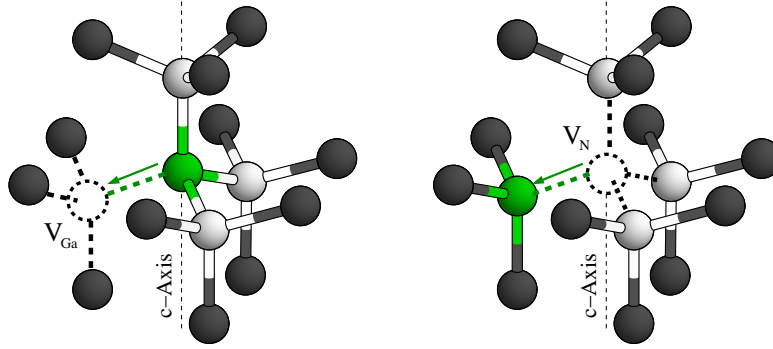


Figure 6.6: The lanthanide in $RE_{Ga} V_N$ defect pairs in hexagonal GaN leaves the N-site to occupy the Ga site.

without any barrier inbetween the migration path. This process (illustrated in Fig. 6.6 can be defined as:



This is a further strong evidence of the fact that lanthanides occupy the Ga site in GaN, either as isolated substitutionals or forming pairs with native defects. Concluding $RE_N V_{Ga}$ pairs cannot be related with the rare earth luminescence.

6.2 Antisites

As a last family of complexes formed by lanthanide impurities and GaN native defects we investigate pairs of lanthanide substitutionals and an antisites. As we have seen in sec. 5.1.5 RE_N substitutionals are not likely to be formed because of their high formation energy which is, for Eu, Er and Tm in the neutral charge state, at least 20 eV higher than the formation energy of the corresponding RE_{Ga} substitutional. For this reason we simulate here only $RE_{Ga} Ga_N$ impurity-antisite pairs depicted in Fig. 6.7.

6.2.1 $RE_{Ga} Ga_N$

Like all the close pair defects in hexagonal GaN also impurity-antisite pairs can have the C_{3v} or the C_{1h} symmetry. We start the investigation with the defect in the C_{3v} symmetry and relax the atomic positions within the LSDA approach. We observe a pronounced lattice relaxation, with the Ga-ligand displaced from its original position along the wurtzite c -axis towards an interstitial position. The RE-Ga bonds are 3.16, 3.07 and 3.02 Å long for Eu, Er and Tm respectively. The rare earths remain substantially on-site, even if it results displaced by 0.07, 0.11 and 0.10 Å for Eu, Er and Tm respectively. The lattice distortion is reflected in the high formation energy of these complexes, calculated in 13.8, 14.7 and 14.7 eV for Eu, Er and Tm in the neutral charge state and N-rich conditions. This formation energy is about 5 eV higher than the formation energy of the other defect pairs like RE_{Ga} -vacancies complexes. In other words, complexes involving a RE substitutional and an antisite have a very high formation energy and are unlikely to occur both in N-rich and in Ga-rich conditions. For this reason we do not investigate these complexes in more detail: we do not relax the atomic positions within the DFTB-FLL approach or in other geometric configurations (i.e. C_{1h}), we do not calculate their binding energy or examine their electronic structure⁷ but rather try to understand why they are energetically so costly. Actually

⁷We assume however that like all the native GaN defects complexed with a lanthanide impurity they will present the perturbed electronic structure of the isolated native defects. The isolated gallium antisite Ga_N has a singlet and

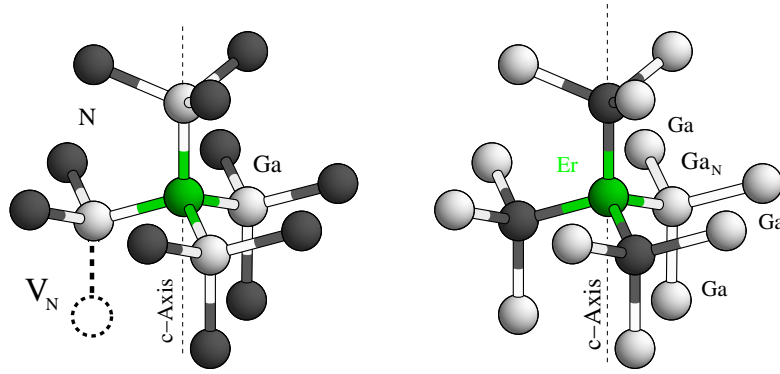


Figure 6.7: Right hand side: $RE_N + V_N$ pairs can have different symmetry depending on the lattice site occupied by the vacancy. The defect here has C_{1h} symmetry. Left hand side: complexes formed by RE_{Ga} substitutionals and the antisite Ga_N in hexagonal GaN. Also in this case the defect can have different symmetries. The defect here has C_{1h} symmetry.

the high formation energy is not unexpected, as isolated antisites in GaN too have a very high formation energy. This is not surprising, as antisites in Ga_N are in general clearly less favorable than other defects, in contrast to other semiconductors like GaAs or ZnS, where they play an important role [182]. The high formation energy of the complex $RE_{Ga} Ga_N$ can again be explained in terms of large lattice mismatch in the covalent radii of gallium ($r_c^{Ga} = 1.26 \text{ \AA}$) and nitrogen ($r_c^{N} = 0.75 \text{ \AA}$). As seen in Sec. 5.1.1 the not complexed substitutional RE_{Ga} induces a compressive stress in the host lattice. Replacing one of the neighbouring N atoms with a gallium atom, three Ga-N bonds are replaced by Ga-Ga atoms. Now, while in wurtzite GaN the Ga-N bond is $\approx 1.95 \text{ \AA}$ (and in zinc-blende GaN 1.91 \AA), the Ga-Ga distance in α -Ga is 2.79 \AA , which is more than 30% bigger. Relaxing the structure results in an outward movement of the Ga atom to reduce the huge stress introduced increasing the Ga-Ga bonds lengths. We calculated for this configuration a relaxation energy of more than 10 eV for all the rare earths in the wurtzite phase and a Ga-Ga bond length up to $\approx 2.23 \text{ \AA}$ (for Er complexes). This is still 14% bigger than the bulk Ga-N bond length, but only 75% of the Ga-Ga bond length in α -GaN, i.e. some strain in the GaN lattice is still present in the structure. Intuitively it is easy to imagine that a group of neighbouring big ions like RE and Ga will build an unfavourable configuration. In fact, while a Ga atom is surrounded by four N atoms in undoped GaN, in the examined case it is surrounded by three other Ga atoms and one lanthanide. Concluding, the Ga antisite introduces such a strain in the GaN lattice that cannot be completely compensated by the atomic relaxation and the complex $RE_{Ga} Ga_N$ is energetically unfavorable.

6.3 Summary and conclusions

In this chapter the defect complexes formed by an intrinsic defect and a lanthanide impurity in hexagonal GaN were investigated with the DFTB-FLL and DFTB-LSDA approach. All of the next neighbour pairs occur in the axial or basal configuration because of the inequivalent lattice sites in hexagonal GaN. Many general trends could be found, in particular it could be asserted that also complexed rare earth impurities prefer the Ga-site and that the presence of these defects causes a noticeable lattice distortion in the GaN host. The presence of the rare earth furthermore affect the charge transition levels of the native defects of the host. In the case of $RE_{Ga} V_N$ pairs a noticeable displacement of the lanthanide from the Ga-site (up to 0.1 \AA) was observed. In the positive charge state this defect behaves isoelectronically with the isolated RE_{Ga} substitutional, i.e. the lanthanides

a doublet in the band gap [182].

are in the 3+ valence state. The binding energy of these defects is a function of the position of the Fermi energy within the GaN band gap. In moderately *n*-type material the high value of the binding energy (1.4 eV in the case of $\text{Er}_{\text{Ga}} \text{V}_{\text{N}}$ axial pairs) would suggest that most of the nitrogen vacancies are bound to the rare earth after annealing. These pairs are furthermore characterised by two charge transitions $\epsilon(+/0)$ and $\epsilon(0/-)$. The presence of the latter close to the conduction band suggests that $\text{RE}_{\text{Ga}} \text{V}_{\text{N}}$ pairs could be important luminescent centers. Similarly, complexes formed by $\text{RE}_{\text{Ga}} + \text{V}_{\text{Ga}}$ pairs, where the vacancy is not directly neighbouring the rare earth are characterised by a relative big relaxation of the lanthanide environment. The formation energy is slightly higher than the formation energy of $\text{RE}_{\text{Ga}} \text{V}_{\text{N}}$. Rare earths and gallium vacancies are bound for every position of the Fermi energy within the band gap. This is due to the strong coupling between Er_{Ga} and V_{Ga} mediated by the displaced N-ligand. The binding energy makes of these pairs one of the dominant defects in GaN. These pairs behave as triple acceptors, with charge transitions $\epsilon(0/-)$, $\epsilon(-/2^-)$ and $\epsilon(2^-/3^-)$ at 0.45, 0.64 and 1.15 eV above the valence band in the case of $\text{Er}_{\text{Ga}} + \text{V}_{\text{Ga}}$ pairs. RE_{Ga} substitutionals and vacancies are bound for almost each position of the Fermi energy within the band gap of the host and in particular in moderately *n*-type material they are strongly bound. This is probably due to the fact that the big sized lanthanide ions fit better in the neighbourhood of an intrinsic defect which leaved additional place for them. On the other hand defect pairs formed by RE_{N} substitutionals and nitrogen vacancy pairs have a much higher (almost 10 eV) formation energy and are not bound. For this reason these pairs are not likely to be formed in appreciable concentrations. $\text{RE}_{\text{N}} \text{V}_{\text{Ga}}$ pairs are not formed, as the lanthanide moves without a barrier within the migration path in the neighbouring vacancy forming a $\text{RE}_{\text{Ga}} \text{V}_{\text{N}}$ pair. Finally RE_{Ga} substitutionals and antisite complexes are characterised by a high formation energy, which could be related to the residual lattice stress due principally to the presence of the antisite. Summarising, the lanthanide-vacancy pairs seem to be able to play a role in the mechanisms that lead to the observed luminescence. The particular role of each single defect is discussed in the last chapter, where a possible model of the processes that lead to the luminescence is proposed.

Chapter 7

Co-doping with oxygen

Even if it has been demonstrated that in semiconductors like Si and GaAs the co-implantation of rare earths with light elements like O is beneficial for the luminescence [17], the issue of co-doping in GaN is still unsettled. In Si and GaAs the co-doping has the dual purpose to increase the luminescence intensity and to reduce the temperature quenching of the emission. This is achieved by the formation of particular RE-O complexes, whose existence in GaN is at least uncertain. Three main opinions are reported in the literature about the effect of oxygen co-doping in RE-doped GaN samples, namely that co-doping with oxygen, carbon or fluorine leads to an improvement of the luminescence [13], that it causes a degradation of the luminescence [245] and finally that it does not influence at all the luminescence [14]. In some case the effect of the co-doping on the luminescence has been found to be depending on the particular GaN sample and even to have a completely opposite behaviour, being beneficial for certain samples and having negative effects for other samples [245]. Summarising, much work on this field has still to be done. In this chapter we want to investigate microscopically the effect of dopants like oxygen and carbon (representative for the class of acceptor and donor dopants in GaN) on RE doped GaN. Our goal is to determine which complexes involving RE and impurities can be created and investigate their stability. From the analysis of characteristics like defect symmetry and binding energy we can then try to identify single defects as compatible with the emission or not. In this chapter we will not investigate all the selected rare earths but will concentrate mainly on Er, which is the experimentally most investigated rare earth and which should be representative for the whole family of lanthanides.

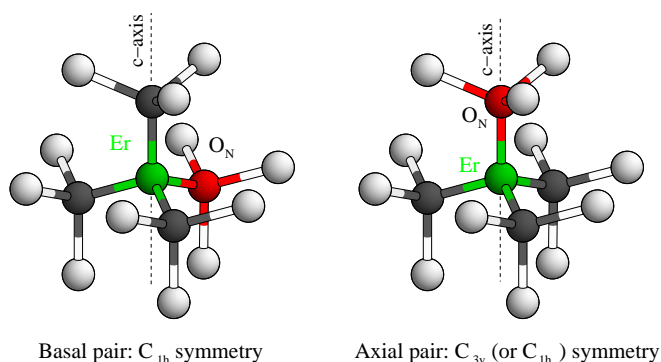


Figure 7.1: $Er_{Ga} O_N$ defect centers in hexagonal GaN can assume two kind of configurations, basal (left hand side with symmetry C_{1h}) and axial (right hand side with symmetry C_{3v} or C_{1h} if a Jahn-Teller distortion occurs) because of the inequivalent N lattice locations in hexagonal GaN. In fact the Er-N bond along the c-axis is longer than the other three.

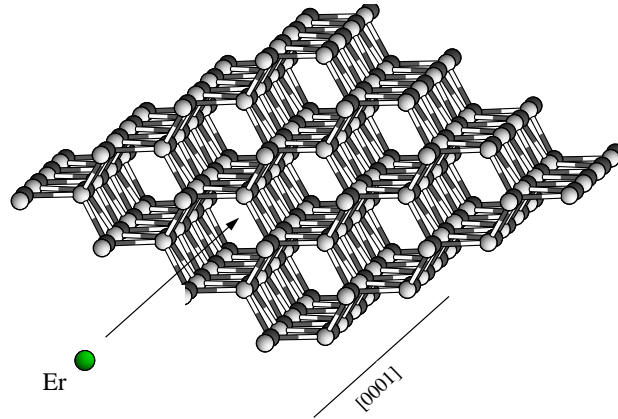


Figure 7.2: *The influence of the atomic rows and planes on the trajectories of energetic particles within the crystal is known as channeling.*

7.0.1 Geometry

By means of EC studies (see chapter 1) it was found that co-implanting erbium together with oxygen or carbon does not result in the occupation of fundamentally different lattice sites of Er [246, 247]. Differences between the co-implanted and the Er-implanted samples are within the error bars, which means that any difference in luminescence caused by co-implantation of Er with O or C into GaN cannot be attributed to a change in the lattice site of Er, in contrast to the case of Er in silicon [17]¹. On the other side, it is also known from previous studies (see chapter 5) that oxygen in GaN forms predominantly O_N substitutionals. We simulate therefore structures with the rare earth atom laying on a Ga site and the oxygen substituting one of the neighbouring N ligands. In the process of ion implantation in GaN samples, the dopants are not shot randomly in the host, but mostly along one of the major lattice directions. In this way the dopants can find an open channel between the rows of atoms and penetrate deeply in the sample without creating a lot of lattice damage². In the case of RE-implanted GaN samples most of the literature refers to samples implanted with the impinging ions along the wurtzite c -axis, as reported in Fig. 7.2. This has an influence on the defect types which are created, especially in the case of co-implanted samples. In lanthanide doped hexagonal GaN there are two inequivalent places for the nitrogen site around the RE_{Ga} substitutional. Indeed the rare earth impurities form with the N-neighbours three equivalent bonds and one somewhat longer along the wurtzite c -axis. This means that the RE-O complexes can occur in hexagonal GaN in two different configurations, depending on the substituted nitrogen atoms. If the substituted atom is one of the three equivalent nitrogens the defect will only have a symmetry plane (through the position of the O atom, of the RE atom and of the inequivalent N) and therefore the C_{1h} symmetry (basal configuration). If the substituted nitrogen is the one along the crystal c -axis (axial configuration) the defect complex can have the C_{3v} or the C_{1h} symmetry. Both configurations are represented in Fig. 7.1. It is known that co-implanting oxygen and lanthanide impurities along the crystal c -axis favours the formation of complexes either in the basal or in the axial configuration, even if it has not be settled under which conditions the one are favoured upon the other [43]. In this work we limit us to the detailed investigation of the axial pairs.

¹Er in oxygen co-doped Si is know to form Er interstitials and other defect centers involving one or more oxygen.

²The influence of the crystal lattice on the trajectories of the incident particles during the implantation is known as *channeling*.

Table 7.1: Geometry of the stablest configuration of the basal and axial Er-O pairs in hexagonal GaN. Er-N₁ and Er-N₂ label inequivalent Er-N bonds. On the left hand side the neutral charge state and on the right hand side the positive charge state.

Conf.	Symm.	Bond	Number	DFTB-LDA	DFTB-FLL	DFTB-LDA	DFTB-FLL
Basal	C_{1h}	Er-N ₁	2	2.21	2.24	2.16	2.18
		Er-N ₂	1	2.22	2.27	2.17	2.21
		Er-O	1	2.04	2.09	2.03	2.03
Axial	C_{3v}	Er-N	3	2.20	2.25	2.16	2.22
		Er-O	1	2.05	2.09	2.03	2.04

As usual we perform our calculations using 256-atoms supercells and a $4 \times 4 \times 4$ Monkhorst-Pack k -point mesh. For the DFTB-FLL calculations we used the usual value of $U-J = 0.27, 0.28$ and 0.27 H for Eu, Er and Tm as we used throughout this work. With these values the piecewise linearity of the total energy is possibly not completely recovered, nonetheless they will suffice to describe the geometry, the band structure and the charge transitions of the system. The defect complexes in the axial configuration can have three different minima, one with the symmetry C_{3v} , where the lanthanide N-ligands and the oxygen Ga-ligands are equivalent, and two minima with the C_{1h} symmetry, where the ligands are inequivalent (two long bonds and one short or two short bonds and a long one). Whether all these minima are formed or not and their energetic stability depends on the occupation of the gap states. We illustrate in some detail the case of erbium-oxygen complexes.

The major difference with the isolated O_N substitutionals is given by the position of the oxygen, which lays in all cases on site and not off-center. The (small) displacement reported in the table is due to the size of the lanthanide ion which introduce some strain in the first neighbour shell.

We notice that the energy difference between the different geometries is very small (15 meV) and of the order of magnitude of the precision of the DFTB-method. We believe though, that the difference is significative, at least qualitatively, because it has been calculated for the same system and with the same supercell, taking advantage of the error cancellation.

Further characteristics of the system, like charge distributions, charge state transition, formation and binding energy are calculated for the axial configuration in its stablest symmetry, i.e. C_{3v} .

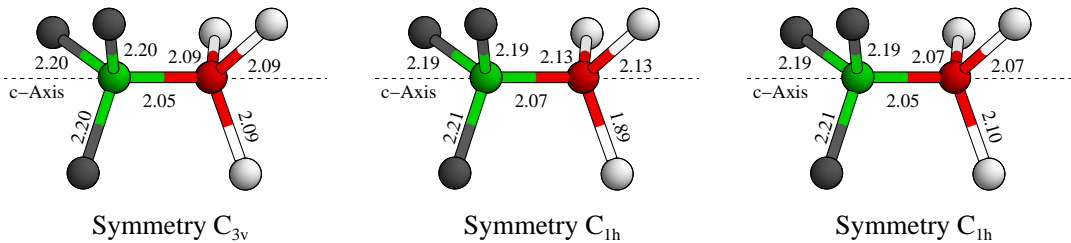


Figure 7.3: The three minima of the Er_{Ga}O_N axial pairs in hexagonal GaN in the neutral charge state: the first one has the C_{3v} symmetry, while the other two the C_{1h} . As usual green circles represent erbium, red ones oxygen, black nitrogen and white gallium atoms. All the distances are given in Å.

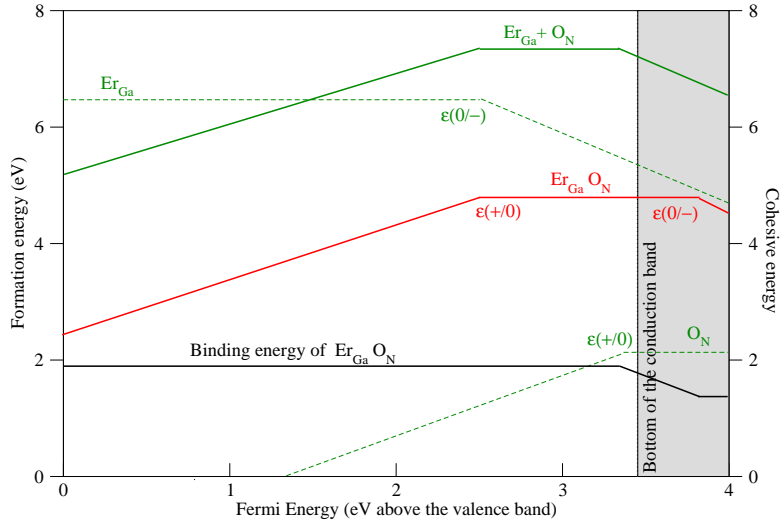


Figure 7.4: Binding energy of the Er-O pair as function of the Fermi energy. Dotted lines are the formation energies of the isolated Er_{Ga} and O_N substitutionals, the green line is their sum, the red line is the formation energy of the $Er_{Ga} O_N$ pair and the black line its binding energy, given as difference of the latter two curves.

7.0.2 Energetics

If from the structural point of view the presence of oxygen does not drastically affect the Er and O co-doped samples, it remains to investigate how it affects the electronic properties of the system. Oxygen is an element which is invisible to some experimental technique³ and oft present as involuntary codopant in grown materials. Oxygen is the principal dopant used to dope n -type GaN. As seen in the 4th chapter it introduces a donor level close to the conduction band edge. The formation energy of the axial pair in the neutral charge state:

$$\begin{aligned}
 E^f &= E^{\text{tot.}}(Er_{Ga} O_n) - \sum_{i=Ga,N,Er,O} \mu_i n_i \\
 &= E^{\text{tot.}}(Er_{Ga} O_n) - 127\mu_{Ga} - 127\mu_N - \mu_{Er} - \mu_O \\
 &= E^{\text{tot.}}(Er_{Ga} O_n) - E_{\text{bulk}}^{\text{tot.}}(\text{GaN}) + \mu_N + \mu_{Ga} - \mu_{Er} - \mu_O
 \end{aligned}$$

and in the C_{3v} symmetry has been calculated to be 4.52 eV (4.66 eV for the basal pairs). DFTB-FLL and DFTB-LDA values are almost identic. As the complex is in the neutral charge state only for values of the Fermi energy close to the conduction band (see following section), and the formation energy of the complex in the positive charge state will be smaller. This is in agreement with the fact that O_N substitutionals in GaN have in general a low formation energy. A low formation energy does not automatically mean that the defect complex will be present in the co-doped samples from which light emission has been observed, as luminescence has only been observed from annealed samples. Only these defect complexes which are stable enough to endure the annealing process can be in fact addressed as possible candidate for the luminescence. Considering a Boltzmann constant of $8.617385 \cdot 10^{-5}$ eV/K, defect complexes whose binding energy is higher than ca. 0.1 eV should remain bound even after annealing at 1000-1200K. The binding energy of Er and O impurities in

³For example in EPR the oxygen ions are invisible, as the only oxygen isotope with non-zero nuclear spin (O^{17}) has a natural abundance of 0.038%. In PL experiments only these ions can be detected, which either are directly excitable or introduce such a distortion of the crystal field to influence the emission spectra of luminescent impurities.

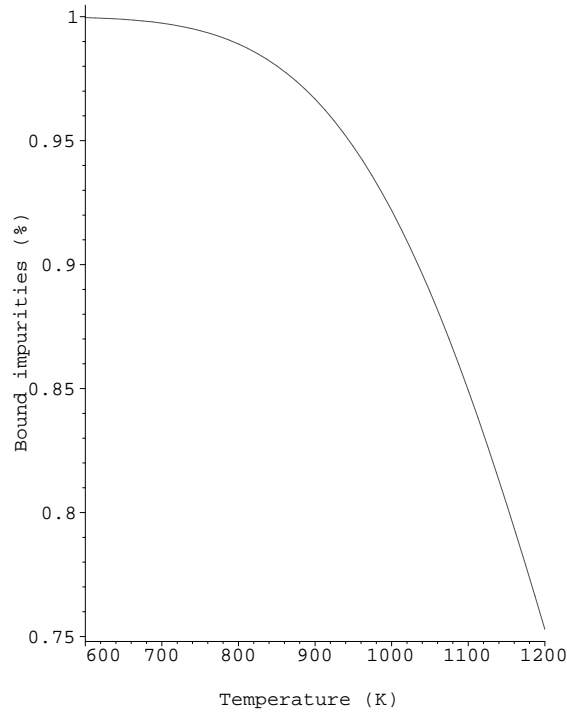


Figure 7.5: Left hand side: Fraction of bound oxygens depending on the annealing temperature, assuming a Er-O binding energy of 1.00 eV.

hexagonal GaN in the dominating positive charge state has been calculated to be 1.86 eV, which is more or less the binding energy of Er and O in Si. This value is considerably higher than the value 390 meV calculated by Filhol *et al.* [57] with a DFT-LDA approach but in agreement with the value of 1.69 eV calculated with a LMTO-ASA approach [237, 238]. The value is almost constant for each position of the Fermi level within the GaN band gap and higher than the binding energy of all other defect complexes involving Er. This large binding energy means that a big fraction of the oxygen impurities will be bound to the lanthanide after annealing. Similarly to the discussion reported in sec. 6.1.1 if we assume that in Er and O co-doped GaN samples the erbium concentration c_{Er} is much bigger than the oxygen concentration c_{O} , the equilibrium concentration of the Er-O pairs is given by:

$$c_{\text{Er-O}} = \frac{c_{\text{Er}}}{c_{\text{Er}} + N e^{-\frac{E_b}{kT}}} \quad (7.1)$$

where, like in Eq. 6.1 N is the density of Ga lattice sites, T is the temperature and k the Boltzmann constant. Considering c_{Er} to be 0.078%⁴, we find at 1000 K 85-95.% of the O atoms to be bound with the Er. The ideal run of the curve representing the fraction of bound oxygens depending on the annealing temperature, assuming a binding energy of 1.00 eV, is plotted in Fig. 7.5.

Strictly speaking the binding energy of the $\text{Er}_{\text{Ga}} \text{O}_{\text{N}}$ pair is a function of the position of the Fermi energy.

⁴This value corresponds to the typical erbium concentration in real samples and is also the erbium concentration we used in our simulations.

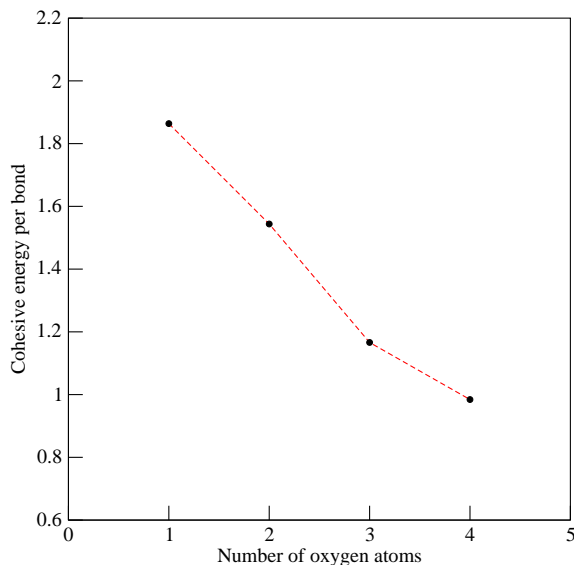


Figure 7.6: Cohesive energy per bond of the Er-O_x complexes. The cohesive energy per bond decreases almost linearly with the number of oxygen atoms, indicating that the most favourable configuration is the Er-O pair.

In Fig. 7.4 we report the value of the binding energy for values of the Fermi energy within the GaN band gap. To gain more informations about the nature of the Er-O bond, Er-O_x complexes in hexagonal GaN were investigated within the DFTB-LSDA approach. In Er-O co-doped Si in fact defect complexes involving different oxygen ions are expected [17]. The cohesive energy per bond has been calculated for complexes including one to four oxygens neighbouring with Er in the neutral charge state. The cohesive energy per bond decreases almost linearly with the number of oxygen atoms, so that once the Er-impurity has bound one oxygen, it will be energetically less favourable to bind a second one. Considering the cohesive energy of a Er-O complex to be the zero of our scale, the cohesive energy per bond of complexes with two, three and four oxygens around the Er-atom will be 0.32, 0.70 and 0.88 eV lower. This is graphically visualised in Fig. 7.6. We observe that the complexes in which the Erbium is surrounded by four oxygen first neighbours are characterised by a pronounced lattice distortion, probably due to the fact that Er and O try to reach a geometric configuration similar to the Er_2O_3 phase. To understand the differences introduced by the oxygen co-doping the difference between the total charge density of the simple substitutionals Er_{Ga} and the total charge density of the complex $\text{Er}_{\text{Ga}}\text{O}_N$ was plotted and reported in Fig. 7.7. It can be observed at first that the differences are limited at the region around the Er and O ions, confirming that the presence of oxygen does not introduce any major difference with respect to the Er doping. The oxygen ion results positively charged, because it is isoelectronic with N, while around the Er ion some charge redistribution is observed. It is interesting to notice that no charge is taken from or accumulated along the Er-O^+ bond. It means that the Er-N and Er-O^+ bonds are similar.

7.0.3 Charge states

The $\text{Er}_{\text{Ga}}\text{O}_N$ pairs are characterised by a donator $\epsilon(+/0)$ transition close to the $\epsilon(0/-)$ transition of the isolated Er_{Ga} substitutionals. We calculated this transition at 2.30 eV above the valence band. To confirm this result the same charge transition was calculated with the already mentioned LDA+ U capable LMTO-ASA approach [237, 238] and found by 2.9 eV above the valence band, which is in qualitative agreement with the DFTB-FLL result. In previous DFT-LDA investigations [57], the $\epsilon(+/0)$ transition of the pair was found to be resonant with the conduction band.

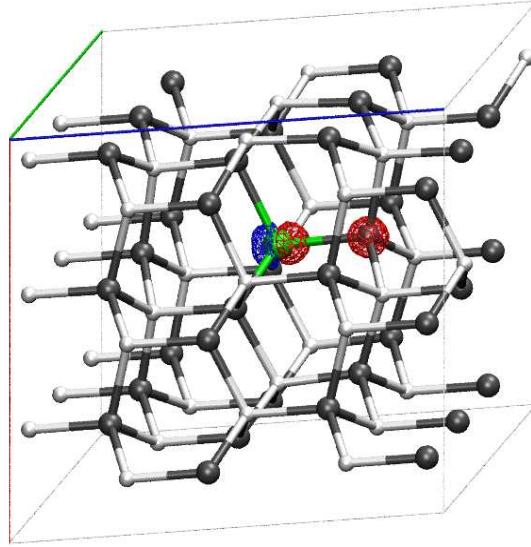


Figure 7.7: Plot of the charge difference of a wurtzite GaN supercell containing an isolated Er_{Ga} substitutional and the same cell containing the isoelectronic impurity-pair $Er_{Ga} O_N^+$. Blue regions indicate accumulation of negative charge and red regions positive charge. The oxygen atom results positively charged (it substitutes a N atom), while a charge redistribution is observed around the Er atom.

The defect pair cannot be negatively charged, as the position of the $\epsilon(0/-)$ charge transition has been calculated at 3.8 eV above the valence band, i.e. in the conduction band (see the right hand side of Fig. 7.4).

As the complex exists in the neutral and positive charge state, properties like binding energy or the geometry have been investigated in both the neutral and positive charge state. An analysis of the Mulliken charges localised on the atoms around the Er substitutional reveals that the presence of the oxygen does not influence the charge distribution on the Er-atom and the other N-ligands. The Mulliken charges calculated with DFTB-FLL for Er_{Ga} substitutionals and $Er_{Ga} O_N$ complexes in the positive charge state are reported on Tab. 7.2: the charges on the Er and N atoms are in the two systems almost identical.

In the neutral charge state there is a further electron which is mostly localised on the Er-atom. This can be observed plotting the charge state difference between the system in the neutral charge state and positively charged, as reported in Fig. 7.8. The difference in the charge density between the two charge states is strongly localised on the Er ion. It means that adding an electron it would not be delocalised but will reside mainly on the lanthanide. The ligands only show on the other side polarisation effects due to the charge accumulation on the Er atom. The O ligand behaves exactly like the N-ligands. It is not surprising that the presence of oxygen in Er-doped GaN-samples does not modify considerably the charge distribution and the geometry of the system, because oxygen

Table 7.2: Mulliken charges localised on the atoms around the Er_{Ga} (left hand side) and $Er_{Ga} O_N$ (right hand side) complexes with C_{3v} symmetry in the positive charge state.

N ₁	5.5151	N ₁	5.5122
N ₂	5.5153	N ₂	5.5133
N ₃	5.5184	N ₃	5.5186
N ₄	5.5227	O	6.3972
Er	13.2227	Er	13.2168

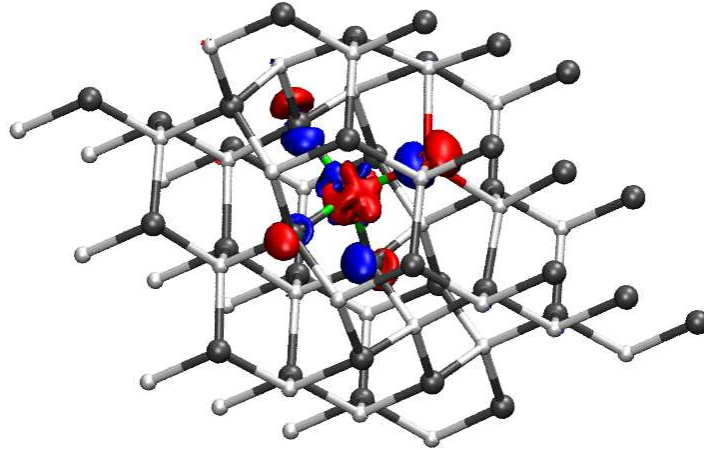


Figure 7.8: Plot of the total charge difference between a wurtzite GaN supercell containing a $\text{Er}_{\text{Ga}} \text{O}_{\text{N}}$ pair in the neutral and positively charged state (the integral of the charge would also be unitary). Blue regions indicate accumulation of negative charge and red regions positive charge. The missing charge is mainly localised on the Er atoms, while in the neighbouring atoms only polarisation effects can be observed.

and nitrogen have similar dimensions and electronegativity. Oxygen can be in fact considered close to an ideal (effective mass) donor in GaN, as it becomes isoelectronic with the substituted N promoting one of its electrons to the conduction band without introducing major changes in the host.

7.1 Summary and conclusions

In this chapter the effect of the co-doping of GaN with erbium and oxygen was investigated. Even if from our investigation cannot be finally settled if the oxygen ions are beneficial for the lanthanide related luminescence, many important informations about the nature of the Er-O complexes could be achieved. The presence of oxygen was found not to alter the structure and the charge distribution around Er centers. Two types of Er-O complexes called axial and basal pairs (with C_{3v} or C_{1h} symmetry) can be formed in hexagonal GaN, depending on the position of the substituted N-ligand with respect to the lanthanide. These configurations are characterised by a very similar energy (the difference is 0.06 eV in the neutral charge state) and similar band structure. The low formation energy of those defects and in particular the relatively high binding energy suggest that Er-O will be formed and remain bound even after annealing. An investigation of the cohesive energy per bond indicates that ErO_x complexes are not likely to be formed (differently from Er-O co-doped Si) but rather, as long as the oxygen fluence does not overtake the Er fluence, different oxygens will be bound to different Er-centers. The high value of the cohesive energy is somehow surprising and has the consequence that almost all present oxygens results bound to the erbium. This high binding energy could be explained by the concurrence of three main factors. The first factor is the already mentioned similarity between oxygen and the substituted nitrogen, which leads to the easy incorporation of oxygen in GaN and to the creation of very stable bonds. The second one is the Coulomb interaction between the substitutionals Er_{Ga} and O_{N} , which is typical for donor-acceptor pairs and which has been also observed for $\text{RE}_{\text{Ga}} \text{V}_{\text{N}}$ complexes. Separating the complex into the constituents we would have Er_{Ga}^- and O_{N}^+ pairs, as can be also deduced from Fig. 7.7. The third factor which could contribute to the high binding energy is a resonance between some state of Er and O. Looking at the energy of the outer states of these atoms it can be observed that the energy of the Er $5p$ -states (and in general of the $5p$ -states of all the lanthanides) is quite close to the energy of the oxygen $2s$ -states and a particularly strong resonance could be created. Unluckily it is not possible within the DFTB approach to proof this idea projecting the atomic states on

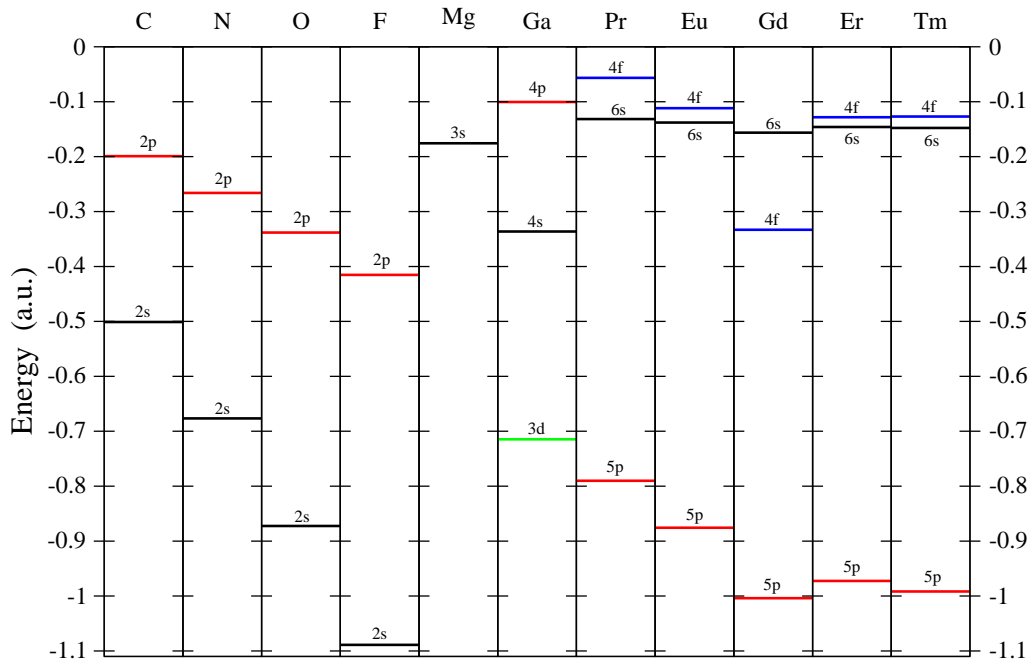


Figure 7.9: Atomic levels of atomic species which are commonly used as dopants for GaN. The levels are calculated with the scalar relativistic atomic program RLCAO. In blue f -orbitals, in black the energy of s -orbitals, in green the d -states and in red the energy of p -orbitals.

the crystal orbitals and its investigation is remanded to future studies. The $\text{Er}_{\text{Ga}}\text{O}_{\text{N}}$ complexes introduce charge transition levels close to the charge transition introduced by the isolated Er_{Ga} substitutionals (i.e. 2.30 eV above the valence band). This means that the pair can be in the neutral or in the positive charge state. In this charge state the oxygen atoms are isoelectronic with the substituted N and the Er atom are in the $3+$ valence state. Because of their symmetry and valence states, $\text{RE}_{\text{Ga}}\text{O}_{\text{N}}$ pairs could play a role in the luminescence observed from co-doped samples, however the excitation process (i.e. in PL experiments) would be difficult because the introduced charge state transition does not lay close to the conduction band. The role which Er-O pairs could play in the luminescence process is further discussed in the next and final chapter of this work.

Chapter 8

Summary and discussion

In this work we investigated the properties of rare earth impurities in GaN by means of self interaction corrected and LDA+ U calculations. The goal of this investigation was to examine from the microscopic point of view single rare earth related impurities, in order to find out whether they can play a role in the RE-related emission or not. In this way we hope to help the general understanding of the emission mechanisms and thus the optimisation of the RE-doped GaN-based devices.

The GaN samples for luminescent devices are today grown, doped and annealed in conditions which empirically have been found to maximise the luminescence but despite many efforts any luminescence band could be definitively assigned to a particular lattice site or defect state.

We start our work reviewing the general properties of the rare earth ions as well as the experimental knowledge of lanthanide-doped GaN samples. We summarise the properties which characterise the luminescent sites (symmetry, valence etc.), which are compared later with the results of our simulation. In the first part of the work we also illustrate the problematic related with the strongly correlated electrons in general and with the lanthanide f -electrons in particular. These systems cannot be modeled with the standard calculation schemes of density functional theory (DFT) in the framework of the local density approximation (LDA). This approach would in fact, due to its approximation and limitations, give a qualitatively wrong description of the strongly correlated electrons, like in the case of the rare earth nitrides or transition metal oxides (e.g. NiO), which are experimentally known to be insulators or semiconductors but appear to be metals in the LDA approximation. As a first step of our investigation we have adapted the existing calculation schemes deriving a formalism (and implementing it in a simulation package), in order to properly handle the strongly correlated electrons. The LDA+ U and pseudo self interaction corrected (pSIC) approaches were adapted to the tight binding formalism and implemented in the density-functional based tight-binding (DFTB) simulation software. This approach is very efficient and allows to circumvent the known gap problem affecting the LDA calculations, even if it does not reach in all cases the precision of the DFT approaches. DFTB needs tight-binding parameters for each atom pair type involved in the calculation. The generation of these parameters was the second step of our path towards the simulation of the rare earths in GaN. Parameters for the simulation of the host (Ga, N) and some of its common dopants (H, C, O) were created and thoroughly evaluated, together of course with the parameters for a selection of lanthanides (Pr, Eu, Gd, Er, Tm) which we thought to be representative and interesting because of their applications and because of the experimental knowledge of their properties which is now available. The DFTB parameters determine in great extent the accuracy of the method and its portability so that great attention has to be paid in their generation and testing. The parameters we created could reproduce the geometry of all the test systems with an accuracy of 1-2% with respect to the experimental values and lead to a qualitative correct description of the band structure of the solid state system investigated. Other physical quantities we simulated like elasticity properties, cohesive energy and formation enthalpies were found to be in reasonable agreement with *ab initio* simulations, of which DFTB can be considered therefore a good approximation.

Armed with a simulation software able to treat strongly correlated electrons in a proper way and

Table 8.1: Charge transition states of some native defect in GaN and of erbium-impurity native-center pairs. Reported are only the charge transitions closest to the conduction band. The values are given in eV above the valence band.

Center	Transition	Position	Center	Transition	Position
—	—	—	Er _{Ga}	$\epsilon(0/-)$	2.35
V _N	$\epsilon(-/3-)$	3.20	Er _{Ga} V _N	$\epsilon(0/-)$	3.14
O _N	$\epsilon(+/0)$	3.35	Er _{Ga} O _N	$\epsilon(+/0)$	2.30

with reliable parameters we were able to start the actual simulation of the RE-related defects in GaN. We started our investigation paradoxically with the simulation of those GaN defects not involving the lanthanides. This has the double goal to give us an even more detailed picture of the DFTB accuracy in the simulation of known GaN native and impurity defects and to determine their properties in both GaN polytypes, wurtzite and zinc-blende. Their understanding and knowledge is in fact fundamental if we want to understand the behaviour of complexes formed by rare earth impurities and native defects. The final part of this work was dedicated to the simulation of the rare earth impurities in the host, both in its hexagonal and cubic polytypes. The effect of oxygen co-doping in lanthanide implanted wurtzite GaN was also investigated. Isolated lanthanide substitutionals, substitutionals complexed with GaN native defects like nitrogen and gallium vacancies, antisites and interstitials and with oxygen impurities were simulated in different charge states, geometric and spin configurations. For key and benchmark systems accurate electronic structure calculations were also performed with different *ab initio* approaches (Wien2k, ABINIT, LMTO-ASA). The results of our investigation are summarised in the following discussion, which is concluded with a possible model for the mechanism leading to the light emission.

Main results

The main goal of our investigation of the rare earth point defect was to find which defect centers are dominant in GaN and to give an overview of their properties and characteristics. Some of these centers in fact could be the luminescent sites which we want to create to optimise the emission from the sample. The luminescent centers have to satisfy determined requirements to be present in the sample (they should have a low formation energy and an high binding energy to be bound after annealing) and have to possess some characteristics known from experimental investigations (e.g. symmetry and valence).

Differences between the rare earths

Many of the chemical and physical characteristics of different elements are mainly due to their outer shell. Most of the lanthanides share the same outer shell and therefore many of their properties. At a first sight the lanthanides impurities in GaN behave similarly. They give rise to similar complexes with the same geometry and minor differences in the bond length due to differences in the ion size. However, from the electronic point of view there are important differences, which can be lead back to different occupations of the *f*-shell. Completely empty, completely filled and half filled *f*-shells are particularly favourable configurations which the system tends to reach. For this reason for example Eu_{Ga} substitutionals (6 *f*-electrons) have an acceptor state $\epsilon(0/-)$ deep in the middle of the GaN gap which many other lanthanides do not have. In the negatively charged state Eu completes the 4*f*-semishell reaching a very stable configuration. For the same reason Gd, which already has an half-filled 4*f*-shell do not change the occupation of the *f*-shell.

Rare earth luminescence was observed for GaN samples doped with almost all lanthanide, but not Gd. This is quite surprising, but can probably be explained with the peculiar electronic configuration of this atom. Unlike other lanthanides the Gd-valence shell includes one 5*d*¹ electron, which plays a particular role in the Gd-N bond and in the charge transitions. While most of the lanthanide promote the two outer 6*s*² and one 4*f* electron to reach the trivalent configuration in GaN, in the

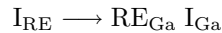
case of Gd the promoted electrons are two outer $6s^2$ and the $5d^1$. The half filled f -shell remains also in the (very stable) atomic configuration. Charging the system with an additional electron will result in the occupation of the $5d$ shell and not of the $4f$ shell. This probably means that it is difficult to bring Gd f -electrons into the excited state from which they can return into the ground state with a radiative process.

The two polytypes

No major differences between lanthanide defects in hexagonal GaN and cubic GaN have been found for the investigated defect centers. This is not surprising, as also native defect and largely used impurities like O and C in wurtzite and zinc-blende GaN do not show qualitative differences. The lower symmetry of hexagonal GaN influences in particular interstitial defects (see section 4.3.1), which however are not likely to be formed in the case of lanthanide doping. The similarity between impurity defect formed in hexagonal and cubic GaN was furthermore observed in the case of the $3d$ transition metals [248]. Instead, major differences have been found between the lanthanide defects in GaN and in other semiconductors like Si, GaAs and ZnO. The literature reports the presence of stable defects in this hosts, like rare earth interstitials or complexes involving rare earths and interstitial oxygen which have not been observed in GaN. It is therefore in most cases misleading to try to interpret the mechanisms underlying the RE-emission from RE-doped GaN with models which have been successfully exploited to explain the RE-emission in the other hosts. Differences between the defects in GaN and other hosts are not peculiar for the lanthanide doping but have been observed for native defects too. The differences can be lead back to the size and electronegativity differences between the constituents (Ga and N), which are far more marked than in other semiconductors like GaAs or SiC.

Lattice site

The first question we try to answer concerns the lattice site of the lanthanide. Rare earth ions in GaN may occupy the Ga-site, the N-site or an interstitial position. Interstitial rare earths ions have been found not to be stable with respect to the configuration:



and are not going to be formed in appreciable concentrations in equilibrium growth conditions. RE_N substitutionals, isolated or complexed with vacancies, introduce a serious lattice distortion in the host and are characterised by a huge formation energy. In particular the $RE_N V_{Ga}$ pair is found not to be stable with respect to the configuration:



confirming the tendency of the rare earth ions to avoid the N-site. Instead lanthanide ions form very stable RE_{Ga} substitutionals¹ which do not introduce major lattice distortion. A parameter was introduced to quantify the stress caused in the host geometry, which was found to be relatively small for all the investigated rare earths. Rare earth ions are readily incorporated in GaN as Ga-substitutionals which are probably the majority centers revealed by EXAFS investigations. Our calculations are in agreement with the experimental evidence of the fact that the lumophore, independently from its particular structure and neighbourhood must be built in such a way that the lanthanide occupies the Ga-site [41]. Consequently the lanthanides in interstitial position and the RE_N substitutionals (isolated or complexed with vacancies, antisites or oxygen impurities) cannot be considered candidates as luminescent center. The strongest luminescence has been detected from samples showing high fractions of rare earth on substitutional Ga places. During the annealing needed to activate the luminescence the lanthanide which were slightly displaced from the ideal lattice site come closer to the Ga-position while the other defect (implantation damage) are reduced. This makes very tempting to assign a relation between the isolated RE_{Ga} substitutionals and the

¹The rare earth ion stays on site in the case of isolated substitutionals and is slightly displaced from the Ga-lattice site in lanthanide-native defect pairs.

luminescence. These defects have been found to be compatible with the luminescence in our work and additionally, no other specific lattice sites have been found to be occupied by RE ions by any technique. However different issues have to be considered, in particular the fact that most of the rare earth ions in the sample do not act as lumophores and that different defect states are responsible for the luminescence. The photoluminescence from RE-doped samples can be investigated as function of the wavelength of the exciting light, a technique called (site-)selective excitation. Different spectra from different wavelengths are an indicator of the presence of different centers actively contributing to the luminescence. Two "majority" and up to four different signatures were found for Er MBE-doped samples [48] and at least four luminescent centers were found in Eu implanted GaN samples [12]. This means that our research cannot be considered concluded even if we identify one class of defect as candidate lumophore because of its characteristics. It was measured that 50-95% of Pr, Nd, Eu, Gd and Er ions implanted in GaN occupies lattice sites that appear to be slightly displaced from the ideal substitutional RE_{Ga} , with a nearly isotropic root mean square (rms). This displacement (of the order of 0.10-0.25 Å) is too large to be explained in terms of lattice vibrations and is an evidence of the fact that if the RE_{Ga} substitutionals participate to the emission process, they probably cannot be considered the only lumophores (but can form defect pair and complexes with GaN intrinsic defects).

Defect states

Apart from the isolated RE_{Ga} substitutionals the further candidates as luminescent centers investigated in this work are the pairs formed with oxygen, antisites (Ga_{N}) and Ga or N vacancies. While the RE_{Ga} Ga_{N} antisites (which are characterised by a high formation energy and a residual lattice stress) are formed only in very low concentrations, the other point defects have lower formation energies (which are relatively similar for all the complexes in the neutral charge state) and the in the case of the of RE_{Ga} V_{N} , RE_{Ga} V_{Ga} and RE_{Ga} O_{N} the complexes results bound after annealing. The similar formation energies of the different centers would signify that different defect centers can be created at the same time in the same sample under certain growth conditions. This would agree with the experimental observation that many different centers contribute to the luminescence. Which of this pairs can be related with the luminescence though?

The RE luminescent transitions have been compared to theoretical models in order to assess definite symmetry properties to the centers. In the cases of Pr, Eu, Er and Tm it was mentioned that the emission spectra are compatible with the C_{3v} symmetry. In any case extracting symmetry informations for RE-centers from emission spectra is difficult, because the observed spectra are the superposition of different centers together with vibronic and satellite lines. Experimental investigations which could unambiguously reveal the symmetry of the defect centers are as far not available, as discussed in Sec. 6.1.1. Furthermore it is unknown how far the rare earth has to be displaced from the wurtzite c -axis in order to reveal a symmetry lower than the C_{3v} in luminescence experiments. We cannot therefore exclude one particular defect center based only on symmetry arguments, rather we think is safe to label a defect as non-luminescent if different parameters are not in agreement with the experimental evidence. The defects complexes investigated in this work which can be formed in the C_{3v} symmetry are the isolated RE_{Ga} substitutionals, the RE_{Ga} V_{N} vacancies, the RE_{Ga} O_{N} and the RE_{Ga} Ga_{N} pairs.

In relation with the experimental evidence of the presence of different luminescent centers, the RE-luminescence has to be related with different defect configurations, some with the RE exactly lying at the Ga lattice site and some with the RE slightly displaced from this position. Among all the investigated configurations the only defects in which the RE lies on-site and which are compatible with the luminescence (because of their symmetry, valence state of the RE, stability against annealing etc.) are the isolated RE_{Ga} substitutionals and the pairs formed by co-doping RE_{Ga} O_{N} (both in the C_{1h} and in the C_{3v} symmetry), while the only defects compatible with the luminescence in which the lanthanide is slightly displaced from the Ga-site are the complexes formed by a lanthanide substitutional and a neighbouring vacancy (RE_{Ga} V_{N} or $\text{RE}_{\text{Ga}}+\text{V}_{\text{Ga}}$). Unfortunately luminescence experiments cannot quantify the number of different defects related to a particular signal. It is therefore not possible to establish if the luminescence is due to a relatively small amount of the implanted ions or by the majority RE ions sitting approximately on the Ga-site

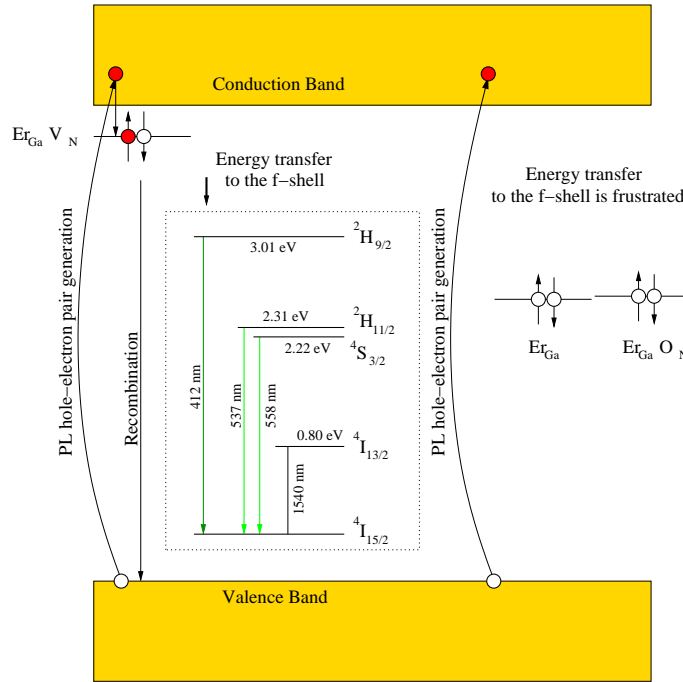


Figure 8.1: Possible excitation mechanism of the $\text{Er}_{\text{Ga}} \text{V}_{\text{N}}$ pairs in GaN. The energy of the charge carriers generated by photoluminescence is transferred to the f-shell through a two step or assisted process in which the PL-generated electron is transferred from the conduction band into an assistant level, from which it can transfer its energy to excite the f-states of the rare earth.

and surrounded by four nitrogen atoms.

The valency of the lanthanide in isolated RE_{Ga} substitutionals in the neutral charge state and in most of the charge states of the defect pairs where the RE occupies the Ga-site is $3+$, which is the valency of the Ga atom the lanthanide replaces and is in accord with the interpretation of photoluminescence experiments [4]. In particular Eu substitutionals in the neutral charge state have been found to be trivalent, despite of the tendency of Eu to be divalent in some compound (elemental metallic phase). Luminescence experiments show that Eu in GaN is trivalent [7, 36] even if there have been reports about divalent Eu in the surface region of Eu-doped GaN [249]. The energy difference between the isolated lanthanide substitutionals in the divalent and trivalent state has been calculate² to be 1.8, 2.3 and 3.0 eV for Eu, Er and Tm substitutionals. This values are in good agreement with the results in Ref. [18].

A model for the excitation mechanisms

Once the different defects created with lanthanide doping in GaN have been examined, a model involving these defects which leads to the luminescence can be suggested. The model resembles the one proposed by Gerstmann *et al.* to explain the Er-related luminescence in SiC [250].

Light emission from lanthanide doped GaN has been observed in photoluminescence (PL), cathodoluminescence (CL) and electroluminescence (EL) experiments. Independently from the excitation mechanism³, the charge carrier energy is transferred to the rare earth impurity (by electron-hole recombination or by impact excitation of hot carriers), which can then relax with a radiative or non-radiative process. Of course in our case only the radiative processes are important.

²The values are the results of LSDA calculation in not relaxed GaN cells. This approach, which is not the approach used throughout this work, has been chosen in order to compare directly the results with the values in [18].

³In PL electron-hole pairs are generated by above band gap excitation, in CL charge carrier are generated by a high-energy electron beam and finally, in EL, charge carriers are injected in the GaN sample applying a bias to the electrical contacts on the layer.

The excitation mechanism however is not straightforward and not all the rare earth related defect states can be excited. Let us see this with an example, e.g. in the case of photoluminescence experiments. In overband excitation a photon with an energy greater than the energetic band gap is absorbed from the material creating an electron-hole pair, i.e. a hole in the valence band and an electron in the conduction band. Electrons can be trapped by donor levels while holes can be trapped by acceptor levels, which results electrically charged. When the trapped electrons and holes recombine, an electron of the f -shell can be brought into an excited state, from which it relaxes with a radiative transition (i.e. photon emission). Normally these transitions (called optical transitions) differ from the electronic transitions because during the recombination the acceptor or donor defects do not relax their atomic structure (as they would do in an electronic transition) so that they possess an energy surplus due to the relaxation energy (Franck-Condon shift). Instead in the case of the lanthanides the environment of the lanthanide ions is not a primary aspect, as the f -shell is screened from the outer atomic shells. Another peculiarity of the photoluminescence effects in lanthanide doped GaN is that the created electron in the conduction band could recombine with the holes in the valence band without exciting the f -states. The process of charge carrier energy transfer can be in fact frustrated by the strong localisation of the f -shells or in the case in which the charge transition levels are deep in the gap and an electron in the conduction band cannot occupy them directly because of the high energy mismatch. This would be the case of the isolated RE_{Ga} substitutionals. In this case the energy transfer to the f -shell can be helped by a so called assistant level (e.g. a level of an isolated donor), a shallow transition-level introduced normally by another nearby defect. An electron from the conduction band can then in a first step occupy the assistant level and from this transfer its energy to the lanthanide f -states. In this model, illustrated in Fig. 8.1, V_N as close pair with RE_{Ga} can play a self-assistant role, as they introduce transition levels in the band gap much closer to the conduction band than the levels introduced by the isolated RE_{Ga} substitutionals (see also Tab. 8.1). The major role of lanthanide-vacancy pairs in the luminescence would be in agreement with the fact that the highest luminescence was measured from sample with rather poor crystalline quality and rich of defects [42].

A look ahead

Understanding the mechanisms leading to the rare earth luminescence is a fundamental step for the realisation of efficient and cost-effective devices. However this step is as difficult as important, due to the nature of the lanthanide and to the multiplicity of configurations at microscopical level caused by the rare earth doping that have to be investigated. In this work we only concentrated on a "small" part of microscopic structures, the isolated point defects. Important issues like the interactions between point and extended defects or the dopant clustering were not examined. The interaction of the rare earth ions with aggregates of several vacancies and acceptors remain for future investigations. The actual luminescence mechanisms could be only addressed indirectly in this work. Nonetheless we were able to describe the physical and chemical characteristics of many rare earth related defect states. On the basis of these results we elaborate a model which would explain why it is difficult to excite a big fraction of the lanthanide dopants and how the presence of GaN native defects would improve the luminescence. In order to identify the defect states responsible for the luminescence, based on the results presented in this work, more future investigations, both theoretical and experimental (e.g. EPR measurements) are required.

Appendix A

Formation Energies

To compare the relative stability of a structural defects in an otherwise ideal crystal the formation energy is used. The formation energy is the energy needed to create the defect and is not constant: it depends from the growth conditions of the crystal, i.e. from the relative abundances of its constituents in the growth phase. These abundances are thermodynamically described by the chemical potentials of the elements involved, which define on turn the reservoir where atoms are taken from or brought to in order to create the defect. The formation energy of charged defects depends also from the position of the Fermi level, which describes the energy position where the electrons are taken from or brought to in order to charge the defect. Summarising, the formation energy of a defect in the charge state q will be:

$$E_{\text{form}} = E_{\text{tot}}(q) - \sum_A n_A \mu_A - q E_{\text{Fermi}} \quad (\text{A.1})$$

where $E_{\text{tot}}(q)$ is the total energy of the crystal in the charge state q . The index A runs over all the atomic species present in the system. μ is the chemical potential and n the number of atoms of type A . In this work only the formation energy of defects in GaN is calculated, and the Eq. A.1 takes the form:

$$E_{\text{form}} = E_{\text{tot}} - n_{\text{Ga}} \mu_{\text{Ga}} - n_{\text{N}} \mu_{\text{N}} - \sum_i n_i \mu_i \quad (\text{A.2})$$

where, n_{Ga} and n_{N} denote the concentrations of Gallium and nitrogen atoms and n_i the concentrations of all impurities i in the crystal. With μ_{Ga} , μ_{N} and μ_i , the chemical potentials of gallium, nitrogen and the impurities are taken into account. Let us calculate here the formation energy of an Erbium substitutional in GaN as example. The chemical potentials of Ga, N and Er are not independent variables, as they have to in equilibrium with GaN and ErN.

$$\begin{cases} \mu_{\text{Ga}} + \mu_{\text{N}} = \mu_{\text{GaN}}^{\text{bulk}} \\ \mu_{\text{Er}} + \mu_{\text{N}} = \mu_{\text{ErN}}^{\text{bulk}} \end{cases} \quad (\text{A.3})$$

In both cases only one chemical potential can be chosen freely. We choose μ_{N} as independent variable in order to have the same independent variable for both relations. The choice of the nitrogen chemical potential is not completely free as μ_{N} has to stay within certain boundary conditions. The chemical potential of any element has to be less than the chemical potential of the corresponding bulk (or molecular) phase, otherwise the element would form during the crystal growth its energetically favorable bulk or molecular structure. The upper limit for μ_{N} is therefore given if GaN is in thermodynamic equilibrium with molecular N_2 . This case is called *N-rich limit*. The lower limit for μ_{N} is instead given when GaN and ErN are in thermodynamic equilibrium with Ga and Er respectively. This case is therefore called *Ga-* (or *Er-*) *rich limit*.

$$\begin{array}{ll} \text{(Ga rich limit)} & \mu_{\text{N}}^{\text{molec.}} + \Delta H^{\text{GaN}} \leq \mu_{\text{N}} \leq \mu_{\text{N}}^{\text{molec}} \quad \text{(N rich limit)} \\ \text{(Er rich limit)} & \mu_{\text{N}}^{\text{molec.}} + \Delta H^{\text{ErN}} \leq \mu_{\text{N}} \leq \mu_{\text{N}}^{\text{molec}} \quad \text{(N rich limit)} \end{array} \quad (\text{A.4})$$

Table A.1: *The chemical potential of elements of interest for this work calculated with DFTB.*

System	Structure	DFTB (eV)	System	Structure	DFTB (eV)
N ₂	Dimer	-71.639	PrN	Rock-salt	-94.933
O ₂	Dimer	-88.602	EuN	Rock-salt	-102.464
Ga ^{bulk}	α-Ga	-71.639	GdN	Rock-salt	-165.531
GaN ^{bulk}	Wurtzite	-101.424	ErN	Rock-salt	-129.503
GaN ^{bulk}	Zinc-blende	-101.424	TmN	Rock-salt	-132.699

where ΔH is the *heat of formation*, defined as

$$\begin{cases} \Delta H_f^0(\text{GaN}) = \mu_{\text{GaN}}^{\text{bulk}} - \mu_{\text{Ga}}^{\text{bulk}} - \mu_{\text{N}}^{\text{molec.}} \\ \Delta H_f^0(\text{ErN}) = \mu_{\text{ErN}}^{\text{bulk}} - \mu_{\text{Er}}^{\text{bulk}} - \mu_{\text{N}}^{\text{molec.}} \end{cases} \quad (\text{A.5})$$

If the heat of formation is negative the reaction is exothermic. The chemical potentials are defined as

$$\mu = \left(\frac{\partial F}{\partial N} \right)_{T,V} \quad (\text{A.6})$$

Where N is the number crystal units, F is the Helmholtz free energy ($F = E - TS$) and T is the temperature, which in our calculations is chosen to be zero. In this case we have

$$\mu = \frac{E_0^N}{N} \quad (\text{A.7})$$

The chemical potential of the molecular and bulk phases have been calculated using the lattice parameters which minimise the DFTB total energy in each case.

Let us come back now to our example, the calculation of the formation energy of the substitutional Er_{Ga} in GaN in the neutral charge state. Eq. A.1 becomes:

$$E_{\text{form}}^0(\text{Er}_{\text{Ga}}) = E_{\text{tot}}^0(\text{Er}_{\text{Ga}}) - n_{\text{Ga}}\mu_{\text{Ga}} - n_{\text{N}}\mu_{\text{N}} - n_{\text{Er}}\mu_{\text{Er}} \quad (\text{A.8})$$

which on turn, because of the relations connecting the chemical potentials becomes:

$$E_{\text{form}}^0(\text{Er}_{\text{Ga}}) = E_{\text{tot}}^0(\text{Er}_{\text{Ga}}) - n_{\text{Ga}}\mu_{\text{GaN}} - n_{\text{Er}}\mu_{\text{ErN}} \quad (\text{A.9})$$

This relation, deriving from a couple of algebraic steps, is very informative as it can be interpreted as follows: to obtain the formation energy of the substitutional Er_{Ga} in GaN one has to subtract from the total energy the chemical potential of all the atomic pairs GaN and of the single couple ErN. Another practical way to calculate the same formation energy, derived with a simple algebraic step is:

$$E_{\text{form}}^0 = E_{\text{tot}}^0(\text{Er}_{\text{Ga}}) - E_{\text{tot}}^0(\text{GaN}) + \mu_{\text{GaN}} - \mu_{\text{ErN}} \quad (\text{A.10})$$

Bibliography

- [1] H. Ennen, J. Schneider, G. Pomrenke and A. Axmann
1.54- μm luminescence of erbium-implanted III-V semiconductors and silicon
Appl. Phys. Lett. **43**, 943 (1983).
- [2] P. N. Favennec, H. L'Haridon, M. Salvi, D. Moutonnet and Y. Le Guillou
Luminescence of erbium implanted in various semiconductors: IV, III-V and II-VI materials
Electron. Lett. **25**, 718 (1989).
- [3] A. J. Steckl and J. M. Zavada
Optoelectronic properties and applications of rare-earth-doped GaN
Mater. Res. Bulletin **24**, 33 (1999).
- [4] A. J. Steckl, J. C. Heikenfeld, D. S. Lee, M. J. Garter, C. C. Baker, Y. Wang and R. Jones
Rare-Earth doped GaN: Growth, properties and fabrication of electroluminescent devices
IEEE J. Sel. Topics in q. Electronics **8**, 749 (2002).
- [5] D. S. Lee and A. J. Steckl
Enhanced blue and green emission in rare earth doped GaN electroluminescent devices by optical photopumping
Appl. Phys. Lett. **81**, 2331 (2002).
- [6] D. S. Lee and A. J. Steckl
Enhanced blue emission from Tm-doped $\text{Al}_x\text{Ga}_{1-x}\text{N}$ electroluminescent thin films
Appl. Phys. Lett. **83**, 2094 (2003).
- [7] E. E. Nyein, U. Hömmerich, J. C. Heikenfeld, D. S. Lee, A. J. Steckl and J. M. Zavada
Spectral and time-resolved photoluminescence studies of Eu-doped GaN
Appl. Phys. Lett. **82**, 1655-1657 (2003).
- [8] J. Stimmer, A. Reittinger, J. F. Nützel, G. Abstreiter, H. Holzbrecher and Ch. Buchal
Electroluminescence of erbium-oxygen-doped silicon diodes grown by molecular beam epitaxy
Appl. Phys. Lett. **68**, 3290-3292 (1996).
- [9] C. G. Duan, R. F. Sabryanov, W. N. Mei, P. A. Dowben, S. S. Jaswal and E. Y. Tsymbal
Electronic, magnetic and transport properties of rare earth mononictides
Invited review article to be published in J. of Phys.: Cond. Matter (2007).
- [10] A. J. Steckl, J. C. Heikenfeld, D. S. Lee and M. J. Garter
Multiple color capability from rare earth doped gallium nitride
Mat. Sci. Eng. **B81**, 97-101 (2001).
- [11] See <http://www.renibel.net>
- [12] K. P. O'Donnell and B. Hourahine
Rare earth doped III-nitrides for optoelectronics
Eur. Phys. J. Appl. Phys. **36**, 91-103 (2006).
- [13] J. T. Torvik, R. J. Feuerstein, J. I. Pankove, C. H. Qiu and F. Namavar
Electroluminescence from erbium and oxygen coimplanted GaN
Appl. Phys. Lett. **69**, 2098 (1996).

- [14] P.H. Citrin, P. A. Northrup, R. Birckhahn and A. J. Steckl
Local structure and bonding of Er in GaN: A contrast with Er in Si,
Appl. Phys. Lett. **76**, 2865 (2000).
- [15] V. Katchkanov, J. F. W. Mosselmann, S. Dalmaso, K. P. O'Donnell, S. Hernandez, K. Wang,
R. W. Martin, O. Briot, N. Rousseau, G. Halambalakis, K. Lorenz and E. Alves
Extended X-ray absorption fine structure studies of thulium doped GaN epilayers
Superlatt. Micr. **36**, 729-736 (2004).
- [16] V. I. Anisimov, F. Aryasetiawan and A. I. Lichtenstein
*First-principles calculations of the electronic structure and spectra of strongly correlated systems:
the LDA+U method*
J. Phys. Cond. Matt. **9**, 767 (1999).
- [17] R. Jones
Structure and electrical activity of RE dopants in semiconductors
Opt. Mat. **28**, 718-722 (2006).
- [18] A. Svane, N. E. Christiansen, L. Petit, Z. Szotek and W. M. Temmerman
Electronic structure of rare-earth impurities in GaAs and GaN
Phys. Rev. B **74**, 165204 (2006).
- [19] Online Reference: www.dftb.org
- [20] M. Haugk, J. Elstner, Th. Frauenheim, T. E. M. Staab, C. D. Latham, R. Jones, H. S. Leipner,
T. Heine, G. Seifert and M. Sternberg
Structures, Energetics and Electronic Properties of Complex III - V Semiconductor Systems
Phys. Stat. Sol B **217**, 473 (2000).
- [21] M. Elstner, Th. Frauenheim, E. Kaxiras, G. Seifert and S. Suhai
A Self-Consistent Charge Density-Functional Based Tight-Binding Scheme for Large Biomolecules
Phys. Stat. Sol B **217**, 375 (2000).
- [22] A. Sieck
Structure and physical properties of Si clusters and of vacancy clusters in bulk Si
Ph.D Thesis, Universität Paderborn (2001).
- [23] E. Rauls
Annealing mechanisms of point defects in SiC.
Ph.D Thesis, Universität Paderborn (2003).
- [24] D. Porezag, Th. Frauenheim, Th. Köhler, G. Seifert and R. Kaschner
*Construction of tight-binding-like potentials on the basis of density-functional theory: Application
to carbon*
Phys. Rev. B **51**, 12947 (1995).
- [25] J. Widany, Th. Frauenheim, Th. Köhler, M. Sternberg, D. Porezag, G. Jungnickel and G. Seifert
*Density-functional-based construction of transferable nonorthogonal tight-binding potentials for B,
N, BN, BH, and NH*
Phys. Rev. B **53**, 4443 (1996).
- [26] J. Elsner, R. Jones, M. I. Heggie, K. Sitch, M. Haugk, Th. Frauenheim, S. Oberg and P. R. Briddon
Deep acceptors trapped at threading-edge dislocations in GaN
Phys. Rev. B **58**, 12571 (1993).
- [27] J. Elsner, M. Haugk, J. Jungnickel and Th. Frauenheim
A density-functional based tight-binding approach to III-V semiconductor clusters
J. Mater. Chem. **6**, 1649 (1996).
- [28] B. Hourahine, S. Sanna, B. Aradi, C. Köhler and Th. Frauenheim
A theoretical study of erbium in GaN
Physica B **376**, 512 (2006).

-
- [29] J. K. Lang, Y. Baer and P. A. Cox
Study of the 4f and valence band density of states in rare earth metals: II Experiment and results
J. Phys. F: Metal Phys. **11**, 121 (1981).
- [30] J. H. Van Vleck
The puzzle of rare earth spectra in solids
J. Phys. Chem. **41**, 67 (1937).
- [31] G. S. Ofelt
Intensities of crystal spectra of rare earth ions
J. Chem. Phys. **37**, 511 (1962).
- [32] G. H. Dieke
Spectra and energy levels of rare earth ions in crystals
Wiley & Sons Inc. New York (1969).
- [33] N. Rousseau, O. Briot, V. Ribes and R. L. Aulombard,
Er doped GaN by Gas Source Molecular Beam Epitaxy on GaN Templates
MRS Symp. Proc. **764**, C3.50.1 (2003).
- [34] G. Halambalakis, N. Rousseau, O. Briot, S. Ruffenach, R. L. Aulombard, P. R. Edwards,
K. P. O'Donnell, T. Wojtowicz and P. Ruterana
Growth and characterisation of Eu doped GaN thin films
Superlatt. Microstr. **36**, 721 (2004).
- [35] T. Wojtowicz, P. Ruterana, N. Rousseau, O. Briot, S. Dalmaso, R. W. Martin and K. P. O'Donnell
The microstructure of Er MBE doped GaN
Mat. Sci. Eng. B **105**, 114 (2003).
- [36] K. Lorenz, U. Wahl, E. Alves, S. Dalmaso, R. W. Martin, K. P. O'Donnell, S. Ruffenach and
O. Briot
High-temperature annealing and optical activation of Eu-implanted GaN
Appl. Phys. Lett. **85**, 2712-2714 (2004).
- [37] E. Nogales, R. W. Martin, K. P. O'Donnell, K. Lorenz, E. Alves, S. Ruffenach and O. Briot
*Failure mechanism of AlN nanocaps used to protect RE-implanted GaN during high temperature
annealing*
Appl. Phys. Lett. **88**, 031902 (2006).
- [38] K. Lorenz, U. Wahl, E. Alves, E. Nogales, S. Dalmaso, R. W. Martin, K. P. O'Donnell, M. Wojdak,
A. Braud, T. Monteiro, T. Wojtowicz, P. Ruterana, S. Ruffenach and O. Briot
High temperature annealing of rare earth implanted GaN films: Structural and optical properties
Opt. Mat. **28**, 750 (2006).
- [39] S. O. Kucheyev, J. S. Williams, C. Jagadish, J. Zou and G. Li
Damage buildup in GaN under ion bombardment
Phys. Rev. B **62**, 7510-7522 (2000).
- [40] K. Lorenz, U. Wahl, E. Alves, T. Wojtowicz, P. Ruterana, S. Ruffenach and O. Briot
Amorphisation of GaN during processing with rare earth ion beams
Superlatt. Microstr. **36**, 737-745 (2004).
- [41] B. Pipeleers, S. M. Hogg and A. Vantomme
Defect accumulation during channeled erbium implantation into GaN
J. Appl. Phys. **98**, 123504 (2005).
- [42] U. Wahl, E. Alves, K. Lorenz, T. Monteiro, A. Vantomme, B. de Vries and R. Vianden
Lattice location and optical activation of rare earth implanted GaN
Mater. Sci. Eng. B **105**, 132-140 (2003).
- [43] B. de Vries
Lattice site location of impurities in group III nitrides using emission channeling
Ph.D thesis, University of Leuven (2006)
-

- [44] S. J. Gurman
Interpretation of EXAFS Data
J.Synchrotron Rad. **2**, 56-63 (1995) and ref. therein.
- [45] V. Katchkanov, J. F. W. Mosselmans, S. Dalmasso, K. P. O'Donnell, R. W. Martin and the RENiBEL Network
Extended X-ray Absorption Fine Structure Studies of GaN Epilayers Doped in situ with Er and Eu During Molecular Beam Epitaxy
MRS Symp. Proc. **798**, Y5.10 (2004).
- [46] V. Katchkanov, J. F. W. Mosselmans, K. P. O'Donnell, E. Nogales, S. Hernandez, R. W. Martin, A. J. Stekl and D. S. Lee
Extended X-ray absorption fine structure studies of GaN epilayers doped with Er
Optical Materials **28**, 785 (2006).
- [47] V. Katchkanov
Ph. D Thesis, University of Strathclyde (2006).
- [48] V. Dierolf, C. Sandmann, J. Zavada, P. Chow and B. Hertog
Site-selective spectroscopy of Er in GaN
J. Appl. Phys. **95**, 5464-5470 (2004).
- [49] S. Kim, S. J. Rhee, D. A. Turnbull, X. Li, J. J. Coleman, S. G. Bishop and P. B. Klein
Trap-mediated excitation of Er³⁺ photoluminescence in Er-implanted GaN
Appl. Phys. Lett. **71**, 2662-2664 (1997)
- [50] F. Pellé, F. Auzel, J. M. Zavada, D. S. Lee and A. J. Stekl
New spectroscopic data of erbium ions in GaN thin films
Mater. Sci. Eng. B **105**, 126-131 (2003).
- [51] V. Katchkanov, K. P. O'Donnell, S. Dalmasso, R. W. Martin, A. Braud, Y. Nakanishi, A. Wakahara and A. Yoshida
Photoluminescence studies of Eu-implanted GaN epilayers
Phys. Stat. Sol. B **242**, 1491 (2005).
- [52] K. Wang, R. W. Martin, K. P. O'Donnell, V. Katchkanov, E. Nogales, K. Lorenz, E. Alves, S. Ruffenach and O. Briot
Selectively excited photoluminescence from Eu-implanted GaN
App. Phys. Lett. **87**, 112107 (2005).
- [53] L. Bodiou, A. Oussif, A. Braud, J-L. Doualan, R. Moncorgé, K. Lorenz and E. Alves
Effect of annealing temperature on luminescence in Eu implanted GaN
Opt. Mat. **28**, 780 (2006).
- [54] A. Braud, J. L. Doualan, R. Moncorgé, B. Pipeleers and A. Vantomme
Er-defect complexes and isolated Er center spectroscopy in Er-implanted GaN
Mat. Sci. Eng. B **105**, 101-105 (2003).
- [55] T. Wojtowicz, P. Ruterana, K. Lorenz, U. Wahl, E. Alves, S. Ruffenach, G. Halambalakis and O. Briot
The atomic structure of defects formed during doping of GaN with rare earth ions
Phys. Stat. Sol. C **2**, 1081 (2005).
- [56] M. Mamor, V. Matias, A. Vantomme, A. Colder, P. Marie and P. Ruterana
Defects induced in GaN by europium implantation
App. Phys. Lett. **85**, 2244-2246 (2004).
- [57] J. S. Filhol, R. Jones, M. J. Shaw and P. R. Briddon
Structure and electrical activity of rare-earth dopants in GaN
Appl. Phys. Lett. **84**, 2841 (2004).
- [58] P. Dorembois and E. van der Kolk
Location of lanthanide impurity levels in the III-V semiconductor GaN
Appl. Phys. Lett. **89**, 061122 (2006).

-
- [59] V. Glukhanyuk, H. Przybylińska, A. Kozanecki and W. Lantsch
Site symmetry of erbium centers in GaN
Phys. Stat. Sol. a **201**, 195 (2004).
- [60] G. Grosso and G. Pastori Parravicini
Solid State Physics,
Academic Press, 273, (2000).
- [61] A. Szabo and N. S. Ostlund
Modern quantum chemistry: introduction to advanced electronic structure theory
McGraw-Hill, (1989).
- [62] Helmut Eschrig
The fundamentals of density functional theory
Teubner, (1996).
- [63] R. G. Parr and W. Yang
Density-Functional Theory of Atoms and Molecules
Oxford University Press, (1989).
- [64] W. Kohn and P. Hohenberg
Inhomogeneous Electron Gas
Phys. Rev. **136**, B864 (1964).
- [65] U. von Barth
Local-density theory of multiplet structure
Phys. Rev. A **20**, 1693 (1979).
- [66] W. Kohn and L. P. Sham
Self-Consistent Equations Including Exchange and Correlation Effects
Phys. Rev. **140**, A1133 (1965).
- [67] R. M. Dreizler and J. da Providencia
Density Functional Methods in Physics
Proceedings of a NATO ASI Held in Alcabideche (Portugal), September, 1983
Plenum Press, (1985).
- [68] V. Barone
Structure, Magnetic Properties and Reactivities of Open-Shell Species From Density Functional and Self-Consistent Hybrid Methods
In D. P. Chong, editor, Recent Advances in Density Functional Methods. Part I. World Scientific Publishing Co. Chapter 8, (1996).
- [69] U. von Barth and L. Hedin
A local exchange-correlation potential for the spin-polarized case
J. Phys. C **5**, 1629 (1972).
- [70] J. F. Janak
Proof that $\frac{\partial E}{\partial n_i} = \epsilon_i$ in density-functional theory
Phys. Rev. B **18**, 7165 (1978).
- [71] C. Göransson, W. Olovsson and I. A. Abrikosov
Numerical investigation of the validity of the Slater-Janak transition-state model in metallic systems
Phys. Rev. B **72**, 134203 (2005).
- [72] H. Eschrig
The fundamentals of Density Functional Theory
Teubner Verlagsgesellschaft, Stuttgart-Leipzig (1996).
- [73] M. Cococcioni and S. de Gironcoli
Linear response approach to the calculation of the effective interaction parameters in the LDA+U method
Phys. Rev. B **71**, 035105 (2005).
-

- [74] J. P. Perdew and A. Zunger
Self-interaction correction to density-functional approximations for many-electron systems
Phys. Rev. B **23**, 5048 (1981).
- [75] O. A. Vydrov, G. E. Scuseria, J. P. Perdew, A. Ruzsinszky and G. I. Csonka
Scaling down the Perdew-Zunger self-interaction correction in many-electron regions
J. Chem. Phys. **124**, 094108 (2006).
- [76] M. T. Czyżyk and G. A. Sawatzky
Local-density functional and on-site correlations: The electronic structure of La_2CuO_4 and LaCuO_3
Phys. Rev. B **49**, 14211 (1994).
- [77] V. I. Anisimov, I. V. Solovyev, M. A. Korotin, M. T. Czyżyk and G. A. Sawatzky
Density-functional theory and NiO photoemission spectra
Phys. Rev. B **48**, 16929 (1993).
- [78] A. G. Pethukov, I. I. Mazin, L. Chioncel and A. I. Lichtenstein
Correlated metals and the LDA+U method
Phys. Rev. B **67**, 153106 (2003).
- [79] X. Gonze, P. Käckell and M. Scheffler
Ghost states for separable, norm-conserving, ab initio pseudopotentials
Phys. Rev. B **41**, 12264 (1990)
- [80] X. Gonze, P. Stumpf and M. Scheffler
Analysis of separable potentials
Phys. Rev. B **44**, 8503 (1991).
- [81] L. Kleinmann and D. M. Bylander
Efficacious form for model pseudopotentials
Phys. Rev. Lett. **48**, 1425 (1982).
- [82] N. Troullier and J. L. Martins
Efficient pseudopotentials for plane-wave calculations
Phys. Rev. B **43**, 1993 (1991).
- [83] D. Vanderbilt
Soft self-consistent pseudopotentials in a generalized eigenvalue formalism
Phys. Rev. B **41**, 7892 (1990).
- [84] C. Hartwigsen, S. Goedecker and J. Hütter
Relativistic separable dual-space Gaussian pseudopotentials from H to Rn
Phys. Rev. B **58**, 3641 (1998).
- [85] S. G. Louie, S. Froyen and M. L. Cohen
Nonlinear ionic pseudopotentials in spin-density functional calculations
Phys. Rev. B **26**, 1738 (1982).
- [86] Th. Frauenheim, F. Weich, Th. Köhler, S. Uhlmann, D. Porezag and G. Seifert.
Density functional based construction of transferable non-orthogonal tight-binding potentials for Si and SiH
Phys. Rev. B **52**, 11492 (1995).
- [87] M. Elstner, D. Porezag, G. Jungnickel, J. Elsner, M. Haugk, Th. Frauenheim, S. Suhai and G. Seifert
Self-consistent-charge density-functional tight-binding method for simulations of complex materials properties
Phys. Rev. B **58**, 7260 (1998).
- [88] Th. Frauenheim, G. Seifert, M. Elstner, Z. Hajnal, G. Jungnickel, D. Porezag, S. Suhai and R. Scholz
A Self-Consistent Charge Density-Functional Based Tight-Binding Method for Predictive Materials Simulations in Physics, Chemistry and Biology
Phys. Stat. Sol. (b) **217**, 41 (2000).

-
- [89] Th. Frauenheim, G. Seifert, M. Elstner, T. Niehaus, C. Köhler, M. Amkreutz, M. Sternberg, Z. Hajnal, A. Di Carlo and S. Suhai
Atomistic simulations of complex materials: groundstate and excited-state properties
J. Phys. Condens. Matter **14**, 3015 (2002).
- [90] C. Köhler
Berücksichtigung von Spinpolarisationseffekten in einem dichtenfunktionalbasierten Ansatz
Ph.D Thesis, Universität Paderborn (2004).
- [91] W. Foulkes and R. Haydock
Tight-binding models and density-functional theory
Phys. Rev. B **39**, 12520 (1989).
- [92] F. W. Averill and G. S. Painter
Harris functional and related methods for calculating total energies in density-functional theory
Phys. Rev. B **41**, 10344 (1990).
- [93] H. Eschrig
Optimized LCAO Method and the Electronic Structure of Extended Systems
Akademie Verlag (1988).
- [94] G. Seifert, H. Eschrig and W. Bieger
Eine approximative Variante des LCAO-Xa- Verfahrens
Zeitung phys. Chemie (Leipzig) **267**, 529 (1986).
- [95] V. Heera, G. Seifert and P. Ziesche
A semi-relativistic variant of the scattered-wave $X\alpha$ method
J. Phys. B: At. Mol. Phys. **17**, 519 (1984).
- [96] J. C. Slater and G.F.Koster
Simplified LCAO method for the Periodic Potential Problem
Phys. Rev. **94**, 1498 (1954).
- [97] K. Lendi
Extension of the Slater-Koster tables for tight-binding calculations to f electrons
Phys. Rev. B **9**, 2433 (1974).
- [98] A. V. Podolskiy and P. Vogl
Compact expression for the angular dependence of tight-binding Hamiltonian matrix elements
Phys. Rev. B **69**, 233101 (2004).
- [99] J. Elsner
Surfaces and Extended Defects in Wurzite GaN
Ph.D thesis, Universität Paderborn (1998).
- [100] M. Elstner
Weiterentwicklung quantenmechanischer Rechenverfahren für organische Moleküle und Polymere
Ph.D thesis, Universität Paderborn (1998).
- [101] D. J. Chadi
Atomic and Electronic Structures of Reconstructed Si(100) Surfaces
Phys. Rev. Lett. **43**, 43 (1979).
- [102] D. A. Papaconstantopoulos and C. S. Hellberg
Comment on "Correlation Induced Paramagnetic Ground State in FeAl"
Phys. Rev. Lett. **89**, 029701 (2002).
- [103] S. L. Dudarev, G. A. Botton, S. Y. Savrasov, C. J. Humphreys and A. P. Sutton
Electron-energy-loss spectra and the structural stability of nickel oxide: An LSDA+ U study
Phys. Rev. B **57**, 1505 (1998).
- [104] M. J. Han, T. Ozaki and J. Yu
 $O(N)$ LDA+ U electronic structure calculation method based on the nonorthogonal pseudoatomic orbital basis
Phys. Rev. B **73**, 045110 (2006).
-

- [105] D. Vogl, P. Krüger and J. Pollmann
Ab initio electronic structure of silver halides calculated with self-interaction and relaxation-corrected pseudopotentials
Phys. Rev. B **58**, 3865 (1998) and **55**, 12838 (1996).
- [106] A. Filippetti and N. A. Spaldin
Self-interaction-corrected pseudopotential scheme for magnetic and strongly-correlated systems
Phys. Rev. B **67**, 125109 (2003).
- [107] C. D. Pemmaraju, T. Archer, D. Sanchez-Portal and S. Sanvito
Atomic self-interaction correction for molecules and solids
cond-mat/0609325, (2006).
- [108] A. I. Liechtenstein, V. I. Anisimov and J. Zaanen
Density-functional theory and strong interactions: Orbital ordering in Mott-Hubbard insulators
Phys. Rev. B **52**, R5467 (1995).
- [109] J. P. Perdew and M. Levy
Physical Content of the Exact Kohn-Sham Orbital Energies: Band Gaps and Derivative Discontinuities
Phys. Rev. Lett. **51**, 1884 (1983).
- [110] L. J. Sham and M. Schlüter
Density-Functional Theory of the Energy Gap
Phys. Rev. Lett. **51**, 1888 (1983).
- [111] V. Fiorentini, M. Methfessel and M. Scheffler
Electronic and structural properties of GaN by the full-potential linear muffin-tin orbitals method: The role of the d electrons
Phys. Rev. B **47**, 13353 (1993).
- [112] <http://physics.nist.gov/PhysRefData/DFTdata/contents.html>
- [113] P. Blaha, K. Schwarz, G. Madsen, D. Kvasnicka and J. Luitz
Wien2k
Inst. f. Materials Chemistry, TU Vienna.
- [114] Michael Sternberg
The atomic structure of diamond surfaces and interfaces
Ph.D Thesis, Universität Paderborn (2004).
- [115] T. Palasyuk and M. Tkacz
Pressure induced hexagonal to cubic phase transformation in erbium trihydride
Sol. St. Comm. **130**, 219-221 (2004).
- [116] T. Palasyuk and M. Tkacz
Pressure-induced structural phase transition in rare-earth trihydrides. Part I. (GdH₃, HoH₃, LuH₃)
Sol. St. Comm. **133**, 481-486 (2005).
- [117] T. Palasyuk and M. Tkacz
Hexagonal to cubic phase transition in YH₃ under high pressure
Sol. St. Comm. **133**, 477-480 (2005).
- [118] F. D. Murnaghan
Finite deformations of an elastic solid
Amer. J. Math. **59**, 235 (1937).
- [119] F. D. Murnaghan
The compressibility of media under extreme pressures
Proc. Nat. Acad. Sci. USA **30**, 244 (1944).
- [120] W. A. Grosshans and W. B. Holzapfel
Atomic volumes of rare-earth metals under pressures to 40 GPa and above
Phys. Rev. B **43**, 5171 (1992).

-
- [121] All the *ab initio* simulations were performed with the simulation package ABINIT, a common project of the Université catholique de Louvain, Coming Incorporated and other contributors (URL <http://www.abinit.org>) and HGH pseudopotentials.
- [122] M. Bernasconi, G. L. Chiarotti and E. Tosatti
Ab initio calculations of structural and electronic properties of Ga solid-state phases
Phys. Rev. B **52**, 9988 (1995).
- [123] M. Fuchs, J. L. F. D. Silva, C. Stampfl, J. Neugebauer and M. Scheffler
Cohesive properties of group-III nitrides: A comparative study of all-electron and pseudopotential calculations using the generalized gradient approximation
Phys. Rev. B **65**, 245212 (2002).
- [124] A. Zoroddu, F. Bernardini, P. Ruggerone and V. Fiorentini
First-principles prediction of structure, energetics, formation enthalpy, elastic constants, polarization, and piezoelectric constants of AlN, GaN, and InN: Comparison of local and gradient-corrected density-functional theory
Phys. Rev. B **64**, 045208 (2001).
- [125] K. R. Lyall and J. F. Cochran
Velocity of sound and acoustic attenuation in pure gallium single crystals
Can. J. Phys. **49**, 1075 (1971).
- [126] C. Kittel
Introduction to solid state physics
Wiley, New York (1996).
- [127] A. L. da Rosa
Dichtenfunktionaltheoretische Untersuchungen zu Anti-Surfactants auf GaN-Oberflächen
Ph. D Thesis, Technische Universität Berlin (2003).
- [128] H. J. Monkhorst and J. D. Pack
Special points for Brillouin-zone integrations
Phys. Rev. B **13**, 5188 (1976).
- [129] D. A. Papaconstantopoulos
Handbook of the band structure of elemental solids
Plenum Press, New York (1986).
- [130] J. Furthmüller, J. Hafner and G. Kresse
Ab initio calculation of the structural and electronic properties of carbon and boron nitride using ultrasoft pseudopotentials
Phys. Rev. B **50**, 15606 (1994).
- [131] H. J. McSkimin and W. L. Bond
Elastic moduli of diamond
Phys. Rev. **105**, 116 (1957).
- [132] M. H. Grimsditch and A. K. Ramdas
Brillouin scattering in diamond
Phys. Rev. B **11**, 3139 (1975).
- [133] A. K. McMahan, C. Huschroft, R. T. Scalettar and E. L. Pollock
Volume-collapse transitions in rare earth metals
J. Comp. Mat. Des. **5**, 131-162 (1998).
- [134] B. I. Min A. J. F. Hansen, T. Oguchi and A. J. Freeman
Local density total energy description of ground and excited state properties of the rare earth metals
J. Mag. Mat. **61**, 139-150 (1986).
- [135] Ralph W. G. Wyckoff
Crystal Structures, VOL. 1
R. E. Krieger Publishing Company, Malabar, Florida (1982).
-

- [136] A. Svane, J. Trygg, B. Johansson and E. Eriksson
Electronic-structure calculations of metal praseodymium by means of modified density-functional theory
Phys. Rev. B **56**, 7143 (1997).
- [137] F. H. Spedding, A. H. Daane and K. W. Herrmann
The crystal structure and lattice parameters of high-purity scandium, yttrium and the rare earth metals
Acta Cryst. **9**, 559 (1956).
- [138] A. E. Curzon and H. G. Chlebek
The observation of FCC Gd, Tb, Dy, Ho, Er and Tm in the form of thin films and their oxidation
J. Phys. F: Met. Phys. **3**, 1 (1973).
- [139] D. R. Lide
Handbook of physics and chemistry 76th ed.
NY, New York (1995).
- [140] C. Stampfl and C G. Van de Walle
Density-functional calculations for III-V nitrides using the local-density approximation and the generalized gradient approximation
Phys. Rev. B **59**, 5521 (1999).
- [141] P. Larson, W. R. L. Lambrecht, A. Chantis and M. van Schilfgaarde
Electronic structure of rare-earth nitrides using the LDA+U approach: Importance of allowing 4f orbitals to break the cubic crystal symmetry
Phys. Rev. B **75**, 045114 (2007).
- [142] M. D. Johannes and W. E. Pickett
Magnetic coupling between nonmagnetic ions: Eu³⁺ in EuN and EuP
Phys. Rev. B **72**, 195116 (2005)
- [143] D. B. McWahn
Effect of pressure on the curie temperature and volume of GdN
J. Chem. Phys. **44**, 3528 (1966).
- [144] C. M. Aerts, P. Strange, M. Horne, W. M. Temmermann, Z. Szotek and A. Svane
Half-Metallic to insulating behaviour of rare-earth nitrides
Phys. Rev. B **69**, 045115 (2004).
- [145] F. Hulliger
Handbook on the physics and chemistry of rare earts Vol. 4
North-Holland Physics Publishing, New York (1979).
- [146] J. Kordis, K. A. Gingerich and E. Kaldis
Heat of vaporisation of EuN and its standard heat of formation,
J. Am. Ceram. Soc. **56**, 581 (1973).
- [147] S. Nishio, T. Nakagawa, T. Arakawa, N. Tomioka, T. Yamamoto, T. Kusunose, K. Niihara, T. Numazawa and K. Kamiya
Specific heat and thermal conductivity of HoN and ErN at cryogenic temperatures
J. Appl. Phys. **99**, 08K901 (2006).
- [148] T. Nakagawa, T. Arakawa, K. Sako, N. Tomioka, T. Yamamoto, T. Kusunose, K. Niihara, K. Kamiya and T. Numazawa
Magnetocaloric effects of ferromagnetic erbium mononitride
J. All. Comp. **408**, 191 (2006).
- [149] Z. Szotek, W. M. Temmerman, A. Svane, L. Petit, P. Strange, G. M. Stocks, D. Ködderitzsch, W. Hergert and H. Winter
Electronic structure of half-metallic ferromagnets and spinel ferromagnetic insulators
J. Phys.: Condensed Matter **16**, S5587 (2004).

-
- [150] A. G. Petukhov, W. R. L. Lambrecht and B. Segall
Electronic structure of rare-earth pnictides
Phys. Rev. B **53**, 4324 (1996).
- [151] C. G. Duan, R. F. Sabiryanov, J. Liu, W. N. Mei, P. A. Dowben and J. R. Hardy
Theoretical study of the magnetic ordering in rare earth compounds with face-centered-cubic structure
J. Appl. Phys. **97**, 10A915 (2005).
- [152] G. Busch, P. Junod, O. Vogt and F. Hulliger
Ferro- and metamagnetism of rare earth compounds
Phys. Lett. **6**, 79 (1963).
- [153] O. Vogt and K. Mattenberger
The magnetism of localised or nearly localised 4f and 5f shells
J. All. Comp. **223**, 226 (1995).
- [154] W. M. Temmerman, Z. Szotek, A. C. Jenkins, A. Svane, H. Winter, S. V. Beiden and G. A. Gehring
An unified band-structure description of localised and delocalised f-states
Proceedings of Magnetism and Electronic Correlations in Local-Moment Systems: Rare-Earth Elements and Compounds, Berlin, Germany, 16-18 March 1998.
- [155] H. Huang, L. Ye, Z. Qin and X. Xie
Interaction between Er atoms and the carbon cage C₈₂
Phys. Rev. B **61**, 12786 (2000).
- [156] O. Ambacher
Growth and application of group III-nitrides
J. Phys. D: App. Phys. **31**, 2653 (1998).
- [157] T. Matsuoka, H. Hokamoto, M. Nakao, H. Harima and E. Kurimoto
Optical bandgap energy of wurtzite InN
Appl. Phys. Lett. **81**, 1246 (2002).
- [158] K. Lischka
Optical properties of cubic group III-nitrides
Phys. Stat. Sol. a **177**, 135 (2000).
- [159] D. J. As, T. Frey, D. Schikora, K. Lischka, V. Cimalla, J. Pezoldt, R. Goldhan, S. Keiser and W. Gebhardt
Cubic GaN epilayers grown by MBE on thin β -SiC/Si (001) substrates
Appl. Phys. Lett. **76**, 1686 (2002).
- [160] D. J. As, S. Potthast, J. Schörmann, S. F. Li, K. Lischka, H. Nagasawa and M. Abe
Molecular beam epitaxy of cubic group III-nitrides on free-standing 3C-SiC substrates
Materials Science Forum **727-529**, 1489 (2006).
- [161] S. Nakamura and G. Fasol
The Blue Laser Diode
Springer-Verlag, Berlin Heidelberg, (1997).
- [162] S. Yoshida, S. Misawa and S. Gonda
Improvement on the electrical and luminescent properties of reactive MBE-grown GaN films by using AlN-coated sapphire substrates
Appl. Phys. Lett. **42**, 427 (1983).
- [163] H. Amano, N. Sawaki, I. Akasaki and Y. Toyoda
Metalorganic vapor phase epitaxial growth of a high quality GaN film using AlN buffer layer
Appl. Phys. Lett. **48**, 353 (1986).
- [164] S. Nakamura
GaN growth using GaN buffer layer
Jpn. J. Appl. Phys. **30**, L1705 (1991).
-

- [165] H. Amano, I. Akasaki, T. Kozawa, K. Hiramatsu, N. Sawaki, K. Ikeda and Y. Ishii
Electron beam effects on blue luminescence of Zn-doped GaN
J. Lumin. **40-41**, 121 (1988).
- [166] J. Neugebauer and C. G. V. de Walle
Hydrogen in GaN: novel aspects of a common impurity
Phys. Rev. Lett. **75** 4452, (1995) and
Role of hydrogen in doping GaN
Appl. Phys. Lett. **68**, 1829 (1996).
- [167] See: <http://compoundsemiconductor.net/articles/news/7/6/8/1>
- [168] J. H. Edgar, S. Strite, I. Akasaki, H. Amano and C. Wetzel
Properties, processing and applications of gallium nitride and related semiconductors
Inspec, (1999).
- [169] A. Rubio, J. L. Corkill, M. L. Cohen, E. L. Shirley and S. Louie
Quasiparticle band structure of AlN and GaN
Phys. Rev. B **48**, 11810 (1993).
- [170] P. E. Van Camp, V. E. Van Doren and J. T. Devreese
High pressure structural phase transformation in gallium nitride
Solid State Commun. **81**, 23 (1992).
- [171] H. P. Maruska and J. J. Tietjen
The preparation and properties of vapor-deposited single-crystalline GaN
Appl. Phys. Lett. **15**, 327 (1969).
- [172] J. C. Nipko, C. K. Loong, C. M. Balkas and R. F. Davis
Phonon density of states of bulk gallium nitride
Appl. Phys. Lett. **73**, 34 (1998).
- [173] K. Karch, J. M. Wagner and F. Bechstedt
Ab initio study of structural, dielectric, and dynamical properties of GaN
Phys. Rev. B **57**, 7043-7049 (1998).
- [174] J. H. Edgar
Properties of Group-III Nitrides and EMIS Datareviews
IEE London,(1994).
- [175] C. G. Van de Walle and J. Neugebauer
First-principles calculations for defects and impurities: Applications to III-nitrides
J. Appl. Phys. **95**, 3851 (2004).
- [176] M. B. Kanoun, A. E. Merad, J. Cibert, H. Aourag and G. Merad
Properties of strained zincblende GaN: first-principles study
Journal of alloys and compounds **366**, 86 (2004).
- [177] S. J. Pearton, C. B. Vartuli, J. C. Zolper, C. Yuan and R. A. Stall
Ion implantation doping and isolation of GaN
App. Phys. Lett. **67**, 1435 (1995).
- [178] J. C. Zolper, R. G. Wilson, S. J. Pearton and R. A. Stall
Ca and O ion implantation doping of GaN
App. Phys. Lett. **68**, 1945 (1996).
- [179] U. Köhler, M. Lübbbers, J. Mimkes and D. J. As
Properties of carbon as an acceptor in cubic GaN
Phys. B **308-310**, 126 (2001).
- [180] J. C. Zolper
Ion implantation in group-III nitride semiconductors: a tool for doping and defect studies
J. Cryst. Growth **178**, 157 (1997).

-
- [181] T. Ogino and M. Aoki *Mechanism of Yellow Luminescence in GaN*
Jap. J. Appl. Phys. **19**, 2395 (1980).
- [182] J. Neugebauer and C. G. V. de Walle
Atomic geometry and electronic structure of native defects in GaN
Phys. Rev. B. **50**, 8067 (1994).
- [183] D. J. As, U. Köhler and K. Lischka
Optical Properties of Carbon Doped Cubic GaN Epilayers Grown on GaAs (001) Substrate by Molecular Beam Epitaxy
MRS Symp. Proc. **798**, 57455 (2001).
- [184] S. Zeng, G. N. Aliev, D. Wolverson, J. J. Davies, S. J. Bingham, D. A. Abdulmalik, P. G. Coleman, T. Wang and P. J. Parbrook
Origin of the red luminescence in Mg doped GaN
Appl. Phys. Lett. **89**, 022107 (2006).
- [185] J. I. Pankove and J. A. Hutchby
Photoluminescence of ion implanted GaN
J. App. Phys. **47**, 5387 (1976).
- [186] S. O. Kucheyev, J. S. Williams and S. J. Pearton
Ion implantation into GaN
Mat. Sci. Eng. R**33**, 51 (2001).
- [187] E. Alves, K. Lorenz, R. Vianden, C. Boemare, M. J. Soares and T. Monteiro
Optical doping of nitrides by ion implantation
Mod. Phys. Lett. B **15**, 1281 (2001).
- [188] T. Monteiro, C. Boemare, M. J. Soares, R. A. Sa Ferreira, L. A. Carlos, K. Lorenz, R. Vianden and E. Alves
PL and lattice location of Eu and Er implanted GaN samples
Phys. Rev. B **308**, 22 (2001).
- [189] C. J. Ellis, R. M. Mair, J. Li, J. Y. Lin, H. X. Jiang, J. M. Zavada and R. G. Wilson
Optical properties of Pr implanted GaN epilayers and $Al_xGa_{1-x}N$ alloys
Mat. Sci. Eng. B **81**, 167 (2001).
- [190] H. J. Lozykowski, W. M. Jadwisieniczak and I. Brown
Photoluminescence and cathodoluminescence of GaN doped with Pr
J. Appl. Phys. **88**, 210 (2000).
- [191] J. M. Zavada, R. A. Mair, C. J. Ellis, J. Y. Lin, H. X. Jiang, R. G. Wilson, P. A. Grudowski and R. D. Dupuis
Optical transitions in Pr-implanted GaN
Appl. Phys. Lett. **75**, 790 (1999).
- [192] E. Silkowski, Y. K. Yeo, R. L. Hengehold, B. Goldenberg, and G. S. Pomrenke
Neodymium and erbium implanted GaN
MRS Symp. Proc. **422**, 69 (1996).
- [193] S. Kim, S. J. Rhee, X. Li, J. J. Coleman and S. G. Bishop
Photoluminescence and photoluminescence excitation spectroscopy of multiple Nd^{3+} sites in Nd-implanted GaN
Phys. Rev. B **57**, 14588 (1998).
- [194] H. J. Lozykowski, W. M. Jadwisieniczak and I. Brown
Cathodoluminescence of GaN doped with Sm and Ho
Solid State Commun. **110**, 253 (1999).
- [195] J. B. Gruber, B. Zandi, H. J. Lozykowski and W. M. Jadwisieniczak
Spectroscopic studies of Sm^{3+} ($4f^5$) in GaN
J. Appl. Phys. **91**, 2929 (2002)
-

- [196] S. Dalmaso, R.W. Martin, P.R. Edwards, V. Katchanov, K.P. O'Donnell, K. Lorenz, E. Alves, U. Wahl, B. Pipeleers, V. Matias, A. Vantomme, Y. Nakanishi, A. Wakahara, A. Yoshida, and the RENiBEL Network
Electron micro-probe analysis and cathodoluminescence spectroscopy of rare earth-implanted GaN
MRS Symp. Proc. **798**, Y5.2 (2003).
- [197] B. de Vries, U. Wahl, A. Vantomme, J. C. Correia, and the ISOLDE collaboration
Emission channeling experiments from the decay of ^{149}Gd to ^{149}Eu in GaN
MRS Symp. Proc. **105**, 106 (2003).
- [198] H. J. Lozykowski, W. M. Jadwisienczak and I. Brown
Photoluminescence and cathodoluminescence of GaN doped with Tb
Appl. Phys. Lett. **76**, 861 (2000).
- [199] H. J. Lozykowski, W. M. Jadwisienczak and I. Brown
Cathodoluminescence study of GaN doped with Tb
Mat. Sci. Eng. B **81**, 140 (2001).
- [200] H. J. Lozykowski, W. M. Jadwisienczak and I. Brown
Visible cathodoluminescence of GaN doped with Dy, Er and Tm
Appl. Phys. Lett. **74**, 1129 (1999).
- [201] E. Alves, M. F. da Silva, J. C. Soares, R. Vianden, J. Bartels and A. Kozanecki
Ion beam and PL studies of Er and O implanted GaN
Nucl. Instr. Meth. B **147**, 383 (1999).
- [202] A. Braud, J. L. Doualan, R. Moncorge, B. Pipeleers and A. Vantomme
Er-defect complexes and isolated Er center spectroscopy in Er-implanted GaN
Mat. Sci. Eng. B **105**, 101 (2003).
- [203] L. C. Chao, B. K. Lee, C. J. Chi, J. Cheng, I. Chyr and A. J. Steckl
Upconversion luminescence of Er-implanted GaN films by focused- ion-beam direct write
Appl. Phys. Lett. **75**, 1833 (1999).
- [204] D. M. Hansen, R. Zhang, N. R. Perkins, S. Safvi, L. Zhang, K. L. Bray and T. F. Kuech
Photoluminescence of erbium-implanted GaN and in situ-doped GaN:Er
Appl. Phys. Lett. **72**, 1244 (1998).
- [205] J. M. Zavada, C. J. Ellis, J. Y. Lin, H. X. Jiang, J. T. Seo, U. Hömmerich, M. Thaik, R. G. Wilson, P. A. Grudowski and R. D. Dupuis
Annealing behavior of luminescence from erbium-implanted GaN films
Mat. Sci. Eng. B **81**, 127 (2001).
- [206] K. Lorenz, U. Wahl, E. Alves, T. Wojtowicz, P. Ruterana, S. Dalmaso, R. W. Martin, K. P. O'Donnell, S. Ruffenach, O. Briot and A. Vantomme
Processing of rare earth doped GaN with ion beams
Mat. Res. Soc. Symp. Proc. **798**, Y5.5 (2003).
- [207] W. M. Jadwisienczak and H.J. Lozykowski
Optical properties of Yb ions in GaN epilayer
Opt. Mater. **23**, 175 (2003).
- [208] D. Vogel, P. Krüger and J. Pollmann
Structural and electronic properties of group-III nitrides
Phys. Rev. B **55**, 12836 (1997).
- [209] J. P. Perdew, M. Ernzerho and K. Burke
Rationale for mixing exact exchange with density functional approximations
J. Chem. Phys. **105**, 9982 (1996).
- [210] M. G. Ganchenkova and R. M. Nieminen
Nitrogen vacancies as major point defects in GaN
Phys. Rev. Lett. **96**, 196402 (2006)

-
- [211] D. W. Jenkins, J. D. Dow and M. H. Tsai
Electronic structure and doping in InN, In_xGa_{1-x}N and In_xAl_{1-x}N
Phys. Rev. B **39**, 3317 (1989).
- [212] D. W. Jenkins and J. D. Dow
N vacancies in Al_xGa_{1-x}N
J. App. Phys. **72**, 4130 (1992).
- [213] X. Zhang, P. Kung, A. Saxler, D. Walker, T. Wang and M. Razeghi
Photoluminescence Study of GaN
Acta Phys. Pol. A **88**, 601 (1995).
- [214] J. Neugebauer and C. G. V. de Walle
Gallium vacancies and the yellow luminescence in GaN
Appl. Phys. Lett. **69**, 503 (1996).
- [215] J. Oila, V. Ranki, J. Kivioja, K. Saarinen, P. Hautojärvi, J. Likonen, J. M. Baranowski, K. Pakula, T. Suski, M. Leszczynski and I. Grzegory
Influence of dopants and substrate material on the formation of Ga vacancies in epitaxial GaN layers
Phys. Rev. B **63**, 045205 (2001).
- [216] K. Saarinen, T. Laine, S. Kuisma, J. Nissilä, P. Hautojärvi, L. Dobrzynski, J. M. Baranowski, K. Pakula, R. Stepniewski, M. Wojdak, A. Wyszomolek, T. Suski, M. Leszczynski, I. Grzegory and S. Porowski
Observation of Native Ga Vacancies in GaN by Positron Annihilation
Phys. Rev. Lett. **79**, 3030 (1997).
- [217] I. H. Lee, I. H. Choi, C. R. Lee and S. K. Noh
Evolution of stress relaxation and yellow luminescence in GaN/sapphire by Si incorporation
Appl. Phys. Lett. **71**, 1359 (1997).
- [218] J. Neugebauer and C. G. Van de Walle
Adv. Solid State Phys. **35**, 25 (1996).
- [219] C. G. Van de Walle
DX-center formation in wurtzite and zinc-blende Al_xGa_{1-x}N
Phys. Rev. B **57**, R2033 (1998).
- [220] C. R. Abernathy, J. D. Mackenzie and S. J. Pearton
CCl₄ doping of GaN grown by metalorganic molecular beam epitaxy Appl. Phys. Lett. **66**, 1969 (1995).
- [221] D. J. As and U. Köhler
Carbon - an alternative acceptor for cubic GaN
J. Phys. Cond. Matter **13**, 8923 (2001).
- [222] U. Birkle, M. Fehrer, V. Kirchner, S. Einfeldt, D. Hommel, S. Strauf, P. Michler and J. Gutowski
J. Nitr. Semicond. Res. **4S1**, G5.6 (1999).
- [223] P. Boguslawski and J. Bernholc
Doping properties of C, Si and Ga impurities in AlN and GaN
Phys. Rev. B **56**, 9496 (1997).
- [224] I. Gorczyca, A. Svane and N. E. Christensen
Theory of point defects in AlN, GaN and BN: Relaxation and pressure effects
Phys. Rev. B **60**, 8147 (1999).
- [225] L. E. Ramos, J. Furthmüller, L. M. R. Scolfaro, J. R. Leite and F. Bechstedt
Substitutional carbon in group-III nitrides: Ab initio description of shallow and deep levels
Phys. Rev. B **66**, 075209 (2002).
- [226] D. S. Lee, J. Heikenfeld, R. Birkhan, M. Garter, B. K. Lee and A. J. Stekl
Voltage-controlled yellow or orange emission from GaN codoped with Er and Eu
Appl. Phys. Lett. **76**, 1525 (2000).
-

- [227] A. J. Stekl, J. Heikenfeld, D. S. Lee and M. Garter
Multiple color capability from rare earth-doped gallium nitride
Mat. Sci. Eng. **N81**, 97 (2001).
- [228] J. M. Zavada, S. X. Jin, N. Nepal, J. Y. Lin, H. X. Jiang, P. Chow and B. Hertog
Electroluminescent properties of erbium-doped III-N light-emitting diodes
Appl. Phys. Lett. **84**, 1061 (2004).
- [229] M. Thaik, U. Hömmerich, R. N. Schwartz, R. G. Wilson and J. M. Zavada
Photoluminescence spectroscopy of erbium implanted gallium nitride
Appl. Phys. Lett. **71**, 2641 (1997).
- [230] S. F. Song, W. D. Chen, J. Zhu and C. C. Hsu
Dependence of implantation-induced damage with photoluminescence intensity in GaN:Er
J. Cryst. Growth **265**, 78 (2004).
- [231] H. Bang, S. Morishima, J. Sawahata, J. Seo, M. Takiguchi and M. Nomura
Concentration quenching of Eu-related luminescence in Eu-doped GaN,
Appl. Phys. Lett. **85**, 227 (2004).
- [232] S. Sanna, B. Hourahine, Th. Gallauner and Th. Frauenheim
An Efficient LDA+U Based Tight Binding Approach
J. Phys. Chem. A **111**, 5671 (2007).
- [233] H. Bang, S. Morishima, Z. Li, K. Akimoto, M. Nomura and E. Yagi
MBE growth of Eu- or Tb-doped GaN and its optical properties
J. Cryst. Growth **237-239**, 1027 (2002).
- [234] DFT-LDA calculations carried out on 72- or 64-atoms supercells (for hexagonal and cubic GaN respectively) containing one impurity atom. HGH-Pseudopotentials and a $4 \times 4 \times 4$ MP k -point mesh was used.
- [235] M. Hashimoto, S. Emura, R. Asano, H. Tanaka, N. Teraguchi, A. Suzuki, Y. Nanishi, T. Honma, N. Umesaki, H. Asahi
Local structure of rare-earth-doped diluted magnetic semiconductor GaGdN
Phys. Stat. Sol. C **0**, 2650 (2003).
- [236] M. Campagna, G. K. Wertheim and Y. Baer
Photoemission in solids II
Lay-Cardona editors, Springer, Berlin (1979).
- [237] O. Gunnarsson, O. Jepsen and O. K. Andersen
Self-consistent impurity calculations in the atomic-spheres approximation
Phys. Rev. B **27**, 7144-7168 (1983).
- [238] U. Gerstmann, *private communication*.
- [239] S. Morishima, T. Maruyama, M. Tanaka, Y. Masumoto and K. Akimoto
Growth of Eu Doped GaN and Electroluminescence from MIS Structure
Phys. Status Solidi A **176**, 113 (1999).
- [240] C. Köhler, B. Hourahine, G. Seifert, M. Sternberg and T. Frauenheim
Spin polarization in the SCC-DFTB formalism
J. Phys. Chem. A **111**, 5622 (2007).
- [241] M. Kotzian, N. Rösch, M. C. Zerner
Intermediate neglect of differential overlap spectroscopic studies on lanthanide complexes
Theor. Chim. Acta **81**, 201 (1992).
- [242] S. Sanna and V. Fiorentini
Lattice constant, effective mass, and gap recovery in hydrogenated GaAs_{1-x}N_x
Phys. Rev. B **69**, 125208-(1-6) (2004).

-
- [243] A. Polimeni, G. Baldassarri, F. Masia, A. Frova, M. Capizzi, S. Sanna, V. Fiorentini, P. J. Klar and W. Stolz
Tunable variation of the electron effective mass and exciton radius in hydrogenated GaAs_{1-x}N_x
Phys. Rev. B **69**, 04120(R) (2004).
- [244] A. Uedono, H. Bang, K. Horibe, S. Morishima and K. Akimoto
Defects in Eu- and Tb-doped GaN probed using a monoenergetic positron beam
J. Appl. Phys. **93**, 5181 (2003).
- [245] E. Alves, M. F. da Silva, J. C. Soares, R. Vianden, J. Bartels and A. Kozanecki
Ion beam and photoluminescence studies of Er and O implanted GaN
Nucl. Inst. Meth. Phys. Res. B **147**, 383-387 (1999) and E. Alves, T. Monteiro, J. Soares, L. Santos, M. F. da Silva, J. C. Soares, W. Lojkowski, D. Kolesnikov, R. Vianden and J. G. Correia
High temperature annealing of Er implanted GaN Mat. Sci. Eng. **B81**, 132-135 (2001).
- [246] B. de Vries, V. Matias, A. Vantomme, U. Wahl, E. M. C. Rita, E. Alves, A. M. L. Lopes and J. G. Correia
Influence of O and C co-implantation on the lattice site of Er in GaN
App. Phys. Lett. **84**, 4304-4306 (2004).
- [247] J. T. Torvik, C. H. Qiu, R. J. Feuerstein, J. I. Pankove and F. Namvar
Photo-, cathodo-, and electroluminescence from erbium and oxygen co-implanted GaN
J. App. Phys. **81**, 6343 (1997).
- [248] U. Gerstmann, A. T. Blumenau and H. Overhof
Transition metal defects in group-III nitrides: An ab initio calculation of hyperfine interactions and optical transitions
Phys. Rev. B **63**, 075204 (2001).
- [249] H. Tanaka, M. Hashimoto, S. Emura, A. Yanase, R. Asano, Y. K. Zhou, H. Bang, K. Akimoto, T. Honma, N. Umesaki and H. Asahi
Magnetic properties of the rare-earth-doped semiconductor GaEuN
Phys. Stat. Sol. C **0**, 2864 (2003).
- [250] U. Gerstmann, E. Rauls, S. Sanna, Th. Frauenheim and H. Overhof
Co-doping of Er-doped SiC with oxygen - a promising way towards 1540 nm emission at room temperature?
Mat. Sci. Forum **527-529**, 655-658 (2006).

Publications

1. A. Polimeni, G. Baldassarri, F. Masia, A. Frova, M. Capizzi, S. Sanna, V. Fiorentini, P. J. Klar and W. Stolz
Tunable variation of the electron effective mass and exciton radius in hydrogenated GaAs_{1-x}N_x
Phys. Rev. B **69**, 04120(R) (2004).
2. S. Sanna and V. Fiorentini
Lattice constant, effective mass, and gap recovery in hydrogenated GaAs_{1-x}N_x
Phys. Rev. B **69**, 125208-(1-6) (2004).
3. A. Pecchia, A. Di Carlo, A. Gagliardi, S. Sanna, Th. Frauenheim and R. Gutierrez
Incoherent electron-phonon scattering in octanethiols
Nano Letters **4**, 2109 (2004).
4. A. Polimeni, G. Baldassarri, F. Masia, A. Frova, M. Capizzi, S. Sanna, V. Fiorentini, P. J. Klar and W. Stolz
Tuning of the electron effective mass and exciton wavefunction size in GaAs_{1-x}N_x
Physica E **21**, 747-751 (2004).
5. B. Szücs, Z. Hajnal, R. Scholz, S. Sanna and Th. Frauenheim
Theoretical study of the adsorption of a PTCDA monolayer on S-passivated GaAs(1 0 0)
Appl. Surf. Sci. **234**, 173-177 (2004).
6. G. Ciatto, F. d'Acapito, F. Boscherini, S. Sanna, V. Fiorentini, A. Polimeni, M. Capizzi, P. J. Klar, W. Stolz and S. Mobilio
Comparison between experimental and theoretical determination of the local structure of the GaAs_{1-y}N_y dilute nitride alloy
Phys. Rev. B **71**, 115210-(1-8) (2005).
7. A. Béré, P. Ruterana, G. Nouet, A. T. Blumenau, S. Sanna, T. Frauenheim, J. Chen and J. Koulidiati
Density-functional tight-binding calculations of electronic states associated with grain boundaries in GaN
Phys. Rev. B **71**, 125211 (2005).
8. S. Sanna
Computational modeling of Rare Earth doped GaN
PC² Year Report, 91 (2005).
9. P. Koskinen, H. Häkkinen, G. Seifert, S. Sanna, Th. Frauenheim and M. Moseler
Density-functional based tight-binding study of small gold clusters
N. J. Phys. **8**, 9 (2006).
10. B. Hourahine, S. Sanna, B. Aradi, C. Köhler and Th. Frauenheim
A theoretical study of erbium in GaN
Phys. B **376**, 512 (2006).

11. U. Gerstmann, E. Rauls, S. Sanna, Th. Frauenheim and H. Overhof
Co-doping of Er-doped SiC with oxygen - a promising way towards 1540 nm emission at room temperature?
Mat. Sci. Forum **527-529**, 655-658 (2006).
12. S. Sanna, B. Hourahine, Th. Gallauner and Th. Frauenheim
An efficient LDA+U based tight binding approach
J. Phys. Chem. A, **111**, 5671 (2007).
13. S. Sanna, B. Hourahine, U. Gerstmann and Th. Frauenheim
An efficient tight binding approach for the study of strongly correlated systems
Accepted for publication in Phys. Rev. B (2007).
14. S. Sanna, B. Hourahine, U. Gerstmann and Th. Frauenheim
Theoretical study of rare earth substitutionals in GaN in preparation
15. B. Hourahine, S. Sanna, B. Aradi, C. Köhler, Th. Niehaus and Th. Frauenheim
Self-interaction and strong correlation in DFTB
J. Phys. Chem. A, **111**, 5665 (2007).
16. S. Sanna, U. Gerstmann and Th. Frauenheim
Proof of the validity of the Slater-Janak transition-state model within the DFTB approach
Submitted to Phys. Rev. B (2007).
17. S. Sanna, B. Hourahine, U. Gerstmann and Th. Frauenheim
Theoretical study of rare earth point defects in GaN
Submitted to Phys. Stat. Sol. B (2007).

Acknowledgements

Exactly five years ago I was, for a semester, an exchange student at the Universität Paderborn. Today, exactly five years later, I'm finishing my Ph.D thesis at the same university. The person who made it possible is Prof. Thomas Frauenheim, which at first invited me and then supported and supervised my work in Paderborn. At him goes my hearty thank!

Volendo ora ringraziare la mia famiglia scrivo in italiano: essendo questa parte rivolta a loro la voglio scrivere nella lingua che abbiamo sempre parlato. Grazie per tutto l'aiuto che solo una famiglia puo dare e sorry per esservi stato vicino solo due volte all'anno in questi quattro anni!

My closest co-workers during my Ph.D have been Dr. Bálint Aradi, Dr. Ben Hourahine and Dr. Uwe Gerstmann. With the first two I also had the pleasure to share the office. Thanks a lot for all the work we did together, for your suggestions and guidance. Each research task is like a recipe which needs a lot of ingredients to be successfully realised. The most important of these ingredients are an efficient computer system with good software running on it and a nice atmosphere in the working group. For the former I owe a thank to Dr. Bálint Aradi, Dr. Ben Hourahine, Dr. Knut Vietze and Dr. Dirk Porezag (DFTB-Software and more) Dr. Christof Köhler and his SHK co-workers (Computer System). For creating this atmosphere and sustaining me with suggestions and help of various nature, I'd like to thank actual and former members of the Frauenheim and Schmidt group in Bremen and Paderborn. At least so important was the daily presence of Prof. Gerhard Leßner and our fruitful discussion about football tactic. The RENiBEL network was the European project for the study of RE in GaN I took part at and which financed this work. For this reason, for providing experimental data, for the clarifying discussion and for the pub crawling around half Europe I want to thank all the RENiBEL members. I'm most grateful to Dr. Andreia da Rosa, Dr. Jens Förstner and Dr. Uwe Gerstmann for the critical reading of this work and suggesting me necessary corrections. They helped me to eliminate most of the "italo-german" flavour from the grammatic and were a great help in identifying those passages of the text which needed rephrasing or clarification. I'd also like to express my gratitude to prof. Donat As for the discussions about GaN and its dopants. I'd also like people who during my stay in Paderborn successfully worked with me on topics, which for various reason could not be included in this thesis. They are Dr. Alessandro Pecchia, Dr. Alessio Gagliardi and the whole group of Prof. Aldo di Carlo from the Università di Tor Vergata in Rom, (work about transport on molecular systems), Bernadette Sücs and Dr. Zoltan Hajnal from the Universität Paderborn (work about molecular covering (PTCDA, Azobenzol and Stylben) on metallic surfaces), Dr. Alexander Blumenau and his group at Max Plank Institut in Düsseldorf (study of thiols on Au surfaces), Dr. Antoine Bére, Prof. Pierre Ruterana and his group at the Centre National de la Recherche Scientifique in Caen (study of dislocations and extended defects in GaN), Prof. Michael Moseler and his group at the Fraunhofer Institut in Freiburg (study of Au clusters). Well, it seems to be a classic to put at the last place the person who mostly deserved our thanks... I thank my wife Hosoon for supporting and sustaining me expecially in this last period, in which my sacrifices were also her sacrifices.

Colophon

This work was entirely written with L^AT_EX2_ε. To maintain a consistent style the number of applications was reduced to the minimum: data plots were prepared with XMGrace (5.1.19), atomic structures were rendered with RasMol (2.7.3.1) and wave functions and charge distribution with VMD (1.8.6) and XFarbe (2.6c). Modifications were then executed with the graphics program XFig (3.2.4). The results of the DFTB+ calculation can be reproduced with the parameters I created for this work, characterised identified by the md5sum reported in Tab. A.2. Parameters are available for everyone who wants to reproduce these results and further simulate rare earth compounds.

Table A.2: *md5sum of the parameter files used in this work.*

C-C	93c4f9fd766d4ad952e549888cbeea8a	C-Er	519a0e1497ea2cb8be41e8c47360e3f4
C-Ga	f60ac30d62e35e5467980f7593505cfd		
C-N	85f202e74756b5e37c89f89b022496a3	C-O	621a08974637b6750cbf6ae6b74e36db
Er-C	d7bce814a65c1471e2d62537bfd99437	Er-Er	bf0896976cf3a6a367509436dc5e6358
Er-Ga	b261dc0d10f50f9d6d426596c34419a4	Er-N	701d968b7c341eb241709f6370a1c582
Eu-O	9c8de0306d6f875fab1e8fafbc8ba89f	Eu-Eu	2421bc072f2f586634b6d58b8afbeb06
Eu-Ga	c504ec5a9c48e9d746dd51f38c344c13	Eu-N	ec5e92c903930b67a8eeebbe3c01e586
Ga-C	620ef4ccd685c23853c46f236ca21957	Ga-Er	f15fd7c39e9a3551bdacd25ff3264b3f
Ga-Eu	af8b3d2b540f1dd79bcde124083e6de9	Ga-Ga	7fb60ea19e4f651f192cf0c317915747
Ga-Gd	f9bc79532fb317f984857d1f70c8c66f	Ga-N	2d4d3470588a34a74a5e1b9ba1590797
Ga-O	3abc46f77baee69ade8bfefc289048e2	Gd-Ga	aba371872ddf7bc95e308141c511724b
Gd-Gd	ff57c8a3c440a8bcf8b41840db7879ed	Gd-N	0e5a4c6c03fce4fc9f4d24b13e867bf3
N-Er	6a766c2fdbd5f283994ca5f1ef98ede9	N-C	126acc90c38a53a1358566aed885ccc1
N-Ga	39507bafb0d5ab97025f3772e2da0c2f	N-Eu	6c8af51589c4da154ce53fe4b9536094
N-N	270b9e66bb19be0d2de61ca7cfe7e93c	N-Gd	8c0e3e1aca5dc3e3bee91fcf0220fdb
O-C	ba395bd0c3aad2142db1099873567068	N-O	359369e1d64d059c1e0e477a3371e4d2
O-Eu	34b4e17173dd43307133bed77183ad96	O-Tm	5f3bb29f7eb3fe1d82211778c2a1f73a
O-N	d794fac915ac6db39c86dda8b1563d7a	O-Ga	78b202198b7aed305b9e6070ee79559a
Pr-Pr	b4e94fe5f5f9a9dc336057e7d29402be	O-O	dfe1ad51b6eb83c69bb8211722cd02aa
Tm-O	88352cd5e66a4bf1085318e7ead576d8	Tm-Tm	60b2e45414cf3705ee36bcfa9021bc8b